NORTH ATLANTIC TREATY ORGANIZATION

SCIENCE AND TECHNOLOGY ORGANIZATION

AC/323(SET-170)TP/600

www.sto.nato.int

STO TECHNICAL REPORT **TR-SET-170**

Mid-Infrared Fiber Lasers

(Lasers à fibre fonctionnant
dans l'infrarouge moyen)

Final Report of Task Group 095.

Published April 2015

NORTH ATLANTIC TREATY ORGANIZATION

SCIENCE AND TECHNOLOGY ORGANIZATION

AC/323(SET-170)TP/600

www.sto.nato.int

STO TECHNICAL REPORT **TR-SET-170**

Mid-Infrared Fiber Lasers

(Lasers à fibre fonctionnant
dans l'infrarouge moyen)

Final Report of Task Group 095.

The NATO Science and Technology Organization

Science & Technology (S&T) in the NATO context is defined as the selective and rigorous generation and application of state-of-the-art, validated knowledge for defence and security purposes. S&T activities embrace scientific research, technology development, transition, application and field-testing, experimentation and a range of related scientific activities that include systems engineering, operational research and analysis, synthesis, integration and validation of knowledge derived through the scientific method.

In NATO, S&T is addressed using different business models, namely a collaborative business model where NATO provides a forum where NATO Nations and partner Nations elect to use their national resources to define, conduct and promote cooperative research and information exchange, and secondly an in-house delivery business model where S&T activities are conducted in a NATO dedicated executive body, having its own personnel, capabilities and infrastructure.

The mission of the NATO Science & Technology Organization (STO) is to help position the Nations' and NATO's S&T investments as a strategic enabler of the knowledge and technology advantage for the defence and security posture of NATO Nations and partner Nations, by conducting and promoting S&T activities that augment and leverage the capabilities and programmes of the Alliance, of the NATO Nations and the partner Nations, in support of NATO's objectives, and contributing to NATO's ability to enable and influence security and defence related capability development and threat mitigation in NATO Nations and partner Nations, in accordance with NATO policies.

The total spectrum of this collaborative effort is addressed by six Technical Panels who manage a wide range of scientific research activities, a Group specialising in modelling and simulation, plus a Committee dedicated to supporting the information management needs of the organization.

- AVT Applied Vehicle Technology Panel
- HFM Human Factors and Medicine Panel
- IST Information Systems Technology Panel
- NMSG NATO Modelling and Simulation Group
- SAS System Analysis and Studies Panel
- SCI Systems Concepts and Integration Panel
- SET Sensors and Electronics Technology Panel

These Panels and Group are the power-house of the collaborative model and are made up of national representatives as well as recognised world-class scientists, engineers and information specialists. In addition to providing critical technical oversight, they also provide a communication link to military users and other NATO bodies.

The scientific and technological work is carried out by Technical Teams, created under one or more of these eight bodies, for specific research activities which have a defined duration. These research activities can take a variety of forms, including Task Groups, Workshops, Symposia, Specialists' Meetings, Lecture Series and Technical Courses.

The content of this publication has been reproduced directly from material supplied by STO or the authors.

Published April 2015

Table of Contents

List of Figures

List of Tables

List of Acronyms

AFB	Air Force Base
AFRL	Air Force Research Laboratory
ALLS	Advanced Laser Light Source
AOM	Acousto-Optic Modulator
AR	Anti-Reflection
ASE	Amplified Spontaneous Emission
BYF	Barium Yttrium Fluoride
CFBG	Chirped Fiber Bragg Grating
COTS	Commercial-Off-The-Shelf
CW	Continuous Wave
DEU	Germany
DFB	Distributed Feedback
DFG	Difference Frequency Generation
DIRCM	Directed Infrared Countermeasures
DRDC	Defence Research and Development Canada
Dstl	Defence Science and Technology Laboratory
EDFA	Erbium-Doped Fiber Amplifier
EOM	Electro-Optic Modulator
ESA	Excited State Absorption
ET	Exploratory Team
ETU	Energy Transfer Up-conversion
EYDFA	Erbium-Ytterbium-Doped Fiber Amplifier
FBG	Fiber Bragg Grating
FFI	Forsvarets Forskningsinstitutt (Norwegian Defence Research Establishment)
FTIR	Fourier Transform Infrared Spectrometer
FWHM	Full-Width Half Maximum
GaAs	Gallium Arsenide
GaP	Gallium Phosphide
GSML	Gain-Switched Mode-Locked
GVD	Group Velocity Dispersion
HIP	Hyperspectral Image Projector
HNLF	Highly Non-Linear Fiber
HR	High Reflector
HVPE	Hydride Vapor Phase Epitaxy
INO	Institut National d'Optique
IR	Infrared
IRCM	Infrared Countermeasures
IRP	IR Photonics
ISL	French-German Research Institute Saint-Louis
LMA	Large-Mode-Area
LVF	Le Verre Fluoré
LWPF	Long Wave Pass Filter

MI	Modulation Instability
MIR	Mid-Infrared
ML	Mode-Locking
MLR	Mode-Locking Resembling
MOPA	Master Oscillator Power Amplifier
MOPAW	Master Oscillator with Programmable Amplitude Wavefront
MUT	Military University of Technology
NA	Numerical Aperture
NIR	Near Infrared
NRL	Naval Research Laboratory
OC	Output Coupler
OPA	Optical Parametric Amplifier
OPGaAs	Orientation-Patterned Gallium Arsenide
OPGaP	Orientation-Patterned Gallium Phosphide
OPO	Optical Parametric Oscillator
OSA	Optical Spectrum Analyzer
PCF	Photon Crystal Laser
PL	Programmable Laser
PM	Polarization Maintaining
PPLN	Periodically-Poled Lithium Niobate
PRF	Pulse Repetition Frequency
QCL	Quantum Cascade Laser
QML	Q-switched Mode-Locked
QPM	Quasi-Phasematching
RTG	Research Task Group
SC	Supercontinuum
SET	Sensors and Electronic Technology
SIF	Step Index Fiber
SMF	Single-Mode Fiber
SPL	Synchronised Programmable Laser
SPM	Self-Phase Modulation
SSFS	Soliton Self-Frequency Shift
TDF	Thulium-Doped Fiber
TDFA	Thulium-Doped Fiber Amplifier
TDFL	Thulium-Doped Fiber Laser
TPA	Two-Photon Absorption
USA	United States of America
UV	Ultraviolet
VBG	Volume Braggs Grating
WDM	Wavelength Division Multiplexing
XPM	Cross-Phase Modulation
YAG	Yttrium Aluminum Garnet
ZBLAN	Family of glasses containing ZrF_4-BaF_2-LaF_3-AlF_3-NaF
ZDW	Zero-Dispersion Wavelength
ZGP	Zinc Germanium Phosphide

Preface

This information is furnished on the condition that it will not be released to another Nation without specific authority of the Department of the Air Force of the United States, that it will be used for military purposes only, that individual or corporate rights originating in the information, whether patented or not, will be respected, that the recipient will report promptly to the United States any known or suspected compromise, and that the information will be provided substantially the same degree of security afforded it by the department of Defense of the United States. Also, regardless of any other markings on the document, it will not be downgraded or declassified without written approval from the originating US agency.

SET-170 Membership List

Dr. Ishwar D. AGGARWAL
US Navy
Naval Research Laboratory Code 5620
4555 Overlook Avenue SW
Washington, DC 20375-5338
UNITED STATES
Email: aggarwal@nrl.navy.mil

Marc EICHHORN, Dr. rer. nat. habil., Dipl.-Phys.
Division III, French-German Research Institute
of Saint-Louis (ISL)
5 rue du Général Cassagnou
68300 Saint-Louis Cedex
FRANCE
Email: Marc.Eichhorn@isl.eu

Henning HEISELBERG, Ph.D
Senior Scientist
Joint Research and Test Centre
DALO
Lautrupbjerg 1-5
DK-2750 Ballerup
DENMARK
Email: heiselberg@mil.dk

Dr. Christelle KIELECK
Directed Photonics and Applications
Division III, French-German Research Institute
of Saint-Louis (ISL)
5 rue du Général Cassagnou
68300 Saint-Louis Cedex
FRANCE
Email: Christelle.Kieleck@isl.eu

Dr. Espen LIPPERT
FFI (Norwegian Defence Research Establishment)
P.O Box 25
NO-2027 Kjeller
NORWAY
Email: Espen.Lippert@ffi.no

Rita D. PETERSON, Ph.D (Chair)
Air Force Research Laboratory
AFRL/RYJW Bldg 620
2241 Avionics Circle
Wright-Patterson AFB, OH 45433
UNITED STATES
Email: rita.peterson@wpafb.af.mil

Jas SANGHERA, Ph.D
Naval Research Laboratory Code 5620
Optical Materials and Devices Branch
4555 Overlook Avenue SW
Washington, DC 20375-5338
UNITED STATES
Email: sanghera@nrl.navy.mil

Jacek SWIDERSKI; Lt. Col., Ph.D
Institute of Optoelectronics
Military University of Technology
2 Kaliskiego Street
00-908 Warsaw
POLAND
Email: jswiderski@wat.edu.pl

Francis THÉBERGE, Ph.D
Defence Scientist
Section Electro-Optic Warfare Section
DRDC Valcartier
2459 route de la Bravoure
Québec (Québec) G3J 1X5
CANADA
Email: francis.theberge@drdc-rddc.gc.ca

Professor David H. TITTERTON
SCD, Dstl
i-SAT:A, Bldg. 5, Room 201
Porton Down, Salisbury
Wiltshire SP4 0JQ
UNITED KINGDOM
Email: DHTITTERTON@mail.dstl.gov.uk

Dr. Denis VINCENT
Defence Scientist
Section Electro-Optic Warfare Section
DRDC Valcartier
2459 route de la Bravoure
Québec (Québec) G3J 1X5
CANADA
Email: Denis.Vincent@drdc-rddc.gc.ca

Contributing Authors

AUTHOR	NATION
Stuart D. JACKSON	AUS
Brian BURGOYNE	CAN
Marc CHÂTEAUNEUF	CAN
Jean-François DAIGLE	CAN
Jacques DUBOIS	CAN
Jean FORTIN	CAN
François LÉGARÉ	CAN
Pierre MATHIEU	CAN
Joseph SALHANY	CAN
Bruno E. SCHMIDT	CAN
Yasaman SOUDAGAR	CAN
Nicolas THIRÉ	CAN
Alain VILLENEUVE	CAN
Antoine BERROU	FRA
Michael ECKERLE	FRA
Gwenael MAZÉ	FRA
Maria MICHALSKA	POL
Rafael R. GATTASS	USA
Shrikrishna M. HEGDE	USA
Vinh Q. NGUYEN	USA
Paul C. PUREZA	USA
L. Brandon SHAW	USA

Mid-Infrared Fiber Lasers

(STO-TR-SET-170)

Executive Summary

Mid-infrared laser technology is critical for active sources to defeat a growing spectrum of heat-seeking missiles, as well as for remote sensing of targets and threats. Fiber lasers have distinct advantages over conventional bulk solid-state lasers in thermal management, resisting misalignment, and tolerating challenging environmental conditions. Their geometry supports distributed system architectures. Despite recent advances, few fiber lasers operate beyond 3 μm, and passive IR fiber and fiber-based components remain rare, lossy and fragile. Extending fiber technology into the mid-IR would provide laser sources that are efficient, robust, compact, high in power, and well-suited to critical military applications like infrared countermeasures.

The SET-170 Programme of Work focused on three tasks:

1) Direct lasing in rare-earth-doped fibers;
2) Supercontinuum generation for broadband output; and
3) Fiber pump sources for bulk mid-IR frequency conversion devices.

To keep the scope manageable, sources with wavelengths shorter than 3 μm and fiber-based components were not considered, in spite of their critical role in eventual systems.

Task 1 identified trivalent holmium at 3.9 μm as the active ion most likely to result in a successful laser, and fluoroindate fiber as the host material due to its transparency to 5.5 μm, and its ability to incorporate the dopant ions. Spectroscopic analysis and modelling were used to evaluate the possibility of developing a viable Ho:fiber laser, and to identify suitable fiber specifications. Funding constraints prevented fabrication of an actual fiber, but lasing was demonstrated in a sample of the Ho-doped glass; an encouraging first result.

Task 2 focused on increasing the output power, bandwidth, and mid-IR efficiency of supercontinuum sources. Key results include power scaling demonstrations in fluoride and chalcogenide fibers; demonstration of the most efficient power distribution at wavelengths longer than 3 μm; and a comparison of different fiber-based pumping techniques. The most significant factors limiting the long-wavelength edge of the supercontinuum spectrum were found to be fiber non-linearities, bend-induced loss and bulk absorption.

Task 3 considered pumping strategies for ZGP, PPLN, and OPGaAs, representing the current spectrum of non-linear materials. A particularly intriguing result was modelling suggesting the viability of pumping an OPGaAs OPO at wavelengths as short as 1550 nm despite the material's two-photon absorption in this region. Unfortunately this result could not be investigated experimentally because the right OPGaAs material was not available, leaving this among our recommendations for future work.

SET-170's programme of work was ambitious, guided by the goal of maximizing our contribution to the field with the resources available. To that end, we were successful in that each task produced results that were noteworthy, and more importantly, useful in the further study of mid-IR fiber lasers. Task Group activity resulted directly in 10 journal publications, plus two planned; and several conference presentations and proceedings. A new Exploratory Team (ET-086) has been approved to continue investigation of mid-IR fiber-based sources, building on the work of this Task Group.

Lasers à fibre fonctionnant dans l'infrarouge moyen

(STO-TR-SET-170)

Synthèse

La technologie des lasers à infrarouge moyen est cruciale si l'on veut que les sources actives mettent en échec un spectre de plus en plus large de missiles à autodirecteur thermique et détectent à distance les objectifs et les menaces. Les lasers à fibre présentent de nets avantages par rapport aux lasers classiques à semi-conducteurs massifs en matière de gestion thermique, résistance au défaut d'alignement et tolérance aux conditions environnementales hostiles. Leur géométrie accepte les architectures de système distribuées. En dépit des progrès récents, peu de lasers à fibre ont une portée supérieure à 3 µm ; la fibre optique passive et les composants à base de fibre restent rares, fragiles et entraînent des pertes de données. L'élargissement de la technologie de fibre au moyen infrarouge produirait des sources laser efficaces, robustes, compactes, très puissantes et bien adaptées aux applications militaires essentielles telles que les contre-mesures infrarouges.

Le programme de travail du SET-170 s'est orienté selon trois directions :

1) Effet laser direct dans les fibres dopées aux terres rares ;
2) Production d'un supercontinuum pour sortie à large bande ; et
3) Sources de pompage pour fibre destinées aux appareils massifs de conversion de fréquence dans le moyen infrarouge.

Afin que l'objectif reste réalisable, les sources à longueur d'onde inférieure à 3 µm et les composants à base de fibre n'ont pas été étudiés, malgré leur rôle crucial dans les systèmes éventuels.

La tâche numéro 1 a déterminé que l'ion holmium trivalent à 3,9 µm était le plus susceptible de donner un laser réussi et a désigné la fibre de fluoroindate en tant que matériau hôte en raison de sa transparence jusqu'à 5,5 µm et de sa capacité à incorporer les ions dopants. L'analyse spectroscopique et la modélisation ont servi à évaluer la possibilité de développer un laser à fibre Ho et à identifier les caractéristiques techniques adéquates de la fibre. Les contraintes de financement ont empêché la fabrication d'une fibre réelle, mais l'effet laser a été démontré dans un échantillon de verre dopé à l'holmium, ce qui est un premier résultat encourageant.

La tâche numéro 2 s'est concentrée sur l'accroissement de la puissance de sortie, de la bande passante et de l'efficacité dans l'infrarouge moyen des sources supercontinuum. Les résultats clés sont notamment des démonstrations d'augmentation de la puissance avec des fibres en fluorure et en chalcogénure, la démonstration de la répartition de puissance la plus efficace à des longueurs d'onde supérieures à 3 µm et la comparaison de différentes techniques de pompage à base de fibre. Les facteurs les plus importants limitant l'élévation de la longueur d'onde en bordure du spectre du supercontinuum se sont révélés être les non-linéarités de fibre, la perte induite par les coudes et l'absorption par la masse.

La tâche numéro 3 a étudié les stratégies de pompage pour les substrats en ZGP, PPLN et OP-GaAs, qui représentent le spectre actuel des matériaux non linéaires. Un résultat particulièrement intrigant a été obtenu : la modélisation a suggéré la viabilité du pompage d'un OPO en OP-GaAs à de courtes longueurs

d'onde (1550 nm) malgré l'absorption à deux photons du matériau dans cette région. Malheureusement, ce résultat n'a pas pu être étudié de manière expérimentale, parce que le matériau en OP-GaAs n'était pas disponible, ce qui nous amène à placer ce sujet dans nos recommandations de travaux futurs.

Le programme de travail du SET-170 était ambitieux, guidé par l'objectif d'optimisation de notre contribution dans le domaine à l'aide des ressources disponibles. Nous avons atteint cet objectif, dans la mesure où chaque tâche a produit des résultats notables et, plus important, utiles à l'étude ultérieure des lasers à fibre dans le moyen infrarouge. L'activité du groupe de travail a directement abouti à 10 publications, deux autres étant en prévision, et à plusieurs présentations et débats en conférence. Une nouvelle équipe exploratoire (ET-086) a été approuvée et continue d'examiner les sources à base de fibre dans le moyen infrarouge, en s'appuyant sur les travaux du présent groupe de travail.

Chapter 1 – INTRODUCTION

1.1 BACKGROUND

A laser is only a relatively sophisticated light source with many special optical properties, such as high directionality and coherence within the beam, which have been applied over the last five decades to a vast range of military as well as civilian applications. As the laser technology continues to develop, so the number of military applications increases. Hence, the "laser" can no longer be considered to be a technical solution looking for a problem.

In the decades since 1960, the developments in general with laser technology have revolutionised the performance of many military systems, providing the operators and war fighters with significant enhancements in performance particularly in remote sensing, countermeasure techniques (hard- and soft-kill options), guidance and navigation systems, as well as a valuable training aid. Consequently, there have been many military projects aimed at exploiting one or more of these special optical properties of the laser, or its fundamental characteristics, since the first reported practical demonstration of laser action in May 1960 by Theodore Maiman.

The first reported application of laser technology concerned sensing and targeting, and in particular, the use of a pulsed source to measure the distance to distant or remote objects. This provided unprecedented measurements of accuracy to a target from the remote "spotter's position". More recent examples of the use of the laser in the sensing function have included gated-imaging and laser-radar applications. There are a number of projects that exploit the high radiant-intensity characteristics of the laser beam for directed-energy applications, particularly for countermeasure systems used for platform protection or anti-air applications.

One of the most significant developments in laser technology over the last decade has been with the fiber laser. The initial catalyst for its development was the so-called telecommunications boom, but as often happens, the techniques developed for that application were relevant to other applications; moreover, the fiber-laser concept has proved to be extremely versatile.

A fiber laser is a solid-state rod laser with a long and very thin gain medium surrounded by an undoped host, such as "glass", which has many advantages for the efficient extraction of waste heat, which can be one of the limiting features of solid-state lasers, leading to very undesirable beam characteristics. The inefficiencies in the generation of photons leading to heat generation within the laser gain medium are usually the fundamental cause of aberrations in the emitted beam intensity profile produced by a conventional solid-state laser.

The operation of a fiber laser can be considered to be a brightness converter, owing to the very high optical-to-optical conversion efficiency, as well as a wavelength changer. The device takes the highly divergent laser light from the pump diodes and usually emits light at a slightly different wavelength in a much brighter beam, i.e. a beam with more optical power and very small divergence. Beam brightness is a fundamental requirement of all directed-energy applications; additionally, beam brightness is important for many sensing applications. Moreover, fiber-laser technology can be configured to control the mode and polarisation of the emission from each fiber laser device. Mode control is normally a fundamental requirement for higher-power devices intending to combine the emission from several lasers in order to create a higher power output. However, not all directed-energy applications require high-power emission, but normally stable and high beam-quality characteristics are necessary.

The basic design of a conventional fiber laser is a doped core surrounded by a so-called cladding region of similar material to the core but not doped and with a slightly reduced refractive index compared with the core. This optical arrangement, with the differing refractive indices, provides the confinement of the light

along the length of the optical fiber core. This core region is often a few microns in diameter and the cladding several orders of magnitude greater, although so-called large-mode area devices have been demonstrated for high-power applications; these fibers have a core diameter of the order of 10 – 50 µm.

Until recently, the main thrust with fiber-laser technology has been with devices that emit in the near and short-wave infrared (up to about 2 µm). These devices have been shown to be highly efficient and robust, so that very small and compact systems can be realised.

The mid-wave infrared (2 – 5 µm), coinciding with an atmospheric window that generally has high beam transmission, is a very important part of the electromagnetic spectrum for many military applications, especially for sensing and countermeasure systems. Other laser technologies are available for operation in this part of the spectrum, but most lack the advantages of fiber-laser sources; moreover, many of these sources are reliant on non-linear techniques using bulk crystals, which tend to make the source more complex and reduce efficiency, leading to a larger system "package".

An Exploratory Team was formed during 2009 under the auspices of the NATO Sensors and Electronic Technologies (SET) Panel to consider the prospects for the application of fiber laser technology, and associated techniques, to generate emission in the mid-wave infrared. This short study identified the following research areas where progress was needed for mid-IR fiber laser technology to advance:

- Fiber gain media based upon materials other than silica, for low-loss transmission through the mid-IR spectral region;
- For writing gratings into non-silica fibers to form resonators to enable monolithic structures to be realised; and
- Optical components such as isolators, modulators, and switches designed for mid-IR operation.

The latter topic was not included in the scope of the planned study group because development of such components entails significant expense and is best left for industry. However, given the growing use of shorter-wavelength fiber lasers as pumps for $\chi^{(2)}$ frequency conversion into the mid-IR, a comparative assessment of fiber-based pumping strategies and architectures was added to the scope of the study group.

The recommendation from the ET to the SET Panel was that the technology base was sufficiently well developed to warrant an investigation of mid-wave IR generation in solid-state devices for military applications. This recommendation was accepted and a technology group was formed to plan and implement a programme of research to investigate these topics. Moreover, the proposed research topic to investigate *fiber gain media based upon materials other than silica, for transmission through the mid-IR*, was expanded and differentiated to include non-linear fibers (Raman, super-continuum), for example, in addition to laser gain media, to reflect existing interest and progress in these techniques.

1.2 OBJECTIVES

The principal objective of this Research Task Group (RTG) was to advance the state-of-the-art in mid-IR fiber laser technology through collaboration involving leading researchers in participating Nations, focusing on the technical areas listed below. Whilst the mid-IR spectral region is often defined as 2 – 5 µm to correspond with the atmospheric transmission window at these wavelengths, the technical challenges of producing coherent output at 3 µm and beyond are more significant and often distinct from those associated with the 2 – 3 µm region. This is demonstrated by the increasing availability of lasers, both fiber and bulk, operating in this region. To extend coverage through the entire mid-IR region, the RTG decided to focus on sources that can emit at 3 µm and longer wavelengths. This, of course, does not exclude sources that can operate at shorter wavelengths in addition to the 3 – 5 µm region.

1.3 GOALS

The specific goals of the TG programme were:

- To investigate direct lasing in fiber gain media at wavelengths longer than 3 μm:
  - Spectroscopic characterisation of doped IR glasses and fibers to augment existing data;
  - Modelling of lasing in candidate fibers using spectroscopic data;
  - Development of specifications for fabrication of promising candidate fiber(s);
  - Exchange of data among panel members; and
  - Demonstration of gain/lasing in IR glass preform, and experimental fiber.
- To investigate non-linear frequency conversion in fibers at wavelengths longer than 3 μm:
  - Measurement non-linearity and dispersion in candidate fibers;
  - Exchange of data among Task Group members;
  - Modelling of frequency conversion behaviour using resulting data;
  - Demonstration of super-continuum generation in suitable fiber(s) using streamlined pump architecture; and
  - Investigation of Raman conversion, if suitable fiber is available.
- Comparison of fiber-based pump techniques for frequency conversion into the mid-IR:
  - Identification and assembly of a standard set of non-linear frequency conversion samples;
  - Development of an experimental protocol for frequency conversion experiments;
  - Evaluation of diverse pumping schemes using the standard sample set and measurement protocol; and
  - Exchange, analysis, and comparison of results.

1.4 RTG MEMBERSHIP

It was decided by consensus that Task Group members should be government or government on-site contractors, to include on-site support contractor scientists involved in national research programmes related to the activities of the Group. The countries that participated in this activity were: Canada, Denmark, France, Germany, Norway, Poland, the United Kingdom and the United States. The lead Nation was the United States and technical team leader was Dr. Rita Peterson of the Air Force Research Laboratory (AFRL).

Chapter 2 – RARE-EARTH-DOPED FIBERS: BACKGROUND

2.1 INTRODUCTION

Fiber lasers are efficient, powerful and versatile waveguide resonant devices that comprise glass optical fiber waveguides for optical gain and Fabry-Pérot resonators for optical feedback. Rapid developments in fabrication capabilities now allow fibers composed of ultralow-loss silicate glass with low scattering, impurity losses and material imperfections, thus providing enormous flexibility in the characteristics and quantity of light that can be generated from fiber lasers. Passively air-cooling an optical fiber is simple owing to its large surface-area-to-volume ratio. Optical excitation using multi-mode semiconductor diode lasers is straightforward and efficient with cladding pumping [1], particularly when the axial symmetry of the fiber is broken [2], and efficiently excites the single-mode core of the fiber to create near-diffraction-limited output with significant enhancement in the brightness [3]. Although doping silicate glass optical fibers using rare-earth cations introduces additional Rayleigh scattering, this drawback is small compared with the gain enhancement. Furthermore, diluted (< 0.1 mol %) rare-earth cation concentrations have a background loss [4] of less than 2 dB km^{-1}, a value that is commensurate with conventional fiber. The lack of long-range order in a silicate glass means that the bandwidth for pump absorption and gain can be up to 50 THz, which relaxes the wavelength tolerance for excitation and creates opportunities for broad tuning and ultrashort pulse generation. The small dimensions of the modes propagating in the core of the fiber provide low-threshold and high-gain characteristics with near-maximum efficiency.

2.2 FIBER LASERS OPERATING AT 1 μM

The highest values of output power and efficiency have been achieved at around 1 μm using Yb^{3+} cations doped into the core of silicate glass fiber and commercial systems [5] capable of supplying output powers of up to 50 kW are now used for a variety of applications, including cutting and welding in the automotive industry. There are a number of reasons for this success. First, the quantum efficiency of the laser transition is close to 100% while the quantum defect, that is, the difference between the pump and laser photon energies, is typically less than 10%. Second, the use of silicate glass optical fiber provides the system with a significant degree of robustness and power-handling capability. Yb^{3+}-doped silicate glass fiber lasers emitting at around 1 μm are therefore incredibly practical devices.

2.3 FIBER LASERS OPERATING BEYOND 1 μM

2.3.1 Pros and Cons

Extending the emission wavelength into the mid-infrared is necessary for a large number of existing and future applications, including IRCM and spectroscopy [6]. The task of engineering a fiber laser becomes easier at longer wavelengths, owing to a number of optical scaling factors. The mode area of the lowest-order mode scales as λ^2, where λ is the laser wavelength; for example, the mode at 2 μm has four times the area of the same mode at 1 μm. This has a profoundly beneficial effect on the power scaling potential of fiber lasers. Because losses due to non-linearity scale with light intensity, Brillouin and Raman scattering are lower at longer wavelengths and so optical damage thresholds are increased. The size of the mode can also be increased by using smaller refractive index contrasts [7] or holey fiber [8]. Translating these methods to longer wavelengths provides further potential for power scaling.

Moving further into the infrared and away from the bandgap of a given glass means that more photons are required to bridge the bandgap, which raises the ablative threshold and thus lowers the loss from two-photon absorption. Stokes emission generated from Raman scattering is also weaker at longer wavelengths [9]. The formation of color centers resulting from localized charge regions is a problem for some Yb^{3+}-doped

silicate glasses because the resulting absorption features located in the visible region have long absorption tails that overlap with the pump and emission wavelengths of Yb^{3+} [10],[11]. The absorption strength diminishes and therefore potentially becomes less problematic at longer wavelengths; for example, with silicate glass fiber lasers that operate at 2 µm.

Unfortunately, extending the emission wavelength of fiber lasers beyond the natural loss-minimum of silicates at 1.5 µm remains a significant challenge. The physical properties of the glass comprising some fibers, such as high background absorption, poor thermal conductivity and low glass transition temperature, negatively impact the output performance beyond this loss minimum. Infrared transmission in the glass is controlled by the phonon density of states, which means that the longest emitting wavelength from a fiber laser is always shorter than its maximum transmissible wavelength because the phonon density of states determines the radiative efficiencies of the fluorescence transitions of the rare-earth cations. Significant research has been directed towards the development of glasses that have the combined characteristics of low maximum phonon energy and fiber 'drawability' while maintaining amorphousness and low loss. Only a small number of glasses currently have these characteristics.

2.3.2 Laser Transitions of the Rare-Earth Cations

The lasing wavelength of fiber lasers is determined by the fluorescence transitions of the rare-earth cation doped into the core of the fiber. Figure 2-1 shows the laser transitions responsible for infrared emission from several rare-earth cation-doped fiber lasers. With a few exceptions, rare-earth cations are consistently in the trivalent oxidation state, and the associated electronic transitions of the cations are the foundation of infrared fiber lasers.

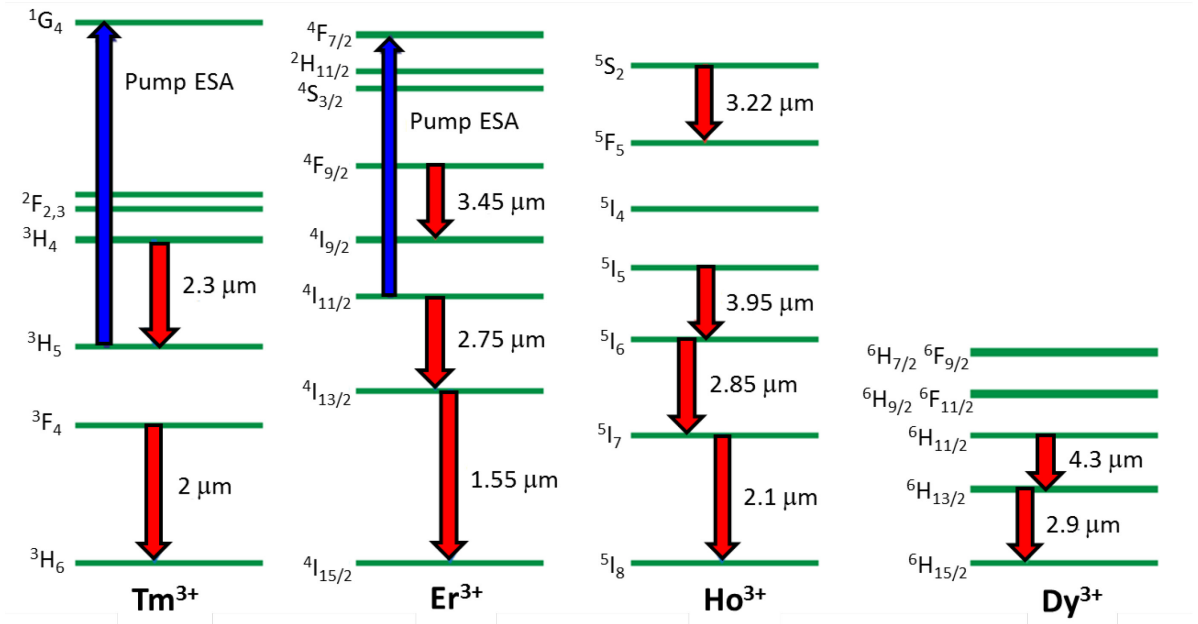

Figure 2-1: Laser Transitions of Rare-Earth Cations for Emission Wavelengths Longer than 1.5 µm.

Phonon broadening acts similarly on all of the rare-earth cations and is therefore homogeneous, but the perturbations to the energy levels of the cations by the surrounding electric fields from nearby glass atoms vary from one cation site to another, which makes them inhomogeneous and temperature-independent. In covalently bonded glasses such as silica, the rare-earth cations form inter-network regions [12] (percolation

channels) comprised of rare-earth cations that bond ionically to non-bridging oxygen atoms that interface with the main covalently bonded network regions. Because their large cationic field strength (defined as Z/r^2, where Z is the atomic number and r is the radius of the ion) requires a high coordination number, rare-earth cations tend to cluster in the inter-network regions to share non-bridging oxygen atoms. The nephelauxetic causes the absorption and emission peaks of rare-earth cation transitions to red-shift to longer wavelengths with increasing covalency of the bonding between the network formers [13].

The relevant fluorescence spectra of the infrared transitions from fiber lasers are shown in Figure 2-2 [14]. The quasi-three-level transitions of the large-Z rare-earth cations Tm^{3+}, Ho^{3+} and Er^{3+}, which fluoresce in the range of 1.5 – 2.2 µm, are responsible for the highest powers available from fiber lasers emitting in the $\lambda > 1.5$ µm region of the near-infrared. The output power performance of such devices relates to strong absorption by cations, which overlaps with the emission from commercial off-the-shelf high-power diode lasers and the excellent physical properties of the silicate glasses used to create the fiber. Extending the laser wavelength further into the infrared has necessitated the use of fluoride glass fiber, owing to its low phonon energy. For the fluorides, the fluorescence spectra tend to cluster in a region that spans approximately 0.6 µm.

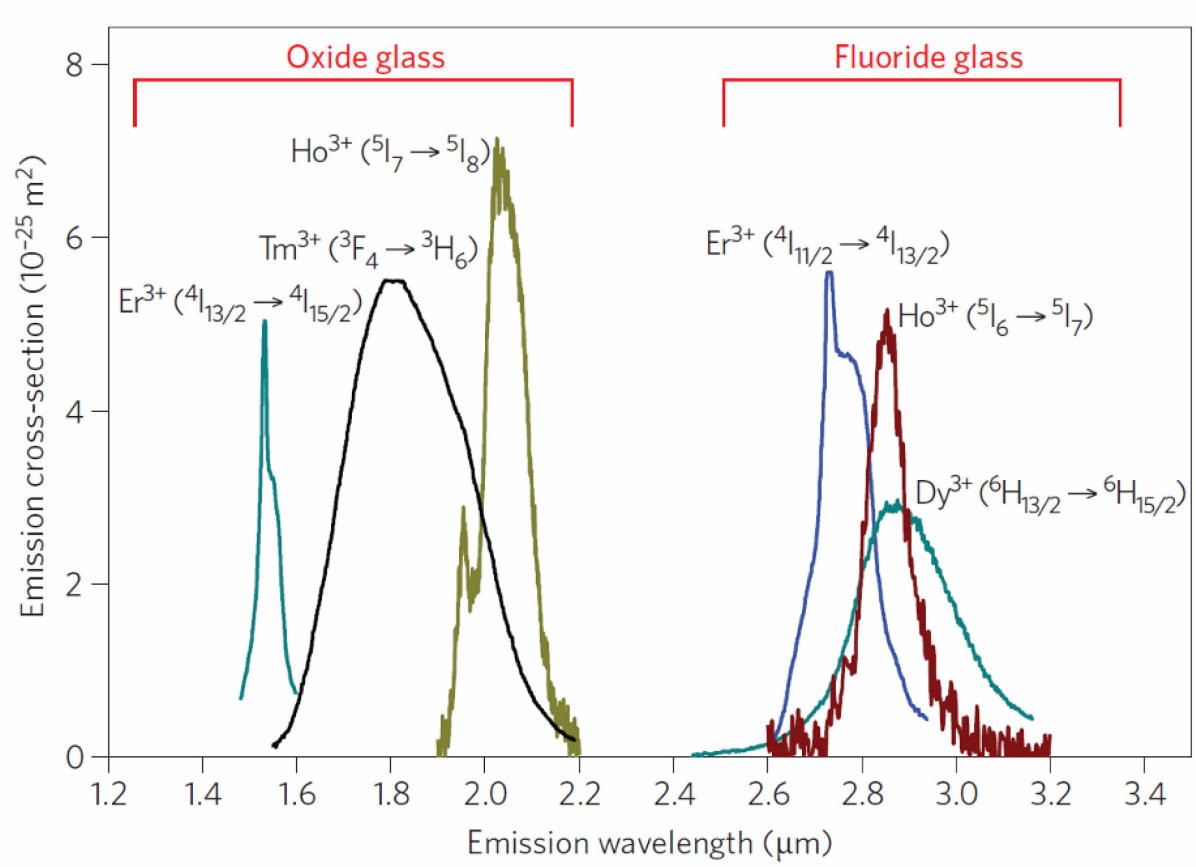

Figure 2-2: Fluorescence Spectra of the Rare-Earth Cation Laser Transitions Used in Fiber Lasers Emitting at Wavelengths Greater Than 1.5 µm. (Oxide glass is a silicate and fluoride glass is ZBLAN) (after S. Jackson [14]).

2.3.3 Host Materials

The typically long (> 1 m) optical path length of a fiber laser means that glasses must exhibit low impurity, low scattering loss, a large Hruby parameter [49] (glass stability) and a low maximum phonon energy.

For emission in the 1 – 2.2 μm region, the low loss and physical strength of silicate glasses has made them remarkably useful hosts for rare-earth cations emitting in this region. Fluoride glasses have high efficiency and moderate output power in the 2.3 – 3.5 μm region. Beyond 3.5 μm, however, only a small number of glasses have the suitably low phonon energy that provides the necessarily high transmission of the fiber and sufficient radiative efficiency for the rare-earth cation transitions.

2.3.3.1 Silicates

Silicate glasses remain the most successful fiber host materials. A high laser damage threshold [50] of approximately 500 MW/cm^2 for doped silicate glass ensures robust high-power operation, and fabrication using modified chemical vapor deposition ensures excellent glass purity. Silicate glasses have high melting points, relatively low thermal expansion coefficients, large tensile strengths, low refractive indices and low non-linearities. All glasses have a low second-order non-linearity, although loss to third-order non-linear processes such as stimulated Raman scattering can be substantial because of the long fiber length and large light intensity in the active core. Silicate glasses consist of strongly covalently bonded atoms that form a disordered matrix with a range of bond lengths and angles. Silica can sustain maximum phonon energies [51] of up to 1,100 cm^{-1}, which sets an upper limit on the emission wavelength. The giant covalent structure of silicate glasses leads to excellent mechanical properties. The maximum 'lattice' vibration or 'phonon' energy is the most active in multi-phonon decay, and the fluctuating Stark field surrounding the rare-earth cation arising from the vibration of the surrounding anions and cations induces non-radiative decay. Because the bandgap of silica is 9 eV, loss to two-photon absorption is small at infrared wavelengths and Rayleigh scattering loss [52] from the frozen-in density fluctuations in the glass can be as low as 0.15 dB km^{-1}. When network formers such as Al_2O_3 and P_2O_5 are added to silica [53], they create the solvation shells necessary for improved rare-earth cation solubility to counteract clustering. Unfortunately, Rayleigh scattering loss increases as a result of the extra refractive index inhomogeneities introduced by the addition of these dopants. Emission at 2 μm from Tm^{3+} and Ho^{3+} cations doped into silicate glasses is highly developed, and a number of commercial systems are now available. The longest laser wavelength [54] from a silicate glass fiber laser is currently 2.188 μm; lasing at longer wavelengths is not expected to be possible in the majority of silicate glasses due to significant phonon quenching.

2.3.3.2 Fluorides

One of the most successful compositions among fluoride glasses is ZBLAN [55], which is comprised of 53 mol % ZrF_4, 20 mol % BaF_2, 4 mol % LaF_3, 3 mol % AlF_3 and 20 mol % NaF. The ZBLAN composition can be varied to introduce certain characteristics: for example, adding PbF_2, ZnF_2 or CaF_2 modifies the viscosity and refractive index; substituting a proportion of ZrF_4 for ThF_4 creates better stability against crystallization; and substituting ZrF_4 with HfF_4 lowers the refractive index. Fluoride fiber preforms can be created by a number of casting processes [56],[57], although crystallization during cooling and reheating often creates scattering centers that limit the dimensions of the preform and the maximum length of useful fiber. Geometrical defects such as inclusions and bubbles formed during fabrication also cause scattering. Reducing the casting pressure of ZBLAN eliminates bubble formation to allow, when combined with anhydrous fluoride precursors, a minimum fiber loss of 0.65 dB km^{-1} at 2.59 μm and < 20 dB km^{-1} at 2.9 μm, which is where the O–H impurity stretching vibration in ZBLAN is located [58].

The maximum phonon energy of ZBLAN [59] is approximately 565 cm^{-1}, which allows fluorescence at room temperature to occur from rare-earth cation transitions comprised of energy gaps larger than 2,825 cm^{-1} (that is, $\lambda <$ 3.5 μm). ZBLAN has low optical dispersion, a low refractive index of 1.49 and a broad transmission window (defined here to have an attenuation of less than 200 dB km^{-1}) in the range of 0.2 – 4.5 μm [60]. Compared with silicate glasses, the lower maximum phonon energy of ZBLAN (and thus the extended infrared transmission) relates to the weaker bond strength and larger reduced mass of the atoms comprising the glass. The fluoride anion is singly charged, which, when combined with weaker bonding, means a higher chemical reactivity compared with silicates, although rare-earth cations substitute the

La3+ cations of the glass to provide comparatively higher doping levels without clustering. The optical damage threshold [61] of ZBLAN for 10 ms pulses at 2.8 μm is approximately 25 MW cm^{-2}, which restricts the achievable peak power levels compared with silicates. However, because the Raman gain coefficient is comparatively smaller [62], significant loss to Raman scattering may never be a concern in future high-power infrared fiber lasers using this glass. The higher thermal loading resulting from the moderate efficiency of 3-μm-class fiber lasers (for which ZBLAN fibers are used), combined with the comparatively poorer physical properties of fluoride glasses, has made power-scaling a significant challenge. The maximum output power from ZBLAN-based fiber lasers is currently 24 W at 2.7 μm [21] and 20 W at 1.94 μm [16].

2.3.3.3 Alternatives

There is ongoing development in the fabrication and testing of glasses for achieving longer emission wavelengths. Germanate glasses [63] have robust mechanical qualities, maximum phonon energies [64] of 900 cm^{-1} and large rare-earth cation solubilities, which allow cluster-reduced Tm^{3+} concentrations in fibers for high-efficiency 1.9 μm emission [65] and short-length devices providing narrow-linewidth output [66]. However, the practicality of germanate glasses for emission beyond 2 μm is reliant on effective removal of OH^- impurity from the glass, which is difficult to achieve. Tellurite glass fiber [67] is a promising alternative, but, like most oxide glasses fabricated from solid-state precursor materials, it contains relatively high concentration of OH^-. Energy transfer from excited Er^{3+} cations to OH^- impurities, combined with the low radiative efficiency of the upper laser level, is sufficient to suppress 3 μm lasing in state-of-the-art Er^{3+}-doped tellurite glass [68]. Chalcogenides [69], glasses based on chalcogens S, Se or Te, are a widely investigated group whose high refractive indices result in large absorption and emission cross-sections. Maximum phonon energies depend on the exact composition of the glass, with values of 350 – 425 cm^{-1} for sulphide glasses [70], 250 – 300 cm^{-1} for selenide glasses [71] and 150 – 200 cm^{-1} for telluride glasses [72]. Optical transmission reaches well into the mid-infrared, up to 15 μm in the case of telluride glass [73], and fluorescence has been measured in sulphide, selenide and telluride glasses from a number of rare-earth cation transitions with emission wavelengths as long as 8 μm [74]. The only demonstration of a rare-earth-doped chalcogenide fiber laser was based on Nd^{3+} emitting at 1.08 μm [75], in which the addition of La_2O_3 to gallium chalcogen glass in order to avoid crystallization during fiber drawing [76] most likely created energetic phonons that suppressed longer-wavelength emission [77]. No laser emission beyond 1 μm has yet been achieved using a rare-earth cation-doped chalcogenide glass fiber, presumably due to the crystallization tendency upon rare-earth doping. Ge–Sb and Ge–As chalcogen glasses, for example, are strongly covalently bonded, which makes the incorporation of rare-earth cations a significant challenge. Alternative co-dopants for chalcogen-based glasses are being developed to improve rare-earth cation solubility and eliminate crystallization [78].

2.3.4 State-of-the-Art CW Fiber Lasers

Despite the variety of rare-earth cation transitions and host materials that have been tested for fiber laser emission, the maximum CW output power produced from demonstrated fiber lasers has a clear exponential decrease when plotted as a function of emission wavelength (Figure 2-3). Table 2-1 lists the maximum output power from reported fiber lasers [14]-[27].

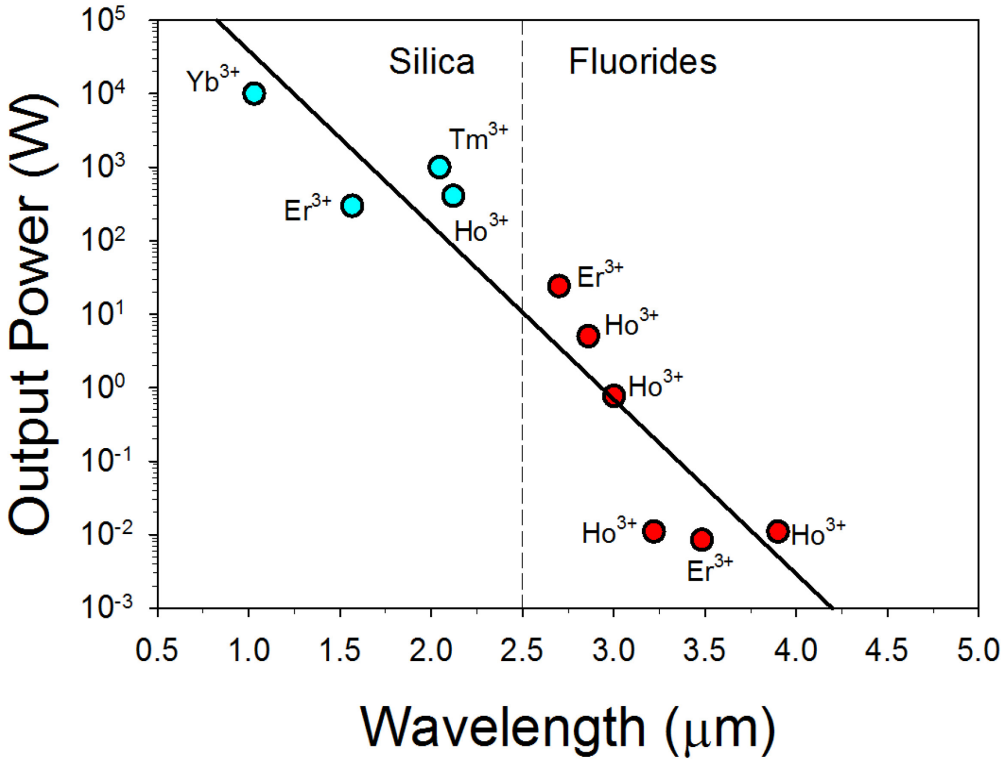

Figure 2-3: Output Power at Different Laser Wavelengths Using Rare-Earth-Doped Silica (Blue Circles) and ZBLAN (Red Circles) Fibers, Respectively. The dashed line is a guide to the eye.

Table 2-1: Characteristics of Infrared Fiber Lasers with Emission Wavelengths ≥ 1.5 μm.

Dopant(s)	Host Glass	Pump λ (μm)	Laser λ (μm)	Transition	Output Power (W)	% Slope Efficiency	Reference
Er^{3+}, Yb^{3+}	Silicate	0.975	1.5	$^4I_{13/2} \rightarrow {}^4I_{15/2}$	297	19	15
Tm^{3+}, Ho^{3+}	ZBLAN	0.792	1.94	$^3F_4 \rightarrow {}^3H_6$	20	49	16
Tm^{3+}	Silicate	0.793	2.05	$^3F_4 \rightarrow {}^3H_6$	1,050	53	17
STm^{3+}, Ho^{3+}	Silicate	0.793	2.1	$^5I_7 \rightarrow {}^5I_8$	83	42	18
Ho^{3+}	Silicate	1.950	2.12	$^5I_7 \rightarrow {}^5I_8$	407	~ 30	19
Tm^{3+}	ZBLAN	1.064	2.31	$^3H_4 \rightarrow {}^3H_5$	0.15	8	20
Er^{3+}	ZBLAN	0.975	2.8	$^4I_{11/2} \rightarrow {}^4I_{13/2}$	24	13	21
Ho^{3+}, Pr^{3+}	ZBLAN	1.1	2.86	$^5I_6 \rightarrow {}^5I_7$	2.5	29	22
Dy^{3+}	ZBLAN	1.1	2.9	$^6H_{13/2} \rightarrow {}^6H_{15/2}$	0.275	4.5	23
Ho^{3+}	ZBLAN	1.15	3.002	$^5I_6 \rightarrow {}^5I_7$	0.77	12.4	24
Ho^{3+}	ZBLAN	0.532	3.22	$^5S_2 \rightarrow {}^5F_5$	0.011	2.8	25
Er^{3+}	ZBLAN	0.653	3.45	$^4F_{9/2} \rightarrow {}^4I_{9/2}$	0.008	3	26
Ho^{3+}	ZBLAN	0.89	3.95	$^5I_5 \rightarrow {}^5I_6$	0.011	3.7	27

The primary cause of this power drop is the increase in quantum defect at longer wavelengths. Efficient high-power diode lasers, the traditional pump sources for silicate glass fiber lasers, typically emit light in the near-infrared region close to 1 μm. Although it would be ideal to use these efficient pump sources for all fiber lasers, the larger quantum defect at longer wavelengths creates heat that becomes an ever-increasing fraction of the absorbed pump energy. The small active-core volume of an optical fiber relative to the total fiber volume of a double-clad fiber results in a small temperature gradient [28]. The temperature within the fiber is governed strongly by the degree of cooling at the air–fiber boundary, which is improved by a large surface area (that is, a larger pump-core diameter). The excellent cooling properties of optical fibers therefore help to alleviate the problem of the growing quantum defect. Developing efficient longer-wavelength pump sources and selecting more appropriate laser transitions can effectively reduce the quantum defect and improve output performance. Laser transition cascading [29], in which multiple transitions lase simultaneously after a single pump photon excitation, offers the opportunity for better photon-to-photon conversion efficiencies and is particularly suited to longer-wavelength transitions for reducing heat loads and improving power-scaling opportunities.

Fiber lasers employing the Tm^{3+} cation [30]-[33] with emission at around 2 μm are the most powerful, efficient and developed of these fiber lasers. These devices are excited with established diode lasers [34] emitting at 0.79 μm, and their output can be tuned from at least 1.86 μm to around 2.09 μm. With the implementation of Tm^{3+} concentrations exceeding 2.5 wt %, combined with cluster-reducing co-dopants that mitigate gain-lowering energy transfer up-conversion processes, cross-relaxation between neighboring Tm^{3+} cations can nearly double the slope efficiency [35]. Cross-relaxation ('two-for-one' excitation) is resonant in silicate glass, thus providing one of the most efficient ways to generate 2 μm light from commercial diode laser pump sources.

The $^5I_7 \rightarrow {}^5I_8$ transition of Ho^{3+} has a peak emission wavelength of 2.1 μm, which overlaps with an important atmospheric transmission window. This transition is also acceptable for resonant pumping with Tm^{3+}-doped silicate glass fiber lasers [36], which introduces a small quantum defect of < 7%. Ho^{3+} fiber lasers were initially co-doped with Tm^{3+} sensitizer cations to exploit the diode-pumpable absorption of Tm^{3+} [37], although loss of excitation to energy-transfer up-conversion and reversible energy-transfer between the first excited states of Tm^{3+} and Ho^{3+} limited the power, extractable energy and efficiency of this technique. Doping silicate glass with only Ho^{3+} cations supports a large short-pulse extraction efficiency and has the potential to reduce the sensitivity of gain to temperature. The demonstration of direct diode pumping with Ho^{3+} [38] opens up additional power-scaling opportunities.

The fluoride glass fiber has a lower phonon energy than silica and so enables emission at longer wavelengths. Er^{3+}-doped fluoride fiber laser can be tuned across the range of 2.71 – 2.88 μm [39]. Engineering the stability and efficiency of the output from a fluoride fiber laser, a necessary requirement for commercial exploitation, is made possible by writing Bragg gratings [40] and splicing glass caps [41] to the ends of the fiber. The overlap of the upper laser level absorption with highly developed diode lasers emitting at 0.98 μm, combined with effective cooling of Er^{3+}-doped double-clad fluoride fiber, has resulted in output powers of up to 24 W at wavelengths of around 2.8 μm [21]. When high-quality Er^{3+}-doped double-clad fluoride fiber with a background loss of < 100 dB km^{-1} is combined with a high Er^{3+} concentration and an optimally engineered fiber laser resonator, energy transfer up-conversion (Figure 2-1) effectively de-populates the lower laser level and 'recycles' the excitation to produce slope efficiencies of 35.6% [42]. Engineering the effective de-population of the lower laser level is required because the upper laser level has a shorter luminescence lifetime than the lower laser level [43]. Cascade lasing [44]-[46] the transitions of 2.8 μm and 1.5 μm offers a solution to the problem of managing the heat generated due to the comparatively low optical conversion efficiencies of single-transition Er^{3+} systems. Pump-excited state absorption from the upper laser level (Figure 2-1) creates a roll-off in the calculated [47] and measured [42] output power and thus presents a significant problem for power-scaling the output from Er^{3+}-doped fluoride fiber lasers pumped to the upper laser level.

Ho^{3+}-doped fluoride fiber [48], which has a wide emission range of 2.8 – 3.02 μm for the $^5I_6 \rightarrow {}^5I_7$ transition, has the advantage of reduced pump-excited state absorption and a higher Stokes limit when the upper laser level is diode-pumped at 1.15 μm. However, the present maximum output power of this system is an order of magnitude lower than that of an Er^{3+}-doped fluoride fiber laser because the low demand for diode lasers operating at 1.15 μm means that beam-combining and brightness-conserving power-scaling technologies have not been expanded to these pump sources. An opportunity to increase the power and wavelength of 3 μm-class fiber lasers has recently been demonstrated [24] using cascade lasing of both the 2.9 μm and 2.1 μm transitions of Ho^{3+}. Laser emission at 3.9 μm was demonstrated under cryogenic conditions from a Ho^{3+}-doped fluoride fiber laser [27]. This result remains the longest wavelength emitted from a fiber laser.

2.3.5 Pulsed Fiber Lasers

Fiber lasers cover a number of pulse width regimes, but the small dimensions of the active core invoke surface damage-threshold limitations. So far, silicate glass fiber has provided the highest peak power, largest pulse energy and widest variety of pulse widths from fiber lasers operating at 2 μm, primarily because of its large damage threshold and the overall maturity of 2 μm fiber lasers. Fiber lasers using Tm^{3+} and Ho^{3+} cations have been mode-locked for ultrashort pulse generation using different approaches [79]-[81]. Because the saturation energy is proportional to the core area, the increased mode size relevant to 2 μm fiber lasers compared with 1 μm fiber lasers benefits energy extraction. Today's shortest pulsewidth at 2 μm from a fiber is 108 fs [82]. Mode-locked fiber lasers operating at 2 μm typically create solitons because silicate fibers are anomalously dispersive at these wavelengths. Larger pulse energies can be achieved by engineering the overall dispersion [83]. Chirped pulse amplification of ultrashort pulses using Tm^{3+}-doped silicate glass fiber leads to near-megawatt peak powers after recompression [84]. For applications that require longer pulses, active Q-switching [85] is capable of generating pulses measuring just a few tens of nanoseconds in duration [86]. Gain-switching [87] using pulsed diode lasers emitting at 1.5 μm for direct excitation of the upper laser level can generate pulses of less than 2 ns in duration [88].

Pulsed fiber laser sources emitting at longer wavelengths make use of fluoride glass, which has a lower surface optical damage threshold but potentially larger mode area than silicate glass. Steady progress has been made with recent demonstrations of Q-switched [89] (90 ns pulsewidth and 0.9 kW peak power) and gain-switched [90] (307 ns pulsewidth and 68 W peak power) operation of Er^{3+}-doped ZBLAN fiber lasers. Recent demonstrations of Q-switched single-transition [91] and cascaded [92] Ho^{3+}-doped fluoride fiber lasers provide 70 ns pulses, emission at 2.87 μm and two-wavelength output. Given that additional mode-size enhancement YF can be achieved by capping the ends of the fiber [41], and that 5 kW peak power has already been demonstrated using fluoride fiber [93], the output performance of pulsed fluoride fiber lasers is likely to see further improvement. The ability to generate clean pulses with smooth transverse mode profiles that prevent localized large intensities will be particularly relevant to future high-peak-power fluoride fiber lasers.

2.4 REFERENCES

[1] Snitzer, E. *et al.* Double clad, offset core Nd fiber laser in *Optical Fiber Sensors*, Vol. 2, Paper PD5 of OSA Technical Digest Series (OSA, 1988).

[2] Zenteno, L. High-power double clad fiber lasers. *J. Lightwave Technol*. 11, 1435-1446 (1993).

[3] Jeong, Y., Sahu, J.K., Payne, D.N. and Nilsson, J. Ytterbium-doped large-core fiber laser with 1.36 kW continuous-wave output power. *Opt. Express* 12, 6088-6092 (2004).

[4] Poole, S.B., Payne, D.N. and Fermann, M.E. Fabrication of low-loss optical fibers containing rare earth ions. *Electron. Lett*. 21, 737-738 (1985).

[5] http://www.ipgphotonics.com/.

[6] Sanghera, J., Shaw, L.B. and Aggarwal, I.D. Chalcogenide glass-fiber-based mid-IR sources and applications, *IEEE J. of Selected Topics in Quantum Electronics* 15, No. 1, 114-119 (2009).

[7] Offerhaus, H.L. *et al.* High-energy single-transverse-mode *Q*-switched fiber laser based on a multimode large-mode-area erbium-doped fiber. *Opt. Lett*. 23, 1683-1685 (1998).

[8] Knight, J.C. *et al.* Large mode area photonic crystal fiber. *Electron. Lett*. 34, 1347-1348 (1998).

[9] Rottwitt, K. *et al.* Scaling of the Raman gain coefficient: applications to germanosilicate fibers. *J. Lightwave Technol*. 21, 1652-1662 (2003).

[10] Koponen, J.J., Söderlund, M.J., Hoffman, H.J. and Tammela, S.K.T. Measuring photodarkening from single-mode ytterbium doped silica fibers. *Opt. Express* 14, 11539-11544 (2006).

[11] Jetschke, S., Unger, S., Röpke, U. and Kirchhof, J. Photodarkening in Yb doped fibers: experimental evidence of equilibrium states depending on the pump power. *Opt. Express* 15, 14838-14843 (2007).

[12] Greaves, G.N. EXAFS and the structure of glass. *J. Non-cryst. Solids* 71, 203-217 (1985).

[13] Caro, P., Beaury, O. and Antic, E. Nephelauxetic effect for 4fN configurations in solid-state. *J. Phys.-Paris* 37, 671-676 (1976).

[14] Jackson, S. Towards high-power mid-infrared emission from a fiber laser. *Nature Photonics* 6, 423-431 (2012).

[15] Jeong, Y. *et al.* Erbium:ytterbium codoped large-core fiber laser with 297 W continuous-wave output power. *IEEE J. Sel. Top. Quant. Electron.* 13, 573-579 (2007).

[16] Eichhorn, M. and Jackson, S.D. Comparative study of continuous wave Tm^{3+}-doped silica and fluoride fiber lasers. *Appl. Phys. B* 90, 35-41 (2008).

[17] Ehrenreich, T. *et al.* 1 kW, all-glass Tm:fiber laser. SPIE Photonics West 2010: LASE, Fibre Lasers VII: Technology, Systems and Applications, Conference 7850 (2010).

[18] Jackson, S.D. *et al.* High-power 83 W holmium-doped silica fiber laser operating with high beam quality. *Opt. Lett.* 32, 241-243 (2007).

[19] Hemming, A. *et al.* A monolithic cladding pumped holmium-doped fiber laser. CLEO: 2013 Technical Digest, Paper CW1M.1, OSA (2013).

[20] El-Agmy, R.M. and Al-Hosiny, N.M. 2.31 μm laser under up-conversion pumping at 1.064 μm in Tm^{3+}:ZBLAN fibre lasers. *Electron. Lett.* 46, 936-937 (2010).

[21] Tokita, S. *et al.* Liquid-cooled 24 W mid-infrared Er:ZBLAN fiber laser. *Opt. Lett.* 34, 3062-3064 (2009).

[22] Jackson, S.D. Single-transverse-mode 2.5-W holmium-doped fluoride fiber laser operating at 2.86 μm. *Opt. Lett.* 29, 334-336 (2004).

[23] Jackson, S.D. Continuous wave 2.9 μm dysprosium-doped fluoride fiber laser. *Appl. Phys. Lett.* 83, 1316-1318 (2003).

[24] Li, J., Hudson, D.D. and Jackson S.D. High-power diode-pumped fiber laser operating at 3 μm. *Opt. Lett.* 36, 3642-3644 (2011).

[25] Carbonnier, C., Többen, H. and Unrau, U.B. Room temperature CW fibre laser at 3.22 μm. *Electron. Lett.* 34, 893-894 (1998).

[26] Tobben, H. Room temperature CW fibre laser at 3.5 μm in Er3+-doped ZBLAN glass. *Electron. Lett.* 28, 1361-1363 (1992).

[27] Schneider, J., Carbonnier, C. and Unrau, U.B. Characterization of a Ho3+-doped fluoride fiber laser with a 3.9 μm emission wavelength. *Appl. Opt.* 36, 8595-8600 (1997).

[28] Brown, D.C. and Hoffman, H.J. Thermal, stress, and thermo-optic effects in high average power double-clad silica fiber lasers. *IEEE J. Quant. Electron*. 37, 207-217 (2001).

[29] Esterowitz, L., Eckardt, R.C. and Allen, R.E. Long-wavelength stimulated-emission via cascade laser action in Ho-YLF. *Appl. Phys. Lett*. 35, 23-239 (1979).

[30] Hanna, D.C., Percival, R.M., Smart, R.G. and Tropper, A.C. Efficient and tunable operation of a Tm-doped fibre laser. *Opt. Commun.* 75, 283-286 (1990).

[31] Jackson, S.D. and King, T.A. High-power diode-cladding-pumped Tm-doped silica fiber laser. *Opt. Lett*. 23, 1462-1464 (1998).

[32] Hayward, R.A. *et al.* Efficient cladding-pumped Tm-doped silica fibre laser with high power single-mode output at 2 μm. *Electron. Lett*. 36, 711-712 (2000).

[33] Moulton, P.F. *et al.* Tm-doped fiber lasers: fundamentals and power scaling. *IEEE J. Sel. Top. Quant. Electron.* 15, 85-92 (2009).

[34] Clarkson, W.A. *et al.* High-power cladding-pumped Tm-doped silica fiber laser with wavelength tuning from 1860 to 2090 nm. *Opt. Lett*. 27, 1989-1991 (2002).

[35] Jackson, S.D. Cross relaxation and energy transfer upconversion processes relevant to the functioning of 2 μm Tm3+-doped silica fibre lasers. *Opt. Commun.* 230, 197-203 (2004).

[36] Jackson, S.D. Midinfrared holmium fiber lasers. *IEEE J. Quant. Electron*. 42, 187-191 (2006).

[37] Oh, K. *et al.* Continuous-wave oscillation of thulium-sensitized holmium-doped silica fiber laser. *Opt. Lett.* 19, 278-280 (1994).

[38] Jackson, S.D., Bugge, F. and Erbert, G. Directly diode-pumped holmium fiber lasers. *Opt. Lett.* 32, 2496-2498 (2007).

[39] Tokita, S. *et al.* Stable 10 W Er:ZBLAN fiber laser operating at 2.71–2.88 μm. *Opt. Lett.* 35, 3943-3945 (2010).

[40] Faucher, D. *et al.* 20 W passively cooled single-mode all-fiber laser at 2.8 μm. *Opt. Lett.* 36, 1104-1106 (2011).

[41] Bernier, M. *et al.* Bragg gratings photoinduced in ZBLAN fibers by femtosecond pulses at 800 nm. *Opt. Lett.* 32, 454-456 (2007).

[42] Faucher, D., Bernier, M., Caron, N. and Vallee, R. Erbium-doped all-fiber laser at 2.94 μm. *Opt. Lett.* 34, 3313-3315 (2009).

[43] Gorjan, M., Marincek, M. and Copic, M. Role of interionic processes in the efficiency and operation of erbium-doped fluoride fiber lasers. *IEEE J. Quant. Electron*. 47, 262-273 (2011).

[44] Schneider, J. Mid-infrared fluoride fiber lasers in multiple cascade operation. *IEEE Photon. Tech. Lett.* 7, 354-356 (1995).

[45] Pollnau, M. *et al.* Three-transition cascade erbium laser at 1.7, 2.7, and 1.6 μm. *Opt. Lett.* 22, 612-614 (1997).

[46] Jackson, S.D. High-power erbium cascade fibre laser. *Electron. Lett*. 45, 830-832 (2009).

[47] Li, J. and Jackson, S.D. Numerical modeling and optimization of diode pumped heavily-erbium-doped fluoride fiber lasers. *IEEE J. Quant. Electron*. 48, 454-464 (2012).

[48] Wetenkamp, L., West, G.F. and Tobben. H. Optical properties of rare earth-doped ZBLAN glasses. *J. Non-cryst. Solids* 140, 35-40 (1992).

[49] Hruby, A. Evaluation of glass-forming tendency by means of DTA. *Czech J. Phys*. B22, 1187-1193 (1972).

[50] Tünnermann, A. *et al.* The renaissance and bright future of fibre lasers. *J. Phys. B* 38, S681-S693 (2005).

[51] Layne, C.B., Lowdermilk, W.H. and Weber, M.J. Multiphonon relaxation of rare-earth ions in oxide glasses. *Phys. Rev. B* 16, 10-20 (1977).

[52] Saito, K. *et al.* Limit of the Rayleigh scattering loss in silica fiber. *Appl. Phys. Lett*. 83, 5175-5177 (2003).

[53] Arai, K. *et al.* Aluminium or phosphorous co-doping effects on the fluorescence properties of neodymium-doped silica glass. *J. Appl. Phys*. 59, 3430-3436 (1986).

[54] Sacks, Z.S., Schiffer, Z. and David, D. Long wavelength operation of double-clad Tm:silica fiber lasers. *Proc. SPIE* 6453, 645320 (2007).

[55] Ohsawa, K., Shibata, T., Nakamura, K. and Yoshida, S. Fluorozirconate glasses for infrared transmitting optical fibers. Paper 1.1, Technical Digest, 7th European Conference on Optical Communication (1981).

[56] Mitachi, S., Miyashita, T. and Kanamori, T. Fluoride-glass cladded optical fibers for mid-infra-red ray transmission. *Electron. Lett*. 17, 591-592 (1981).

[57] Tran, D.C., Fisher, C.F. and Sigel, G.H. Jr. Fluoride glass performs prepared by a rotation casting process. *Electron. Lett*. 18, 657-658 (1982).

[58] Carter, S.F. *et al.* Low loss fluoride fibre by reduced pressure casting. *Electron. Lett*. 26, 2115-2117 (1990).

[59] Almeida, R.M. and Mackenzie, J.D. Vibrational spectra and structure of fluorozirconate glasses. *J. Chem. Phys*. 74, 5954-5961 (1981).

[60] Day, C.R. *et al.* Fluoride fibres for optical transmission. *Opt. Quant. Electron*. 22, 259-277 (1990).

[61] Zhu, X. and Jain, R. 10-W-level diode-pumped compact 2.78 μm ZBLAN fiber laser. *Opt. Lett*. 32, 26-28 (2007).

[62] Fortin, V., Bernier, M., Carrier, J. and Vallée, R. Fluoride glass Raman fiber laser at 2185 nm. *Opt. Lett*. 36, 4152-4154 (2011).

[63] Wang, J., *et al.* Fabrication and optical-properties of lead-germanate glasses and a new class of optical fiber lasers doped with Tm3+, *J. Appl. Phys.* 73, 8066-8075 (1993).

[64] Lincoln, J.R. *et al.* New class of fibre laser based on lead-germanate glass. *Electron. Lett.* 28, 1021-1022 (1992).

[65] Wu, J., Yao, Z., Zong, J. and Jiang, S. Highly efficient high-power thulium-doped germanate glass fiber laser. *Opt. Lett*. 32, 638-640 (2007).

[66] Geng, J., Wu, J., Jiang, S. and Yu, J. Efficient operation of diode-pumped single-frequency thulium-doped fiber lasers near 2 μm. *Opt. Lett*. 32, 355-357 (2007).

[67] Mori, A., Ohishi, Y. and Sudo, S. Erbium-doped tellurite glass fibre laser and amplifier. *Electron. Lett*. 33, 863-864 (1997).

[68] Gomes, L. *et al.* Energy level decay and excited state absorption processes in erbium-doped tellurite glass. *J. Appl. Phys*. 110, 083111 (2011).

[69] Eggleton, B.J., Luther-Davies, B. and Richardson, K. Chalcogenide photonics. *Nature Photon.* 5, 141-148 (2011).

[70] Julien, C. *et al.* Raman and infrared spectroscopic studies of Ge–Ga–Ag sulfide glasses. *Mat. Sci. Eng*. B22, 191-200 (1994).

[71] Weszka, J. *et al.* Raman scattering in In2Se3 and InSe2 amorphous films. *J. Non-cryst. Solids* 265, 98-104 (2000).

[72] Uemura, O., Hayasaka, N., Tokairin, S. and Usuki, T. Local atomic arrangement in Ge–Te and Ge–S–Te glasses. *J. Non-cryst. Solids* 205, 189-193 (1996).

[73] Maurugeon, S. *et al.* Telluride glass step index fiber for the far infrared. *J. Lightwave Technol*. 28, 3358-3363 (2010).

[74] Shaw, L.B., Cole, B., Thielen, P., Sanghera, J. and Aggarwal, I.D. Mid-wave IR and long-wave IR laser potential of rare earth doped chalcogenide glass fiber. *IEEE J. Quantum Electronics* 37 1127-1137 (2001).

[75] Schweizer, T. *et al.* Rare-earth doped chalcogenide glass laser. *Electron. Lett*. 32, 666-667 (1996).

[76] Brady, D.J. and Schweizer, T. Minimum loss predictions and measurements in gallium lanthanum sulfide based glasses and fibers. *J. Non-cryst. Solids* 242, 92-98 (1998).

[77] Seddon, A.B. *et al.* Progress in rare-earth-doped mid-infrared fiber lasers. *Opt. Express* 18, 26704-26719 (2010).

[78] Aggarwal, I.D. and Sanghera, J.S. Development and applications of chalcogenide glass optical fibers at NRL. *J. Optoelectron. Adv. Mat*. 4, 665-678 (2002).

[79] Nelson, L.E., Ippen, E.P. and Haus, H.A. Broadly tunable sub-500 fs pulses from an additive-pulse mode-locked thulium-doped fiber ring laser. *Appl. Phys. Lett*. 67, 19-21 (1995).

[80] Sharp, R.C., Spock, D.E., Pan, N. and Elliot, J. 190-fs passively mode-locked thulium fiber laser with a low threshold. *Opt. Lett*. 21, 881-883 (1996).

[81] Solodyankn, M.A. *et al.* Mode-locked 1.93 μm thulium laser with a carbon nanotube absorber. *Opt. Lett*. 33, 1336-1338 (2008).

[82] Imeshev, I. and Fermann, M.E. 230-kW peak power femtosecond pulses from a high power tunable source based on amplification in Tm-doped fiber. *Opt. Express* 13, 7424-7431 (2005).

[83] Engelbrecht, M., Haxsen, F., Ruehl, A., Wandt, D. and Kracht, D. Ultrafast thulium-doped fiber-oscillator with pulse energy of 4.3 nJ. *Opt. Lett*. 33, 690-692 (2008).

[84] Haxsen, F. *et al.* Pulse energy of 151-nJ from ultrafast thulium-doped chirped-pulse fiber amplifier. *Opt. Lett*. 35, 2991-2993 (2010).

[85] El-Sherif, A.F. and King, T.A. High-peak-power operation of a *Q*-switched Tm^{3+}-doped silica fiber laser operating near 2 μm. *Opt. Lett*. 28, 22-24 (2003).

[86] Eichhorn, M. and Jackson, S.D. High-pulse-energy actively *Q*-switched Tm^{3+}-doped silica 2 μm fiber laser pumped at 792 nm. *Opt. Lett*. 32, 2780-2782 (2007).

[87] Jiang, M. and Tayebati, P. Stable 10 ns, kilowatt peak-power pulse generation from a gain-switched Tm-doped fiber laser. *Opt. Lett*. 32, 1797-1799 (2007).

[88] Ding, J.W. *et al.* A monolithic thulium doped single mode fiber laser with 1.5 ns pulsewidth and 8 kW peak power. *Proc. SPIE* 7914, 79140X (2011).

[89] Tokita, S. *et al.* 12 W *Q*-switched Er:ZBLAN fiber laser at 2.8 μm. *Opt. Lett*. 36, 2812-2814 (2011).

[90] Gorjan, M., Petkovšek, R., Marinček, M. and Čopič, M. High-power pulsed diode-pumped Er:ZBLAN fiber laser. *Opt. Lett*. 36, 1923-1925 (2011).

[91] Hu, T., Hudson, D.D. and Jackson, S.D. Actively *Q*-switched 2.9 μm $Ho^{3+}Pr^{3}$+-doped fluoride fiber laser. *Opt. Lett*. 37, 2145-2147 (2012).

[92] Li, J., Hu, T. and Jackson, S.D. *Q*-switched fiber cascade laser. *Opt. Lett*. 37, 2208-2210 (2012).

[93] Eichhorn, M. High-peak-power Tm-doped double-clad fluoride fiber amplifier. *Opt. Lett*. 30, 3329-3331 (2005).

Chapter 3 – RARE-EARTH-DOPED FIBERS: EXPERIMENT AND MODEL

3.1 INTRODUCTION

Lasers delivering high pulse energies or output power directly from an electronic transition are rare in the mid-infrared region of the spectrum. For that reason we are investigating new materials that could be used as laser media and more particularly as fiber lasers. The choice of the fiber material involves multiple considerations: the maximum phonon energy, the environmental durability, the draw ability and the rare-earth solubility. Fiber lasers operating on laser transitions which have wavelengths > 3 µm need to use glasses with very low phonon energies. ZBLAN fibers have been widely used for fiber laser source emitting below 3 µm. For longer wavelengths, the use of heavier metal fluoride glasses reduces the phonon energies, and therefore, the already demonstrated fluoroindate-based fiber is a good host material candidate for the development of mid-IR fiber lasers.

We chose two rare-earth dopants for the focus of our investigations: dysprosium (Dy^{3+}) and holmium (Ho^{3+}), based on the availability of emission at wavelengths longer than 3 µm. The $^6H_{11/2} \rightarrow {}^6H_{13/2}$ transition of Dy^{3+} corresponds to a wavelength of about 4.3 µm. Lasing has been demonstrated on this transition in crystal hosts [1], but so far only on the shorter wavelength $^6H_{13/2} \rightarrow {}^6H_{15/2}$ transition in fibers [2]. The second candidate, emitting at 3.9 µm, is Ho^{3+}:ZBLAN (ZBLAN : ZrF_4-BaF_2-LaF_3-AlF_3-NaF). The first investigation of this fiber laser used 640 nm pumping and resulted in ~ 1 mW of output power at 3.9 µm [3]. In a second set-up, a 3.4-m long Ho^{3+}:ZBLAN fiber (2000 ppm Ho^{3+}) was used and emitted up to 11 mW on the 3.9 µm transition when pumped at 885 nm with a launched pump power of 900 mW [4]. However, room-temperature operation of Ho^{3+}:ZBLAN on the 3.9 µm transition could not be achieved and the fiber had to be cooled with liquid nitrogen. In order to realize 3.9 µm fiber lasers at room temperature, new host materials are needed that show even lower phonon energies than ZBLAN; fluoroindate may prove suitable.

3.2 SPECTROSCOPY

Contributors to this section: Rita D. Peterson[1], Shrikrishna M. Hegde[2], Francis Théberge[3], Denis Vincent[3], Pierre Mathieu[3]

3.2.1 Dy:fluoroindate Glass

The samples tested here are fluoroindate glasses fabricated by two different companies: Le Verre Fluoré (LVF) and IR Photonics (IRP). The sample from LVF (S/N:110614/3220) was 5 mm in diameter and 10-mm long. The two end faces were optically polished and the cylindrical surface was rough fire polished. The IRP sample (S/N:4000979) had dimensions of 11.54 mm diameter and 9.84 mm length.

The energy-level diagram of the Dy-doped glass samples and their measured absorption spectra are presented in Figure 3-1(a). The most interesting transition is the $^6H_{11/2} \rightarrow {}^6H_{13/2}$ one at 4.2 µm. In Figure 3-1(b) and Figure 3-1(c), we can clearly observe the absorption bands centered around 1.1 µm, 1.3 µm, 1.7 µm, and 2.8 µm. Spectra in (b) are measured with a spectrophotometer UV-Vis-NIR CARY 6000i from AGILENT. Spectra in (c) are measured with a FTIR spectrometer Excalibur FTS 3000MX from DigiLab. The relative absorption ratio between the samples from Le Verre Fluoré (LVF) and IR Photonics

[1] Air Force Research Laboratory, AFRL/RYDH Bldg 620, 2241 Avionics Circle, Wright-Patterson AFB, OH 45433, United States.

[2] University of Dayton Research Institute, Dayton, OH 45469, United States.

[3] DRDC Valcartier, 2459 route de la Bravoure, Québec (Québec) G3J 1X5, Canada.

(IRP) indicates that the Dy concentration was 2.8 times higher in the sample from Le Verre Fluoré. The strongest IR absorption appears at 1280 nm with a weaker, broader mid-IR absorption near 2830 nm. The contribution to phonon absorption begins at ~ 6000 nm and rapidly increases reaching ~ 10 cm^{-1} in these samples. The material thus may be useful up to ~ 6000 nm with further improvements in growth techniques and Dy^{3+} doping concentrations. It also appears that the background absorbance for the lower concentration IRP sample is more than the higher-doped LVF material in the near UV region. The phonon absorption also increases at a shorter wavelength in the IR region in this sample. Assuming the optical polish and surface quality of the two materials are the same, this suggests that the sample growth conditions are different for the two samples and optically, the higher-doped material may be more desirable than the lower doped material.

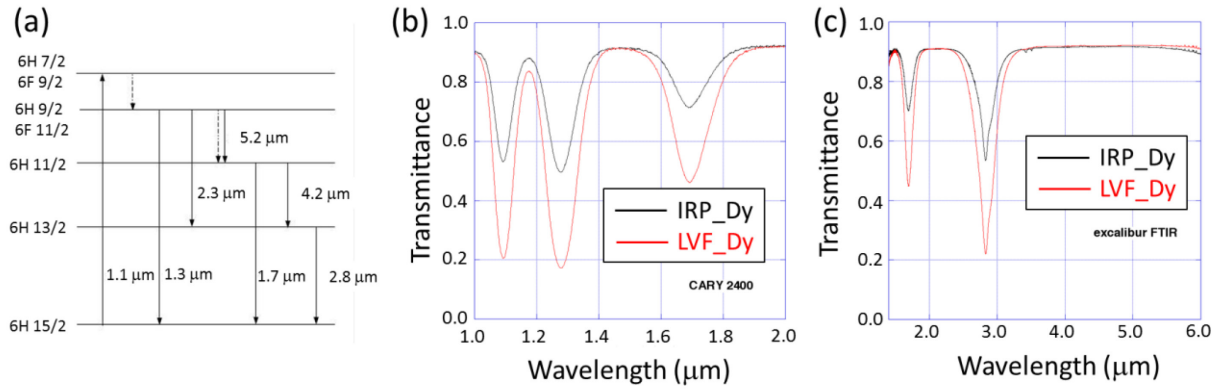

Figure 3-1: (a) Energy-Level Diagram of Dy:fluoroindate Glass; (b) Dy:fluoroindate Absorption Spectra Measured Between 1 µm and 2 µm; and (c) Between 1.5 µm and 6 µm for IR Photonics (IRP_Dy) and Le Verre Fluoré (LVF_Dy) Samples.

Fluorescence in the two Dy:glass samples was measured using a SPEX 220M spectrometer fitted with a liquid N_2 cooled InSb detector and 300 g/mm grating. A Spectra Physics Nd:YVO_4 laser was used to pump the sample. The typical power level used was ~ 400 mW measured at the sample position. A synchronous detection technique using a lock-in amplifier and a mechanical chopper (f ~ 200 Hz) was used to detect the emitted fluorescence in the mid-IR region (2400 nm to 6000 nm). Proper order-sorting longpass filters were used to identify distinct emission peaks. The fluorescence spectra corrected for the spectral response of the system (Figure 3-2), show two peaks at 2900 nm and 5700 nm. The longer wavelength peak at 5700 nm is a second order of the main band at 2900 nm as shown in Figure 3-2. The intensity of the peak is extremely weak, due to the low concentration of Dy in the samples. The expected fluorescence on the $^6H_{11/2} \rightarrow {}^6H_{13/2}$ transition of interest at 4.2 – 4.3 µm cannot be observed at all.

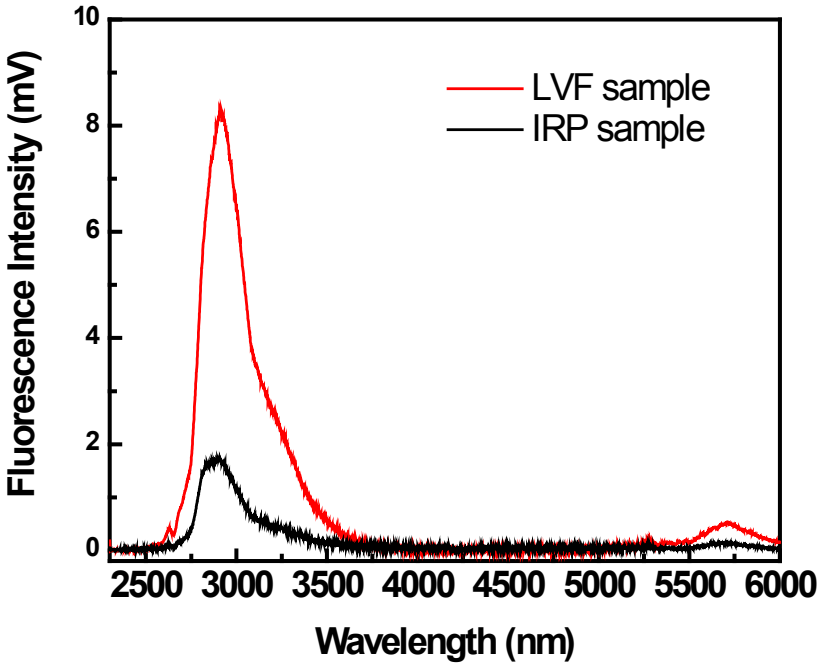

Figure 3-2: Fluorescence in Dy:fluoroindate Glass Samples.

The fluorescence lifetime at different wavelengths was also measured using the set-up presented in Figure 3-3. The Dy-doped glass samples were pumped by 12 ns pulsewidth 1.064 µm Nd:YAG laser. Each fluorescence lines were isolated by coupling the emitted signal into a monochromator. At the output of the monochromator, the lifetime of the isolated fluorescence lines was measured using an InSb detector having a response time of 10 ns.

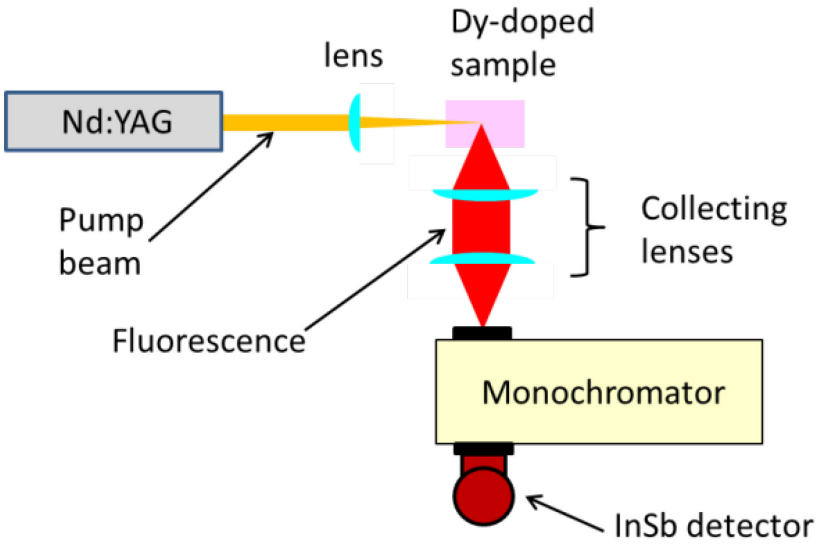

Figure 3-3: Set-Up for Measuring Fluorescence Lifetime of Various Electronic Transitions in Dy:fluoroindate Glass Samples.

The measured fluorescence lifetime at 1.7 µm ($^6H_{11/2} \rightarrow {}^6H_{15/2}$) and at 2.9 µm ($^6H_{13/2} \rightarrow {}^6H_{15/2}$) are presented in Figure 3-4 for both glass samples at room temperature. The measured fluorescence lifetime at 1/e decay was

0.6 ms at 2.9 µm and around 0.9 ± 0.1 µs at 1.7 µm. Once again, using a completely different experimental set-up, no fluorescence was detected around 4.2 µm for the transition $^6H_{11/2} \rightarrow {}^6H_{13/2}$. In order to avoid the coupling loss from the monochromator slits, we replaced this one by a Long Wave Pass Filter (LWPF) transmitting wavelength above 3.3 µm. Although the collection efficiency was increased by more than 10 times, no fluorescence signal around 4.2 µm was detected using the LWPF and the InSb detector for both glass samples at room temperature. The fact that fluorescence at 1.7 µm from the $^6H_{11/2}$ level was detected whereas none was observed at 4.2 µm could be explained by a very low branching ratio for the latter emission. In view of the very short life time of less than 1 µs and the low branching ratio, it seems that lasing from the 4.2 µm transition at room temperature could be difficult to obtain and that it might require operation at much lower temperature.

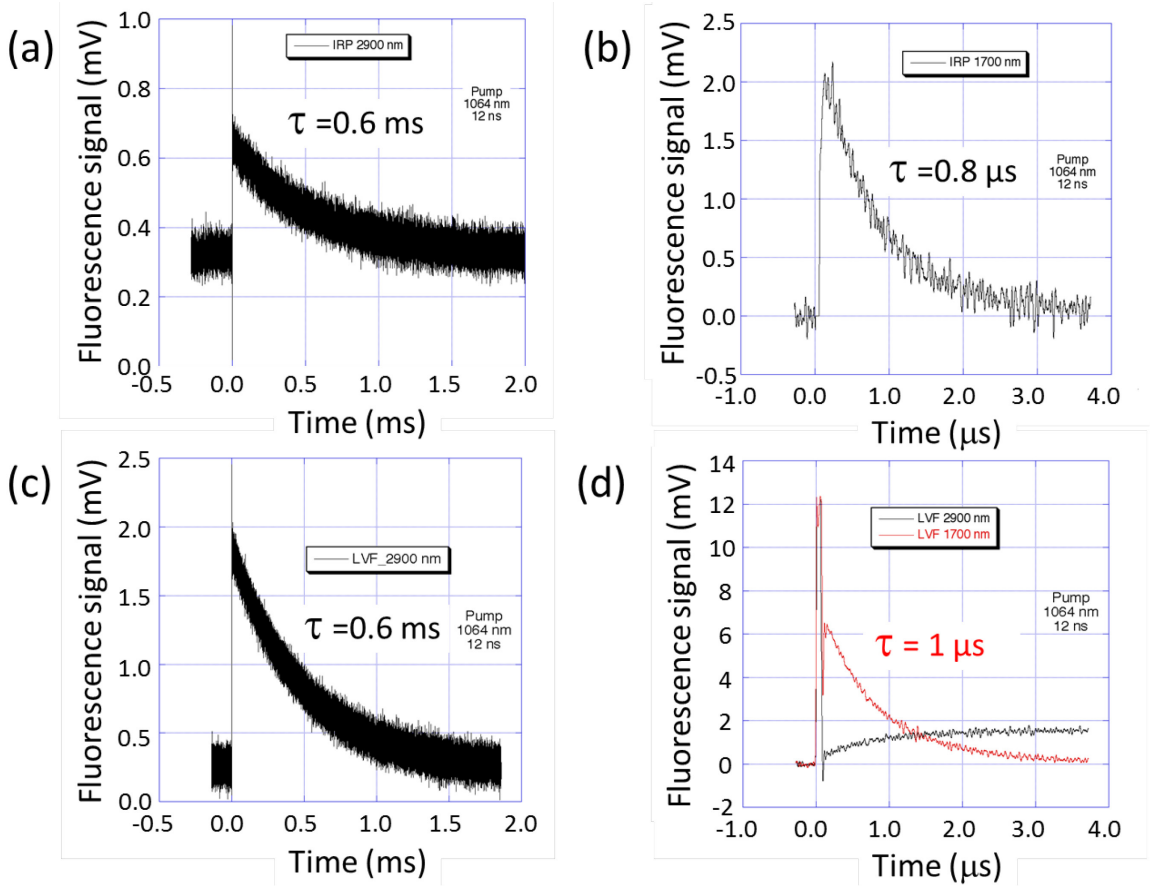

Figure 3-4: Fluorescence Decay for Dy:fluoroindate Pumped by 12-ns Nd:YAG Laser. (a) At 2.9 µm in the *IR photonics* sample (IRP_2900 nm); (b) At 1.7 µm in the *IR photonics* sample (IRP_1700 nm); (c) Fluorescence decay at 2.9 µm in the *Le Verre Fluoré* sample (LVF_2900 nm); (d) At 1.7 µm in the *Le Verre Fluoré* sample (LVF_1700 nm). For comparison, the fluorescence curve at 2.9 µm is superposed in (d) and shows the $^6H_{13/2}$ level being populated by the decay from the $^6H_{11/2}$.

3.2.2 Ho:fluoroindate Glass and Ho:BYF

A single sample of 10% Ho:fluoroindate glass was available for spectroscopic study, in the form of a 10 mm^3 cube, highly polished on all sides. The sample was fabricated by Le Verre Fluoré (LVF), and cut from a larger glass sample, the remainder of which was fabricated into a Brewster-cut sample for lasing experiments, described later in this chapter. Emission experiments were also made on a Ho-doped BaY_2F_8 crystal (Ho:BYF), since we have the means to reproduce lasing experiments in this material, and can use it to

help understand how spectroscopic properties relate to lasing behavior. The BYF host crystal is monoclinic and therefore emission results are polarization dependent. The sample was in the form of a rectangular parallelepiped (~ 4 x 5 x 7 mm^3), with the two 4 x 5 mm^2 end faces optically polished. The Ho concentration was 30%.

Room temperature absorption in the Ho:fluoroindate glass sample was measured using a Cary 5000 dual-beam spectrophotometer. The results are shown in Figure 3-5. Several intense and sharp absorption peaks in the near UV and visible region (300 nm – 650 nm) were observed. Three near IR absorption bands around 750 nm, 1200 nm and 2000 nm were also seen. The visible band around 640 nm showed intense absorption and peak saturation (OD > 10) at 640 nm. Similarly, the near IR band around 2000 nm showed strong absorption and peak saturation (OD > 10) at 1950 nm.

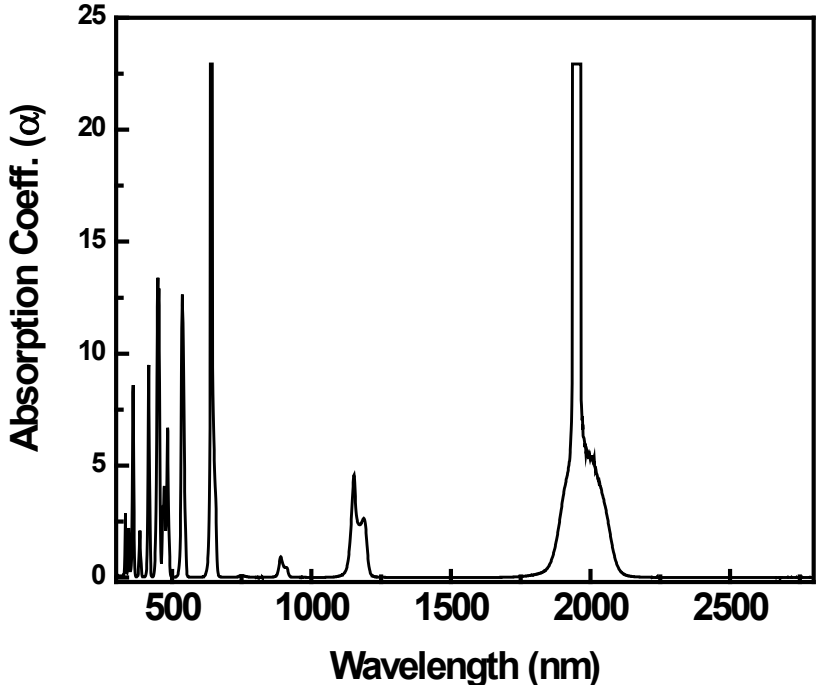

Figure 3-5: Absorption in 10% Ho:fluoroindate Glass Sample.

For measuring emission, a SPEX 220M spectrometer was used, along with a liquid-nitrogen-cooled InSb detector and preamplifier system, in the experimental set-up shown in Figure 3-6. The spectrometer was fitted with a 150 Gr/mm grating blazed at 4 μm. The sample was pumped with a CW Coherent Verdi laser at 532 nm. At this wavelength, the Ho^{3+} absorption is only ~ 45% of the peak absorption at 640 nm. The laser beam was slightly focused on the optically polished end face and emission was collected from the same face in a back reflection geometry. Typical pump power was ~ 500 mW at the sample position. A synchronous detection technique using a lock-in amplifier and a mechanical chopper ($f \leq 200$ Hz) was used to detect the fluorescence. Suitable longpass filters were used to suppress higher orders of the pump and shorter-wavelength emission lines. The room temperature emission spectra for both Ho-doped samples, corrected for the spectral response of the system, are shown in Figure 3-7 and Figure 3-8.

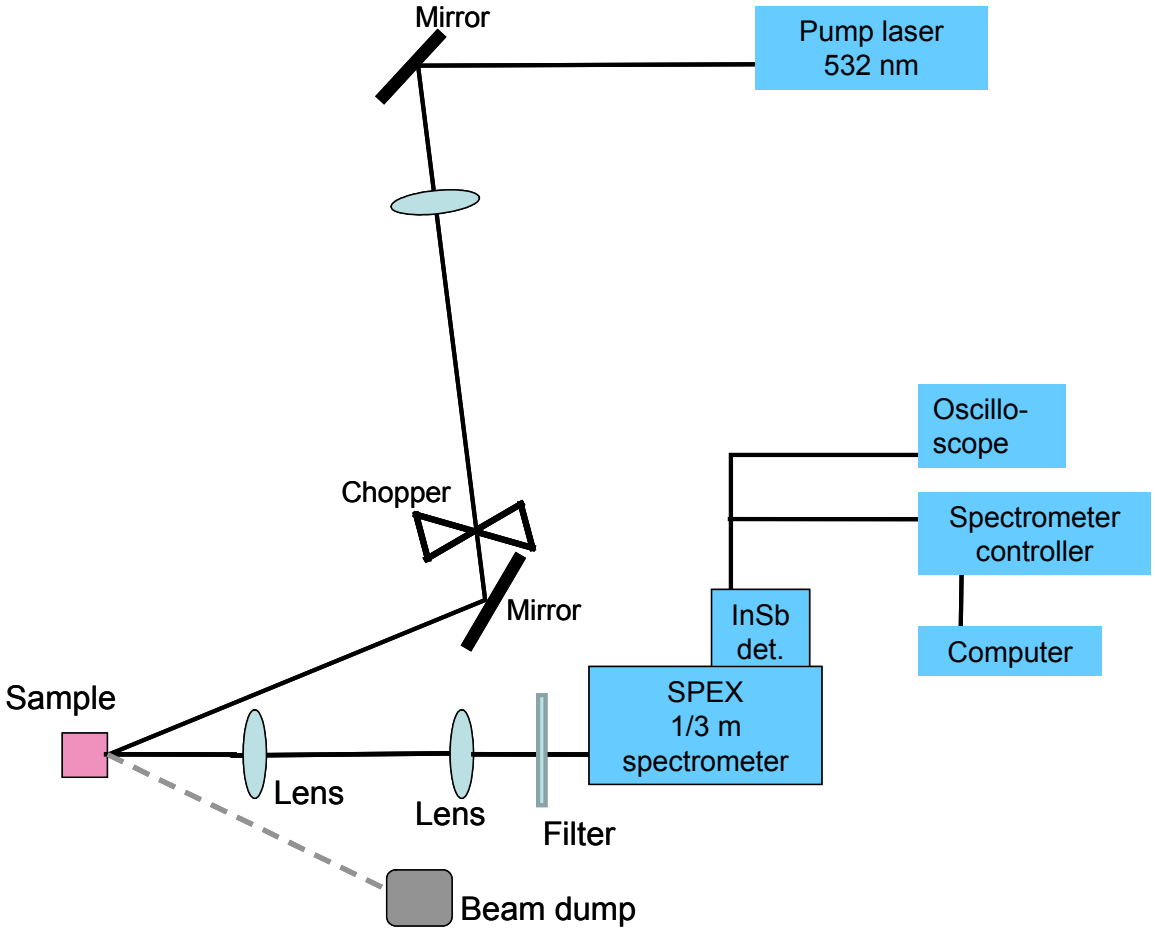

Figure 3-6: Experimental Set-Up for Measuring Emission.

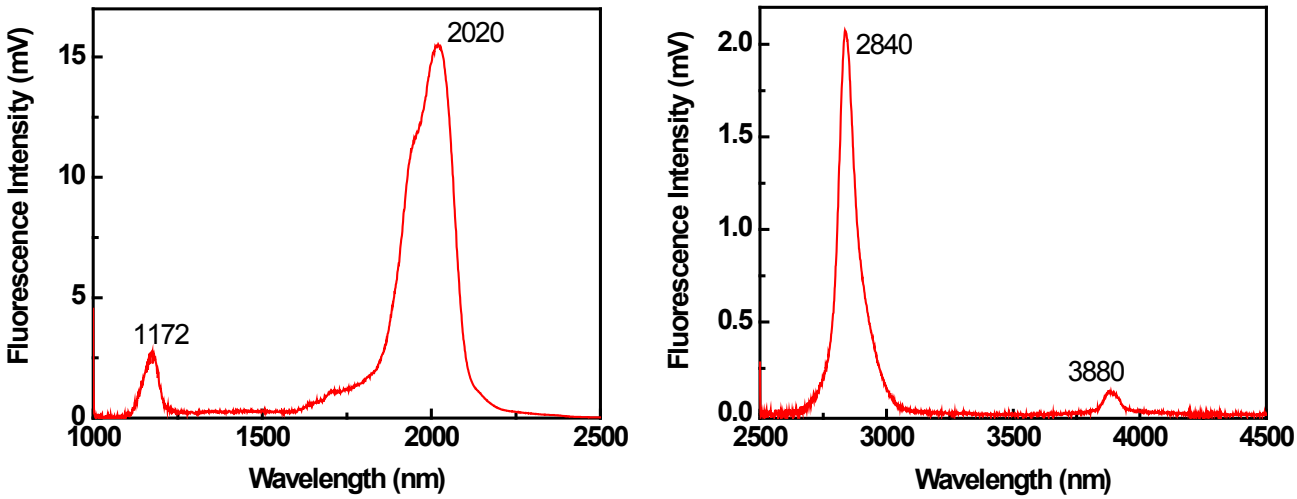

Figure 3-7: Fluorescence in 10% Ho:fluoroindate Glass from 1000 – 2500 nm (Left) and 2500 – 4500 nm (Right).

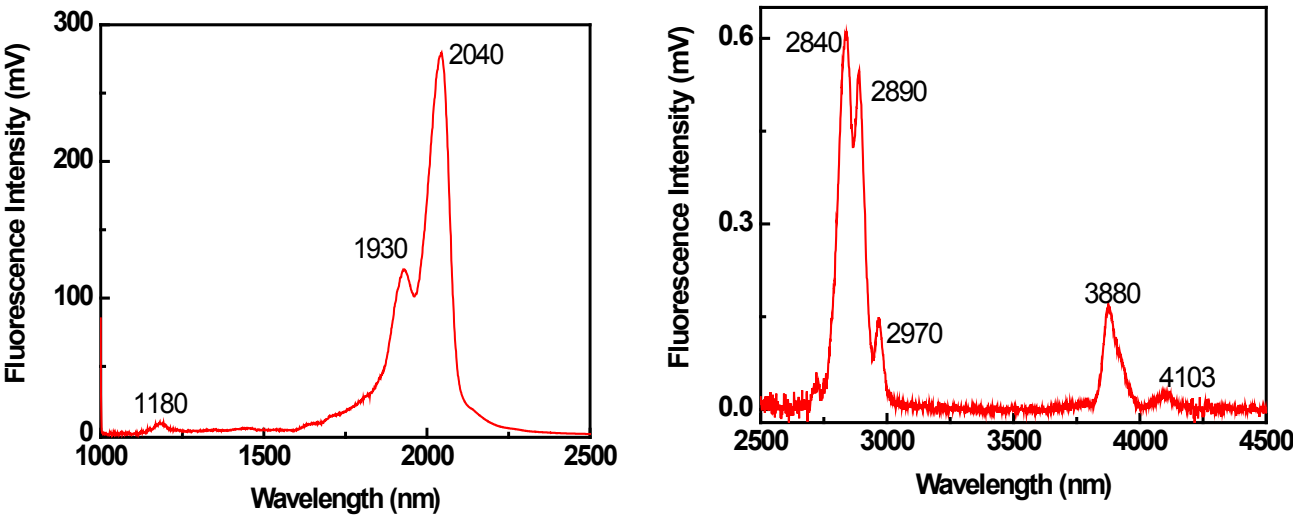

Figure 3-8: Fluorescence in 30% Ho:BYF from 1000 – 2500 nm (Left) and 2500 – 4500 nm (Right).

A number of emission peaks were observed. The strongest by far in both samples was from the $^5I_7 \rightarrow {}^5I_8$ transition around 2020 – 2040 nm, the basis for many highly successful laser systems. Emission from the $^5I_5 \rightarrow {}^5I_6$ transition around 4 μm was considerably weaker than this and the other peaks. The splitting of the peaks seen in the 3000 nm and 4000 nm regions for Ho:BYF is probably due to polarization effects arising from the low symmetry of the host crystal. For experimental simplicity, polarization was not controlled in these experiments.

Fluorescence lifetime was measured in both Ho-doped samples, at room temperature and at 25 K using a helium-cooled cryostat system. The $^5I_5$ lifetime in particular is very short – just tens of μs – so the pump beam was focused near the outside edge of the chopper wheel. The chopper could then be run at its maximum frequency of 200 Hz for measuring this level, giving a pump pulse fall time of less than 10 μs. These results are summarized in Table 3-1.

Table 3-1: Fluorescence Lifetime Data for Ho-Doped Samples at Room Temperature and 25 K.

Level	Ho:fluoroindate RT	Ho:fluoroindate 25 K	Ho:BYF RT	Ho:BYF 25 K
$^5I_5$	30 μs	105 μs	42 μs	58 μs
$^5I_6$	1.3 ms	2.7 ms	2.3 ms	1.1 ms
$^5I_7$	10.6 ms	8.7 ms	20.2 ms	12 ms

The decrease in lifetime in certain cases suggests the influence of up-conversion processes that are favored at low temperature, or possibly even the influence of radiation trapping and reabsorption. To eliminate the latter effect and to obtain more accurate lifetime values, measurements were repeated using a pinhole to limit the pumped area, a method described thoroughly in [5]. The pinhole was placed in the path of the pump beam after the chopper, such that it would be imaged onto the face of the sample by a lens placed between the pinhole and the sample. The pinhole size was varied, changing the area of the sample that was excited. Measured fluorescence lifetime was plotted as a function of pinhole size, shown in Figure 3-9 and

Figure 3-10. The lifetime value t_0 corresponding to a pinhole size of zero was taken to describe the lifetime in the absence of radiation trapping effects, as annotated on each plot.

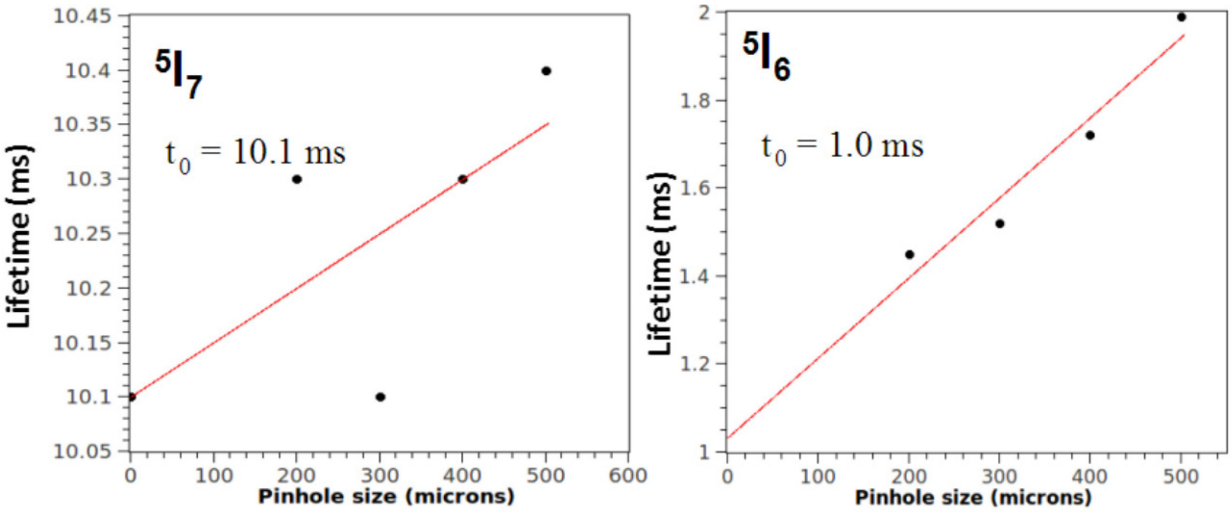

Figure 3-9: Fluorescence Lifetime in Ho:fluoroindate as a Function of Pump Pinhole Size for the $^5I_7$ and $^5I_6$ Levels.

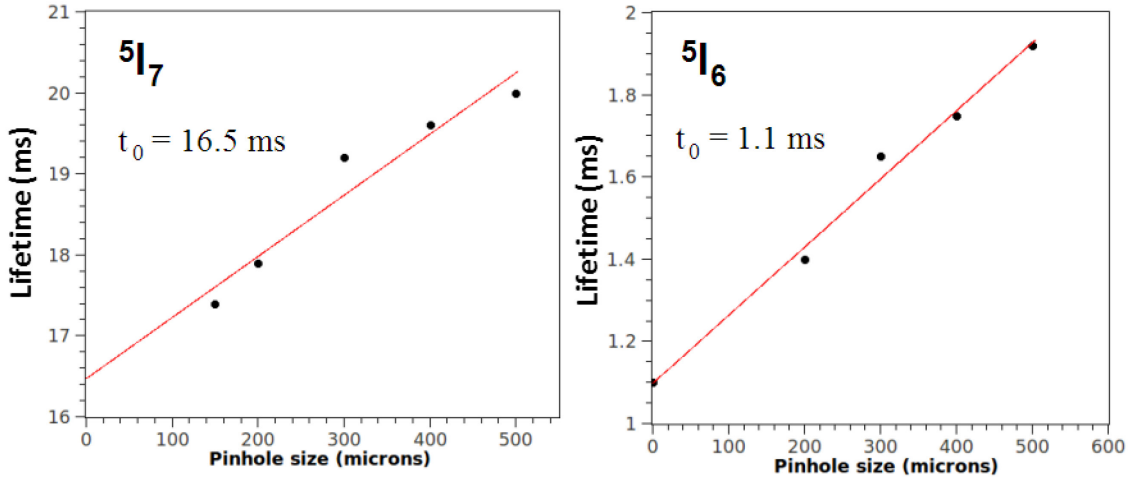

Figure 3-10: Fluorescence Lifetime in Ho:BYF as a Function of Pump Pinhole Size for the $^5I_7$ and $^5I_6$ Levels.

A similar analysis of the critical $^5I_5$ lifetime was attempted but not possible in the current experimental set-up due to excessive noise in the signal for smaller sizes of pinhole. Addressing this and repeating the measurement at low temperature remain incomplete due to unforeseen funding and personnel limitations, and are left as future tasks for a follow-on Task Group, should it decide to continue this line of investigation.

3.3 HO:GLASS MODELLING

Contributors to this section: Espen Lippert[4], Marc Eichhorn[5]

Numerical modelling can be a very useful tool for evaluating new laser systems. This is particularly the case for fiber lasers where the development and manufacturing of the glass fiber itself can be a costly process. The goal of this numerical study has been to evaluate the possibility of designing a Ho^{3+} fiber laser with emission close to 4 µm ($^5I_5$ to $^5I_6$ transition). To make this laser transition efficient it is necessary to use a glass host with low loss (< 1 dB/m) and low phonon energies, to avoid quenching of the laser transition. In this study we have evaluated fluoroindate (fluoroindate) glass as a possible host for a 4-µm Ho laser. In this glass system low loss Ho-doped material is available, but it remains an unanswered question whether or not the lifetime of the $^5I_5$ level is sufficiently long to support continuous laser action under obtainable pumping conditions.

Parameters used in this modeling have been taken from the literature, and some from the spectroscopic measurements described in a previous section. The up-conversion parameters are not easily obtainable and have just been estimated from fitting modeling results to gain-switched laser experiments in Ho:BYF, which is a crystal host with comparable properties.

In order to validate the model it has been applied to Ho laser experiments reported in literature, although they were operating on the 3-µm transition ($^5I_6$ to $^5I_7$).The ability to recreate these results gives greater confidence in the model.

The major challenge in making the 3.9-µm transition in Ho^{3+} lase is depopulating the lower lying manifolds to obtain sufficient gain at the $^5I_5$ to $^5I_6$ transition, which are the second and third exited manifolds in Ho^{3+}. To achieve this, three techniques have been studied:

- Cascade lasing the lower $^5I_6$ to $^5I_7$ transition;
- High doping concentration to achieve beneficial up-conversion; and
- Co-doping to quench the long-lived $^5I_7$ manifold.

High doping concentration and up-conversion is crucial in the operation of Ho:BYF lasing at 3.9 µm, and co-doping and cascade lasing have both previously been applied to Ho:ZBLAN lasers to achieve low threshold and efficient lasing at 2.9 µm. We have investigated whether or not the combination of these three techniques will make it possible to lase the 3.9-µm transition in Ho-doped fluoroindate glass, even with a quite short lifetime of the $^5I_5$.

3.3.1 Model Description

The approach used to model the fiber laser is similar to that used by Quimbye et al. for Dy^{3+}-chalcogenides, and the first test of the model was indeed to recreate his results [6]. The only major difference between his approach and the one used in his work is that we choose to directly integrate the rate equation instead of solving for a steady-state solution.

The lower energy levels of Ho^{3+} together with the pump, fluorescence, stimulated emission, absorption, and up-conversion transitions are shown in Figure 3-11. The ion is modeled as a 4-level system, and the lifetime of the fifth $^5I_4$ level is assumed to be short compared to the others so that the ions converted up to $^5I_4$ end directly up in the $^5I_5$ level.

[4] FFI (Norwegian Defence Research Establishment), P.O. Box 25, NO-2027 Kjeller, Norway.

[5] ISL, French-German Research Institute of Saint-Louis, 5 rue du Général Cassagnou, 68300 Saint-Louis Cedex, France.

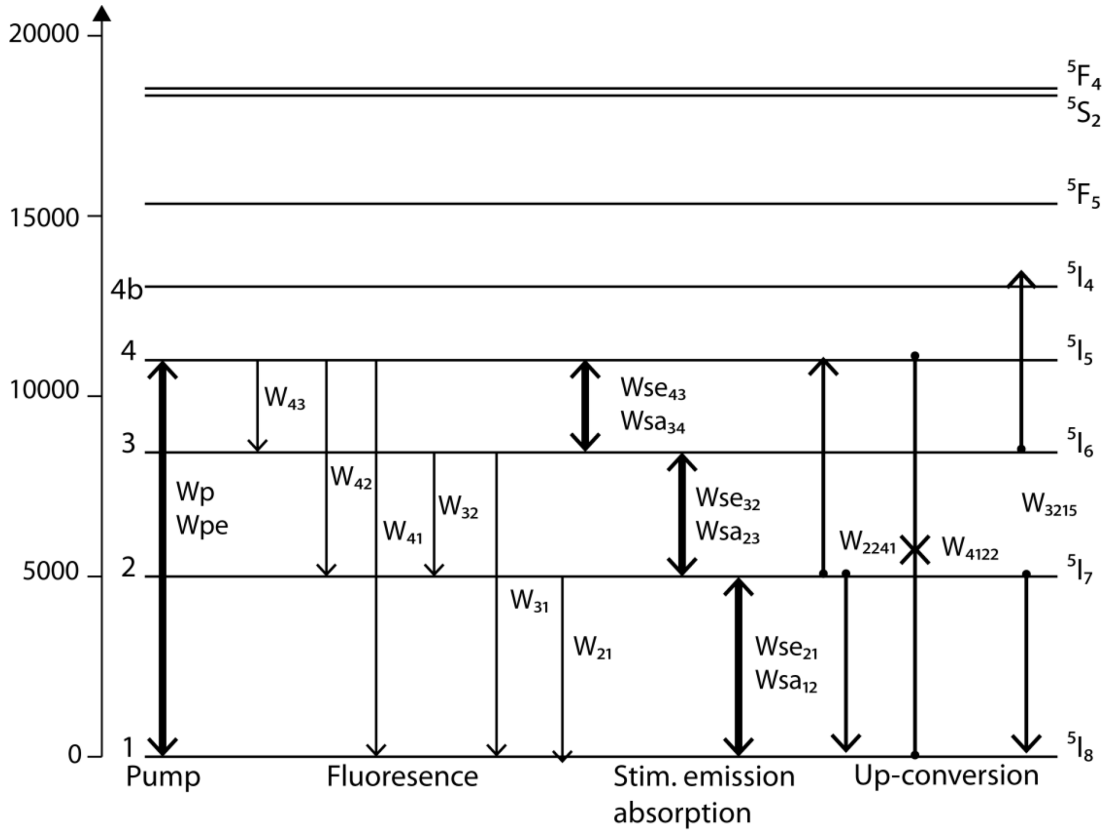

Figure 3-11: Simplified Energy-level Diagram with the Transitions Included in the Model.

The levels and transitions indicated in Figure 3-11 are described by the rate equations in (0.1):

$$\begin{aligned}
\frac{dN_1}{dt} &= -\left(W_{sa12}+W_p\right)N_1+\left(W_{se21}+W_{21}\right)N_2+k_{2241}N_2^{\,2}+k_{3215}N_2N_3-k_{4122}N_1N_4+W_{31}N_3+\left(W_{pe}+W_{41}\right)N_4\\
\frac{dN_2}{dt} &= W_{sa12}N_1-\left(W_{21}+W_{sa23}+W_{se21}\right)N_2-2k_{2241}N_2^{\,2}+2k_{4122}N_1N_4-k_{3215}N_2N_3+\left(W_{32}+W_{se32}\right)N_3+W_{42}N_4\\
\frac{dN_3}{dt} &= W_{sa23}N_2-\left(W_{32}+W_{31}+W_{sa34}+W_{se32}\right)N_3+\left(W_{43}+W_{se43}\right)N_4-k_{3215}N_2N_3\\
\frac{dN_4}{dt} &= W_pN_1+k_{2241}N_2^{\,2}-k_{4122}N_4N_1+k_{3215}N_3N_2+W_{sa34}N_3-\left(W_{pe}+W_{43}+W_{42}+W_{41}+W_{se43}\right)N_4
\end{aligned} \tag{0.1}$$

where $N_i i = 1,2,3$ *or* 4, are the population densities, W_{saij} and W_{seij} are the rates of absorption between level i and j, W_{ij} are the transfer rates between level i and j, and k_{ijkl} are the coefficients for the up-conversion processes.

When the new population has been found by integrating the rate equation over a desired time step, the gain for each section along the fiber is calculated by integrating the difference between the absorption and emission over the transversal mode, which is assumed to be Gaussian with a radius calculated from the fiber core size and NA. Using this calculated gain, the power distribution along the fiber is shifted one step in the fiber. This new power distribution is then used in solving the rate equations in a new iteration. This continues until the solution is stable. Finding a steady-state solution using this direct integrating method can be time consuming due to the oscillatory nature of the problem; this can be helped by scaling the rate equations without changing the steady-state solution, which can be achieved by scaling down the population and compensating by scaling up the cross-sections, and up-conversion rates.

3.3.2 Validation of Model

In order to gain confidence in the numerical model, it was validated by applying it to experiments reported in literature. The fiber material used in these experiments was ZBLAN, which is a fluoride material with comparable properties to fluoroindate. The parameter values used in these validations give guide lines for what could be reasonable values for fluoroindate, but they are not directly used in the fluoroindate model. The experiments we chose were lasers on the 2.9-µm transition ($^5I_6$ to $^5I_7$), and although our aim was to obtain lasing on the 3.9-µm transition ($^5I_5$ to $^5I_6$) the model's ability to recreate these experiments will show that the lower levels are modelled correctly.

The first experiment we modelled was reported by Jackson [7]. It is simple to model in the sense that it pumped directly to the upper laser level ($^5I_6$), and the lower laser level ($^5I_7$) is depopulated by co-doping with Pr^{3+}, which effectively reduces the lifetime of the lower laser level to probably on the order of 100 µs. The parameters used in the model are shown in Annex A. This results in an efficient laser with very low threshold. The experimental points and the model fit shown in Figure 3-12 are in good agreement. We also tried to vary the parameters in the simulations, such as lifetimes and cross-sections, and found that the results were very insensitive to this. This is reasonable since the threshold is very low and the slope is limited by the quantum defect and the ratio of output coupling to total loss. Although the fit was insensitive to some parameter values the fit show that the model can give reasonable results.

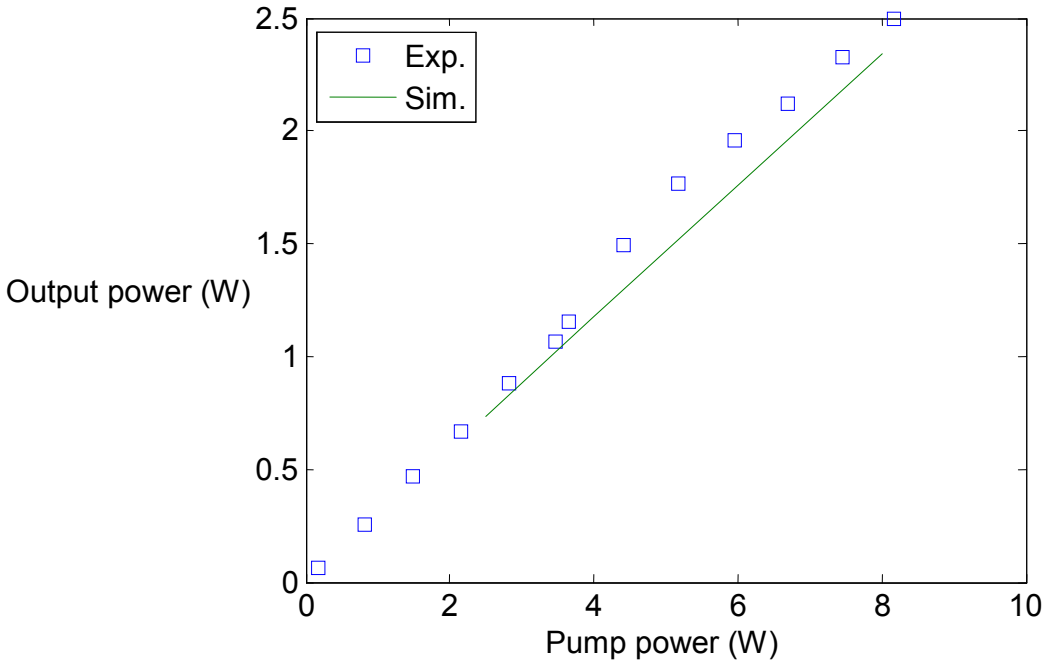

Figure 3-12: Model Fit to 2.94 µm Ho:ZBLAN Fiber Laser.

The second experiment used in the model validation was more challenging. The laser was also a Ho:ZBLAN laser, but without Pr^{3+} co-doping. Instead the $^5I_7$ level was depopulated through cascade lasing of the 2-µm transition [8]. This laser had a much more complex behavior and high threshold. The parameters used are shown in Annex A. The result of the model fit is shown in Figure 3-13.

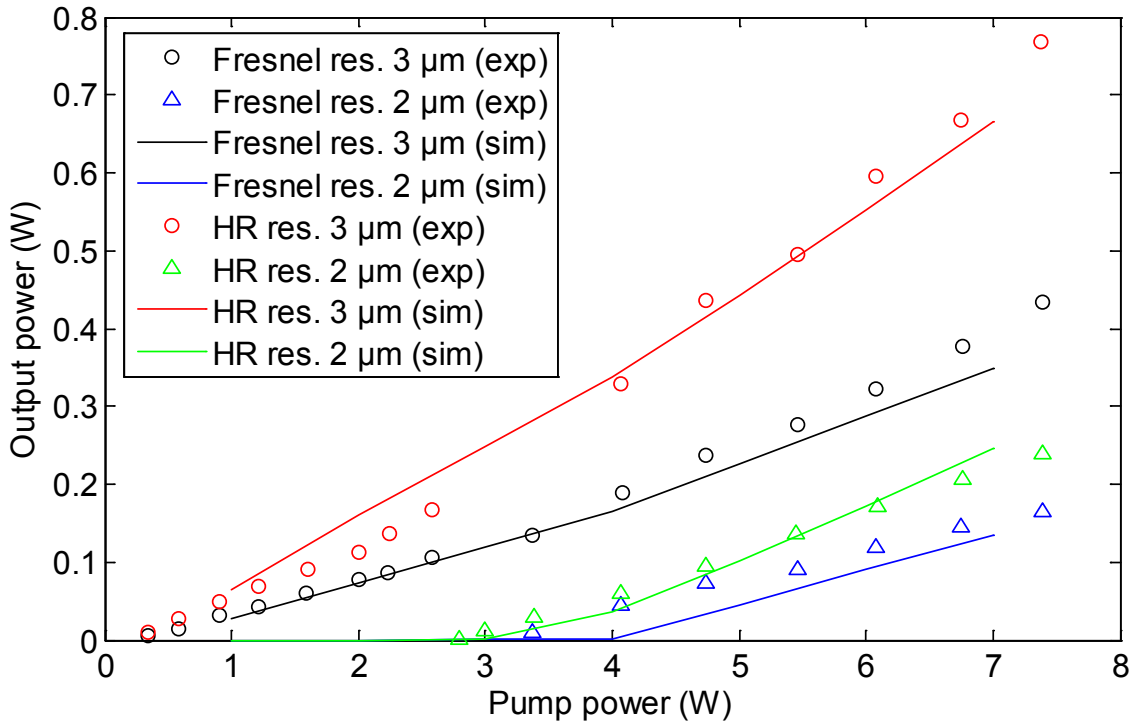

Figure 3-13: Model Fit to Cascade Lasing in Ho:ZBLAN.
Two sets of resonator mirrors were applied to the fiber laser.

As Figure 3-13 shows, the fit between the model and the experiments are not as good as for the previous case, but still much of the behavior is recreated. This example is much more sensitive to the input parameter values, and making the model fit the experiment reasonably well greatly adds to the confidence that it can model the behavior of a cascade fiber laser system.

3.3.3 Model Predictions

Lasing the 3.9-µm transition in Ho^{3+} is challenging even without lifetime quenching from the phonon coupling. The lifetime of the $^5I_5$ level is shorter than that of the $^5I_6$ level, which in turn is shorter than the $^5I_7$ lifetime, and the substantial non-radiative transfer only makes this situation worse. These unfortunate lifetime ratios inhibit population inversion between the manifolds. Even though this can be overcome to some extent by lasing to a level high up in the lower lying manifold, it tends to be very difficult to make transitions to these high lying levels lase in continuous operation for feasible pump intensities. There is only one demonstration of lasing the 3.9-µm transition continuously in a fiber laser, and they achieved only 11 mW and had to cryogenically cool the fiber to 77 K [9]. To mitigate this lifetime problem, some mechanism had to be found to depopulate the $^5I_6$ level. The obvious way to do this is to lase both the 3.9-µm and the 2.9-µm transition simultaneously. If the threshold of the 2.9-µm transition can be made low, the population in the $^5I_6$ level can be kept down, thus allowing for a more favorable population ratio. A second effect which not only depopulates the $^5I_6$ level, but also repopulates the $^5I_5$ level is the up-conversion from both the $^5I_6$ and $^5I_7$ level, as indicated by Figure 3-11. This effect will increase with increasing doping concentration, making the doping level an important parameter in the design of a Ho:fluoroindate fiber laser. A challenge with the cascade lasing scheme is that the lower level of the 2.9-µm transition ($^5I_7$) also has a longer lifetime than the upper level ($^5I_6$). It has been shown, however, that this transition can lase in spite of this to lines high up in the $^5I_7$ manifold. It has also been shown that depopulating this level, e.g. using co-doping like in the first validation experiment, will reduce the threshold of the 2.9-µm transition.

This simple analysis led us to investigate two approaches to make the Ho-fiber laser at 3.9 µm, both using cascade lasing at the 2.9-µm transition, but one with co-doping to reduce the lifetime of the $^5I_7$ level and one without.

It is also clear that having high pump intensity is advantageous, and therefore we chose a fiber structure where the pump core was as small as possible, but still large enough to allow pumping with high brightness laser diodes. We chose to investigate a dual-cladding fiber with an inner core with a 10-µm diameter and an outer pump core of 50 µm. We applied dual-end pumping with 10 W launched pump power in both directions at 895 nm. In the model we used the up-conversion coefficient estimated from the Ho:BYF model fit reported by Eichhorn, and we further assumed that these coefficients will be proportional to the doping concentration [10]. The assumption of linearity has been shown to be valid at least for low doping concentration (< 4 mol %) [11]. Our values were estimated for ionic distances equal to that of 10% doping in fluoroindate and are most accurate around this concentration, but will probably not overestimate the up-conversion at lower concentration. The lifetimes we used were the ones we determined experimentally, which were considerably shorter than what we had hoped when this host material was chosen for investigation. We used the absorption and emission experiments to estimate the energy levels of the laser manifold and the shape of the emission lines. The rest of the parameters were estimated from literature values of Ho^{3+} in similar hosts [12]. Where the values were uncertain, conservative estimates were used. A list of the parameters is given in Annex A.

The results from the modeling of the Ho-doped double-clad fiber are shown in Figure 3-14 and show that for high doping concentrations the 3.9-µm transition lases efficiently even with a very short lifetime of 30 µs assumed for the $^5I_5$ level. Using 20% Ho doping the optical efficiency is ~ 40%, which is almost twice the ratio of pump wavelength to laser wavelength, usually limiting the efficiency of an optically pumped laser. The reason for this is that the electrons are recirculated by the strong up-conversion from the $^5I_6$ and $^5I_7$ levels, and can contribute to laser action several times. This process greatly reduces the detrimental effect of the short lifetime of the $^5I_5$ level. Even though the long lifetime of the $^5I_7$ level reduces the efficiency of the 2.9-µm transition, co-doping to mitigate this does not help since this also reduces the efficiency of the up-conversion recirculation. Only for the lowest doping concentration, where the up-conversion is less important, is the co-doping beneficial.

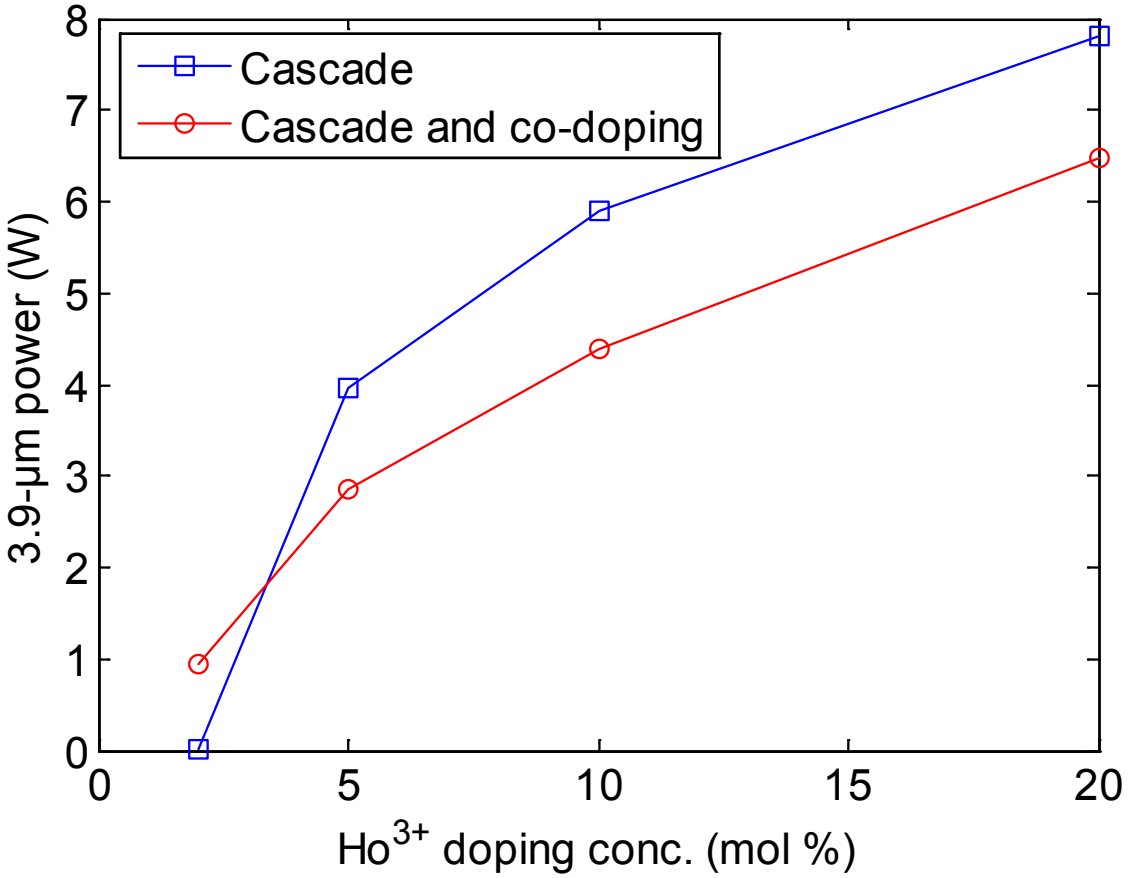

Figure 3-14: Model Predictions of Two Cases of Cascade Lasing a Double Clad Fiber, Pumped by Two 10 W Pumps, With (Red Curve) and Without Co-Doping (Blue Curve) for Varying Doping Concentrations.

To study the effect of the $^5I_5$ lifetime we varied the lifetime. The results in Figure 3-15 show that at this pump level with this fiber geometry the efficiency is saturated already at a lifetime of 100 µs. This shows that the modeled up-conversion processes are very efficient in re-circulating the electrons which undergo non-radiative or radiative transfer to the $^5I_6$ and $^5I_7$ levels. The only lost energy in the system is across the $^5I_7$ to $^5I_8$ transition, which takes place in the up-conversion process.

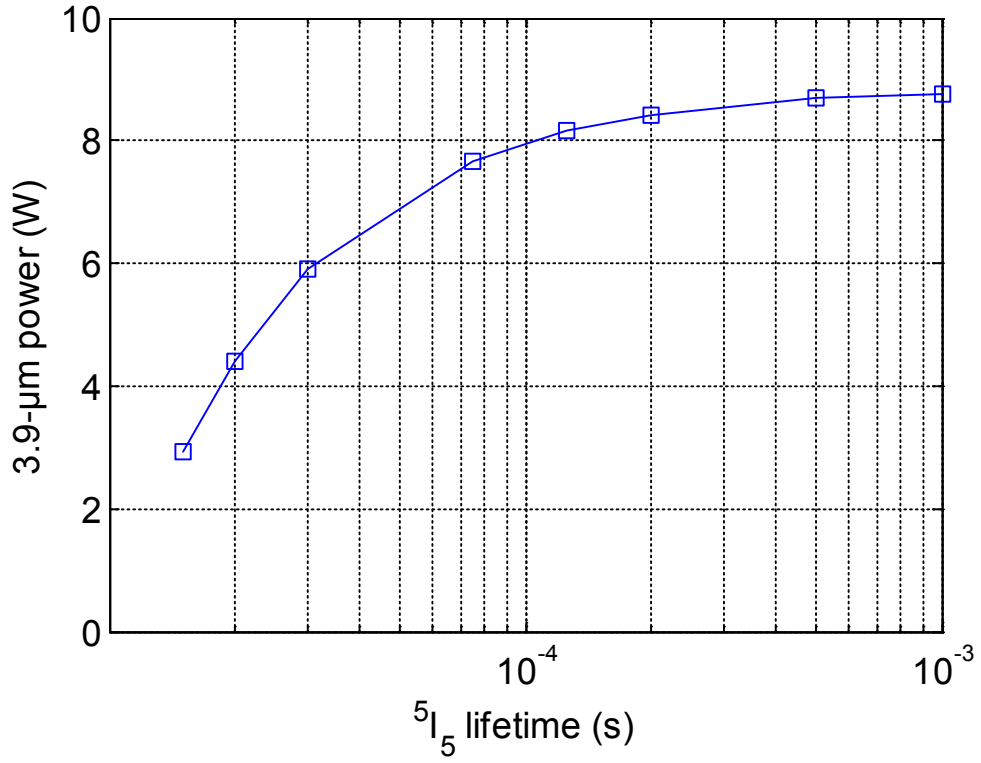

Figure 3-15: Output Power at 3.9 µm from a Fiber with 10 mol % Ho^{3+}, for Varying Lifetime of the $^5I_5$ Level.

3.3.4 Conclusions

We have shown that a double-clad Ho-doped fluoroindate glass fiber can be lased efficiently at 3.9 µm for doping concentrations greater than ~ 5 mol %, provided that the up-conversion coefficients we have used are correct. It should be noted, though that the values we have used have been extracted from model fitting in a different crystalline host (BYF), and that more work should be done on extracting better values for emission cross-sections and up-conversion coefficients. The peak emission cross-sections should be easily available from Judd-Ofelt analysis, whereas the up-conversion coefficients can be estimated from model fitting to fluorescence measurements under strong pumping. If the true values are similar to what we have assumed, it should be feasible to design an efficient diode pumped 4-µm fiber laser.

3.4 HO:GLASS LASING

Contributors to this section: Marc Eichhorn[6], Christelle Kieleck[6], Antoine Berrou[6]

Like Ho:ZBLAN, Ho^{3+}:fluoroindate glass exhibits an absorption peak around 890 nm (Figure 3-16). Thus we need an intense pump source at this wavelength. We will use Cr^{3+}:LiSAF laser to pump, as a first demonstration, a bulk Ho^{3+}:fluoroindate glass. In this sub-section we present first the characteristics of the Cr^{3+}:LiSAF laser that was used as pump source. In order to compare the performance of our new material (Ho^{3+}:fluoroindate glass) to well-known materials, we built a laser based on a Ho^{3+}:BYF crystal. Its performance is reported thereafter. Replacing the Ho^{3+}:BYF crystal by Ho^{3+}:fluoroindate glass in the laser cavity we recorded, to the best of our knowledge, the first laser activity of this glass.

[6] ISL, French-German Research Institute of Saint-Louis, 5 rue du Général Cassagnou, 68300 Saint-Louis Cedex, France.

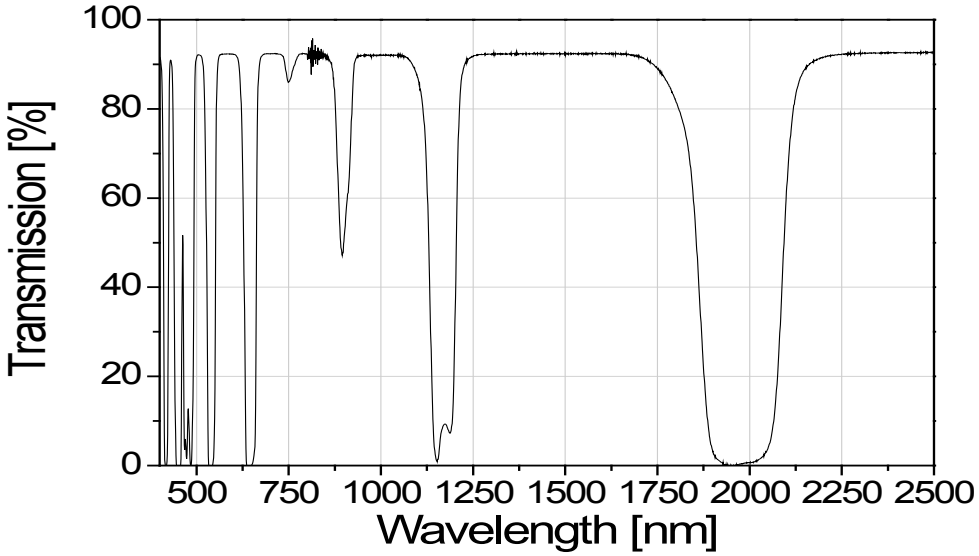

Figure 3-16: Transmission of Uncoated Ho^{3+}:fluoroindate Glass as Function of Wavelength.

The experimental set-up of the Cr^{3+}:LiSAF (Cr^{3+}:$LiSrAlF_6$) laser is presented in Figure 3-17. The crystal rod is 101.6-mm long and 6 mm in diameter. The chromium doping concentration is 0.8%. It is flash lamp-pumped, resulting in available pump energies for holmium pumping of several joules at pulse widths of ~ 80 µs in free-running mode. In order to obtain a narrow emission linewidth from the laser, a threefold SF4-prism monochromator was inserted into the cavity, resulting in a linewidth of 2.5 nm, centered at 889 nm.

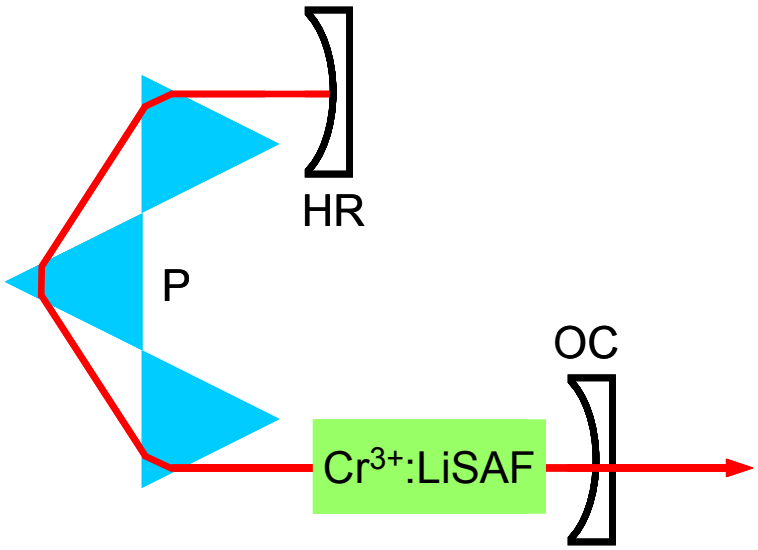

Figure 3-17: Cr^{3+}:LiSAF Laser Layout. HR: High Reflectivity Mirror; P: Prisms; OC: Output Coupler.

The laser output energy as function of the electrical flashlamp energy is reported in Figure 3-18. The laser set-up is presented in Figure 3-19. Ho3+:BYF crystal is 15-mm long, it is not coated therefore its faces are cut off with an angle to reduce the Fresnel loss. It is pumped from both sides and its temperature is not controlled. As the pump source beam is polarized, we used a polarized beam splitter to separate the pump

beam into two parts. The ratio between the two arms can be controlled with the half-wave plate 1. The pump beam is focused inside the crystal using plano-concave lenses. The laser cavity which is approximately 250-mm long is composed of three mirrors. The dichroic mirrors M1 and M2 are highly transmissive for the pump beam and highly reflective for the laser beam. The output coupler M3 has a reflectivity of 80%. Maximum output energy of 650 mJ was achieved at 150 J electrical energy. The conversion slope efficiency was measured to be 0.63%, which is lower than what we obtained few years ago with this laser [10].

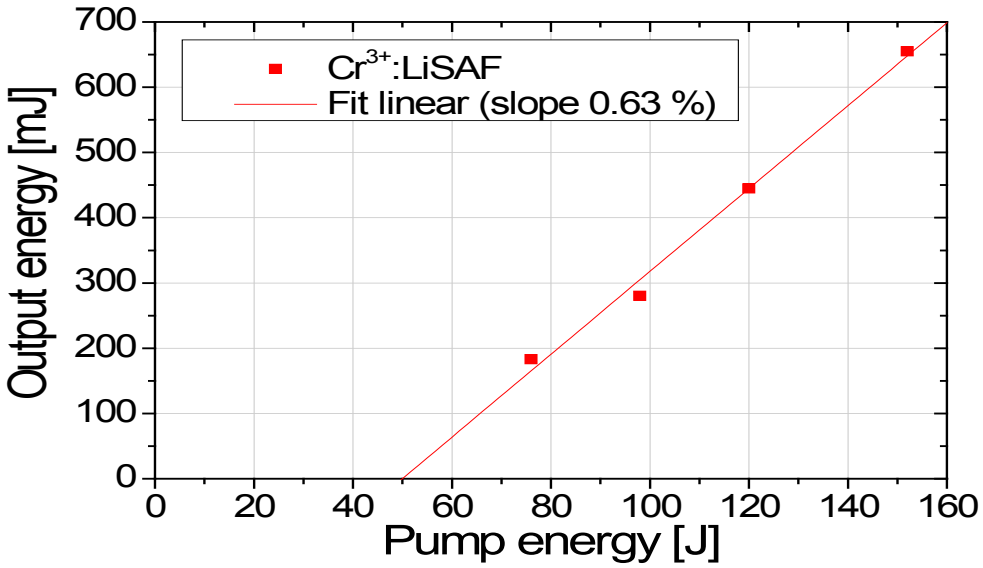

Figure 3-18: Cr^{3+}:LiSAF Laser Output Energy as Function of Electrical Flashlamp Energy (80 µs Pulse Duration).

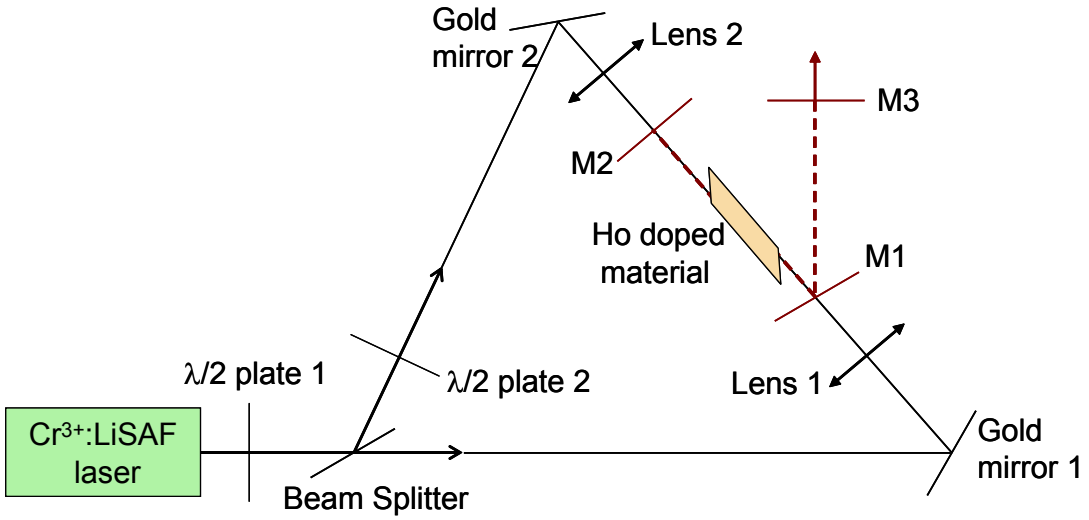

Figure 3-19: Mid-Infrared Laser Set-Up.

Ho3+:BYF crystal (Ho:BaY2F8) is an interesting material because it can be pumped in the near-infrared at 889 nm and emit in the mid-infrared at 3.9 µm. Due to the longer lifetime of the terminating level compared to the upper laser level, this transition can be regarded as a quasi-three-level transition. Moreover due to the strong difference in upper and lower-state lifetimes (52 µs and 5.45 ms respectively), the laser can be

operated efficiently only in pulsed mode with repetition rates smaller than the inverse lower level lifetime. However, when strongly doped with Ho^{3+} (> 20%) an Energy Transfer Up-conversion (ETU) process allows for recycling of used inversion and thus can allow for cw operation [10]. Here, we only run the pump source in single shot (80 µs pulse duration).

The laser output energy as a function of the pump energy is reported in Figure 3-20. Three different pump conditions were examined. First, in blue, we roughly separated the pump beam into equal parts. Then, in green, we rotated the half-wave plate 1 for maximum pump energy in the first arm. Finally, in red, we blocked the pump beam of the second arm. The evolution of the slope efficiency between the three curves shows that the second arm pumping is less efficient than the first arm. We need more investigations to determine the cause of this behavior. Nevertheless we obtained a threshold energy of 125 mJ, a slope efficiency of 6.9% and maximum output energy of nearly 35 mJ at 650 mJ pump energy. The temporal profile of the laser beam in Figure 3-21 shows a quasi-continuous emission after spikes at the beginning. This behavior is well explained with numerical simulation in [10].

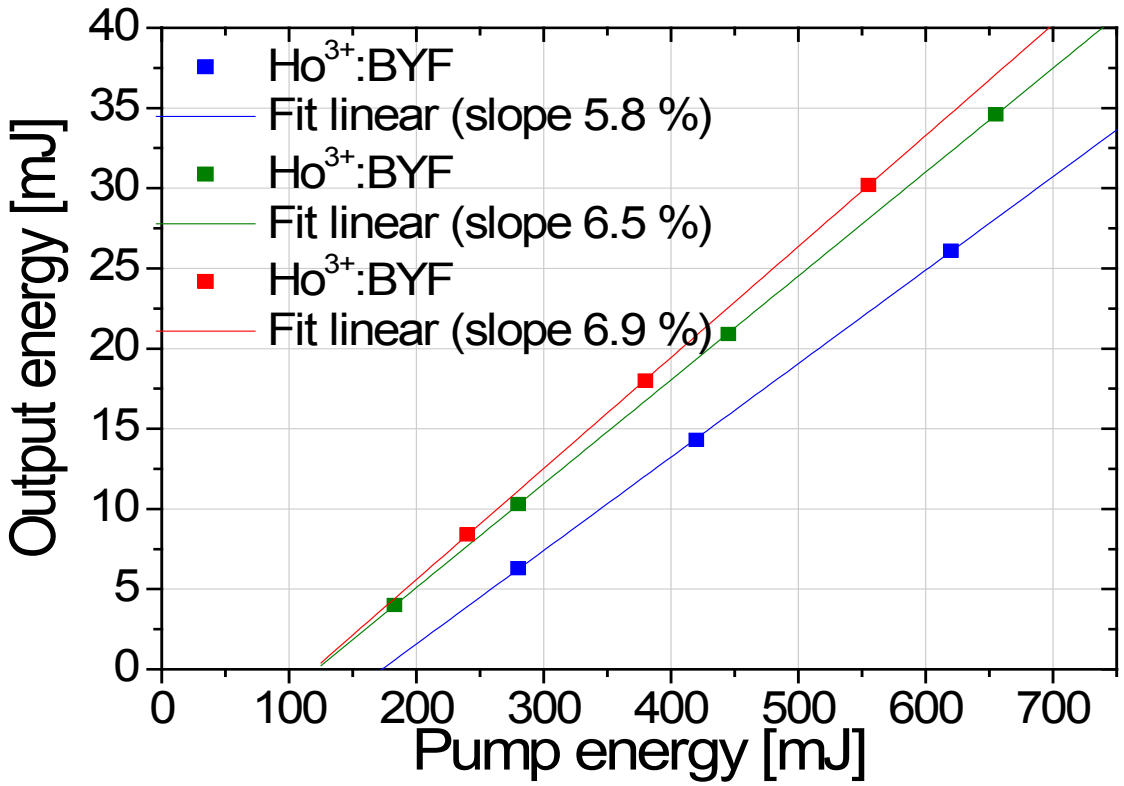

Figure 3-20: Ho^{3+}:BYF Output Energy as Function of Cr^{3+}:LiSAF Energy for Three Different Repartitions of Pump Intensity Between the Two Arms: 57% in the First Arm and 43% in the Second (Blue); 85% in the First Arm and 15% in the Second (Green); and 100% in the First Arm (Red).

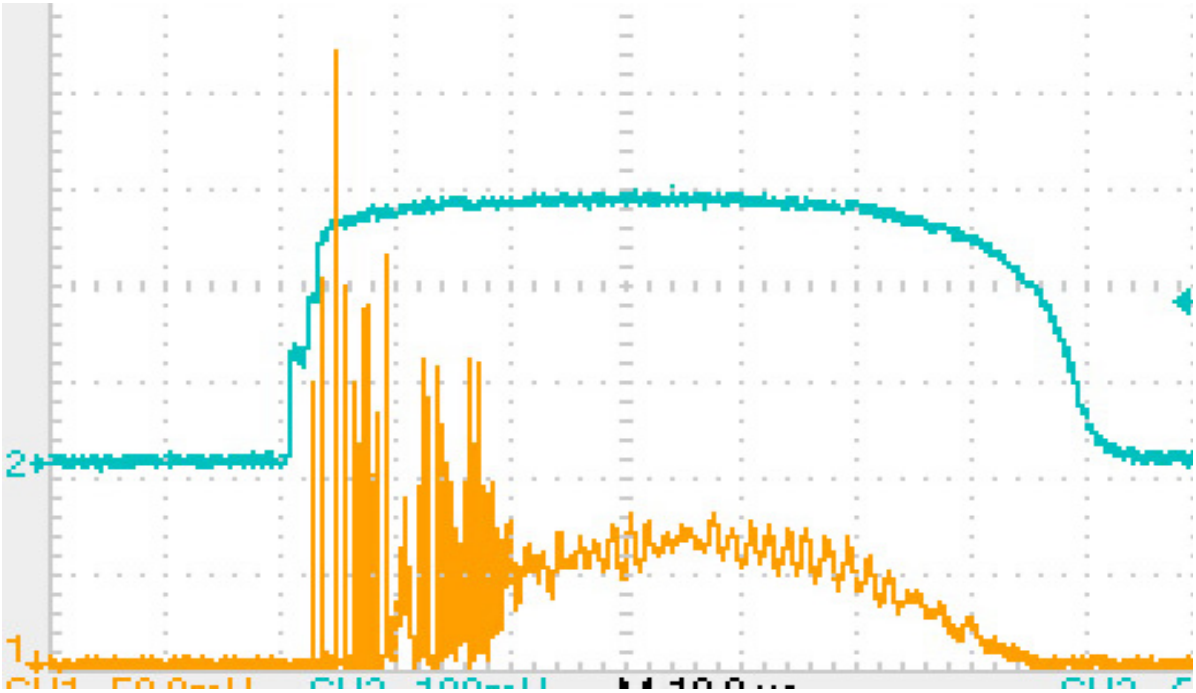

Figure 3-21: Temporal Profile of Cr^{3+}:LiSAF Laser Pulse (Cyan) and Ho^{3+}:BYF Laser Pulse (Orange) at Maximum Output Energy.

A picture of our Ho^{3+}:fluoroindate glass is presented in Figure 3-22. It shows high optical quality (bulk) and surface finish. It is 30-mm long and has a holmium doping concentration of 10%. Like the Ho^{3+}:BYF crystal, it has no optical coating. Thus it is Brewster cut to limit the Fresnel loss.

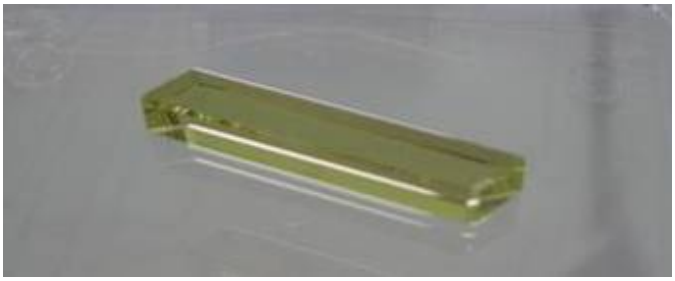

Figure 3-22: Ho^{3+}:fluoroindate Glass.

We used the set-up presented in Figure 3-19, replacing the Ho^{3+}:BYF crystal with this fluoroindate glass. Since this glass is two-times longer than the BYF crystal, we needed to realign the pump and the cavity. The laser output energy as a function of the pump energy is reported in Figure 3-23. We recorded the output energy for two configurations. The first configuration was with 85% of the pump energy in the first arm and the remaining 15% in the second one. For the second configuration we blocked the pump of the second arm, keeping the same power in the first arm. The laser threshold energy was approximately 230 mJ. The conversion slope efficiency was 1.3% with 5.4 mJ maximum output energy. It appears that this laser is not as efficient as the Ho^{3+}:BYF laser, but we must emphasize that the laser cavity was almost the same for the two lasers therefore it was not optimal for the second experiment with a longer active medium.

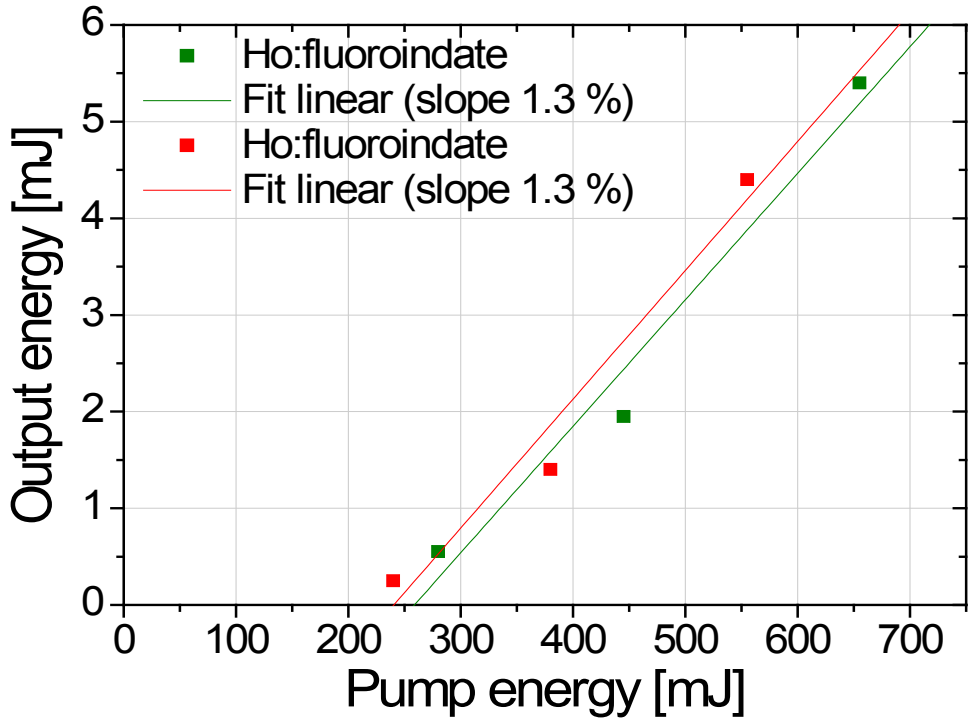

Figure 3-23: Ho^{3+}:fluoroindate Output Energy as Function of Cr^{3+}:LiSAF Energy for Two Different Repartitions of the Pump Energy Between the Two Arms: 85% in the First Arm and 15% in the Second (Green) and 100% in the First Arm (Red).

The temporal profile of the Ho^{3+}:fluoroindate laser beam at maximum output energy is reported in Figure 3-24. This profile shows separated spikes for 30 µs and then nearly quasi-continuous emission with weak power during 20 µs. This behavior is expected when pumping few times above threshold and is comparable to Ho^{3+}:BYF laser beam profile at this laser energy level.

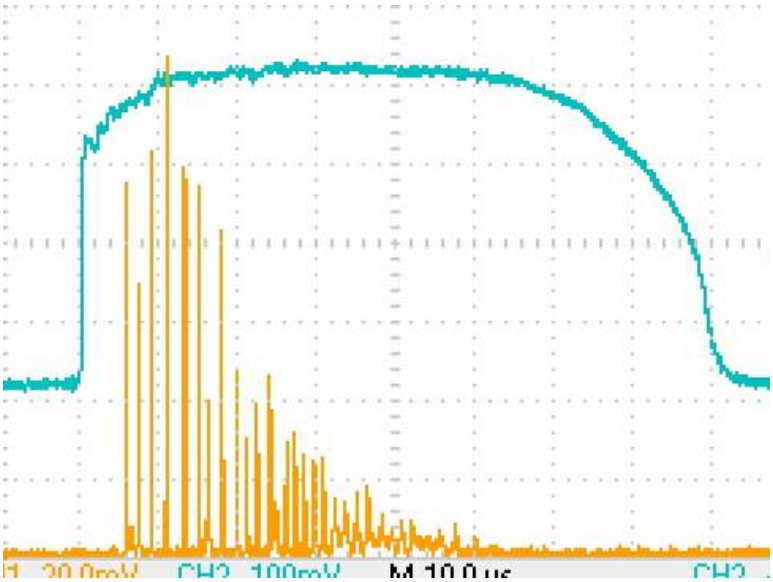

Figure 3-24: Temporal Profile of the Cr^{3+}:LiSAF Laser Pulse (Cyan) and the Ho^{3+}:fluoroindate Laser Pulse (Orange) at Maximum Output Energy.

The set-up was not optimized for a 30-mm long laser material. Nevertheless we obtained, for the first time to our knowledge, a laser emission from a Ho^{3+}:fluoroindate glass. We think that this is the first step towards a pulsed mid-infrared fiber laser based on this material.

3.5 REFERENCES

[1] Barnes, N.P. and Allen, R. Room temperature Dy:YLF laser operation at 4.34 mm, IEEE Journal of Quantum Electronics v. 27, 277-282 (1991).

[2] Jackson, S.D. Continuous wave 2.9 μm dysprosium-doped fluoride fiber laser, Appl. Phys. Lett. 83, 1316 (2003).

[3] Schneider, J. Fluoride fibre laser operating at 3.9 μm, *Electron. Lett.*, Vol. 31, pp. 1250-1251 (1995).

[4] Schneider, J., Carbonnier, C. and Unrau, U. Characterization of a Ho^{3+}-doped fluoride fiber laser with a 3.9-μm emission wavelength, *Appl. Opt.*, Vol. 36, pp. 8595-8600 (1997).

[5] Eichhorn, M. Fluorescence reabsorption and its effects on the local effective excitation lifetime, Appl Phys B 369-377 (2009).

[6] Quimbye, R.S., Shaw, L.B., Sanghera, J.S. and Aggarwal, I.D. Modeling of Cascade Lasing in Dy:Chalcogenide Glass Fiber Laser With Efficient Output at 4.5 μm, IEEE Photonics Technology Letters 20, 123-125 (2007).

[7] Jackson, S.D. High-power and Highly efficient diode-cladding-pumped holmium-doped fluoride fiber laser operating at 2.94 μm, Opt. Lett. 34, 2327-2329 (2009).

[8] Li, J., Hudson, D.D. and Jackson, S.D. High-power diode-pumped fiber laser operating at 3 μm, Opt. Lett. 36, 3642-3644 (2011).

[9] Schneider, J., Carbonnier, C. and Unrau, U.B. Characterization of a Ho^{3+}-doped fluoride fiber laser with a 3.9-μm emission wavelength, Appl. Opt. 36, 8595-8599 (1997).

[10] Eichhorn, M. Quasi-three-level solid-state lasers in the near and mid infrared based on trivalent rare earth ions, Applied Physics B 93, 269-316 (2008).

[11] Barnes, N.P., Walsh, B.M. and Filer, E.D. Ho:Ho upconversion: applications to Ho lasers, J. Opt. Soc. Am. B 20, 1212-1219 (2003).

[12] Jackson, S.D. Towards high-power mid-infrared emission from a fiber laser, Nature Photonics 6, 423-431 (2012).

Chapter 4 – NON-LINEAR FIBERS

4.1 BACKGROUND AND PREVIOUS WORK

High brightness broadband sources in the 2 µm to 5 µm atmospheric window with good beam quality and small divergence are needed for spectroscopy and metrology as well as defence applications. Optical fibers are the most interesting technology for Supercontinuum (SC) generation because they permit confining the pump laser pulse into a very small area core and thus the laser pulse interacts with a non-linear medium (here the fiber glass) over a long distance with relatively low losses. Now, the majority of SC sources developed are based on silica fibers, for example [1]-[5]. Especially silica photonic crystal fibers are very unique media in which dispersion and non-linear properties can be tailored by a suitable design of their microstructures [6]. However, as a result of multi-photon absorption, spectral broadening in silica glasses is limited to below 3 µm [7], which makes them unsuitable for continuum generation in the Mid-Infrared (MIR) spectral band. Therefore, soft glasses including tellurite [8]-[10], chalcogenide [11]-[13], fluoride [14]-[16], and lead-bismuth-gallate [17] glasses have been adopted for MIR SC generation. Tellurite, fluoride and lead-bismuth-gallate glasses exhibit high optical transparency in the long-wavelength range of up to ~ 5 µm [8],[17],[18], while chalcogenide glasses are transparent even above 7 µm wavelength [19].

There have been several demonstrations of SC generation with soft glass optical fibers [2],[9],[15],[20]-[25]. SC sources using fluorozirconate based fibers have reached watt level powers, but are restricted to wavelengths below 4 µm when using long fibers. The intrinsic fiber loss due to the multi-phonon absorption edge in fluorozirconate-based fibers is the main limitation on the long-wavelength side for SC generation [26]. Emission beyond the multi-phonon absorption edge can be overcome using short lengths of fiber and high pump intensity and has been demonstrated also in telluride [9] and fluoride fibers [15], but requires the use of high peak power laser sources which are sensitive to mechanical vibrations and temperature fluctuations. On the other hand, micron-sized suspended core fibers offer the possibility to adjust the fiber dispersion and enhance the SC generation; however, these small core fibers cannot sustain high average laser powers. Chalcogenide fibers are chemically stable to air humidity and their non-linear responses is about 500 times higher than fluoride glasses [27]-[30], but their damage threshold is lower than fluoride glasses. Usually, the chalcogenide fiber damage threshold is about 10 times lower than for fluoride fiber which is an important issue when multi-watt average power is required at the output of a single-mode fiber. The proper fiber for the conception of a ruggedized multi-watt SC fiber source into the 2 µm to 5 µm atmospheric windows is explored intensively by many research groups and the recent progresses in fiber technologies indicate that such objectives should be reached in a near future.

SC generation in soft glass fibers is a relatively new research domain and the number of research groups dealing with this topic is still very small. Nevertheless, the results already achieved are very impressive and promising regarding practical applications of SC sources. A very important issue for MIR SC sources ($\lambda > 2$ µm) is the efficiency of SC power distribution towards red wavelengths in relation with the wavelength of pump signal. It directly affects their practical usage in such areas as direct infrared countermeasure or infrared spectral fingerprinting. In this section, we review 3 main techniques for mid-infrared SC generation, i.e. in step-index ZBLAN fibers, in step-index chalcogenide fibers, and in Tellurite fibers. Others micro-structured fibers or exotic glasses are not considered here because the achieved output power is generally low, i.e. less than 100 mW in the MIR spectral range. For this review, Table 4-1 points out the main results published in the literature before the NATO SET-170 started in September 2010 with the emphasis on the results having the highest average power and/or the broadest MIR spectrum. On the other hand, Table 4-2 presents the MIR supercontinuum parameters for the most powerful laser sources developed by various groups during the 3-year mandate of the NATO SET-170. By comparing the data of both tables, we clearly see a rapid increase of the MIR supercontinuum bandwidth and its average power during the last few years. It is interesting to note that the members of the NATO SET-170 obtained similar results that the one listed in Table 3-1 for the ZBLAN fibers while it is Dr. Sanghera's group (member of NATO SET-170) that obtained the highest average power and the broadest supercontinuum in chalcogenide fibers [31].

Table 4-1: Parameters of Supercontinuum Fiber-Based Laser Sources Prior to NATO-SET-170.

Fibers	References	Total Average Power	Spectral Width	MIR Power	
				> 2 µm	> 3 µm
Step-Index ZBLAN	[32]	1.3 W	1.95 – 2.55 µm	~ 0.6 W	~ 0.2 W
	[33]	10.5 W	0.8 – 4.2 µm	~ 5 W	~ 1.1 W
Step-Index Chalcogenide	[34]	0.04 W	1.2 – 2.5 µm	~ 0.0001 W	N/A
Tellurite Fiber	[9]	0.09 W	0.8 – 4.8 µm	~ 0.01 W	~ 0.006 W

Table 4-2: Parameters of Supercontinuum Fiber-Based Laser Sources Developed by Various Groups During the Mandate of the NATO-SET-170.

Fibers	References	Total Average Power	Spectral Width	MIR Power	
				> 2 µm	> 3 µm
Step-Index ZBLAN	[35]	3.9 W	0.75 – 4.3 µm	~ 2.5 W	1.3 W
	[23]	2.6 W	1.9 – 4.5 µm	~ 2.5 W	~ 1 W
	[36]	7.1 W	1.9 – 3.9 µm	~ 6.5 W	~ 2.5 W
Step-Index Chalcogenide	[31]	0.56 W	1.9 – 4.8 µm	~ 0.55 W	~ 0.18 W
Tellurite Fiber	[37]	0.1 W	0.9 – 4.2 µm	N/A	N/A

In order to achieve significant spectral broadening, the zero Group Velocity Dispersion (GVD) of the fiber should be close to the center wavelength of the laser pulse used for SC generation, with the laser wavelength slightly shifted towards the anomalous GVD regime. This minimizes the walk-off between the different regions of the generated spectrum, allowing for further spectral broadening [38]. The GVD of a fiber is first determined by its core material and the diameter of the fiber core. Depending of the refractive indexes of the glass used for the fiber, the fiber GVD is very similar to the glass GVD when its core diameter is larger than ~ 10 µm. For smaller core, the waveguide dispersion tends to shift the zero GVD wavelength towards shorter wavelengths. Such tendency explains the development of microstructured core fibers in order to match the zero GVD wavelength of the fiber with the central wavelength of ultrashort and powerful lasers for the generation of supercontinuum.

For all the results presented above in Table 4-1 and Table 4-2, the supercontinuum generation is generally initiated by self-phase modulation and four-wave mixing which induce primarily the spectral broadening before higher order dispersion causes fission of the laser pulse. After the fission of the laser pulse into multiple solitons, the individual solitons redshift by the Raman self-frequency shift effect and emit phase-matched dispersive waves at wavelengths shorter than the zero GVD [39]. All these non-linear effects are intensity dependent, therefore the fiber core diameter, the fiber dispersion, the initial laser pulsewidth and peak power are important parameters that directly impact the supercontinuum efficiency.

From the results presented in Table 4-1 and Table 4-2 there is a very interesting approach to generate SC in a tandem of silica and fluoride fibers which was proposed by Xia et al. [32],[33] – a technique permitting to eliminate the need of using high peak power mode-locked lasers. The SC generation was initiated by the breakup of amplified nanosecond pulses in a piece of conventional silica Single-Mode Fiber (SMF) into a train of soliton-like sub-pulses through Modulation Instability (MI) and then, as a result of Raman scattering, the spectrum was further broadened in a ZBLAN fiber to over ~ 4 μm wavelength. A unique feature of this solution, differencing it from the other approaches mentioned above, is the possibility of boosting the output average power while keeping the spectrum shape and width relatively constant. The group has already presented the linear scaling up of the average output power to 10.5 W with a spectrum of ~ 0.8 μm to 4 μm using erbium and erbium:ytterbium power fiber amplifiers [33] as well as 5.3 W in a continuum extending from ~ 1.9 μm to 4.5 μm when applying an additional amplification stage based of Tm-doped fibers [23].

In the following sections, we present different experimental schemes for supercontinuum generation obtained by the NATO SET-170 Task Group members. In Section 4.2.1 we demonstrate broadband and powerful supercontinuum generation in step-index ZBLAN fiber. Supercontinuum generation in chalcogenide fiber is also presented in Section 4.2.2, and finally, Section 4.2.3 presents recent results on supercontinuum generation in Indium fluoride-based fibers.

4.2 EXPERIMENTAL RESULTS

4.2.1 Supercontinuum Generation in ZBLAN Fibers

4.2.1.1 Three-Octave Spanning Supercontinuum Generated in a Fluoride Fiber Pumped by Er and Er:Yb-Doped and Tm-Doped Fiber Amplifiers

Contributors to this section: Jacek Swiderski[1], Maria Michalska[1]

From: Optics & Laser Technology 52, 75-80 (2013)

In this section we demonstrate broadband 0.9 – 3.6 μm supercontinuum generation with 0.66 W of output power, using a single-mode fluoride (ZBLAN) fiber pumped by 1.55 μm nanosecond pulses amplified in a cascade of fiber amplifiers. Expanding the pump source by adding an additional amplification section based on thulium-doped fibers, the long-wavelength edge of the spectrum was shifted to ~ 4 μm and was limited by intrinsic losses of the used non-linear ZBLAN fiber. For this cases, the average SC power as high as 288 mW was recorded, of which 266 mW (92%), 167 mW (58%) and 60 mW (21%) corresponds to wavelengths longer than 2 μm, 3 μm and 3.6 μm, respectively.

4.2.1.1.1 SC Generation with the Use of 1.55 μm Fiber Amplifier

The SC generator schematic is shown in Figure 4-1. The pump source was arranged as a fiber MOPA system consisting of a seed and a cascade of three fiber amplifiers. The MOPA output was directly spliced to a piece of SMF followed by a single-mode ZBLAN fiber.

[1] Institute of Optoelectronics, Military University of Technology, 2 Kaliskiego Street, 00-908 Warsaw, Poland.

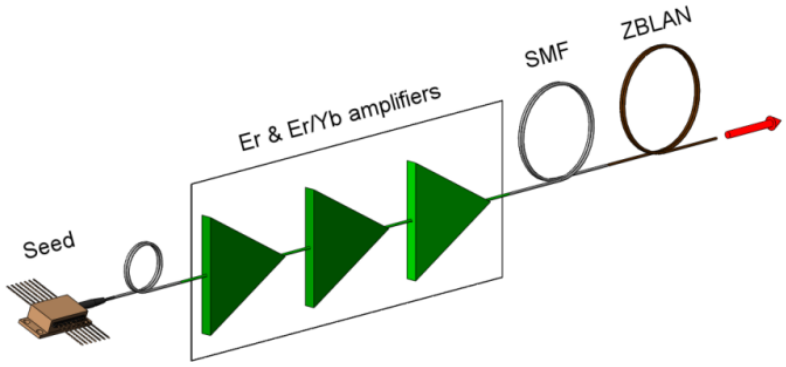

Figure 4-1: Set-Up of SC Source Pumped by a 1.55 µm MOPA.

A 1549.5 nm Distributed Feedback (DFB) laser was used as a seed of ~ 1 ns pulses generated at the Pulse Repetition Frequency (PRF) of 200 kHz. The average output power for this duty cycle was 3 µW, which corresponds to the pulse energy and pulse peak-power of 15 pJ and 15 mW, respectively. Such a pulse train was amplified in a three-stage fiber amplifying cascade, formed by two erbium preamplifiers (EDFAs) and a booster erbium/ytterbium amplifier (EYDFA).The EDFAs utilized single-mode, single-clad erbium-doped fibers with the core diameter of 4 µm and they were pumped by up to 1.5 W of total power at 976 nm wavelength. The booster amplifier was made with the use of 2.4-m long Er:Yb-co-doped double-clad fiber characterized by 6.5 µm / 0.19 NA core and 125 µm / 0.45 NA octagonal clad pumped in counter-propagating scheme (via a multi-mode pump power combiner) by a fiber-coupled laser diode delivering of up to 10 W of continuous power at a wavelength of 976 nm. The power amplifier provided gain of up to 12.5 dB. To block any back reflections, each laser system stage was optically isolated. Also, to eliminate the out-of-band amplified spontaneous emission generated by the active ions, the 100 GHz band-pass filters were used. The entire system provided up to 58.5 dB of total gain. All the SC system components were fusion spliced, thus providing an all-fiber architecture.

The fiber MOPA output (that is 0.5-m long output fiber pigtail of the pump combiner used in the construction of EYDFA) was fusion spliced with a standard SMF-28 having a length of ~ 2.5 m. Finally, the laser radiation coming out of the SMF was launched via bulk optics to a ZBLAN fiber with a ~ 55% efficiency. The 20-m long ZBLAN fiber, with attenuation curve shown in Figure 4-2, had a core/clad diameter of 7/125 µm and a NA of 0.23. The ZDW and cut-off wavelength of this fiber were 1.9 µm and 2.04 µm, respectively.

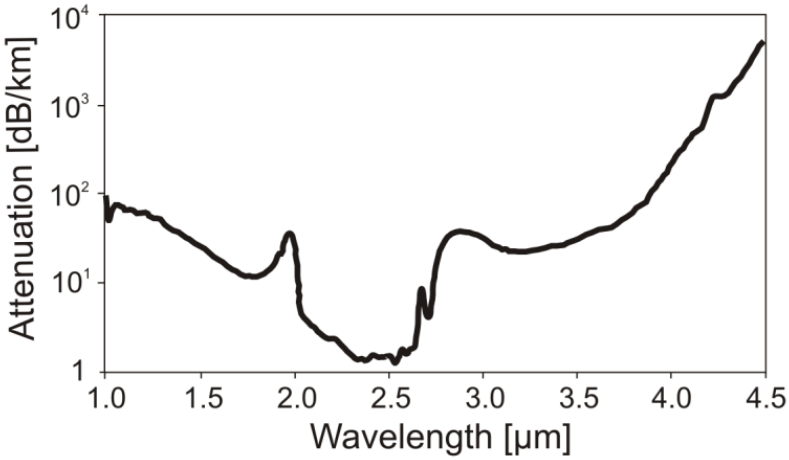

Figure 4-2: Attenuation of the ZBLAN Fiber.

Output SC spectra from 0.6 to 2.4 µm wavelength were measured by using two optical spectrum analyzers whereas the longer wavelengths were recorded with a grating monochromator and a HgCdTe detector. Then the measured spectra were spliced together. The output average SC power was measured by a power meter (Ophir, Laserstar) with thermal sensor (response range of 0.19 to 20 µm).

4.2.1.1.2 SC Generation with the Use of Tm-Doped Fiber Amplifier

The principle scheme of the SC laser source built with the use of Tm^{3+}-Doped Fiber Amplifiers (TDFAs) is shown in Figure 4-3. A significant part of the system is based on the MOPA described in Section 4.2.1.1.1. In this approach, two TDFAs were added.

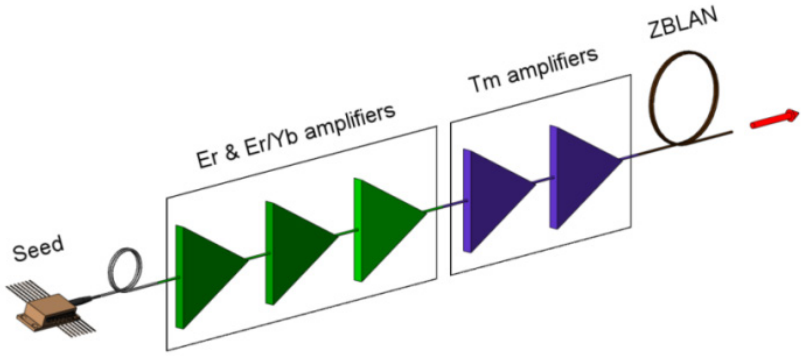

Figure 4-3: Set-Up of SC Source Pumped by Tm-Fiber Amplifiers.

The MOPA fiber output was spliced to a 1-m long single-mode double-clad Tm^{3+}-Doped Fiber (TDF) (dopant concentration, 2 wt. %) with core/clad diameter of 10/130 µm and corresponding NA of 0.15/0.46. It was core-pumped by the 1.55 µm signal coming out of the Er and Er:Yb amplifiers. Then the output from the first TDF was launched into the second 2.5-m long TDF with the same parameters as defined above. It was cladding pumped (in forward configuration) via a (2 x 1) + 1 pump combiner combining two fiber-pigtailed 4.75 W 790-nm pump laser diodes with 105 µm core diameter and 0.22 NA. The fiber end was angle-cleaved to prevent any back reflections. Like in the previous set-up, all the SC system components were fusion spliced to provide an all-fiber format. Finally, the signal amplified and initially broadened in a cascade of TDFAs was launched into the ZBLAN fiber with the use of a telescope allowing for coupling efficiency of ~ 60%. Since fluoride glass has a much lower melting point of about 260°C than silica glass (~ 1200°C), it was not possible to directly fusion splice the two fibers. Both ends of the fluoride fiber as well as the output fiber end of the second TDFA were polished at an angle of 8° to avoid any back reflections.

4.2.1.1.3 SC Generation with the Use of 1.55 µm Fiber Amplifier

The maximum average output power provided by the MOPA system, measured at the SMF output, was 1.56 W. About 0.85 W of this power was coupled into the ZBLAN fiber indicating to ~ 55% launching efficiency. The output SC power as a function of launched pump power is shown in Figure 4-4.

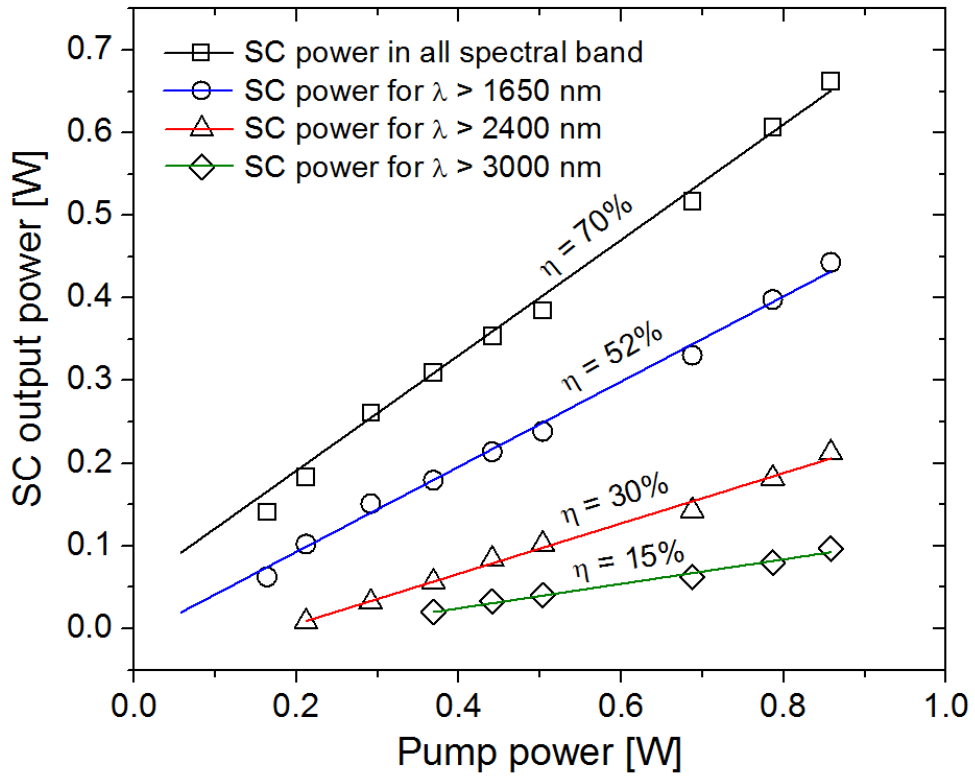

Figure 4-4: Average SC Output Power as a Function of Incident Pump Power (η – Slope Efficiency).

The output power increases linearly with the increase in pump power and was only limited by the available pump power. For 0.86 W of the pump power the SC power as high as 0.66 W in the whole wavelength range with a slope efficiency of 70% was recorded. A distribution of SC power in different spectral bands is presented in Table 4-3. It can be noticed that over 60% of the power corresponded to wavelengths longer than 1.65 µm and 15% (0.1 W) of the power was detected for wavelengths longer than 3 µm.

Table 4-3: SC Power Distribution in Different Spectral Bands.

Spectral Range	Output Power	% of Output Power
All Range	0.66 W	100%
λ > 1.65 µm	0.44 W	66.7%
λ > 2.4 µm	0.21 W	31.8%
λ > 3 µm	0.10 W	15.2%

The measured SC output spectra, recorded for selected pump power levels and corrected for the spectral responsivity of the HgCdTe detector and the monochromator gratings response are presented in Figure 4-5. The inset in each figure depicts the spectrum of light generated at the SMF output. For pump power of 150 mW the output SC spectrum with a characteristic peak at 1.55 µm spreads from ~ 1.4 µm to 1.9 µm (Figure 4-5(a)). In the spectrum of pump signal, presented in the inset, two sets of side lobes spaced symmetrically from the signal at 1550 nm by ~ 25 nm can be distinguished. This spectral signature is characteristic for MI process leading to the break of pump pulses propagating through the SMF into many

shorter sub-pulses and consequently, to the spectrum broadening along with increasing the pump power [34]. Applying the pump power of 300 mW results in the spectrum broadening from ~ 1.4 µm to 1.9 µm and from ~ 1 µm to 3 µm, measured after SMF and ZBLAN fiber, respectively (Figure 4-5(b)). The output SC power for this case was 260 mW. Further increase in pump power leads to further broadening of the output spectrum. For the maximum applied pump power of 860 mW, the 3-octave spanning (from ~ 0.9 µm to 3.6 µm) SC output spectrum generated out of the ZBLAN fiber was obtained (Figure 4-5(d)). It is worth noting here that the pump signal propagating in the SMF was broadened to ~ (1.4 – 2.2) µm. A 10 dB level flatness was obtained in the wavelength interval from ~ 1 µm to 2.7 µm (1700 nm of spectral span). Assuming 20 dB changes in intensity distribution, the spectrum spreads from ~ 1 µm to 3.45 µm (span of 2450 nm). One can see that the intensity falls rapidly for wavelengths longer than 3.4 µm, which can be attributed to the increase in the fluoride fiber attenuation (Figure 4-2).

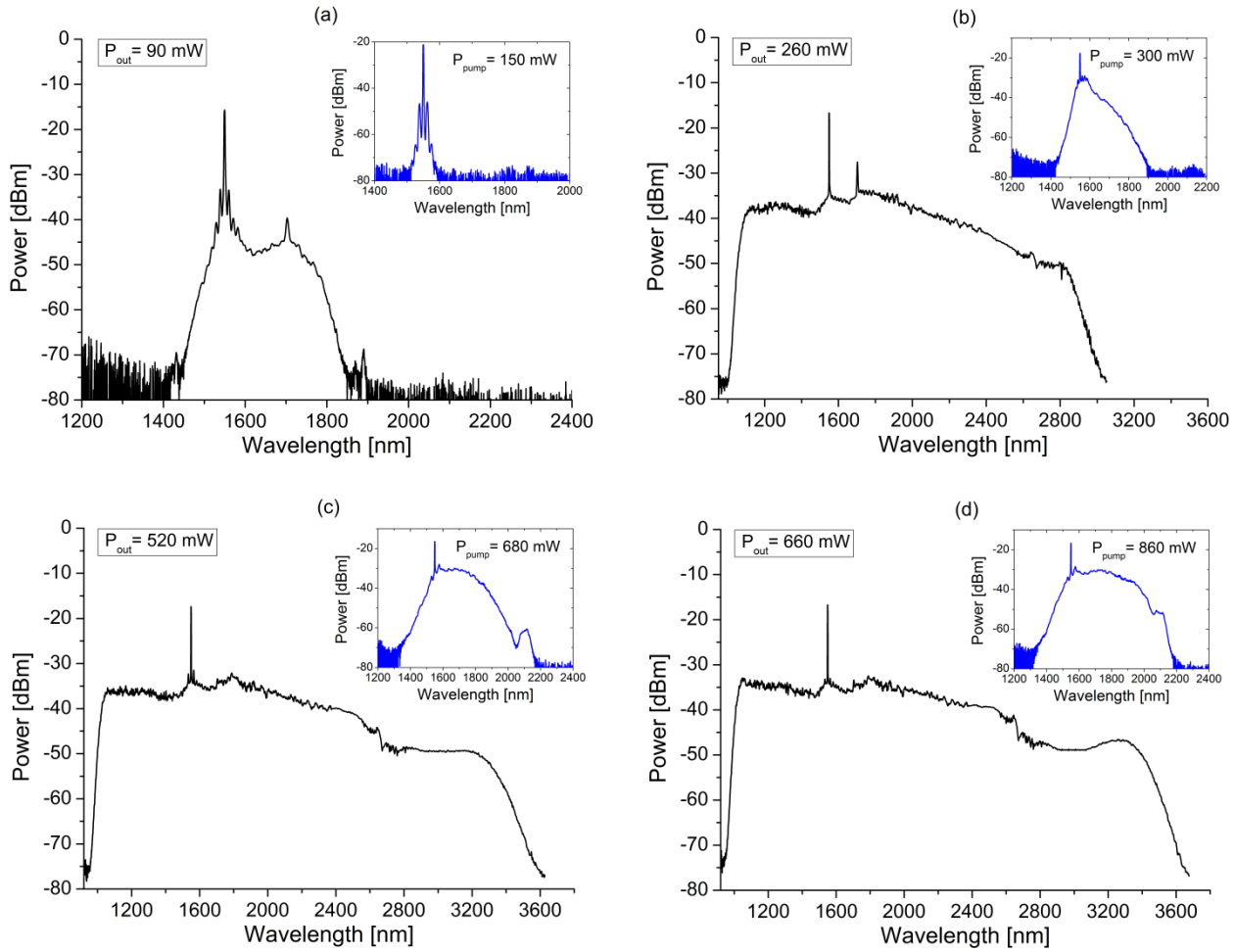

Figure 4-5: Evolution of Output SC Spectrum with Pump Power. Power launched into the ZBLAN fiber: 150 mW (a), 300 mW (b), 680 mW (c), 860 mW (d). Insets present spectrum generated at the SMF output.

As it was mentioned earlier, the initial spectrum broadening in the SMF is caused by MI effect and Soliton Self-Frequency Shift (SSFS) [16],[40],[41]. In the fluoride fiber, the SSFS phenomenon is also responsible for further broadening the spectrum towards longer wavelength while SPM is responsible for blue-shifting of the spectrum [40].

4.2.1.1.4 SC Generation with the Use of Tm-Doped Fiber Amplifier

The general concept of the second experiment was to extend the output SC spectrum only towards mid-IR ($\lambda > 2$ µm). Like in, for example [42]-[44], the active fibers played a role of both non-linear and amplification media. The power of signal initially broadened into the SMF (as high as 0.89 W, of which 58 mW corresponded to $\lambda > 2.4$ µm) was launched to the core of the first TDFA. It allowed absorbing of almost entire pump radiation at 1550 nm and its Raman-scattering components of the wavelength < 1.8 µm by Tm^{3+} ions and finally converting it into longer wavelengths lying in amplification bands of TDF (the first one extends from ~ 1.8 µm to 2.1 µm and the second one from ~ 2.2 µm to 2.5 µm). Applying a Tm-doped fibers as non-linear media allowed us to extend the spectrum from ~ 1.8 µm to ~ 2.7 µm at 40 dB below the peak with 2.37 W for $\lambda > 1.65$ µm and 0.49 W for wavelength beyond 2.4 µm. This spectral extension can be attributed to parallel amplification in both emission bands of Tm^{3+} ions in a silica host. Detailed description of the results can be found in [2]. The radiation generated out of the second TDFA was coupled to the ZBLAN fiber, the same as described in Section 4.2.1.1.1, by bulk optics allowing for launch efficiency of 60%.

The output SC power versus the launched pump power is shown in Figure 4-6. The output power increases linearly along with the pump power increase. The total SC average power of 288 mW is achieved for the launched power of 790 mW. By using different long-pass filters cutting below 1.65, 2, 2.4, 3 and 3.6 µm, it was possible to determine the SC power distribution in different spectral bands, as is presented in Table 4-4. The power as high as 266 mW constituting 92% of total SC output power corresponds to mid-IR spectral band ($\lambda > 2$ µm). The pump-to-signal conversion efficiency was 22.9% with respect to the launched pump power. The power of over 160 mW (58% of total SC output power) lies in wavelengths beyond 3 µm leading to an efficiency of 18.6%.

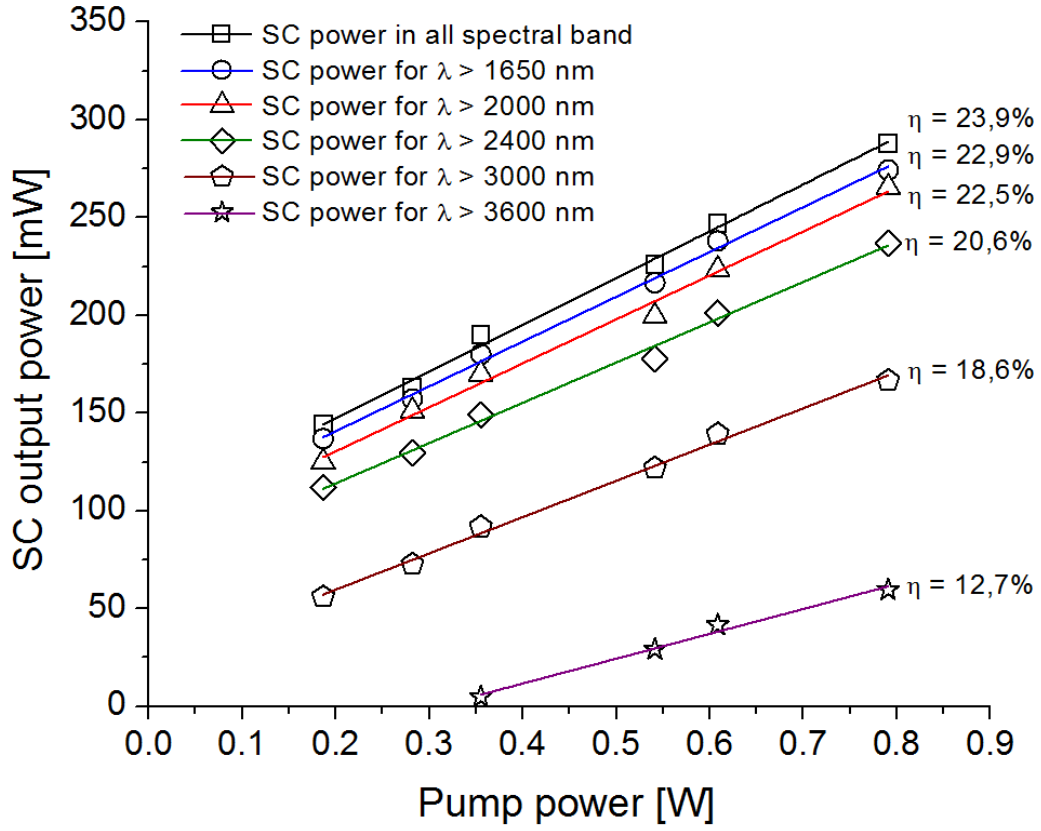

Figure 4-6: Average SC Output Power vs. Launched Pump Power (η – Slope Efficiency).

Table 4-4: SC Power Distribution in Different Spectral Bands.

Spectral Range	Output Power	% of Output Power
All range	288 mW	100%
$\lambda > 1.65$ µm	274 mW	95%
$\lambda > 2.0$ µm	266 mW	92%
$\lambda > 2.4$ µm	240 mW	83%
$\lambda > 3.0$ µm	167 mW	58%
$\lambda > 3.6$ µm	60 mW	21%

The evolution of SC spectrum generated in the fluoride fiber is depicted in Figure 4-7. The inset shows the spectrum generated by the second TDFA at its maximum performance. Higher power generated by the cascade of TDFAs corresponds to higher average SC output power and larger SC spectrum extension limited by fluoride glass transparency. As can be seen, the spectrum spreads from ~ 0.9 µm to 4 µm, however, it is mostly broadened towards infrared wavelengths. The spectrum covers the range of ~ (1.9 – 3.8) µm constituting an octave-spanning mid-IR SC when measured within -25 dB level with respect to the maximum peak. The dip in the spectrum around 2.7 – 2.9 µm corresponds to OH ions absorption in the medium. Another characteristic feature of the spectrum is that it reveals a maximum peak at ~ 3.7 µm, which shows that the light was efficiently converted towards mid-IR (58% of total output power was recorded for $\lambda > 3.0$ µm) and further spectral broadening was difficult due to the rapidly increasing fiber attenuation > 100 dB/km at ~ 4 µm and > 1000 dB at 4.5 µm (Figure 4-2), caused longer wavelengths generated in a 20-m long fluoride fiber to be highly attenuated preventing red wavelengths cut-off extension. Besides, a fiber bend-induced loss contributed to the overall attenuation due to the fluoride fiber was coiled on a 20 cm diameter spool.

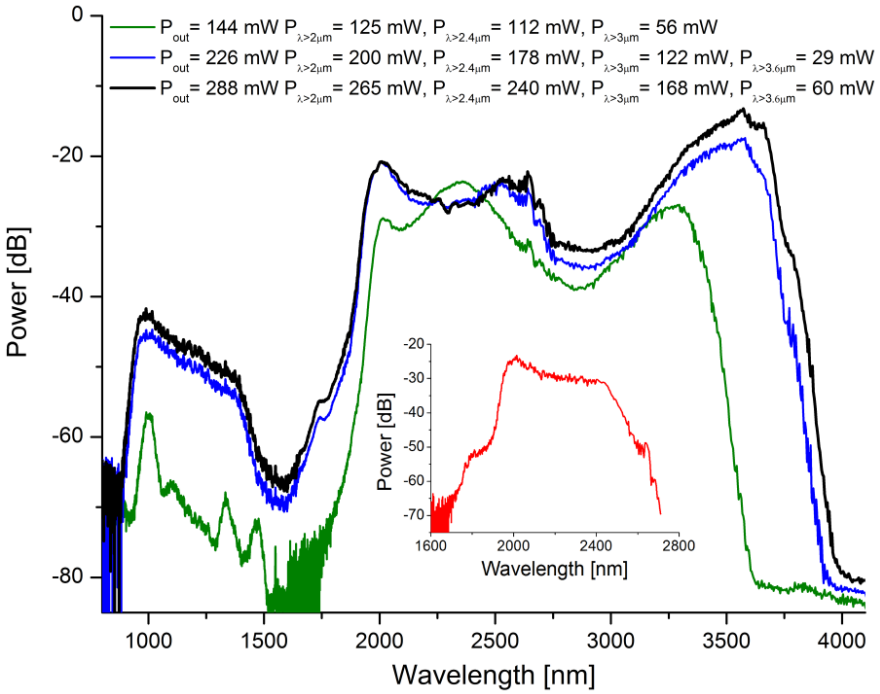

Figure 4-7: SC Spectrum After Propagation Through ZBLAN Fiber, for Selected Values of Output Power. Inset: Spectrum generated by cascade of TDFAs (pump signal) at its maximum performance.

The ZBLAN fiber used has its ZDW at ~ 1.9 µm so that it was mostly pumped in anomalous Group Velocity Dispersion (GVD) region, which means that the main non-linear process leading to spectrum extension is MI effect responsible for solitons formation and soliton self-frequency shift [16],[40]. As the MI process is noise driven, a distribution of many solitons, with different energies are created, resulting in different rates of self-frequency shifting. They are additionally broadened by Self-Phase Modulation (SPM) and Cross-Phase Modulation (XPM) making the SC spectrum relatively smooth and flat. However, as can be seen in Figure 4-7, the spectrum also broadens towards shorter wavelengths (in the band of ~ 0.9 to 1.6 µm) with the average power of 14 mW (only 5% of total output power). It is associated with generation of phase-matched dispersive waves at wavelengths shorter than the ZDW accompanying the MI-induced solitons propagating in the fiber [45]-[47].

In conclusion, we report broadband low-power SC generation in a single-mode fluoride (ZBLAN) fiber with a core/clad diameter of 7/125 µm. When the fiber was pumped by 0.86 W of average power delivered by the 1.55 µm MOPA system, the produced continuum covered 3 octaves from ~ 0.9 µm to 3.6 µm with 0.66 W of average output power. Expending the pump system by applying a cascade of TDFAs providing the average output power as high as 2.37 W in a spectral band of ~ (1.75 – 2.7) µm it was possible to extend the spectrum generated in the ZBLAN fiber from ~ 0.9 µm to 4 µm. The average power as high as 288 mW was recorded, of which 266 mW corresponded to wavelengths longer than 2 µm. Contrary to the first experiment, the output spectrum was mainly distributed towards mid-infrared, the -25 dB bandwidth (measured from the top peak) covers the span of 1900 nm, from ~ 1.9 µm to 3.8 µm.

The difference in the spectrum evolution between the two experiments carried out can be attributed to different spectral bands of the pump signal. In case of the first system, significant part of the pump was located in the normal GVD region of the ZBLAN fiber thus supporting the spectrum extension towards shorter wavelengths with much contribution from SPM. Contrary to that, the second system was mostly pumped in anomalous GVD region and the output spectrum extended mainly towards mid-IR, as a result of Raman induced scattering.

4.2.1.2 Mid-IR Supercontinuum Generation in a ZBLAN Fiber Pumped by a Gain-Switched Tm-Doped Fiber Laser and Amplifier System

Contributors to this section: Jacek Swiderski[2], Maria Michalska[2], Gwenael Mazé[3], Christelle Kieleck[4], Marc Eichhorn[4]

In this section, covered partly in *Optics Express* 21, pp. 7851-7857 (2013), we demonstrate a novel method of Mid-Infrared (MIR) Supercontinuum (SC) generation with the use of a 2 µm gain-switched thulium-doped fiber laser. SC radiation ranging from ~ 1.8 µm to 4.15 µm, generated in a single-mode ZBLAN fiber with a zero-dispersion wavelength (ZDW) shifted to ~ 1.9 µm, is reported. An average output power of 1.25 W with 0.6 W at wavelengths longer than 2.4 µm was measured. It is, to the best of our knowledge, the first report on such an approach to generate a MIR SC in fluoride fibers.

4.2.1.2.1 SC Experimental Set-Up

The SC source consists of a 1.55 µm fiber MOPA, a gain-switched Thulium-Doped Fiber Laser (TDFL) and a Thulium-Doped Fiber Amplifier (TDFA). The principal scheme of this configuration is shown in Figure 4-8.

[2] Institute of Optoelectronics, Military University of Technology, 2 Kaliskiego Street, 00-908 Warsaw, Poland.

[3] Le Verre Fluoré, Campus KerLann, F-35170 Bruz, Brittany, France.

[4] French-German Research Institute of Saint-Louis ISL, 5, rue du Général Cassagnou, B.P. 70034, 68301 Saint-Louis Cedex, France.

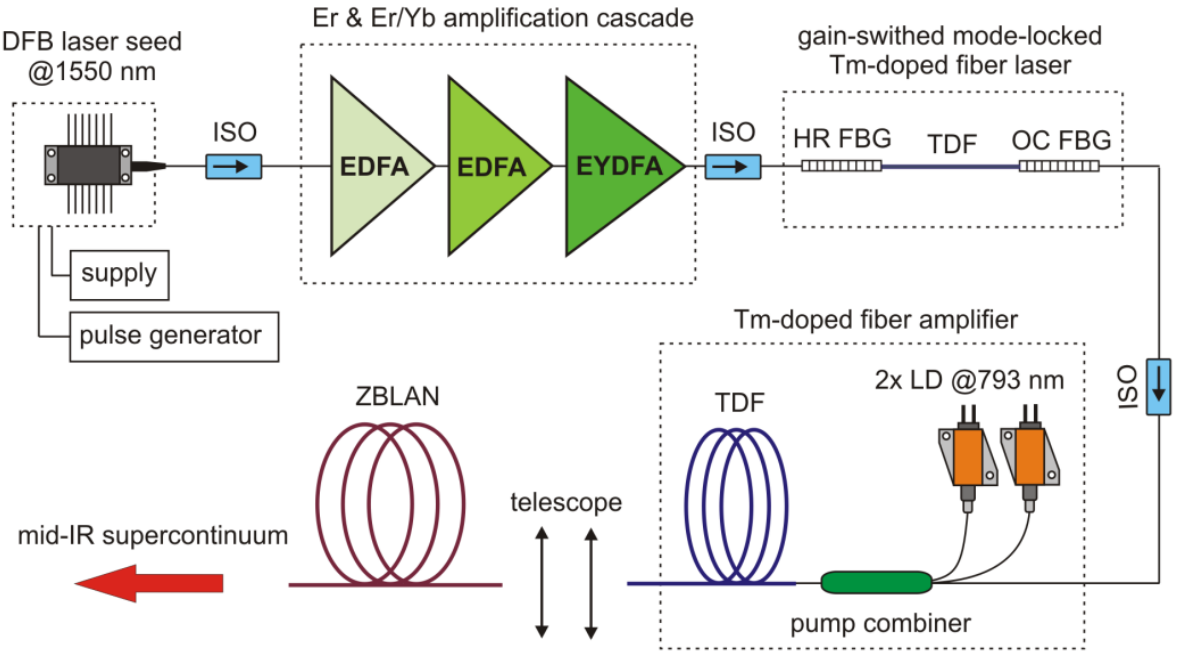

Figure 4-8: Block Diagram of Fiber Mid-IR SC Source. ISO – Optical Isolator.

To obtain a stable pulse train, fast gain-switching and resonant pumping are required. In-band pumping ensures a rapid population inversion that can be depleted by a single short gain-switched pulse. Then the cross-relaxation and excited state absorption processes can be reduced leading to generation of stable, short 2-µm pulses, as was shown in [48]. Furthermore, in gain-switched TDFLs, an output pulse duration is determined by an active medium gain and the round-trip time, which means that the length of active fiber directly affects output time characteristics of a laser. In such a situation, only core-pumping can provide a suitable gain while keeping a resonator length short and thus supports generation of short (tens of ns) pulses [48]. For this reason, a ~ 20-cm long, single-mode double-clad, Tm-doped (~ 2 wt. %), silica fiber (TDF) was used as an active medium of the GSML laser. It had a 10/130 µm core/clad diameter and a corresponding numerical aperture NA of 0.15/0.46. The active fiber was core-pumped by a 1.55 µm fiber MOPA system, delivering pulses of 20 – 700 ns duration at the frequency independently changeable in the range from 26 to 320 kHz.

The MOPA system consisting of a DFB laser seed followed by a cascade of Erbium- and Erbium:Ytterbium-Doped Fiber Amplifiers (EDFA and EYDFA) was capable to deliver pulses with energy of several tens of µJ and average power of up to 3.5 W. About 90% of pump power was absorbed by the active dopant. The output from the MOPA system was directly spliced to the pigtail of a 3-cm long High Reflector (HR) Fiber Bragg Grating (FBG). The laser cavity was formed by a HR FBG having a reflectivity of > 99% at 1994.5 nm, and an Output Coupler (OC) FGB with a reflectivity of 90% at 1994.6 nm and a 3 dB reflection bandwidth of 1.5 nm. The FBGs were cleaved and fusion spliced very close to the active fiber to keep the resonator short. In the next step, the TDFL output was optically isolated and spliced to an input of TDFA that was built with the use of ~ 2.5-m long TDF, characterized by the same parameters as mentioned above. The amplifier was cladding-pumped by two fiber-pigtailed 4.75 W 790-nm pump laser diodes with 105 µm core diameter and 0.22 NA via a (2 x 1) + 1 pump combiner with a signal feedthrough. Finally, the 2 µm amplified pulse train was launched into a ZBLAN fiber with the use of a telescope allowing for coupling efficiency of ~ 60%. The 20-m long ZBLAN fiber (manufactured by Le Verre Fluoré) had a core/clad diameter of 7/125 µm and a NA of 0.23. The ZDW and cut-off wavelength of this fiber were 1.9 µm and 2.04 µm, respectively. Both ends of the fluoride fiber as well as the output fiber end of the TDFA were polished at an angle of 8° to avoid any back reflections.

The benefit of using the GSML Tm^{3+}-doped fiber laser as a pump source is the lower cost and reduced complexity of the system, compared to, for example Q-switched or QML lasers. Besides, comparing with CW pumping scheme, the increased peak power of self-mode-locked pulses, amplified in a chain of fiber amplifiers, can eliminate the critical dependence on the ZDW, as it was reported in [49].

SC spectrum from 1.2 µm to 2.4 µm wavelength was measured by using an Optical Spectrum Analyzer (OSA), whereas the longer wavelengths were measured with a grating monochromator and a thermoelectrically cooled HgCdTe detector. A sampling digital oscilloscope with 6 GHz bandwidth and two detectors with rise/fall time of < 35 ps were used to measure time characteristics.

4.2.1.2.2 Experimental Results and Discussion

The gain-switched TDFL was pumped by ~ 100 ns 1.55 µm pulses with the energy of up to 80 µJ at the Pulse Repetition Frequency (PRF) ranging from 26 to 40 kHz. After reaching the lasing threshold, the 2 µm output pulses of long duration appeared and with the increase in pump power both the pulse build-up time and pulse width shortened. Further increase in pump energy led to Mode-Locked Resembling (MLR) operation with a full modulation depth, which is shown in Figure 4-9.

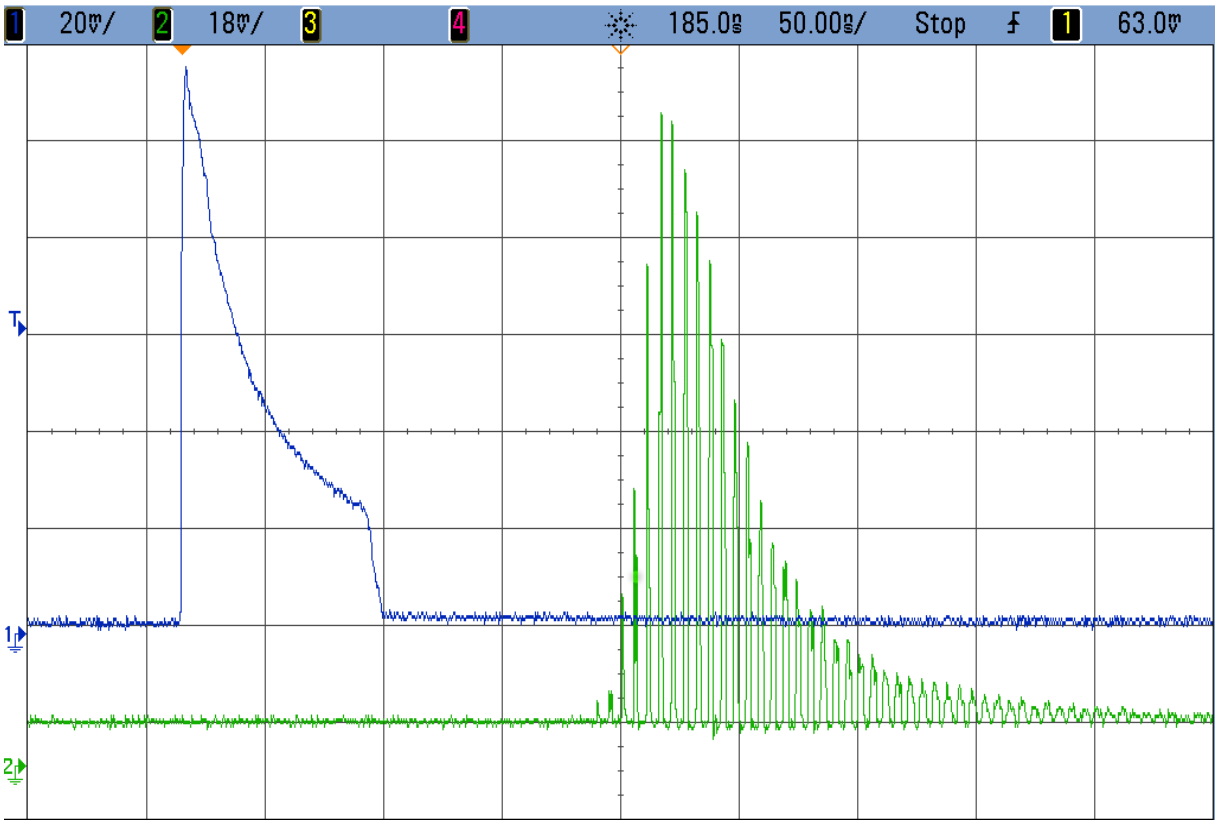

Figure 4-9: An Example of Oscilloscope Picture of Recorded Gain-Switched Mode-Locked-Like Output Laser Pulse. Trace 1 (upper) – pump 1.55 µm pulse; Trace 2 (lower) – output 2 µm laser pulse.

The envelope width of the gain-switched pulse was ~ 50 ns, whereas the duration of the most intensive sub-pulses was 200 – 300 ps (190 MHz spectral space), the time of which is much shorter than the laser cavity round-trip time (5.3 ns). The mode-locking depth as well as the exact form of generated pulse train was strictly dependent on the pumping conditions (PRF, pump pulse width and shape, pump pulse energy).

We believe that the origin of self-starting MLR operation in our gain-switched fiber laser is the beating effect of laser longitudinal modes [50].

In the next step, the MLR pulses from the gain-switched fiber laser (presented in Figure 4-9) were boosted in the TDFA. Figure 4-10 shows the evolution of output average power at 2 µm for the PRF of 26 kHz and 40 kHz as a function of TDFA pump power. For 26 kHz (Figure 4-10(a)), the average power of 2.3 W, with corresponding 88 µJ energy in 50 ns duration gain-switched pulse was measured. Increasing the PRF to 40 kHz results in average power scaling up to 2.6 W with a corresponding pulse energy of 65 µJ (Figure 4-10(b)). The amplifier operated with a 26.5% and 31% slope efficiency for 26 kHz and 40 kHz, respectively.

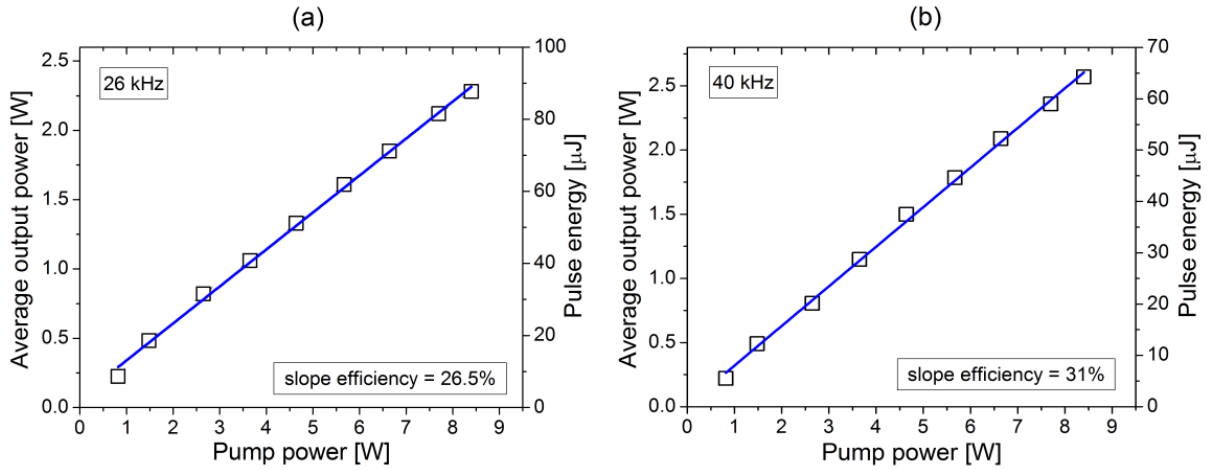

Figure 4-10: Average Output Power at 2 µm Wavelength for 26 kHz (a) and 40 kHz (b) vs. Launched TDFA Pump Power.

Figure 4-10 presents pulse energy and peak power for selected MLR pulses in a 50-ns gain-switched envelope for the PRF of 26 kHz. The inset presents a typical MLR pulses within an envelope of a gain-switched pulse. During the experiment we did not carry out autocorrelation measurements and the pulse structure was recorded with the use of a sampling oscilloscope and a fast photodiode and then analyzed in OriginPro software. The timing of the sub-pulses was slightly unstable, owing to amplitude fluctuations of 1.55 µm pump pulses. Furthermore, we also noticed that careful adjustment of the pump power and the pump pulse time characteristic led to the improvement of output pulse structure stability.

As can be seen in the inset in Figure 4-11, the width of the first and last sub-pulses was longer than those in the center of the gain-switched envelope. The highest peaks were characterized by the shortest duration and thus the highest peak-power. The generated pulse train consisted of ~ 15 – 20 sub-pulses. The maximum energy of the gain-switched pulse (calculated by dividing the average output power by the PRF) was 88 µJ, whereas the energies of three highest MLR peaks (marked in the inset as 4, 5 and 6) were 8.3 µJ, 13.7 µJ and 15.7 µJ (with corresponding peak power of 22.2 kW, 24.7 kW and 27.8 kW), respectively.

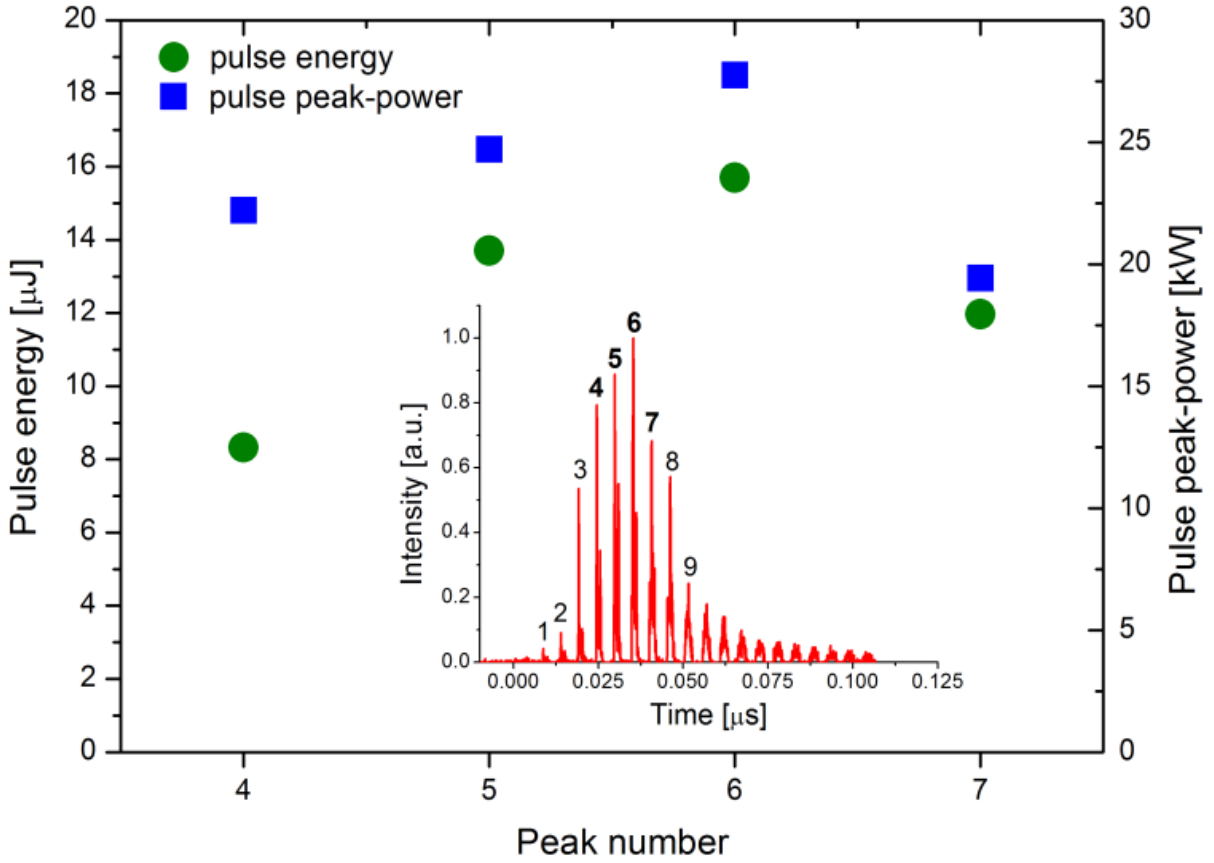

Figure 4-11: Pulse Energy and Peak Power for Selected MLR Sub-Pulses in a Gain-Switched Pulse Envelope (Inset).

Finally, the amplified pulse train was launched into the ZBLAN fiber with ~ 60% coupling efficiency. As was mentioned earlier, the fluoride fiber had the ZDW at 1.9 μm in order to be pumped in anomalous dispersion region but relatively close to the ZDW, which facilitates spectral broadening towards mid-IR [40]. The output SC power as a function of launched pump power, for both PRFs applied, is shown in Figure 4-12. The output power increases linearly with the increase of pump power and was only limited by the available pump power. For instance, for 26 kHz increasing the incident pump power to 1.23 W results in the total SC power of 0.74 W, out of which 0.27 W is in the wavelength range beyond 2.4 μm. Over 0.12 W was detected for $\lambda > 3$ μm. When operating at 40 kHz, the output power was as high as 0.9 W, where 240 mW and 86 mW were measured for $\lambda > 2.4$ μm and 3 μm, respectively. The slope efficiency η of generated SC in all spectral SC band was 62.8% and 60% for the PRF of 40 kHz and 26 kHz, respectively. Even though higher PRFs provided higher generation efficiency of total output power, the generation efficiency of longer wavelength radiation was higher for lower PRF, being a consequence of higher peak power of pump pulses.

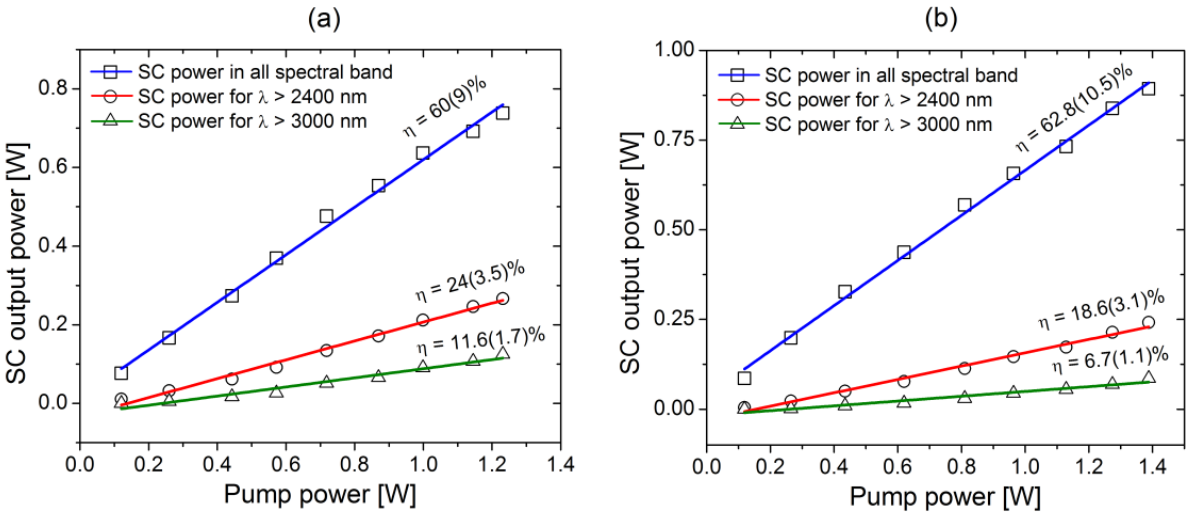

Figure 4-12: Average SC Output Power for 26 kHz (a) and 40 kHz (b) vs. Launched Pump Power. Slope efficiencies η in brackets indicate slope efficiency with respect to TDFA pump power.

The measured SC output spectrum, corrected for the spectral responsivity of the HgCdTe detector and the monochromator gratings response, is presented in Figure 4-13.

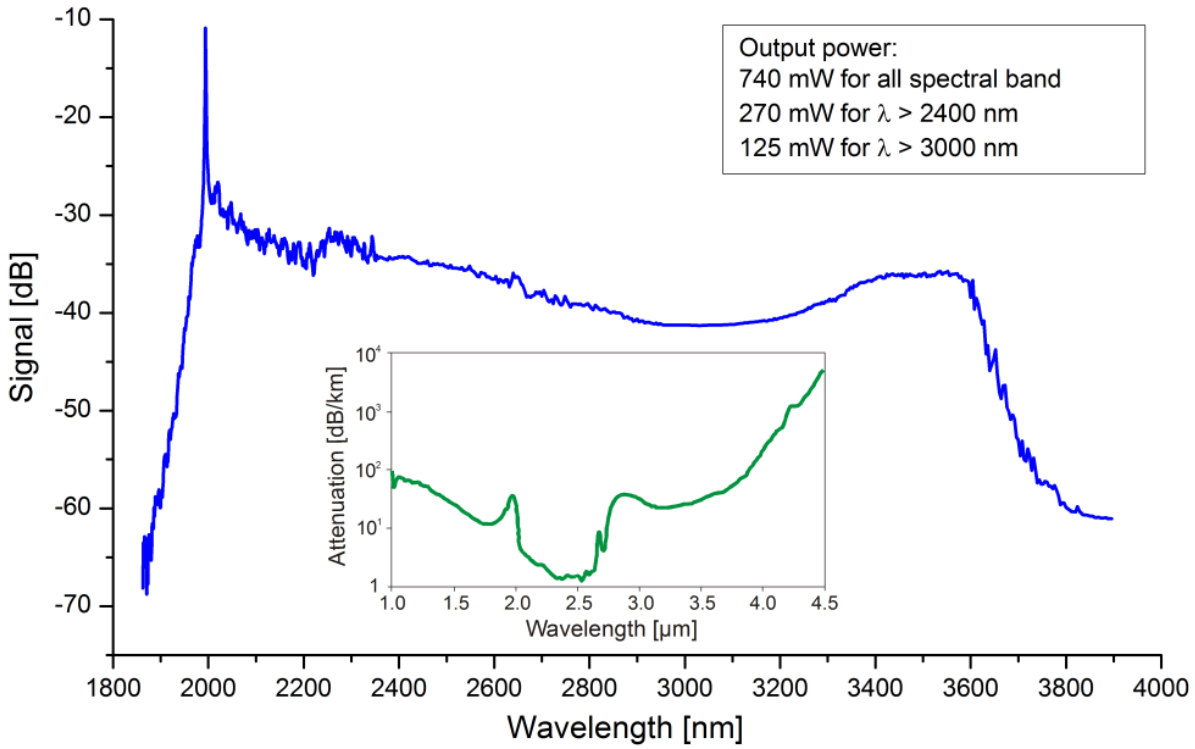

Figure 4-13: SC Spectrum After Propagation Through the ZBLAN Fiber for the Maximum Output Power and the PRF of 26 kHz. Inset: Attenuation of the ZBLAN fiber.

A modulation instability effect leading to the creation of solitons and then soliton self-frequency shift are mostly responsible for spectrum extension in Figure 4-13, which is typical for pumping a non-linear medium

in the anomalous Group Velocity Dispersion (GVD) region [16],[22],[40]. Additionally, the red-shifted solitons were broadened by self-phase modulation and cross-phase modulation, making the SC spectrum smooth and flat. As can be seen in Figure 4-13, the 10 dB flatness of spectral intensity was maintained in the wavelength interval from ~ 2100 to 3600 nm (span of 1500 nm). Another characteristic feature of the spectrum is that it is mainly broadened towards longer wavelength with reference to the pump wavelength, in contrary to spectra obtained in laser systems utilizing 1.55 µm pulses and pumping in the normal GVD of ZBLAN fibers [e.g. [15],[16],[22],[33]]. Further spectral broadening towards mid-IR was difficult due to the rapidly increasing fiber attenuation > 100 dB/km at ~ 4 µm and > 1000 dB at 4.5 µm (inset in Figure 4-13), such that red wavelengths generated in the fluoride fiber were highly attenuated preventing long wavelengths cut-off extension. The length of the ZBLAN fiber used in the experiment was not optimized. It will be the subject of further investigation, taking into account the pump pulse characteristics of our laser source. As was shown for example in [15], by proper selection of fluoride fiber length with regard to pump pulse peak power the inherent material losses of a fiber can be overcome leading to spectrum extension even beyond 6 µm.

In the next experiment we decided to scale up the output SC power. To this end, we modified the TDFA section by using a ~ 4.5-m long Large-Mode-Area (LMA) Tm-Doped Fiber (TDF) characterized by a core/clad diameter of 25/250 µm and corresponding numerical apertures of 0.1/0.46. It was cladding pumped in co-propagation configuration by a 793-nm, 30-W laser diode, which radiation was launched into the gain fiber via a (2 + 1) x 1 pump combiner with a signal feedthrough (signal input port: 10/125 µm, 0.15/0.46 NA; pump input ports: 105/125 µm, 0.22 NA; output port: passive double-clad 25/250 µm fiber, 0.11/0.46 NA). The output of the LMA TDF was first equipped with a home-made mode field adaptor (fiber taper) with a 25/250 µm (0.11/0.46 NA) fiber at the input and 11/125 µm (0.11 NA) fiber at the output, providing the mode conversion to a single mode fiber (0.5-m long SM2000). The maximum average output power provided by the 2 µm laser system, measured at the SM2000 fiber output, was 4.8 W. All the pump system components were fusion spliced, thus making it all-fiber. Finally, the 2 µm amplified pulses were launched into the ZBLAN fiber. The output spectrum generated from the ZBLAN fiber, for maximum recorded output SC power, is presented in Figure 4-14. The inset presents SC average output power recorded in different bands vs. launched pump power.

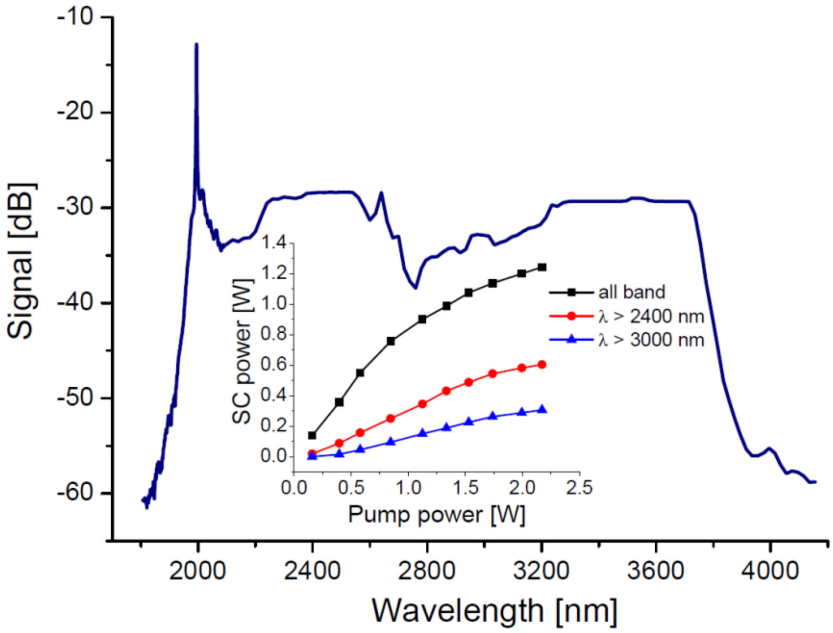

Figure 4-14: SC Emission Spectrum Generated in the ZBLAN Fiber. The inset shows SC power evolution in different spectral bands as a function of lunched pump power.

As can be seen in Figure 4-14, the spectrum covers more than one octave in frequency that is from ~ 1.8 µm to 4.15 µm with a residual peak at the pump wavelength. The maximum average output power was measured to be 1.25 W, for ~ 2.2 W of launched pump power. It can be noticed that 48.5% of the power (0.6 W) corresponded to wavelengths longer than 2.4 µm and 24.6% (0.31 W) of the power was detected for wavelengths longer than 3 µm. The dip in the spectrum around 2.8 µm corresponds to OH ions absorption in the non-linear medium and detection system. The 10 dB spectral flatness was maintained in the range of ~ 2 µm to 3.8 µm. The pump light peak at 1994.5 nm was not included into the calculation of the bandwidth.

In conclusion, we have demonstrated for the first time, to the best of our knowledge, an over octave spanning MIR supercontinuum generation in a step-index ZBLAN fiber, pumped by a gain-switched Tm^{3+}-doped fiber laser and amplifier system. The pump laser delivered ~ 50 ns gain-switched pulses with simultaneously mode-locked resembling sub-pulses. The maximum SC output average power for 26 kHz of repetition rate was 1.25 W and the power beyond 2.4 µm and 3 µm were measured to be 0.6 W and 0.31 W, respectively. Both an output power and spectrum width can be further scaled up.

4.2.1.3 Actively Q-Switched and Mode-Locked Tm^{3+}-Doped Silicate 2 µm Fiber Laser for Supercontinuum Generation in Fluoride Fiber

Contributors to this section: Michael Eckerle[5], Christelle Kieleck[5], Jacek Świderski[6], Stuart D. Jackson[7], Gwenael Mazé[8], Marc Eichhorn[5]

From: OPTICS LETTERS, **37**, pp. 512-514 (2012)

In this section we demonstrate a diode-pumped actively Q-switched and actively mode-locked Tm^{3+}-doped double-clad silicate fiber laser is reported providing up to 5 W of average output power at ~ 60 kHz Q-switch envelope repetition rate and ~ 8 µJ sub-pulses with up to 2.4 kW peak power. Using this source as a pump laser for supercontinuum generation in a ZBLAN fiber, over 1080 mW of supercontinuum from 1.9 µm to beyond 3.6 µm was obtained at an overall efficiency of 3.3% with respect to the diode pump power.

Supercontinuum fiber lasers based on fluoride glass emitting at eye-safe wavelengths between 2 µm and 5 µm are promising laser sources for countermeasures, spectroscopy, and remote sensing. For mid-infrared SC generation short pulse durations and thus high peak powers are necessary. These pulses break up by modulation instabilities into femtosecond pulses, which create the supercontinuum, e.g. in fluoride glasses [22],[23],[32],[33],[51]. The required pump pulses, usually on the (sub-)nanosecond scale with kW peak powers, are not achievable from fiber lasers by simple Q-switching. Passive mode-locking results in pulse energies that are too low, thus creating a limit in the average power. Up to now, pulsed laser diodes and amplifier schemes were the necessary pump sources for SC generation [22],[32],[33]. To optimize the relation among pulse width, pulse peak power, and accessible pulse energy while providing a simple, one-oscillator solution, active cw Mode-Locking (cw-ML) is a good choice [52]. In addition, active mode-lockers show much higher damage thresholds so that > 10 W of average output power can be achieved [52]. Further scaling of the pulse energy and peak power of the nanosecond to sub-nanosecond SC pump pulses can be achieved by simultaneous intracavity Q-switching of an actively Mode-Locked (Q-ML) fiber laser.

This section presents a simultaneous actively Q-switched and actively mode-locked 2 µm Tm^3 fiber laser in a single-fiber-oscillator arrangement and its use as a pump source for SC generation by pumping a ZBLAN fluoride fiber. Figure 4-15 shows the set-up of the Tm^3 fiber laser. The active medium is a 2.4-m long silica double-clad fiber (from the former Optical Fiber Technology Center, Australia) with a 20 µm diameter

[5] ISL, French-German Research Institute of Saint-Louis, 5 rue du Général Cassagnou, 68300 Saint-Louis Cedex, France.

[6] Institute of Optoelectronics, Military University of Technology, 2 Kaliskiego Street, 00-908 Warsaw, Poland.

[7] Institute of Photonics and Optical Science, School of Physics, University of Sydney, NSW 2006, Australia.

[8] Le Verre Fluoré, Campus KerLann, F-35170 Bruz, Brittany, France.

(NA 0.20) core doped with 2.8% Tm^3. The hexagonally shaped cladding has a flat-to-flat diameter of 300 µm (NA 0.40). The fiber end facing the cavity end mirror is cleaved at an angle of 8° to reduce Fresnel back reflections. The opposite end is cleaved perpendicular to the fiber axis to act as an Output Coupler (OC) with a reflectivity of ~ 4%. The dielectric end mirror of the 0.4-m long free-space external cavity has a high reflectivity about 2 µm. A 50 µm thick etalon with a reflectivity of 90% on both sides was inserted into the cavity to obtain a well-defined output spectrum. An Anti-Reflection (AR)-coated Acousto-Optic Modulator (AOM) mode-locker was placed directly in front of the cavity end mirror. A second AR-coated AOM with a deflection efficiency of > 80% for Q-switching was inserted between the fiber end and the etalon. The high deflection efficiency and the 8° cleave of the fiber ensure a high Amplified Spontaneous Emission (ASE) threshold to obtain a high initial gain before Q switching. The mode-locker was tunable in its drive frequency to allow accurate adjustment to the cavity round-trip time to establish mode-locking.

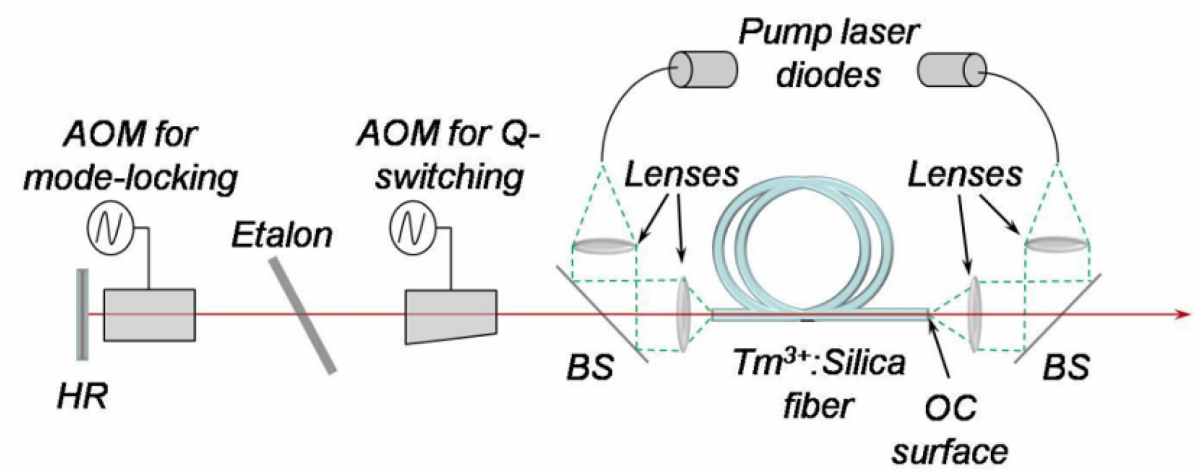

Figure 4-15: Set-Up of the Q-Switched, Mode-Locked Tm^{3+}:silica Fiber Laser.

The fiber was symmetrically pumped at 792 nm using fiber-coupled laser diodes, which each emitted 25 W from a 200 µm multi-mode fiber (NA 0.22). The pump light was collimated using lenses with an effective focal length of 11 mm. Identical lenses were used to focus the pump light onto the fiber and to collimate the fiber laser output at both ends. The lenses were AR coated for the pump and laser radiation. Dichroic mirrors reflective for the pump and highly transmissive for the laser wavelength were used to combine laser and pump light and to direct the pump light onto the fiber. Because of the small core and low NA of the pump fibers relative to the cladding and NA of the laser fiber, a pump launch efficiency of ~ 96% was achieved.

As fiber lasers are extremely sensitive to back reflections, optical isolation was provided by a home-built polarization-independent optical isolator attributable to the non-polarization maintaining properties of the fiber laser. The isolator set-up consisted of splitting the beam into two arms, one for each polarization, which were separately isolated and then recombined. Using half-wave plates placed within the arms, it was possible to change the output power of the set-up while keeping the actual pulse parameters unchanged.

When both AOMs were activated, the laser produced pulse trains with a repetition rate of ~ 60 kHz at an average output power of 5 W. For the Q-ML set-up, mode-locking could be achieved at different ML frequencies and resulted in the pulse widths and average output powers shown in Figure 4-16. There the pulse width [Full Width At Half Maximum (FWHM)] of the strongest sub-pulse in the generated pulse trains and the relative power drop, occurring when switching from simple Q-switched to Q-ML operation, is depicted. This effect, which arises from coupling of non-evenly spaced modes, has already been investigated under cw-ML operation [52]. However, in contrast to the cw-ML results, where for one ML frequency the pulses obtained were < 100 ps, while all other operation points resulted in > 2 ns pulses,

the Q-ML operation provides pulses of 2 ns duration even for the ML frequency in which the drop in average output power is minimal.

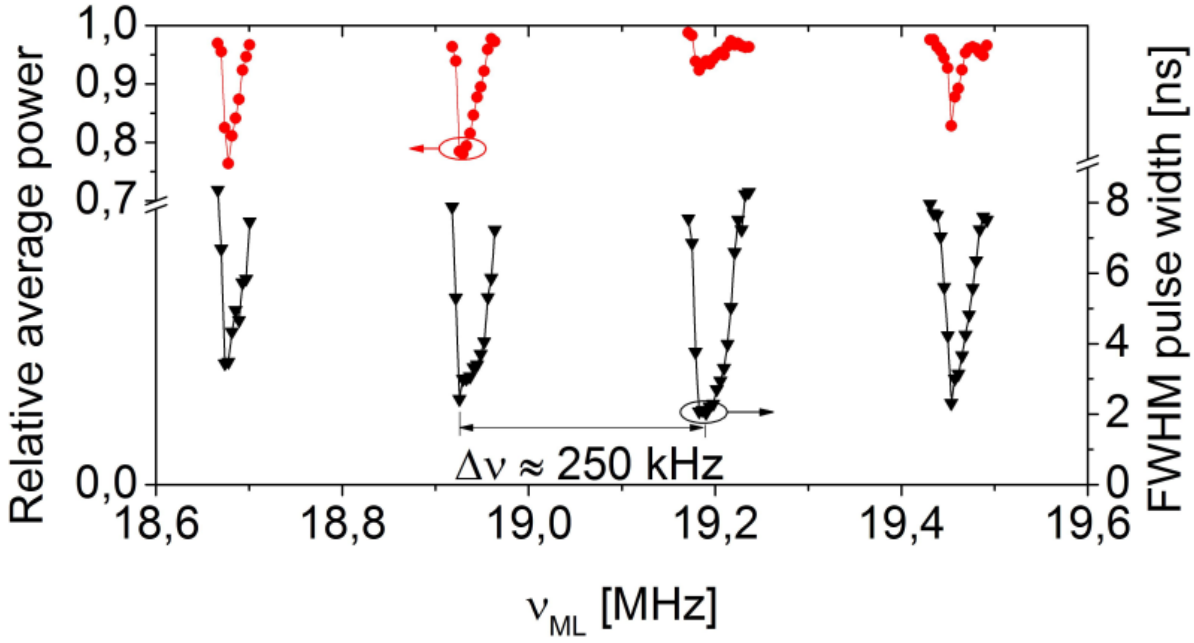

Figure 4-16: Relative Average Power and FWHM Pulse Width of the Major Sub-Pulse in the Q-Switch Envelope for Different Mode-Locking Frequencies.

The pulse trains consisted of 5 – 12 pulses within one Q-switch envelope. The corresponding energies and peak powers of these sub-pulses for ν_{ML} =19.1905 MHz are shown in Figure 4-17. The peak power P_{peak} was calculated under the assumption of a Gaussian pulse shape resulting in $P_{peak} = 0.94\ Ep/\Delta t_{FWHM}$, with Ep being the pulse energy and Δt_{FWHM} the pulse width measured at FWHM. Because of the approximately equal pulse widths within one Q-switch envelope, the distribution function of energy and peak power follows the Q-switch envelope. For the measurement shown in Figure 4-17, the maximum pulse energy was ~ 8 µJ at a peak power of 2.5 kW. After a new alignment and recleaving of the fiber, the maximum pulse energy could be increased to ~ 9 µJ; however, at a larger pulse width thus resulting in a lower peak power of 1.5 kW. The emission peaks of the laser with a spectral width of 1 – 2 nm were located at 1950.7 nm, 1976.6 nm, 2003.5 nm, and 2030.8 nm. The Q-switch envelope phase is not stable with respect to the ML pulse train and the number of sub-pulses can change by ± 1, resulting in pulse-to-pulse fluctuations in peak power ~ 10%.

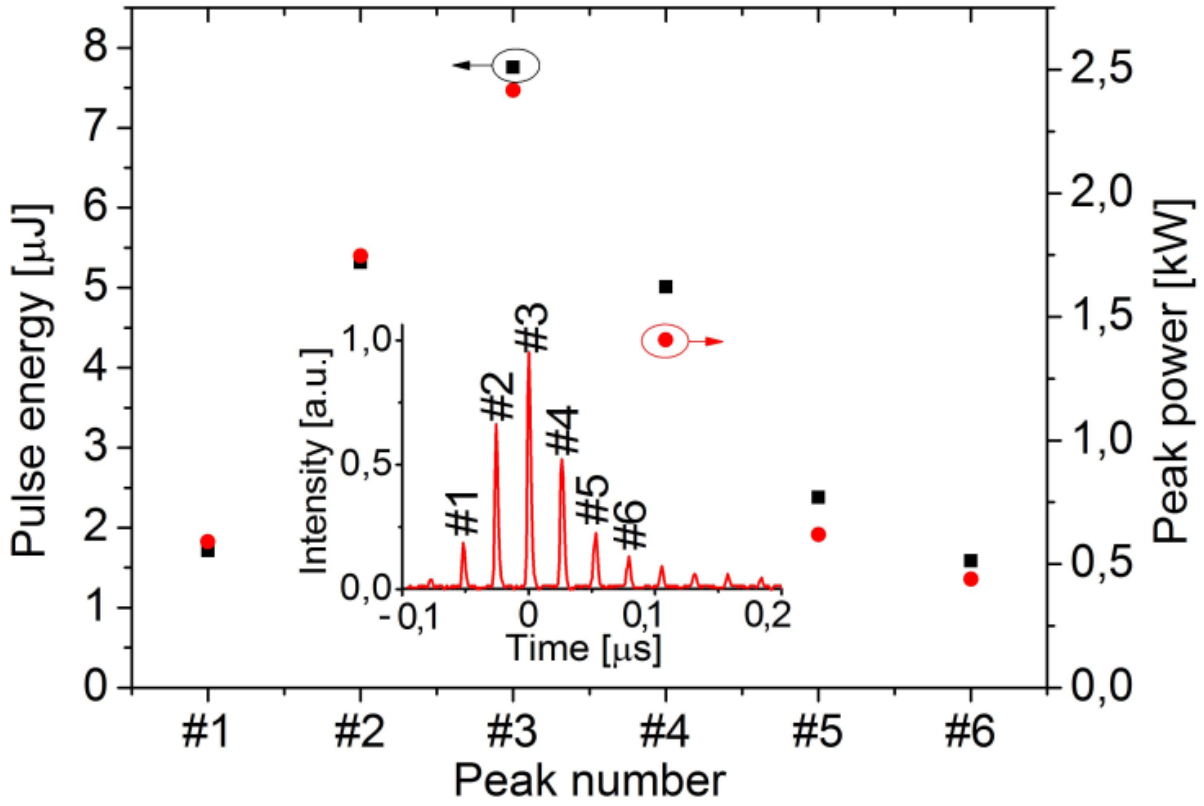

Figure 4-17: Pulse Energy and Peak Power for Succeeding Pulses in One Q-Switch Envelope (Inset).

In a second experiment the Tm^3 fiber laser was used as the pump source for SC generation in a 15-m long ZBLAN fiber with an 8 µm diameter core, a cut-off wavelength of 3.13 µm, and a 125 µm diameter cladding. A fiber with a zero-dispersion wavelength at about 1.54 µm was chosen so that it could be pumped in its anomalous dispersion regime necessary for SC generation. This allows for SC wavelength conversion by four-wave mixing, self-phase modulation, and Raman scattering [32],[51]. The pump was mode matched to the ZBLAN fiber by a telescope, allowing for launch efficiencies of over 60% despite the not optimum beam quality of the pump, caused by the slightly multi-mode nature of the Tm^3 fiber and the recombining after isolation. Using a scanning grating spectrometer, an InAs detector, and a lock-in amplifier for noise reduction and correcting for the overall detection response results in the spectra depicted in Figure 4-18, recorded with a resolution of 6.27 nm. As the InAs detector was the only type available at the time of the experiment, the measured spectra were limited to ~ 3600 nm – see inset in Figure 4-18. Using the optical isolator set-up, the fiber was independently pumped with both polarizations. As can be seen in the inset, there is no clear impact to the conversion efficiency for pumping with different polarizations, in agreement with the fact that the ZBLAN fiber is not polarization maintaining and not exposed to any symmetry breaking constraints. In some cases, however, a p-polarized pump performs better, which can be attributed to slightly different pulses in the two polarizations, e.g. envelope shape and number of sub-pulses, resulting from a symmetry breaking by the angle cleave and the tilted etalon in the free-space cavity of the Q-ML fiber laser.

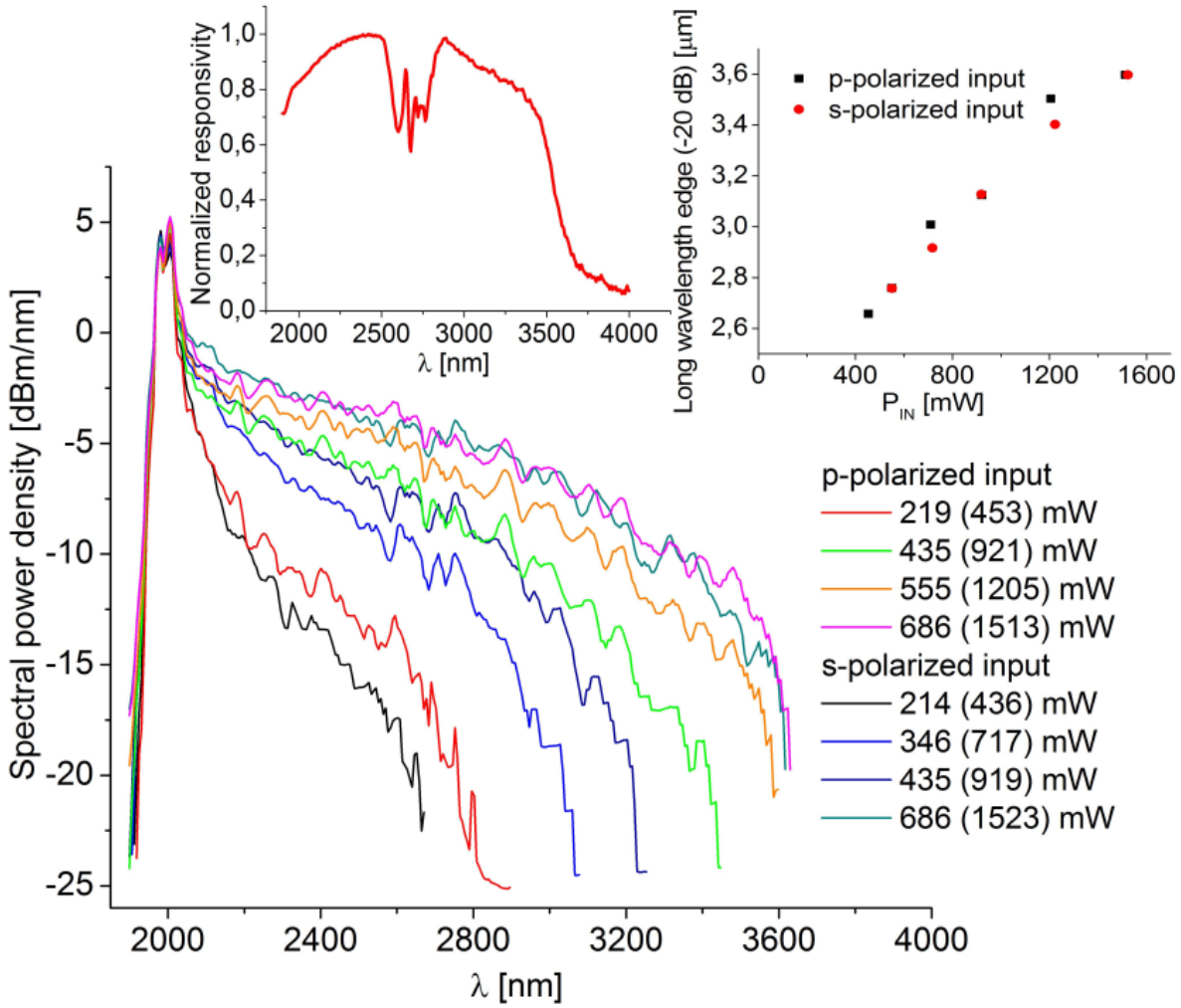

Figure 4-18: SC Output Spectra Resulting from Different Incident Powers from the Q-ML Pump. The value in the legend denotes the overall average output power P_{OUT}, and the value in brackets the corresponding average incident pump power P_{IN}. The right inset shows the wavelength at which the power dropped by 20 db relative to the peak of the spectrum, and the left inset depicts the overall spectrometer response.

Using a long-wave pass filter with a 3 dB edge at 2340 nm, the amount of power shifted beyond 2340 nm was investigated and is depicted in Figure 4-19. Up to ~ 105 mW was measured for $\lambda > 2340$ nm. For comparison the upper inset shows the overall SC power including residual pump, reaching over 700 mW. The black line is a linear interpolation of the first five measurement points. The rollover of the total SC power for input powers larger than 800 mW results from increasing absorption of the fiber for longer wavelengths (see lower inset in Figure 4-19) owing to the 15-m long fiber used. As the fiber was coiled on a 20 cm diameter spool, bend-induced losses contribute, which have been shown to be significant at these long wavelengths even for a radius of 40 cm [33]. Increasing the incident pump power to 3 W resulted in an SC power of over 1080 mW and more than 216 mW beyond 2340 nm. The overall wavelength conversion efficiency from the Tm^3 fiber laser pump diodes to the final total supercontinuum output is ~ 3.3%, which is comparable to recent results of 2 μm pumped SC [23],[33]. The current arrangement exhibits a reduced complexity compared to multi-stage amplifier systems.

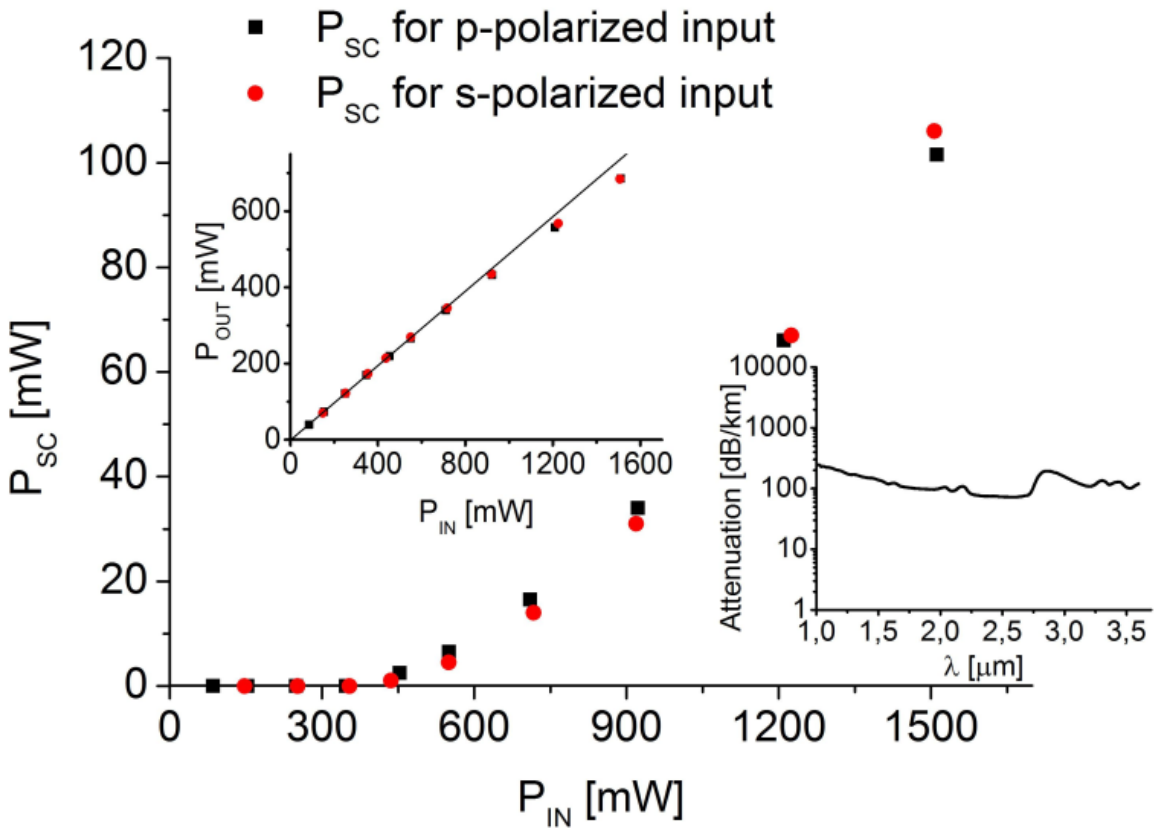

Figure 4-19: Power Shifted Beyond 2340 nm for Different Average Pump Powers. The upper inset shows for comparison the overall average output power (the black line being a linear interpolation of the first five points). The second inset shows the passive attenuation of the ZBLAN fiber.

The SC generated in this work is comparable to the spectra presented by other 2 μm pumped SC experiments [23] regarding the power drop from peak spectral pump power to SC plateau and the negligible amount of spectral power that is shifted to short wavelengths below the pump wavelength.

In conclusion, a simultaneous actively Q-switched and actively mode-locked Tm^{3+} fiber laser with up to 5 W of average output power at ~ 60 kHz Q-switch envelope repetition rate was presented. Up to ~ 8 μJ sub-pulses with peak powers reaching 2.4 kW were generated. Using this laser as a pump source for SC generation in a ZBLAN fiber over 1080 mW of supercontinuum from 1.9 μm to beyond 3.6 μm was obtained. The overall efficiency with respect to the diode pump power of the total laser set-up was 3.3%. The scalability of the pump laser (not average power limited) makes this scheme promising for future high-average-power SC sources with reduced complexity due to the single-oscillator approach.

4.2.2 Supercontinuum Generation in Chalcogenide Fibers

Contributors to this section: Rafael R. Gattass[9], L. Brandon Shaw[9], Vinh Q. Nguyen[9], Paul C. Pureza[9], Ishwar D. Aggarwal[10], Jasbinder S. Sanghera[9]

From: Optical Fiber Technology, 18, pp. 345-348 (2012)

[9] U.S. Naval Research Laboratory, 4555 Overlook Avenue SW, Washington, DC 20375-5338, United States.
[10] Sotera Defense Solutions, 2200 Defense Highway, Crofton, MD 21114, United States.

In this section we present an all-fiber based supercontinuum source with emission covering the wavelength range of 1.9 – 4.8 µm is demonstrated. The laser source is based on a combination of silica Commercial-Off-The-Shelf (COTS) components and a chalcogenide-based non-linear optical fiber. The system provides 10 dB spectral flatness from 2.0 µm to 4.6 µm, and 20 dBm points from 1.9 µm to 4.8 µm. The output power is 565 mW, but scalable by scaling the repetition rate. The limit on the long-wavelength edge of the system is identified as an extrinsic absorption feature in the fiber used; confirming the system could be scaled to generate a broadband source even further in the infrared.

There have been several demonstrations of mid-infrared supercontinuum generation with optical fibers [9],[15],[20]-[23],[53]-[56]. Chalcogenide fibers (fibers based on chalcogen elements S, Se and Te) are natural candidates for infrared supercontinuum sources due to their long-wavelength multi-photon absorption edge. For example, the multi-photon absorption edge for an As_2S_3 is 7.4 µm [19], and can be even further for Se-based and Te-based chalcogenide fibers. For applications involving non-linear optical processes, chalcogenide fibers are even more suitable [19] given their high non-linear refractive index n_2 (~ 5 x $n_2^{tellurite}$, ~ 500 x n_2^{silica} and ~ 1000 x $n_2^{fluoride}$) [55] and high peak Raman gain g_r (~ 65 x g_r^{silica} [57],[58], ~ 46 x $g_r^{fluoride}$ [59], ~ 2 x $g_r^{tellurite}$ [60]). In addition, chalcogenides have high optical damage threshold (e.g. > 25 GW/cm^2 at 2.4 µm for As_2S_3 [54]) and environmental stability (e.g. non-hydroscopic for most chalcogenide glasses including As_2S_3, As_2Se_3). It is the combination of wide transmission range, strong non-linear properties, high optical damage threshold and environmental stability that make chalcogenide fibers an ideal system from fiber-based supercontinuum laser sources. The first mid-infrared fiber supercontinuum source was demonstrated using chalcogenide fibers in 2005 [53],[61], but was based on an optical parametric amplifier pumped by a Ti:sapphire laser. The supercontinuum source was limited in spectral range (2 – 3.5 µm) and average power (< 10 mW). In [54] we transitioned to a fiber-based pump source which still emitted close to 2.5 µm, increasing the average power (140 mW) and extending the spectral range to cover from 1.5 to 4.8 µm. The supercontinuum laser system was based on a custom picosecond mode-locked laser seed system [62], amplified in a Er-doped fiber amplification stage, soliton-self frequency shifted to 2 µm and further amplified in a Tm-doped fiber amplification stage. In this paper, we transition to an all COTS-based laser system still using a chalcogenide fiber in the last stage for high non-linear mid-infrared supercontinuum source.

4.2.2.1 Experimental Set-Up

Figure 4-20 shows a schematic of the laser system developed for the supercontinuum source. Multi-stage master oscillator power amplifier geometry is used following a similar approach as the one described in [63]. A 40-ps, 10-MHz Er-fiber-based laser with 200 mW average output power was sourced from a commercial vendor and is used as a seed for the system. The use of a picosecond pulse duration seed minimizes the effect of Brillouin scattering as power is increased while being fairly insensitive to dispersion. Spectral filtering with narrow band filters and temporal filtering with an acousto-optic modulator are done to the output of the seed laser to reduce power carried by amplified spontaneous emission to 30 dB of the peak wavelength. The seed is amplified in multiple stages, and the power is soliton shifted into the Tm amplification band. Because the soliton shifting occurs in a non-Tm-doped fiber, no amplified spontaneous emission is present in the emission band of Tm and the soliton-shifted pulses act as a new background free “seed” for the Tm amplification. Propagation in a highly non-linear fiber continues to shifts the center wavelength further into the infrared. The chalcogenide fiber used in the last stage is a step-index core-clad As_2S_3 fiber with a 10 µm core diameter and numerical aperture of 0.3 and 2 m length. The step-index fiber was fabricated through a double crucible process and has a minimum transmission loss of 0.7 dB/m at 1.5 µm. The end faces of the fiber are cleaved and mechanically coupled to the silica without any patterning or treatment resulting in a total 68% reflection loss from both end faces.

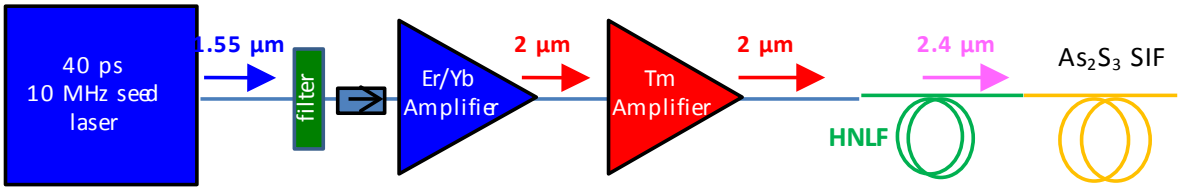

**Figure 4-20: Schematic of All Fiber Laser System.
HNLF: Highly Non-Linear Fiber; SIF: Step Index Fiber.**

4.2.2.2 Results

The laser system was characterized before and after the insertion of the chalcogenide fiber in the system. The optical beam's wavelength prior to entering the chalcogenide fiber is centered around 2.45 µm and has approximately 100 nm bandwidth. At this stage, the output is approximately 1.4 W of average power. After propagating through the As_2S_3 chalcogenide fiber, 565 mW broadband supercontinuum is observed.

Figure 4-21 shows the generated supercontinuum spectrum. The spectrum is measured with a scanning monochromator and three-stage thermo-electrically cooled HgCdTe detector. Higher order diffraction orders are removed by a series of longpass filters.

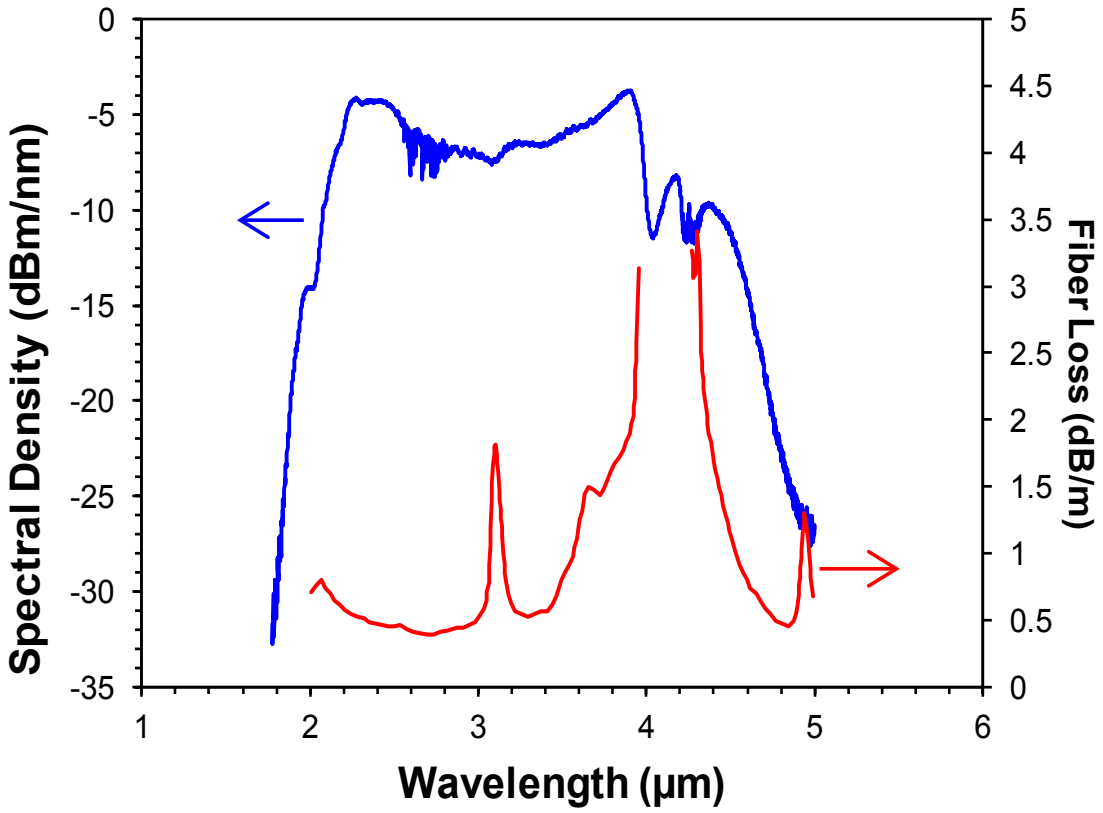

Figure 4-21: Supercontinuum Spectrum (Blue Curve) and Estimated Loss Curve for Chalcogenide Fiber (Red Curve).

The spectrum, at the 20 dBm points, spans from 1.9 µm to 4.8 µm. The noise observed around 2.8 µm is due to atmospheric absorption bands caused by the use of a non-purged monochromator system. The system

provides 10 dB spectral flatness over 2.0 – 4.6 µm. We have measured the beam profile for the output beam at 2.2 µm with an infrared camera. Although the fiber supports a low number of modes, the system is aligned to excite only the lowest order mode at this wavelength. Given the fiber numerical aperture and core diameter, as the supercontinuum continues to broaden, the fiber becomes single mode at approximately 3.8 µm. Although we have not been able to measure the mode between 2.2 and 3.8 µm, we believe the short length of fiber used and the efficient energy transfer indicates that the beam remains single mode over all the emission wavelengths. The laser system was tested over a period of approximately one month. Average power and spectrum broadening were monitored weekly and remained repeatable over the whole monitoring time. Detailed characterization of noise and further long-term stability by a NIST-calibrated sensor system is currently underway. Figure 4-22 shows the evolution of the supercontinuum spectrum with respect to increase pump power. As can be seen the spectrum broadens mostly to longer infrared wavelengths with increasing pump power. The supercontinuum spectrum seems to be attenuated at the same location as a known impurity band (shown in Figure 4-21), although some power is still observed beyond the impurity band.

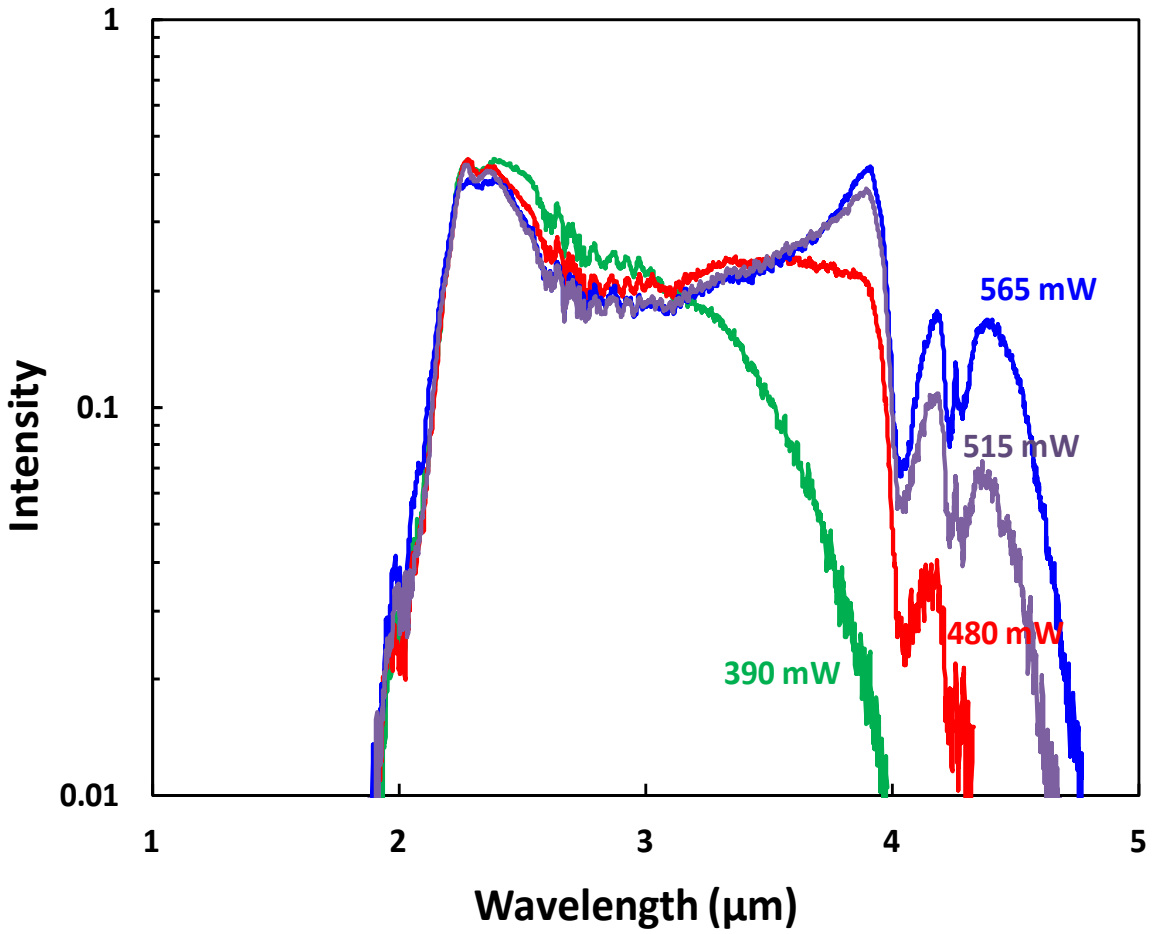

Figure 4-22: Spectral Evolution of Supercontinuum Source as a Function of Measured Output Power.

4.2.2.3 Discussion

Previous demonstrations of MIR supercontinuum generation in other materials systems used anomalous dispersion pumping for supercontinuum generation [6],[19],[55]. Here, normal dispersion pumping is

utilized for supercontinuum generation. The process of supercontinuum generation in a normal dispersion fiber is known and is primarily interplay between stimulated Raman scattering and self and cross-phase modulation [63]. We speculate that given the asymmetric power induced broadening towards infrared wavelength, the bandwidth of the laser beam before entering the chalcogenide fiber (100 nm) and the bandwidth of the Raman gain in As_2S_3 fiber (85 cm^{-1}) [59], the observed spectrum can be attributed to about 6 or 7 stokes shifts, with spectral broadening at each shift caused by a convolution of the Raman gain spectrum with the broadband pulse out of the silica stage as well as smoothing from self-phase modulation and cross-phase modulation.

While a photonic crystal design to enable anomalous dispersion pumping could have been used in the system [20], photonic crystal fibers designs to shift the zero dispersion wavelengths in As_2S_3 result in small core fiber diameters which can be difficult to fabricate and typically have higher transmission losses as well as high insertion losses. Power scaling with such small core structures is also problematic, especially with suspended core microstructured fiber where the core is effectively thermally isolated from the cladding by an air layer. The use of normal dispersion pumping in step index fiber was chosen instead of a photonic crystal fiber design to allow for increased power handling and future power scaling. The transmission range of As_2S_3 fiber extends further out than the maximum wavelength observed in the supercontinuum spectrum of Figure 4-21. The drop in power around 4.1 µm is not due to an intrinsic limit in the material system, but instead to an extrinsic impurity present in the fiber. Overlaid in Figure 4-21 is the measured fiber loss for a multi-mode fiber batched under similar processing conditions as the 10 µm core fiber used in this experiment. The large absorption peak around 4.1 µm is due to ppm-level hydrogen impurities, which bond to form H-S in the fiber. Because the supercontinuum process involves broadening the spectrum from shorter wavelengths, the H-S absorption band attenuates the power and halts the broadening. Given the width of the absorption band and the bandwidth of the Raman cross-section in As_2S_3, theoretically if there is enough power present below the absorption peak, a Raman scattering event could leap enough energy over the absorption band and continue broadening the supercontinuum even further. The power dependent “hop” over the absorption band is clearly seen in the power evolution of the supercontinuum shown in Figure 4-22. The spectrum broadens towards longer wavelengths with increasing pump power. At the low end, output power level of 390 mW, spectral broadening has not yet reached the impurity band. At 480 mW output power, there is not enough power in the fiber to induce enough non-linearity to hop over the absorption band and spectrum broadening stops at about 4 µm. As the pump power is further increased (515 mW output power), a peak beyond 4.1 µm is visible with enough power to continue broadening towards longer wavelengths. Even further increase in pump power is one alternative for broader sources, but the same effect could be accomplished by reducing the losses due to the impurity band. There are known processes for reducing the level of impurities in chalcogenide fibers with attenuations of less than 3 dB/m at 4.0 µm already demonstrated [64]. A combination of increased power and better purification should significantly improve the bandwidth of the supercontinuum. Besides improvements to the bandwidth of the system, the fiber-based architecture used in this experiment can be scalable to higher average powers. Two common approaches can be used for power scaling: increasing repetition rate while maintaining peak power (as done in [33]); and increasing peak power per pulse while maintaining repetition rate.

For the first approach, the current system is limited to 10 MHz by one of the time-filters being used, but there are other commercial alternatives up to 100s of MHz. The repetition rate could be scaled up while maintaining the peak power constant, thereby reducing the risk of optical damage.

In the second approach, the peak power per pulse can be increased, resulting in scaling of the average power. In the system presented here, we have been limited to the maximum pump power. However, because the current supercontinuum scheme operates in the normal dispersion regime of the fiber, the core size of the fiber can be increased while maintaining intensity in the core of the fiber to scale to higher powers.

We have used a combination of both approaches to scale the peak power from our preliminary results of 140 mW [54] to 565 mW. Previously, the pump source operated at 560 kHz with a peak power per pulse

> 10 kW. Our power scaled supercontinuum pump source operates at a 10 MHz repetition rate with a peak power per pulse of 3.5 kW. By operating the system with the peak power of the first demonstration (10 kW) and the repetition rate of the second system (10 MHz), we project a scaled average power between 1.5 and 2.5 W.

A limitation to power scaling through repetition rate scaling would be reaching the damage threshold for the fiber. However for our pulse width of less than 100 ps and an incident pump far from the two-photon absorption edge (as in our case with a pump around 2.45 µm), we observe the peak intensity damage threshold to be very high. For example, for the system described in this paper, the incident peak intensity at the fiber front face is approximately 4.5 GW/cm^2, while a previous interaction of this system with a lower repetition rate lead to an incident peak intensity of approximately 12 GW/cm^2 [54]. The scalable fiber-based mid-infrared supercontinuum source demonstrated in this section addresses immediate needs for infrared sources in metrology such as the one for the Hyperspectral Image Projector (HIP) being developed at National Institute of Standards and Technology [65]-[67]. Requirements for illumination of the HIP system are spectral power density of 10 dBm/nm or higher, spectral flatness of 10 dB within the band of interest (3 – 5 µm) and continuous wave or high repetition rate pulse trains with rates much faster than the temporal response of the system under test (typically 1 MHz or better repetition rate). The output diameter of the fiber can be no greater than 20 µm in diameter to maintain spectral resolution of the system. Currently, we are power scaling and packaging the supercontinuum source for implementation in the HIP.

In conclusion, we presented in this section an all-fiber chalcogenide-based supercontinuum source with emission covering the wavelength range of 1.9 – 4.8 µm. The system architecture is based on a combination of silica commercial-off-the-shelf components and an As_2S_3 step index non-linear optical fiber. The supercontinuum spectrum has 10 dB spectral flatness from 2.0 µm to 4.6 µm, 20 dBm points from 1.9 µm to 4.8 µm, with a total output power of 0.565 W. We identify the current long-wavelength limit of the system to be due to an extrinsic absorption in the fiber, acknowledging further broadening is still possible in this glass system.

4.2.3 Supercontinuum Generation in Fluoroindate Fibers

4.2.3.1 Supercontinuum Generation in Fluoroindate Fiber with Ultrashort Laser Pulses

Contributors to this section: Francis Théberge[11], Jean-François Daigle[11], Denis Vincent[11], Pierre Mathieu[11], Jean Fortin[11], Bruno E. Schmidt[12], Nicolas Thiré[12], François Légaré[12]

In this section we present the first demonstration of SC generation in a fluoroindate based single-mode fiber. These fibers exhibit a minimal loss of 0.1 dB/m at 3.2 µm and a loss inferior to 0.8 dB/m at 5 µm. With this fiber, we demonstrated the generation of 20 dB spectral flatness SC spanning from 2.7 µm to 4.7 µm.

The attenuation spectrum for the single-mode fluoroindate based fiber is presented in Figure 4-23 (black line). For comparison, Figure 4-23 presents also the attenuation spectrum for a single-mode fluorozirconate based fiber having similar core diameter. In this section, we compare the SC generation in these two fibers and their specifications are listed in Table 4-5. The fluoroindate fiber has been produced by Le Verre Fluoré and its glass composition is similar to Ref. [69].

[11] DRDC Valcartier, 2459 route de la Bravoure, Québec (Québec) G3J 1X5, Canada.

[12] INRS-EMT, 1650 Lionel-Boulet Blvd, Varennes (Québec) J3X 1S2, Canada.

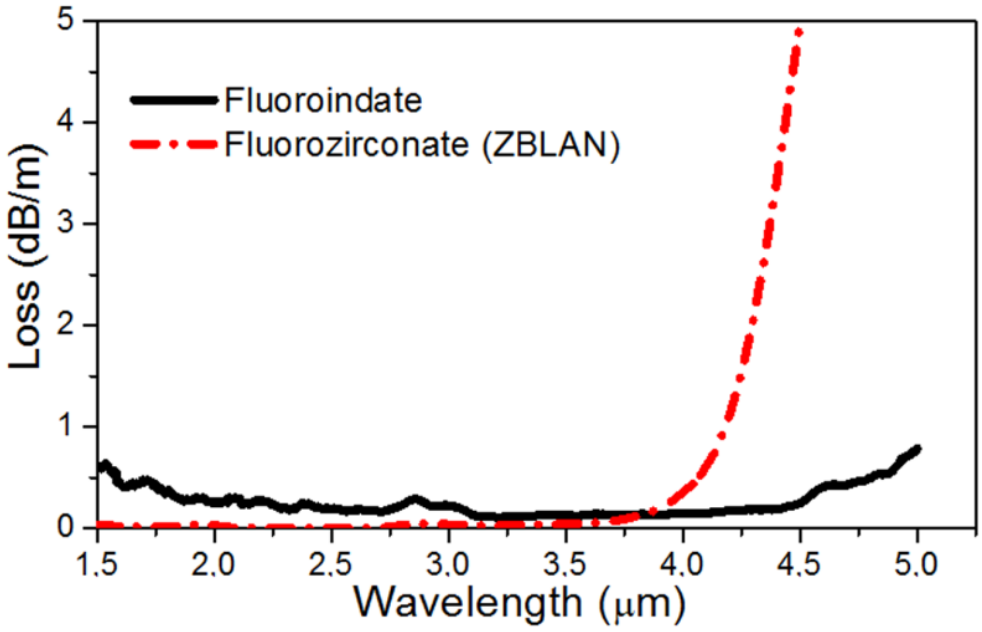

Figure 4-23: Attenuation Spectrum of the Fluoroindate-Based Fiber (Black Line) and ZBLAN Fiber (Red Dash-Dot).

Table 4-5: Parameters of Fluoride Fibers.

Fiber	Fluoroindate	ZBLAN
Core Diameter	16 μm	16 μm
Cladding Diameter	120 μm	125 μm
Numerical Aperture	0.14	0.19
Cut-Off Wavelength	2.8 μm	4.2 μm
Zero Dispersion	1.83 μm	1.63 μm
Length	9.5 m	9.0 m

The fibers described in Table 4-5 have a relatively large core diameter for SC generation applications enabling these fibers to sustain high average laser powers. Various laser pulse parameters have been injected into these fibers with pulse durations ranging from 70 fs to 20 ns and with central wavelength between 1.5 μm and 3.4 μm. For the fluoroindate based fiber, more than 12 W of average power centered at 1.5 μm and with peak power exceeding 10 kW (20 ns pulsewidth) can be injected into the fiber core without any damage, which makes this fiber interesting for multi-watt SC sources.

In order to achieve significant broadening, the zero Group Velocity Dispersion (GVD) of the fiber should be close to the center wavelength of the laser pulse used for SC generation, with the laser wavelength slightly shifted towards the anomalous GVD regime. This minimizes the walk-off between the different regions of the generated spectrum, allowing for further spectral broadening [38]. The zero GVD wavelength of the fluoroindate-based fiber is 1.83 μm, but more interesting is the very small dispersion variation beyond the zero GVD wavelength from 1.8 μm to 4 μm with a value inferior to 10 ps/km•nm around 3 μm [69]. Therefore, the central wavelength of the laser pulse injected into the fiber can be tuned over a wide spectral range without undergoing severe temporal broadening due to large anomalous GVD.

In order to investigate the SC generation, different pulse duration at different center wavelengths were coupled into the fluoroindate fiber. The experiments were performed using the infrared beam line at the Advanced Laser Light Source (ALLS) [70]. An optical parametric amplifier pumped by a Titanium-sapphire allows the generation of wavelength-tunable laser pulses in the range of wavelength between 1.4 µm to 4 µm. For wavelengths between 1.4 µm to 2 µm, different transform limited pulse duration from 70 fs up to 850 fs were achieved through spectral filtering by closing a variable slit in the Fourier plane of a 4-f set-up. At longer wavelengths up to 4 µm, narrow band-pass filters were used for this purpose.

Both fiber ends were cleaved by a diamond stylus to ensure a sufficiently flat interface. The generated and transmitted SC was measured by an $f = 12.5$ cm monochromator equipped with a 300 lines/mm diffraction grating and a PbSe detector, giving a spectral resolution around 5 nm. In order to block any second diffraction order of the grating overlapping with the SC spectrum, a Germanium window was used in front of the detector to record the spectrum from 1.9 µm up to 3.5 µm. To record the spectrum from 3 µm up to 5.5 µm, a long-wavelength pass filter transmitting above 3 µm was used in front of the detector.

Figure 4-24 presents the generated SC in the fluoroindate and the ZBLAN fibers, when 70 fs, 3.4 µm laser pulses were injected in these fibers. Figure 4-24(a) presents the spectral broadening into the 9.5-m long single-mode fluoroindate based fiber. We observe the continuous broadening as we increased the laser pulse energy injected into the fiber. For the lowest pulse energies, the spectral broadening is asymmetric and occurs mainly towards the longer wavelength due to the self-phase modulation occurring in anomalous dispersion regime. For a laser pulse energy of 120 nJ injected into the fiber, the peak power of the laser was 1.7 MW. Such peak power is about 20 times lower than the critical power for self-focusing (Pcr ≅ 39 MW) in fluoride glasses [28],[68]. At 120 nJ per pulse, the SC produced in the fluoroindate fiber provides 20 dB spectral flatness from 2.7 µm to 4.7 µm.

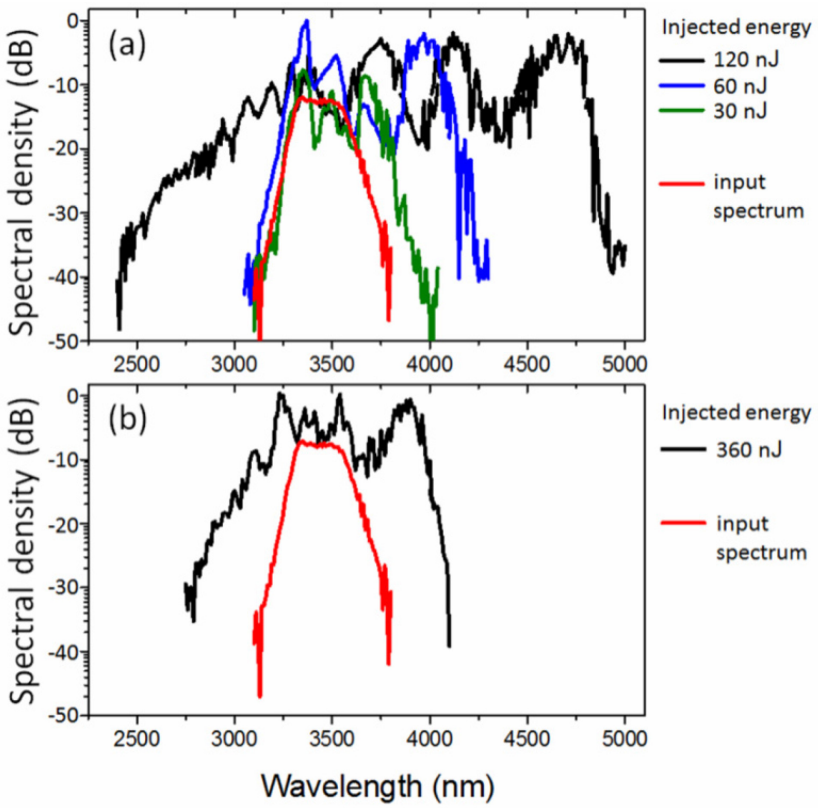

Figure 4-24: (a) Spectral Evolution of Supercontinuum as a Function of Measured Energy per Pulse Injected in Fluoroindate-Fiber; (b) Supercontinuum Generation in ZBLAN Fiber.

During SC generation, self-phase modulation and four-wave mixing induce initially the spectral broadening before higher order dispersion causes fission of the laser pulse. After the fission of the laser pulse into multiple solitons, the individual solitons redshift by the Raman self-frequency shift effect and emit phase-matched dispersive waves at wavelengths shorter than the zero GVD [39].

The spectral modulations observed in the SC of Figure 4-24(a) are partly attributed to the spectral interference resulting from the spectral broadening and phase-shift induced by the self-phase modulation. The stronger spectral modulations for the red-shifted part of the SC are probably enhanced by the generation of self-frequency shift Raman solitons [39],[71]. In Figure 4-24(b), it is interesting to compare the SC generation in ZBLAN. Because the dispersion in ZBLAN is 2 – 3 times larger at 3.4 µm than for the fluoroindate fiber, more energetic laser pulses have to be injected into the ZBLAN core in order to preserve similar soliton order $N \cong 7$ for the maximum pulse energy injected in both fibers. For the ZBLAN fiber, SC generation could not expand beyond 4.1 µm because of the important absorption beginning around 4 µm (see Figure 4-23). On the other hand, the blue-shifted extension of the SC in ZBLAN is weaker because the ZBLAN dispersion is larger and induces the lengthening of the laser pulses at shorter distance into the fiber [68]. The 20 dB spectral flatness in ZBLAN spans from 2.9 µm to 4.0 µm which is two times narrower than for the fluoroindate fiber.

The absorption edge in fluoroindate was not the dominant factor limiting the SC expansion observed in Figure 4-24(a), because we did not observe a decrease of the SC as sharp as in Figure 4-23(b) and the attenuation was only 0.5 dB/m in the fluoroindate fiber around 4.7 µm. In fact, the SC extension in the fluoroindate fiber was probably limited by the dispersion of the very broad SC laser pulse generated into the fluoroindate fiber.

Usually the maximum spectral broadening of the laser pulse is achieved for the distance at which soliton fission occurs. Optimizing the fiber length just shorter than this point is the basis of the higher-order soliton effect compression technique, and a number of empirical expressions for this characteristic distance have been developed [38]. It is particularly useful to refer to this distance as the fission length (L_{fiss}), written in the simplified form:

$$L_{fiss} = \sqrt{L_D L_N}$$

where $L_D = {\tau_0^2}/{|\beta_2|}$ is the dispersion length, $L_N = {(cA_{eff})}/{(n_2 \omega_0 P_0)}$ is the non-linear length, τ_0 is the initial pulsewidth, β_2 is the group velocity dispersion, c is the light speed, A_{eff} is the effective core area, n_2 is the non-linear index of refraction, ω_0 is the central frequency, and P_0 is the initial peak power. According to the initial laser parameters, the fiber core diameter and the fluoroindate dispersion of 10 ps/km•nm around 3.4 µm, we obtain a fission length $L_{fiss} \approx$ 2 cm. Also, when estimating the soliton order (N) for the 120 nJ laser pulse injected into the fluoroindate fiber, we obtain a relatively low order:

$$N = \sqrt{\frac{L_D}{L_N}} \cong 7$$

which indicates that the fission did not occur randomly due to modulation instability and the coherence of the laser pulse was preserved during the SC generation [6].

Considering the fluoroindate fiber dispersion, the 70 fs initial laser pulse duration and the few centimeters long fission length, we determined that most of the spectral broadening from self-phase modulation and Raman-shift occurred within the first tens of centimeters of the fiber. Thereafter, the dispersion lengthened the broadband laser pulsewidth and decreased significantly the peak intensities. Finally, linear propagation of the generated SC occurred for the rest of the fiber length (or approximately for 8.5 m of propagation). At the

fluoroindate fiber output, the pulse duration of the chirped SC laser pulse is estimated to be ~ 100 ps and its peak power is ~ 1 kW. These estimations and the SC presented in Figure 4-24(a) point out the very good transmission of the fluoroindate fiber for the whole SC generated at the beginning of the fiber because no absorption bands or absorption cut-off were observed in the measured output spectra.

In summary, the anomalous dispersion of step-index fluoroindate fiber in the mid-infrared is relatively low and permits the SC generation from a wider range of initial central wavelength for the injected laser pulses. Moreover, the very low loss between 1 µm and 5 µm allows a continuous expansion of the SC without any interception from an absorption edge or an absorption band as in the case of long ZBLAN or long chalcogenide fibers, respectively. With a large core single-mode fluoroindate fiber, we demonstrated the generation of 20 dB spectral flatness SC from 2.7 µm to 4.7 µm, which covers almost entirely the mid-infrared atmospheric windows. Single-mode fluoroindate fiber represents unambiguously a promising fiber for the generation of multi-watt SC over a wide spectral range.

4.2.3.2 High Average Power Supercontinuum Generation in an Indium Fluoride Fiber

Contributors to this Section: Jacek Swiderski[13], Francis Théberge[14], Maria Michalska[13], Pierre Mathieu[14], Denis Vincent[14]

In this section we report the first demonstration of Watt-level Supercontinuum (SC) generation in a step index indium fluoride (fluoroindate) fiber pumped by a 1.55 µm fiber Master-Oscillator Power Amplifier (MOPA) system. The SC is generated in two steps: first ~ 1 ns amplified laser diode pulses are broken up into soliton-like sub-pulses leading to initial spectrum extension and then launched into a fluoride fiber to obtain further spectral broadening. The pump MOPA system can operate at a changeable repetition frequency delivering up to 19.2 W of average power at 2 MHz. When the 8-m long fluoroindate fiber was pumped with 7.54 W at 420 kHz output average SC power as high as 2.09 W with 27.8% of slope efficiency was recorded. The achieved SC spectrum spread from 1 to 3.05 µm.

To extend the transmission range in the mid-IR while providing the high-power capacity at the same time, indium fluoride (fluoroindate) fibers seem to be a good choice. They have lower phonon energy than ZBLAN glasses which increases their transparency in the mid-IR region to ~ 5.5 µm [72]. Furthermore, to obtain SC generation, they can be pumped effectively by the novel pulsed laser system already developed, for example [14],[16],[36],[50],[73]-[74]. Even though fluoroindate fibers (and suitable pump sources) are accessible, there have been no reports on high-power SC generation in these media.

The experimental arrangement for SC generation is shown in Figure 4-25. Basically it consists of two parts – a pump laser (developed at MUT, Poland) and a non-linear fluoride fiber (provided by DRDC, Canada). The pump MOPA system is a four-stage fiber amplifier, seeded with a directly modulated Distributed Feedback (DFB) laser delivering 1 ns pulses at λ = 1.55 µm and at variable Pulse Repetition Frequency (PRF) in the range of 0.2 – 2 MHz.

[13] Institute of Optoelectronics, Military University of Technology, 2 Kaliskiego Street, 00-908 Warsaw, Poland.

[14] DRDC Valcartier, 2459 route de la Bravoure, Québec (Québec) G3J 1X5, Canada.

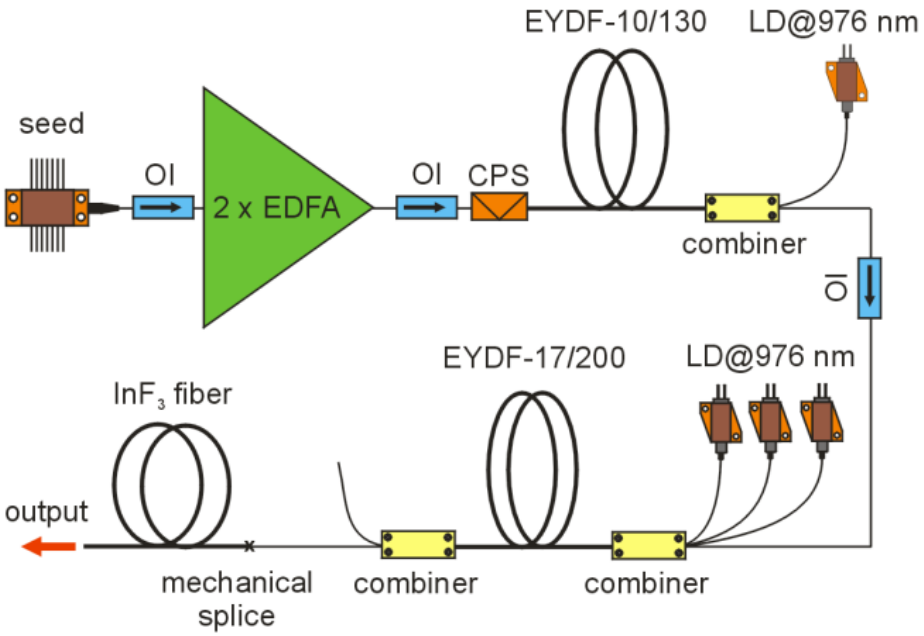

Figure 4-25: Set-Up for SC Generation. OI – Optical Isolator; EDFA – Erbium-Doped Fiber Amplifier; EYDF – Erbium:Ytterbium-Doped Fiber; CPS – Cladding Power Stripper; LD – Laser Diode.

The optical pulses delivered by the seed diode are first pre-amplified in two core-pumped Er-Doped Fiber Amplifiers (EDFAs) and one cladding pumped Er:Yb-Doped Fiber mid-Amplifier (EYDFA1). This system part could generate up to 2.1 W of average output power providing up to 58.5 dB of total gain, as reported in [2],[74]. The pulse train from the EYDFA1, after optical isolation, is then boosted in an Er:Yb-Doped Fiber power Amplifier (EYDFA2). The gain medium of EYDFA2 is a ~ 4.5-m long Er^{3+}:Yb^{3+}-co-doped, polarization maintaining, double-clad, Large-Mode-Area (LMA) fiber (EYDF) with a core diameter of 17 µm and a clad diameter of 200 µm, the NA was 0.17 for the core and 0.46 for the inner clad. A (6 + 1) x 1 pump combiner with a signal feedthrough (signal input: SMF-28; pump ports: 105/125 µm, 0.22 NA; signal output: passive double-clad 17/200 µm fiber, 0.17/0.46 NA) was used to deliver pump radiation to the active fiber. It combined power emitted by three 30 W multi-mode fiber-pigtailed (core diameter of 105 µm) laser diodes operating at the central wavelength of λ = 976 nm. Over 90% of the launched pump light was absorbed in the active fiber. The output of the LMA EYDF was first equipped with a home-made mode field adaptor (fiber taper) with a 17/200 µm (0.1/046 NA) fiber at the input and 25/300 µm (0.1/046 NA) fiber at the output. Then it was fusion spliced to a second pump combiner (signal input: passive double-clad 25/300 µm fiber, 0.1/0.46 NA; pump ports: 105/125 µm, 0.22 NA; signal output SMF-28) providing > 85% signal transmission. This allowed for filtering the unabsorbed pump power at λ = 976 nm from the amplified 1.55 µm pulse train. Furthermore, the 1.5-m long output pigtail fiber of the second combiner with ~ 8 µm core diameter permitted easy pump light coupling into the non-linear fiber. The active fiber of the EYDFA2 was coiled on a 10-cm diameter cylinder placed on a water-cooled heat-sink that was kept at 18 – 19 °C. Finally, the output signal fiber port of the combiner was mechanically spliced to the input end of the fluoroindate fiber with over 90% launching efficiency. Both fibers ends were angle-cleaved to prevent any reflection in the system.

Figure 4-26 presents the MOPA system average output power (after the 1.5-m long SMF fiber), for the PRF of 0.42, 1, and 2 MHz versus absorbed pump power in the EYDFA2. The inset in the top-left corner presents the spectrum generated at the system output for 2 MHz repetition rate and 19.2 W of output power while the inset in bottom right corner depicts the spectrum measured for 0.42 MHz repetition rate and 7.54 W of output power.

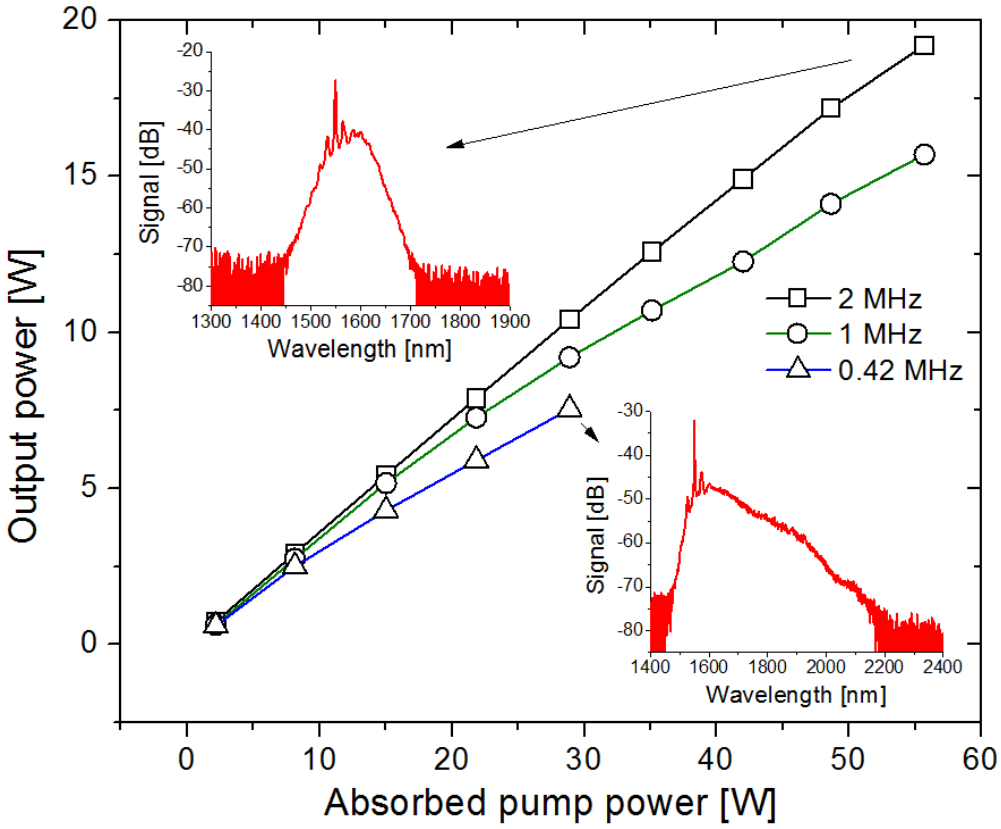

Figure 4-26: The Pump MOPA System Output Power. Top inset – Signal spectrum at 2 MHz and 19.2 W of output power; Bottom inset – Signal spectrum at 0.42 MHz and 7.54 W of output power.

As can be seen in Figure 4-26, average output power increases almost linearly with the rise of absorbed pump power. The maximum average output power for 55.7 W of absorbed pump power, measured at the highest PRF, was 19.2 W with 35% of slope efficiency determined with respect to absorbed pump power. For the lowest applied repetition rate of 0.42 MHz and 29 W of absorbed pump power, the output power was measured to be 7.54 W with 26% slope efficiency. The limit of output power for the lower PRF resulted from the presence of Amplified Spontaneous Emission (ASE) emitted by the Yb^3-dopant of the gain fiber. With the increase in pump power, the output spectrum gradually extended towards mainly mid-IR region. For instance, at 420 kHz repetition rate and output power of 7.54 W the spectrum covered the band of ~ 1.45 – 2.15 μm. The shape of the spectra presented in the insets is typical for pumping in the anomalous dispersion region of the fiber – with signature of a residual peak at the pump wavelength and a continuum signal spread about 15 – 20 dB below the maximum peak. Furthermore, the spectra show a set of two sidebands, symmetrically separated from the pump wavelength. It is a characteristic feature for Modulation Instability (MI) phenomenon which causes the breakup of 1 ns pulses in the 1.5-m long SMF into femtosecond pulses [16] leading to boosting pulse peak power and thus spectrum extension.

In the next step, the pump pulse train with an initially broadened spectrum was launched into the 8-m long fluoroindate fiber with a core/clad diameter of 16.7/125 μm and a core NA of 0.17. Its attenuation curve is shown in Figure 4-27. The losses in the range of 1.5 – 5 μm were measured to be < 0.8 dB/m. The minimum losses of 0.3 dB corresponded to $\lambda = 4.15$ μm. The peak at ~ 2.9 μm is related to OH absorption. The Zero Dispersion Wavelength (ZDW) of the fiber was at 1.83 μm, as specified by the manufacturer. The cut-off wavelength was measured to be at 3.72 μm, which means that the fiber is multi-mode at the pump wavelength and single-mode for $\lambda > 3.72$ μm.

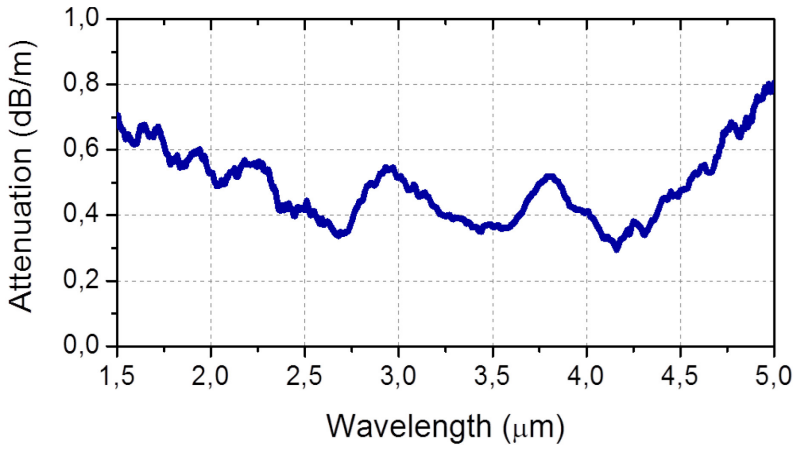

Figure 4-27: Attenuation Curve of the Fluoroindate Fiber.

During the experiment we decided not to exceed 8 W of pump power at 1.55 μm launched into the non-linear fiber, which we considered to be safe for it. To determine the best conditions for SC generation we changed the PRF of the MOPA system from 2 MHz to 0.4 MHz while keeping its output power constant and monitoring a spectrum at the fluoride fiber output end. Best continua extension was achieved at lower repetition rates (< 500 kHz) which can be attributed to the boost of peak power launched into the 1.5-m long SMF and then into the fluoride fiber. It leads to the enhancement of non-linearity and thus efficiency of SC generation process. Pumping the fluoroindate fiber with 7.54 W at 0.42 MHz repetition rate we achieved 2.09 W of total average output SC power, of which 0.96 W (45.9%), 0.57 W (27.3%) and 177 mW (8.5%) corresponded to wavelengths longer than 1.65 μm, 2 μm, and 2.4 μm, respectively (Figure 4-28). In the present MOPA system configuration it was difficult to lower the PRF below 400 kHz while keeping the output power at > 5 W, which resulted from the presence of ASE at ~ 1.06 μm coming from the EYDFA2, affecting the whole system performance at lower repetition rates.

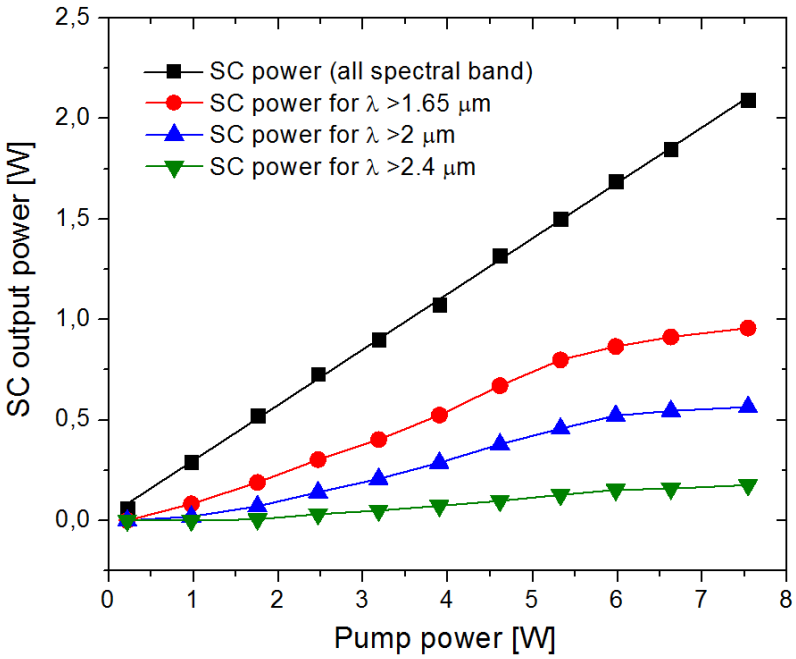

Figure 4-28: SC Average Output Power vs. Launched Pump Power, Measured for 1 ns Pulses and 0.42 MHz Repetition Rate.

Figure 4-29 illustrates the output SC spectrum at the fluoride fiber output. The inset shows the ratio of SC output power measured for λ > 1.65 μm to SC power in the whole spectral band versus launched pump power. The spectrum was measured using two optical spectrum analyzers (measurement in the range of 0.6 – 2.4 μm) and a monochromator with a thermoelectrically cooled HgCdTe detector (for wavelength beyond 2.4 μm). The pump signal was first broadened in the 1.5-m long SMF covering the band of 1.45 – 2.15 μm and then it was launched into the fluoride fiber. Since the fluoroindate fiber has the ZDW at 1.83 μm, it was pumped both in normal and anomalous dispersion region. It means that Raman-induced scattering was mainly responsible for the spectrum extension towards the mid-IR while self-phase modulation and dispersive wave generation contribute to spectrum extension towards shorter wavelengths [39],[40]. As can be seen, the output spectrum spreads from ~ 1 μm to 3.05 μm with a residual peak at the pump wavelength. The 10 dB flatness, excluding the pump peak, is kept in the range of ~ 1.2 – 2.4 μm. For wavelengths longer than 2.4 μm the output signal slowly drops, which results mainly from the fiber attenuation. Further spectral extension could be possible by decreasing the PRF. However the current pump system at lower frequencies (< 400 kHz) reveals significant growth of the 1 μm ASE in the power erbium:ytterbium amplifier. The build-up of the ASE may arise from the high ytterbium doping concentration of the LMA Yb^{+3}-doped fiber, manifesting itself at low duty factors. As Figure 4-29 illustrates, at the short-wavelength part of the spectrum, the ASE signal at about 1.06 μm is clearly visible.

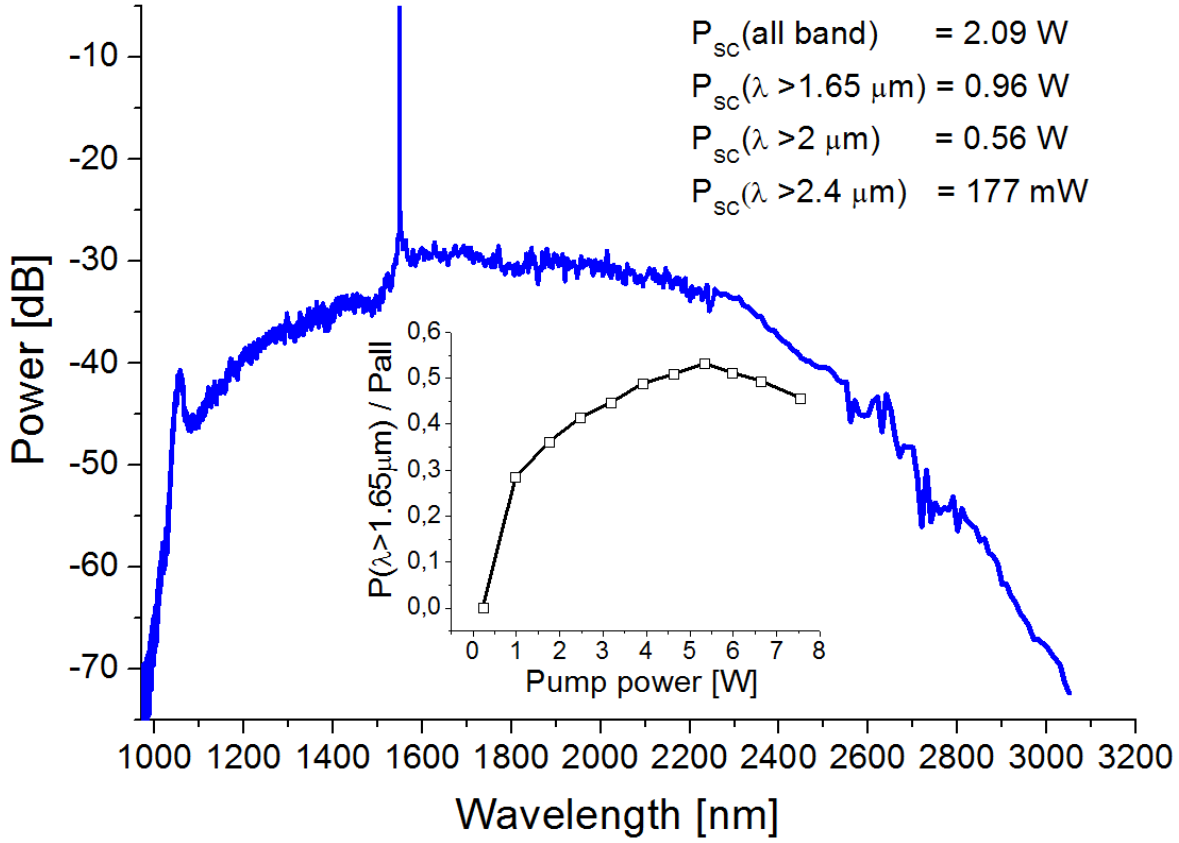

Figure 4-29: SC Spectrum after Propagation Through the Fluoroindate Fiber for the Maximum Output Power. Inset, the ratio of SC output power measured for λ > 1.65 μm to SC power in the whole spectral band versus launched pump power.

Another feature of the observed SC generation is that there was a pump power level, at which spectral broadening towards longer wavelengths was ineffective. As can be seen in the inset in Figure 4-29, for pump power > 5.3 W the ratio of SC power at λ > 1.65 μm to SC in the whole recorded spectral band started to

drop and the power was distributed more effectively towards shorter wavelengths. As Figure 4-28 illustrates, the SC power measured in the whole spectral band increases linearly with the increase in pump power reaching 27% of slope efficiency. However, in case of SC power measured for $\lambda > 1.65$ μm, the slope efficiency is 15.7% (for pump power up to 5.3 W) and then with further increase in pump power it falls to 7.1%. We believe that such behaviour is caused by more effective conversion to a shorter wavelength range, probably due to pumping the fluoroindate fiber more intensively in the normal dispersion region.

The measured spectrum covers over 2000 nm span and it could be further extended by applying more powerful pump source and by using an indium fluoride fiber with smaller core. The fiber non-linearity is defined by the non-linear parameter $\gamma = 2\pi n_2/\lambda A_{eff}$, where n_2 is the non-linear refractive index, λ is the wavelength of the pump pulse and A_{eff} is the effective mode area of a mode propagating inside the fiber. It means that the effective mode area and thus fiber core directly affects the fiber non-linearity. In our case the fluoroindate fiber has the core diameter of 16.7 μm, which is large comparing, e.g. with ZBLAN fibers, where a core diameter is ~ 7 μm, allowing for efficient SC generation even beyond 4.4 μm [23]. The fiber attenuation could be also reduced leading to more effective non-linear interaction and lower thermal load.

In conclusion, the first demonstration of high average power SC generation in a 8-m long step-index indium fluoride fiber pumped by a 1.55 μm MOPA system is reported. A SC extending from 1 μm to 3.05 μm with 2.09 W of total average output power was demonstrated. The system was tested over a week for several hours per day and any fiber degradation was not noticed. The output power of the system should be further scaled up by applying more pump power, lowering the PRF and using a fluoroindate fiber with lower material losses. It should also provide more efficient SC spectrum extension.

4.3 CONCLUSIONS

Mid-Infrared (MIR) Supercontinuum (SC) generation has attracted great attention from the research community, mainly due to its numerous potential applications in infrared microscopy, spectroscopy, medicine, and military technique. Most of the applications require high power, broadband sources emitting radiation in the 2 – 5 μm spectral band. Up to now, there have been many reports on mid-infrared SC generation in soft-glass fibers, including telluride, chalcogenide, and fluoride fibers pumped by a variety of laser sources. However, most of the reported works concern experiments with high peak power femtosecond lasers or optical parametric amplifiers, where output average pump power and thus output SC power is limited to mW-level. To achieve high average power, longer pump pulses on the picosecond or nanosecond scale are needed. Sparse literature reports on high-power (> 0.5 W) SC generation show that this technology is still in its infancy. However, the latest results, including the ones reported by the NATO SET-170 RTG, indicate that the objective of developing ruggedized, ready-to-use, multi-watt supercontinuum sources should be met in the near future.

The highlights of the research on mid-IR SC generation carried out by the members of NATO SET-170 RTG are as follows:

- The first demonstration of the highest average SC power (0.565 W) and the broadest spectrum (1.9 – 4.8 μm) directly emitted from a step-index chalcogenide (As_2S_3) fiber.
- The first demonstration of broadband (2.7 – 4.7 μm) mid-IR SC generation in a step-index indium fluoride (fluoroindate) fiber.
- The first demonstration of Watt-level (2.09 W in the 1 – 3.05 μm spectral band) SC generation in a step-index indium fluoride (fluoroindate) fiber.
- The first demonstration of Watt-level (1.08 W) SC generation (from 1.9 μm to 3.6 μm) in a ZBLAN fiber pumped by an actively Q-switched and mode-locked Tm-doped fiber laser (the pump laser is an example of single pump oscillator approach, making this pump scheme promising for future high power SC sources).

- The first demonstration of Watt-level (1.25 W in the 1.8 – 4.15 μm spectral band) SC generation in a step-index ZBLAN fiber pumped by a fast gain-switched Tm-doped fiber laser and amplifier system.
- The first demonstration of most efficient SC power distribution towards the mid-IR (from 288 mW of output power, 266 mW (92%), 240 mW (83%), 167 mW (58%) and 60 mW (21%) were measured for wavelengths beyond 2 μm, 2.4 μm, 3 μm and 3.6 μm, respectively).

Analyzing the foregoing results as well as the results presented in the available literature recently it can be stated that practical realization of broadband, high average power mid-IR supercontinuum sources that could meet requirements imposed by many applications (especially military applications) is still challenging. This challenge concerns both non-linear media suitable for mid-IR SC generation as well as pump lasers. The most significant factors that limit the long-wavelength edge of the SC spectrum are fiber non-linearities, bend-induced loss and fiber material absorption. The most promising non-linear fibers are telluride, chalcogenide and fluoride based fibers. The first two groups are characterized by very high non-linearity facilitating efficient spectrum extension over short fiber lengths, however these glasses are susceptible to thermally induced damage at high powers thus limiting the output average power < 2 W. The most perspective fibers for high-power SC generation seem to be fluoride (ZBLAN) fibers, in which 10.5 W of average power (in the 0.8 – 4 μm spectral band) has been reported recently. According to the theoretical analysis [33] the average power of the mid-IR SC generated in a single-mode ZBLAN fiber can be further scaled up to ~ 15 W and even to ~ 40 W by implementing better thermal management and heat dissipation techniques (e.g. wrapping an optical fiber with a thermal pad with high thermal conductivity). The same power limitation could be addressed to fluoroindate fibers, but contrary to ZBLAN fibers they are transparent to ~ 5.5 μm, therefore enabling covering the whole 2 – 5 μm spectral band.

Using novel, reliable and high-power fiber-based laser systems facilitating coupling the pump light into a non-linear fiber, output average power of > 20 W from a single-mode fluoride fiber covering the mid-IR band should be achieved within the next 2 – 5 years.

4.4 REFERENCES

[1] Kudlinski, A., George, A.K., Knight, J.C., Travers, J.C., Rulkov, A.B., Popov, S.V. and Taylor, J.R. Zero-dispersion wavelength decreasing photonic crystal fibers for ultraviolet-extended supercontinuum generation, Opt. Express 14, 5715-22 (2006).

[2] Swiderski, J. and Michalska, M. Mid-infrared supercontinuum generation in a single-mode thulium-doped fiber amplifier, Laser Phys. Lett. 10, 035105 (2013).

[3] Cumberland, B.A., Travers, J.C., Popov, S.V. and Taylor, J.R. 29 W high power CW supercontinuum source, Opt. Express 16, 5954-62 (2008).

[4] Baronio, F., Conforti, M., Angelis, C.D., Modotto, D., Wabnitz, S., Andreana, M., Tonello, A., Leproux, P. and Couderc, V. Second and third order susceptibilities mixing for supercontinuum generation and shaping, Opt. Fiber Technol. 18, 283-9 (2012).

[5] Moller, U., Sorensen, S.T., Larsen, C., Moselund, P.M., Jakobsen, C., Johansen, J., Thomsen, C.L. and Bang, O. Optimum PCF tapers for blue-enhanced supercontinuum sources. Opt. Fiber Technol. 18, 304-314 (2012).

[6] Dudley, J.M., Genty, G. and Coen, S. Supercontinuum generation in photonic crystal fiber, Rev. Modern Phys. 78, 1135-84 (2006).

[7] Izawa, T., Shibata, N. and Takeda, A. Optical attenuation in pure and doped fused silica in their wavelength region, Appl. Phys. Lett. 31, 33-35 (1977).

[8] Liao, M., Gao, W., Duan, Z., Yan, X., Suzuki, T. and Ohishi, Y. Supercontinuum generation in short tellurite microstructured fibers pumped by a quasi-cw laser, Opt. Lett. 37, 2127-29 (2012).

[9] Domachuk, P., Wolchover, N.A., Cronin-Golomb, M., Wang, A., George, A.K., Cordeiro, C.M.B., Knight, J.C. and Omenetto, F.G. Over 4000 nm bandwidth of mid-IR supercontinuum generation in sub-centimeter segments of highly nonlinear tellurite PCFs, Opt. Express 16, 7161-68 (2008).

[10] Ebendorff-Heidepriem, H., Kuan, K., Oermann, M.R., Knight, K. and Monro, T.M. Extruded tellurite glass and fibers with low OH content for mid-infrared applications, Opt. Mat. Express 2, 432-42 (2012).

[11] Gattass, R.R., Shaw, L.B., Nguyen, V.Q., Pureza, P.C., Aggarwal, I.D. and Sanghera, J.S. All-fiber chalcogenide-based mid-infrared supercontinuum source, Opt. Fiber Technol. 18, 345-8 (2012).

[12] Sanghera, J.S., Aggarwal, I.D., Shaw, L.B., Florea, C.M., Pureza, P., Nguyen, V.Q. and Kung, F. Nonlinear properties of chalcogenide glass fibers, J. Optoelectron. Advan. Mat. 8, 2148-55 (2006).

[13] Marandi, A., Rudy, C.W., Plotnichenko, V.G., Dianov, E.M., Vodopyanov, K.L. and Byer, R.L. Mid-infrared supercontinuum generation in tapered chalcogenide fiber for producing octave-spanning frequency comb around 3 μm, Opt. Express 20, 24218-25 (2012).

[14] Eckerle, M., Kieleck, C., Swiderski, J., Jackson, S.D., Mazé, G. and Eichhorn, M. Actively Q-switched and mode-locked Tm^{3+}-doped silicate 2 μm fiber laser for supercontinuum generation in fluoride fiber, Opt. Lett. 37, 512-14 (2012).

[15] Qin, G., Yan, X., Kito, C., Liao, M., Chaudhari, C., Suzuki, T. and Ohishi, Y. Ultrabroadband supercontinuum generation from ultraviolet to 6.28 μm in a fluoride fiber, Appl. Phys. Lett. 95, 161103 (2009).

[16] Alexander, V.V., Kulkarni, O.P., Kumar, M., Xia, C., Islam, M.N., Terry Jr., F.L., Welsh, M.J., Ke, K., Freeman, M.J., Neelakandan, M. and Chan, A. Modulation instability initiated high power all-fiber supercontinuum lasers and their applications, Opt. Fiber Technol. 18, 349-74 (2012).

[17] Buczynski, R., Bookey, H.T., Pysz, D., Stepien, R., Kujawa, I., McCarthy, J.E., Waddie, A.J., Kar, A.K. and Taghizadeh, M.R. Supercontinuum generation up to 2.5 μm in photonic crystal fiber made of lead-bismuth-galate glass, Laser Phys. Lett. 7, 666-72 (2010).

[18] Saad, M. Fluoride glass fiber: state of the art, Proc. SPIE 7316, 73160N-1-16 (2009).

[19] Monro, T.M. and Ebendorff-Heidepriem, H. Progress in microstructured optical fibers, Annual Review of Material Research 36, 467-95 (2006).

[20] Hu, J., Menyuk, C.R., Shaw, L.B., Sanghera, J.S. and Aggarwal, I.D. Computational study of 3–5 μm source created by using supercontinuum generation in As2S3 chalcogenide fibers with a pump at 2 μm, Opt. Lett. 35, 2907-2909 (2010).

[21] Hu, J., Menyuk, C.R., Shaw, L.B., Sanghera, J.S. and Aggarwal, I.D. Maximizing the bandwidth of supercontinuum generation in As2Se3 chalcogenide fibers, Opt. Express 18, 6722-6739 (2010).

[22] Xia, C., Kumar, M., Kulkarni, O.P., Islam, M.N., Terry Jr., F.L., Freeman, M.J., Poulain, M. and Mazé, G. Mid-infrared supercontinuum generation to 4.5 μm in ZBLAN fluoride fibers by nanosecond diode pumping, Opt. Lett. 31, 2553-2555 (2006).

[23] Kulkarni, O.P., Alexander, V.V., Kumar, M., Freeman, M.J., Islam, M.N., Terry, J., Neelakandan, M. and Chan, A. Supercontinuum generation from 1.9 to 4.5 μm ZBLAN fiber with high average power generation beyond 3.8 μm using a thulium doped fiber amplifier, J. Opt. Soc. Am. B 28, 2486-2498 (2011).

[24] Gao, W., Amraoui, M.E., Liao, M., Kawashima, H., Duan, Z., Deng, D., Cheng, T., Suzuki, T., Messaddeq, Y. and Ohishi, Y. Mid-infrared supercontinuum generation in a suspended-core As2S3 chalcogenide microstructured optical fiber, Opt. Exp. 21, 9573-9583 (2013).

[25] Swiderski, J. and Michalska, M. Watt-level, all-fiber supercontinuum source based on telecom-grade fiber components, Appl. Phys. B 109, 177-181 (2012).

[26] Monro, T.M. and Ebendorff-Heidepriem, H. Progress in microstructured optical fibers, Annu. Rev. Mater. Res. 36, 467-495 (2006).

[27] Tolstik, N., Sorokin, E., Kalashnikov, V. and Sorokina, I. Soliton delivery of mid-infrared femtosecond pulses with ZBLAN fiber, Opt. Express 2, 1580-1587 (2012).

[28] Zhu, X. and Peyghambarian, N. High-Power ZBLAN Glass Fiber Lasers: Review and Prospect, Adv. In OptoElect. 2010, 1-23 (2010).

[29] Asobe, M., Suzuki, K., Kanamori, T. and Kubodera, K. Nonlinear refractive index measurement in chalcogenide-glass fibers by self-phase modulation, Appl. Phys. Lett. 60, 1153 (1992).

[30] Sanghera, J.S., Aggarwal, I.D., Shaw, L.B., Florea, C.M., Pureza, P., Nguyen, V.Q., Kung, F. and Aggarwal, I.D. Nonlinear properties of chalcogenide glass fibers, J. Opto-Elect. & Adv. Mat. 8, 2148-2155 (2006).

[31] Gattass, R.R., Shaw, L.B., Nguyen, V.Q., Pureza, P.C., Aggarwal, I.D. and Sanghera, J.S. All-fiber chalcogenide-based mid-infrared supercontinuum source, Opt. Fiber Technol. 18 345-348 (2012).

[32] Xia, C., Kumar, M., Cheng, M.-Y., Hegde, R.S., Islam, M.N., Galvanauskas, A., Winful, H.G. and Terry, Jr., F.L. Power scalable mid-infrared supercontinuum generation in ZBLAN fluoride fibers with up to 1.3 watts time-averaged power, Opt. Express 15, 865-871 (2007).

[33] Xia, C., Xu, Z., Islam, M.N., Terry, Jr., F.L., Freeman, M.J., Zakel, A. and Mauricio, J. 10.5 W Time-Averaged Power Mid-IR Supercontinuum Generation Extending Beyond 4 μm With Direct Pulse Pattern Modulation, IEEE Quantum Elect. 15, 422-434 (2009).

[34] Lamont, M.R.E., Luther-Davies, B., Choi, D.-Y., Madden, S. and Eggleton, B.J. Supercontinuum generation in dispersion engineered highly nonlinear (γ = 10 /W/m) As_2S_3 chalcogenide planar waveguide, Opt. Express 15, 14938-14944 (2008).

[35] Kumar, M., Islam, M.N., Terry, F.L., Freeman, M.J., Chan, A., Neelakandan, M. and Manzur, T. Stand-off detection of solid targets with diffuse reflection spectroscopy using a high-power mid-infrared supercontinuum source, Appl. Opt. 51, 2794-2807 (2012).

[36] Yang, W., Zhang, B., Yin, K., Zhou, X. and Hou, J. High power all fiber mid-IR supercontinuum generation in a ZBLAN fiber pumped by a 2 μm MOPA system, Opt. Express 21, 19732-19742 (2013).

[37] Thapa, R., Rhonehouse, D., Nguyen, D., Yao, Z., Zong, J. and Chavez-Pirson, A. Ultra-wide mid-IR supercontinuum generation in W-type tellurite fiber pumped by 2 micron ultrashort laser, in Frontiers in Optics 2012/Laser Science XXVIII, OSA Technical Digest (Optical Society of America), Paper FW4D.2 (2012).

[38] Dudley, J.M. and Taylor, J.R. Supercontinuum generation in optical fibers (Cambridge University Press, 2010).

[39] Agger, C., Petersen, C., Dupont, S., Steffensen, H., Lyngsøn, J.K., Thomsen, C.L., Thøgersen, J., Keiding, S.R. and Bang, O. Supercontinuum generation in ZBLAN fibers—detailed comparison between measurement and simulation, , J. Opt. Soc. Am. B 29, 635-645 (2012).

[40] Agrawal, G.P. Nonlinear Fiber Optics, 4th Edition (Academic Press, 2007).

[41] Dudley, J.M., Provino, L., Grossard, N., Maillotte, H., Windeler, R.S., Eggleton, B.J. and Coen, S. Supercontinuum generation in air-silica microstructured fibers with nanosecond and femtosecond pulse pumping, J. Opt. Soc. Am. B 19, 765-71 (2002).

[42] Geng, J., Wang, Q. and Jiang, S. High-spectral-flatness mid-infrared supercontinuum generated from a Tm-doped fiber amplifier, Appl. Opt. 51, 834-40 (2012).

[43] Kurkov, A.S., Kamynin, V.A., Sholokhov, E.M. and Marakulin, A.V. Mid-IR supercontinuum generation in Ho-doped fiber amplifier, Laser Phys.Lett. 8, 754-57 (2011).

[44] Pioger, P.H., Couderc, V., Leproux, P. and Champert, P.A. High spectral power density supercontinuum generation in a nonlinear fiber amplifier, Opt. Express 15, 11358-63 (2007).

[45] Akhmediev, N. and Karlsson, M. Cherenkov radiation emitted by solitons in optical fibers, Phys.Rev. A 51, 2602-07 (1995).

[46] Dudley, J.M., Genty, G., Dias, F., Kibler, B. and Akhmediev, N. Modulation instability, Akhmediev breathers and continuous wave supercontinuum generation. Opt. Express 17, 21497-21508 (2009).

[47] Skryabin, D.V. and Yulin, A.V. Theory of generation of new frequencies by mixing of solitons and dispersive waves in optical fibers, Phys. Rev. E 72, 016619 (2005).

[48] Jiang, M. and Tayebati, P. Stable 10 ns, kilowatt peak-power pulse generation from a gain-switched Tm-doped fiber laser, Opt. Lett. 32, 1797-1799 (2007).

[49] Larsen, C., Sorensen, S.T., Noordegraaf, D., Hansen, K.P., Mattsson, K.E. and Bang, O. Zero-dispersion wavelength independent quasi-CW pumped supercontinuum generation, Opt. Commun. 290, 170-174 (2013).

[50] Swiderski, J. and Michalska, M. Generation of self-mode-locked resembling pulses in a fast gain-switched thulium-doped fiber laser, Opt. Lett. 38, 1624-1626 (2013).

[51] Hagen, C.L., Walewski, S.W. and Sanders, S.T. IEEE Photon. Technol. Lett. 18, 91 (2006).

[52] Hübner, P., Kieleck, C., Jackson, S.D. and Eichhorn, M. Opt. Lett. 36, 2483 (2011).

[53] Shaw, L.B., Thielen, P.A., Kung, F.H., Nguyen, V.Q., Sanghera, J.S. and Aggarwal, I.D. IR supercontinuum generation in As–Se photonic crystal fiber, in: Proc. Advanced Solid State Photonics, Paper TuC5 (2005).

[54] Shaw, L.B., Gattass, R.R., Sanghera, J.S. and Aggarwal, I.D. All-fiber mid-IR supercontinuum source from 1.5 to 5 um, in: Proc. SPIE 7914, 7914-24 (2011).

[55] Price, J.H., Monro, T.M., Ebendorff-Heidepriem, H., Poletti, F., Horak, P., Finazzi, V., Leong, J.Y., Petropoulos, P., Flanagan, J.C., Brambilla, G., Feng, X. and Richardson, D.J. Mid-IR supercontinuum generation from nonsilica microstructured optical fibers, IEEE J. Sel. Top. Quant. Electron. 13, 738-749 (2007).

[56] Hagen, C.L., Walewski, J.W. and Sanders, S.T. Generation of a continuum extending to the midinfrared by pumping ZBLAN fiber with an ultrafast 1550-nm source, IEEE Photon. Technol. Lett. 18, 91-93 (2006).

[57] Ta'eed, V., Baker, N.J., Fu, L., Finsterbusch, K., Lamont, M.R.E., Moss, D.J., Nguyen, H.C., Eggleton, B.J., Choi, D.-Y., Madden, S. and Luther-Davies, B. Ultrafast all optical chalcogenide glass photonic circuits, Opt. Express 15, 9205-9221 (2007).

[58] Asobe, M., Kanamori, T., Naganuma, K., Itoh, H. and Kaino, T. Third-order nonlinear spectroscopy in As_2S_3 chalcogenide glass fibers, J. Appl. Phys. 77, 5518-5523 (1995).

[59] Xiong, C., Magi, E., Luan, F., Tuniz, A., Dekker, S., Sanghera, J.S., Shaw, L.B., Aggarwal, I.D. and Eggleton, B.J. Characterization of picosecond pulse nonlinear propagation in chalcogenide As2S3 fiber, Appl. Opt. 48, 5467-5474 (2009).

[60] Fortin, V., Bernier, M., Carrier, J. and Vallée, R., Fluoride glass Raman fiber laser at 2185 lm, Opt. Lett. 36, 4152-4154 (2011).

[61] Sanghera, J.S., Brandon Shaw, L. and Aggarwal, I.D., Chalcogenide glass-fiber-based mid-IR sources and applications, IEEE J. Sel. Top. Quant Electron. 15, 114-119 (2009).

[62] Lou, J.W. and Currie, M. High-energy saturable absorber mode-locked fiber laser system, Opt. Lett. 30, 406-408 (2005).

[63] Imeshev, G. and Fermann, M. 230-kW peak power femtosecond pulses from a high power tunable source based on amplification in Tm-doped fiber, Opt. Express 13, 7424-7431 (2005).

[64] Nguyen, V.Q., Sanghera, J.S., Cole, B., Pureza, P., Kung, F.H. and Aggarwal, I.D. Fabrication of arsenic sulfide optical fiber with low hydrogen impurities, J. Am. Ceram. Soc. 85, 2056-2058 (2002).

[65] Rice, J.P., Brown, S.W. and Neira, J.E. Development of hyperspectral image projectors, Proc. SPIE 6297, 629701 (2006).

[66] Rice, J.P., Neira, J.E., Kehoe, M. and Swanson, R. DMD diffraction measurements to support design of projectors for test and evaluation of multispectral and hyperspectral imaging sensors, Proc. SPIE 7210, 72100D (2009).

[67] Shaw, L.B., Gattass, R.R., Sanghera, J.S., Aggarwal, I.D. and Rice, J.P. Broadband mid-IR fiber supercontinuum source for hyperspectral image projection, in: 2011 IEEE Photonics Society Summer Topical Meeting Series, IEEE, pp. 93-94 (2011).

[68] Tolstik, N., Sorokin, E., Kalashnikov, V. and Sorokina, I. Soliton delivery of mid-infrared femtosecond pulses with ZBLAN fiber, Opt. Express 2, 1580-1587 (2012).

[69] Soufiane, A., Can, F., Helgouach, H.L. and Poulain, M. Material dispersion in optimized fluoroindate glasses, J. Non-Cryst. Sol. 184, 36-39 (1995).

[70] Schmidt, E., Shiner, A.D., Giguère, M., Lassonde, P., Trallero-Herrero, C.A., Kieffer, J.-C., Corkum, P.B., Villeneuve, D.M. and Légaré, F. High harmonic generation with long-wavelength few-cycle laser pulses, J. Phys. B: At. Mol. Opt. Phys. 45, 074008 (2012).

[71] Yan, X., Kito, C., Miyoshi, S., Liao, M., Suzuki, T. and Ohishi, Y. Raman transient response and enhanced soliton self-frequency shift in ZBLAN fiber, J. Opt. Soc. Am. B 29, 238-243 (2012).

[72] Saad, M. Indium fluoride glass fibers, Proc. SPIE 8275, 82750D (2012).

[73] Heidt, M., Li, Z., Sahu, J., Shardlow, P.C., Becker, M., Rothhardt, M., Ibsen, M., Phelan, R., Kelly, B., Alam, S.U. and Richardson, D.J. 100 kW peak power picosecond thulium-doped fiber amplifier system seeded by a gain-switched diode laser at 2 μm, Opt. Lett. 38, 1615-1617 (2013).

[74] Swiderski, J. and Michalska, M. Over three-octave spanning supercontinuum generated in a fluoride fiber pumped by Er&Er:Yb-doped and Tm-doped fiber amplifiers, Opt. & Laser Technol. 52, 75-80 (2013).

Chapter 5 – FIBER-PUMPED FREQUENCY CONVERSION DEVICES

5.1 BACKGROUND AND PREVIOUS WORK

Contributors to this section: Christelle Kieleck[1], Antoine Berrou[1], Marc Eichhorn[1]; Francis Théberge[2], Pierre Mathieu[2], Denis Vincent[2], Jean-François Daigle[3], Alain Villeneuve[4], Joseph Salhany[4], Brian Burgoyne[4], Yasaman Soudagar[4], Marc Châteauneuf[2], Jacques Dubois[2], Rita D. Peterson[5]

Mid-IR lasers find interesting applications in medicine, remote sensing [1], molecular spectroscopy of pollutants [2], detection of threats [3], etc. Ideally, the ultimate mid-IR laser should be intrinsically robust to mechanical vibrations, stable over temperature fluctuations, tunable over a broad spectral range, and efficient for low power consumption. A technology that could meet all these goals is the mid-IR fiber laser. Efficient and tunable rare-earth-doped mid-IR fiber lasers do not exist yet, and they still require the development of single-mode Infrared (IR) fibers and highly efficient pump sources [4]. Chalcogenide, fluoride and telluride fibers are under development to access spectral bands beyond the capability of silica, both as laser hosts and as non-linear materials. Fiber laser and mid-infrared supercontinuum generation studies are in progress. Substantial improvements in areas such as loss, power/energy handing, and active ion incorporation must occur, however, to allow for an all-fiber solution in the mid-IR.

An intermediate step toward completely fiber-based sources is a mid-IR source based on fiber-pumped frequency converters. The most mature and readily available fiber pump sources emitting in the near-infrared are Tm^{3+}- and Ho^{3+}-doped fibers operating around 2 µm. These are available as commercial products that are relatively robust, compact, efficient, and high in power and energy. In addition, their output is already farther in the infrared than that of more common Yb-based fibers. However, 2 µm fiber technology still suffers from a lack of commercial fiber components for high power and high energy operation – even though some fiber components are emerging [5].

On the non-linear material side, only a few crystals can fulfill the wavelength requirements associated with high-power applications in the atmospheric windows (3 – 5 µm and 8 – 12 µm): PPLN, covering only part of the 3 – 5 µm region; $ZnGeP_2$ (ZGP); and Orientation-Patterned Gallium Arsenide (OPGaAs). The website of Inrad, a vendor of ZGP, already claims that "recent advances in 2 µm fiber laser technology have increased the potential of ZGP for use in ruggedized, compact optical set-ups. Pumping ZGP with a fiber laser instead of a solid-state source could substantially reduce the footprint of the entire system (IRCM System)" [6]. Unfortunately ZGP and OPGaAs crystals are still not readily available, and other emerging non-linear crystals, though promising, remain untested.

Up to now, Optical Parametric Oscillators (OPO) that could generate mid-IR laser radiation have been developed, but these OPOs can generate only a few wavelengths at a time. Moreover these OPOs are sensitive to mechanical vibrations and temperature fluctuations, and thus difficult to implement for real applications in the field. Another high-potential mid-IR laser source under development is the Quantum Cascade Laser (QCL) which is based on microstructured semi-conductors usually requiring low-temperature cooling for achieving high power output. QCLs are however, not tunable over a broad spectral range, and thus several QCLs are needed in parallel to cover some specific wavelengths in the mid-IR spectral region [7].

[1] ISL, French-German Research Institute of Saint-Louis, 5 rue du Général Cassagnou, 68300 Saint-Louis Cedex, France.

[2] DRDC Valcartier, 2459 route de la Bravoure, Québec (Québec) G3J 1X5, Canada.

[3] AEREX Avionics Inc., 324 St-Augustin Avenue, Breakeyville (Québec) G0S 1E1, Canada.

[4] Genia Photonics Inc., 500 Cartier Blvd. West, Suite 131, Laval (Québec) H7V 5B7, Canada.

[5] Air Force Research Laboratory, AFRL/RYDH Bldg 620, 2241 Avionics Circle, Wright-Patterson AFB, OH 45433, United States.

This chapter will give part of the state-of-the-art of non-linear converters directly pumped by a fiber laser, and will concentrate only on those devoted to 3 – 5 µm emission, especially for DIRCM applications.

5.2 EXPERIMENTAL RESULTS

5.2.1 PPLN-Based Systems

Periodically Poled Lithium Niobate (PPLN) is a mature and widely available commercial non-linear crystal that can readily be directly fiber-pumped. As it is limited by intrinsic absorption to a maximum operating wavelength of approximately 4 µm, complete wavelength coverage for DIRCM application is not possible with this material system. As an example, set-ups are briefly described which can deliver average power in excess of 1 W in the 3.8 – 4.0 µm wavelength range at a pulse repetition frequency of 100 kHz and an average power of 0.25 W at 4.5 µm wavelength. The original design and performance of tunable mid-IR generation by fiber-pumped difference frequency mixing in PPLN, undertaken at DRDC, Canada, is described in detail.

5.2.1.1 Singly Resonant PPLN OPO Pumped by an Adjustable PRF 100 kHz, Linearly Polarized, 1545 nm Wavelength Pulsed Fiber Source

A mid-IR source consisting of a 10 W average-power, linearly polarized 1.54 µm wavelength pulsed fiber source pumping an optical parametric oscillator was reported, (Figure 5-1) [3]. From this source, average power in excess of 1 W in the 3.8 – 4.0 µm wavelength range at a pulse repetition frequency of 100 kHz was obtained. With a slightly different set-up, an average power of 0.25 W at 4.5 µm wavelength was achieved. Components are bulk with free-space coupling.

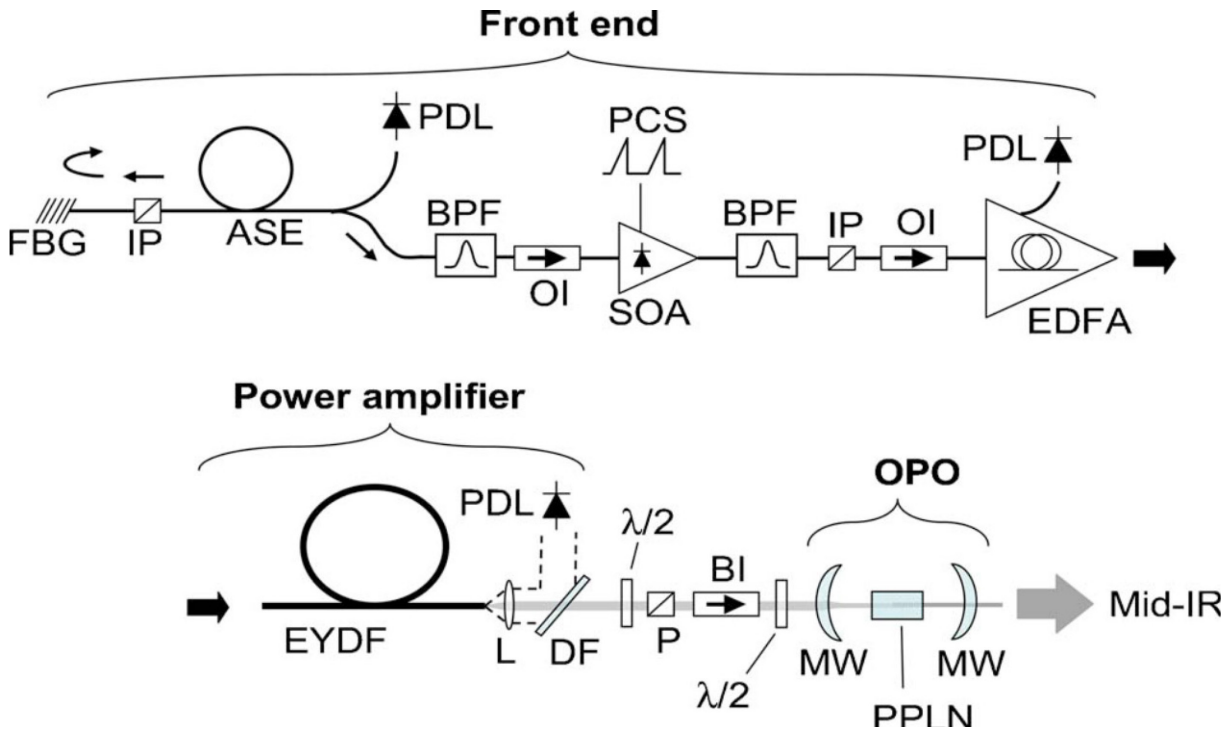

Figure 5-1: Layout of Mid-IR Source: Singly Resonant PPLN OPO Pumped by an Adjustable PRF 100 kHz, Linearly Polarized, 1545 nm Wavelength Pulsed Fiber Source.

5.2.1.2 Tunable Mid-Infrared Generation by Fiber-Pumped DFM in PPLN

Contributors to this section: Francis Théberge[6], Jean-François Daigle[7], Alain Villeneuve[8], Joseph Salhany[8], Brian Burgoyne[8], Yasaman Soudagar[8], Marc Châteauneuf[6], Jacques Dubois[6]

We present here a design based on Difference-Frequency Generation (DFG) in a non-linear crystal pumped by synchronized and tunable commercially available Near-Infrared (NIR) fiber lasers. This idea is not new and has been explored by others groups [8]-[12], but the latest innovations in NIR fiber lasers [13] have enabled the creation of fast-scanning picosecond fiber lasers.

The key element for the generation of a fast tunable mid-IR laser source through DFG is the programmable Erbium-doped fiber laser which combines dispersive elements with a synchronized Electro-Optic Modulator (EOM). This first fiber laser can emit any wavelength within the gain band, quickly tune to any wavelength in this range, and program any spectrally encoded signal. The basis of this laser is schematically presented in Figure 5-2(a). With an Erbium-doped fiber used as gain medium, a Wavelength Division Multiplexer (WDM) couples the energy of a 980 nm laser diode to provide core pumping. An Optical Coupler (OC) extracts a portion of the amplified light and delivers it to the next stage (Figure 5-3). The Programmable Laser (PL) is dispersion-tuned. A series of three Chirped Fiber Bragg Gratings (CFBG) serve as the dispersive element for covering as much of the Erbium-gain spectrum as possible, and are addressed by a circulator. The timing of the pulses to the EOM then determines which wavelength will see amplification by coordinating activation of the EOM with the arrival of the desired wavelength's pulse wavefront.

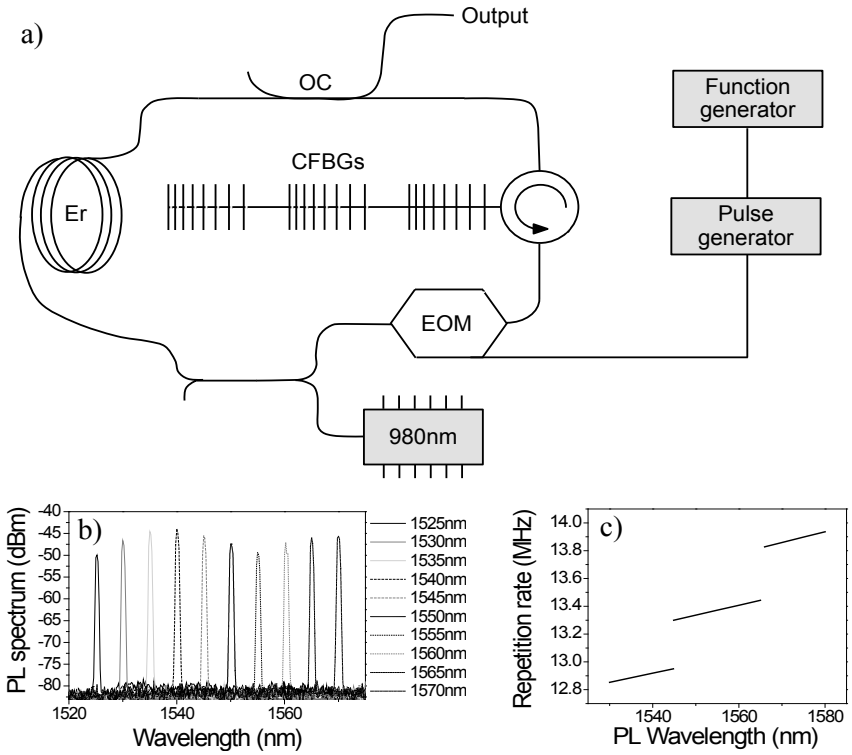

Figure 5-2: (a) Schematic of the Programmable Erbium-Doped Fiber Laser, Including: Electro-Optic Modulator (EOM), Output Coupler (OC), Chirped Fiber Bragg Grating (CFBG), Wavelength Division Multiplexer (WDM); (b) Samples of Laser Output Spectrum; (c) Repetition Rate as a Function of Amplified Wavelength.

[6] DRDC Valcartier, 2459 route de la Bravoure, Québec (Québec) G3J 1X5, Canada.

[7] AEREX Avionics Inc., 324 St-Augustin Avenue, Breakeyville (Québec) G0S 1E1, Canada.

[8] Genia Photonics Inc., 500 Cartier Blvd. West, Suite 131, Laval (Québec) H7V 5B7, Canada.

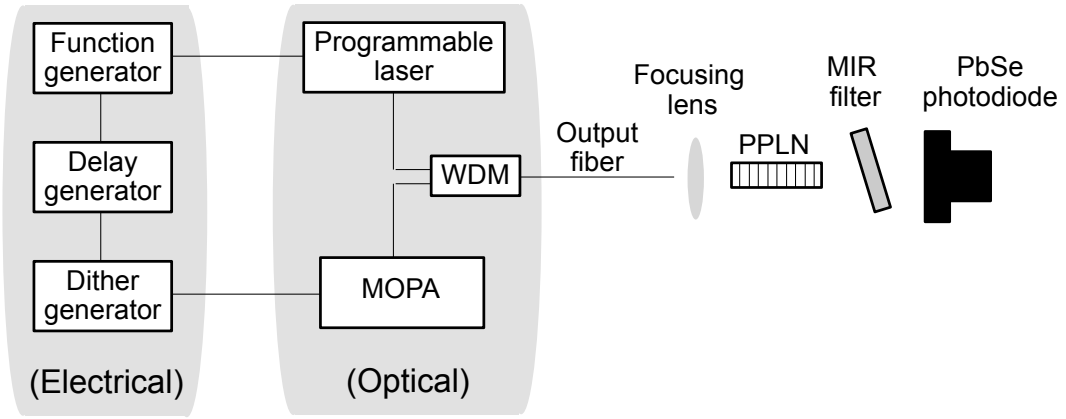

Figure 5-3: Set-Up for Generation and Characterization of the Tunable Mid-IR Laser. The programmable laser and MOPA outputs are combined by a broadband WDM. Both lasers are synchronized and controlled by high-speed electronics driven by software. At the output end of the fiber, the combined beams are focused into the PPLN crystal. The mid-IR output is filtered and its power measured by the PbSe photodiode.

Because of the small distance between the three CFBGs in this system, we observe two jumps in Figure 5-2(c), the graph of repetition rate as a function of wavelength. In fact, the signal applied to the EOM controls four parameters:

- Wavelength;
- Wavelength sweep;
- Repetition rate; and
- Optical pulsewidth.

The EOM is driven by a function generator/pulse generator combination. Operated on its own, the PL can output more than 10 million different optical frequencies per second with very high accuracy, stability, and reproducibility. Since the PL is a dispersion-tuned actively mode-locked laser, wavelengths may be selected in any arbitrary order, enabling wavelength sweeps in either sequential or arbitrary wavelength sequences. Wavelengths can be selected from the entire range or a partial range. The steps between adjacent wavelengths may be arbitrary or may be defined through the user interface in any arbitrary order.

In order to generate mid-IR signal through DFG, we needed an Ytterbium-doped fiber laser synchronized with the Erbium-based PL. One such picosecond laser system is the Synchronized Programmable Laser (SPL) from Genia Photonics that combines these two picosecond fiber laser systems in which both output pulses are synchronized at the DFG crystal (Figure 5-3). The SPL system used for these works consists of the Erbium-doped PL combined with an Ytterbium-doped fiber-based Master Oscillator Power Amplifier (MOPA). A WDM combines the two laser outputs into a single beam. The PL and MOPA use high-speed electronics to drive their internal EOM with precisely timed picosecond pulses.

The synchronization lies within a novel low-jitter function generator circuit capable of generating multiple signals to trigger the pulse generators of each laser. These signals can compensate for any delay in the external optical set-up, ensuring that pulses from both lasers are synchronized at the DFG crystal. Because the 9 µm core output fiber guides both laser beams, spatial overlap is automatically achieved and maintained up to the DFG crystal without the need for any alignment. The laser beams are focused into a 25-mm long PPLN crystal in single pass geometry. For the DFG scheme, the Ytterbium laser corresponds to the pump and the tunable Erbium laser is the signal, with the frequency of the mid-IR output given by the difference of frequency between the pump and the signal. After the PPLN crystal, residual pump and signal from the NIR lasers are filtered out by an AR-coated Germanium window. A calibrated PbSe photodiode is used to measure the power of the generated mid-IR beam.

The PL was continuously tunable from 1525 nm to 1600 nm while the wavelength of the MOPA was fixed at 1080 nm. In principle, the DFG could produce a mid-IR source tunable from 3.32 – 3.7 µm. However the temperature control of the PPLN oven limited the phase-matching such that tunability was possible only from 3.52 – 3.57 µm, with a quantum efficiency of 44% (Figure 5-4(a)). For a 25-mm long PPLN crystal with a grating period of 29.6 µm, the DFG phase-matching bandwidth for a fixed temperature was 2.6 nm, broad enough for our 25 ps pulse train having a spectral width of 0.25 nm.

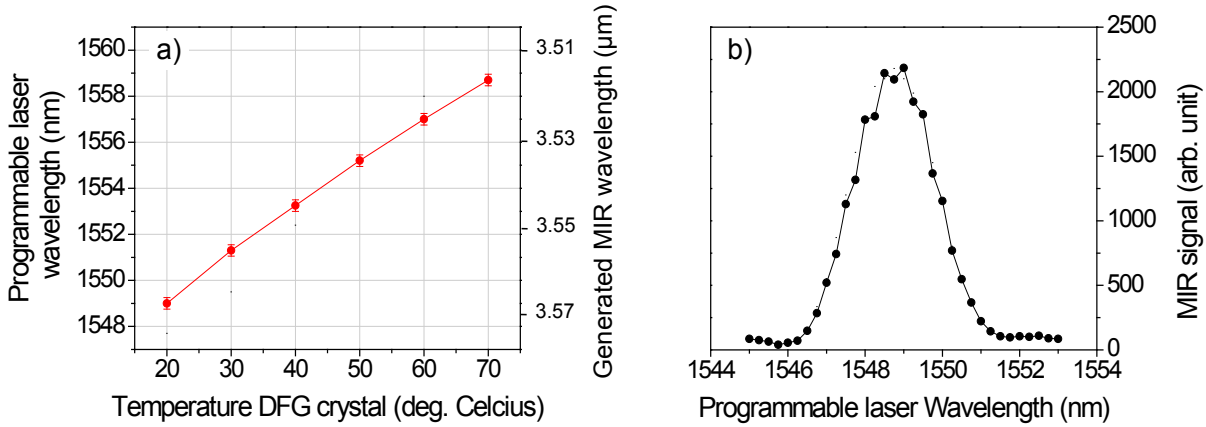

Figure 5-4: Measured DFG Phase-Matching in the PPLN Crystal as a Function of the Temperature (a) and DFG Phase-Matching Window of the PPLN (25 mm long) at Temperature of 20°C (b).

In order to exploit the entire spectral range of the PL, we used two other PPLN crystals with periods of 29.5 µm and 29.7 µm. Figure 5-5(a) presents examples of mid-IR spectra generated using the SPL at the maximum power for both the PL (35 mW) and the MOPA (32 mW). These spectra were measured with a grating-based monochromator and a Mercury Cadmium Telluride detector, and were obtained at the optimum delay between the PL and the MOPA pulses to produce maximum mid-IR output power. In these cases, we could almost cover the entire spectral range of the PL and an efficient mid-IR output was obtained from 3.4 – 3.7 µm. The double-peak structure observed in each spectrum is due to the Self-Phase Modulation (SPM) of the PL pulse occurring in the 2-m long fiber used to transport the output of the WDM to the PPLN crystal.

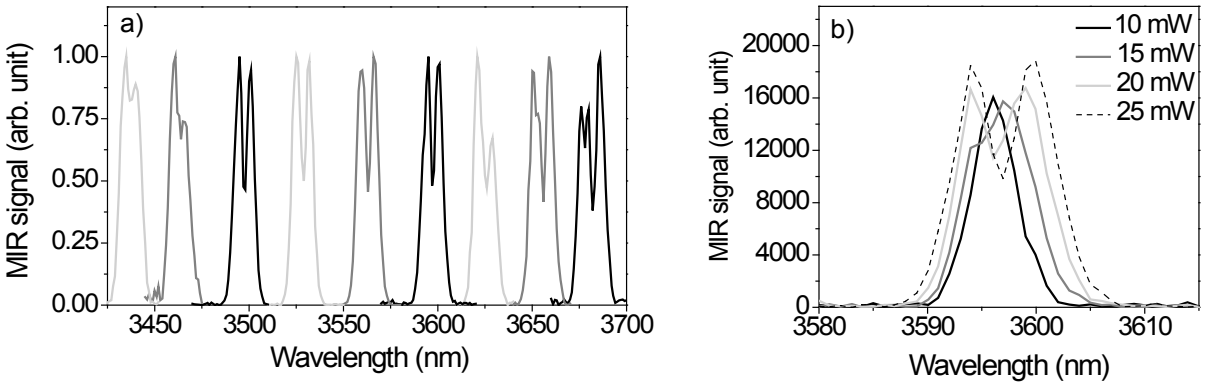

Figure 5-5: Normalized Mid-IR Spectrum Measured for Different PL Wavelengths, and PPLN Crystals with Periods of 29.7 µm and 29.5 µm (a); Mid-IR Spectrum Centred at 3.6 µm as a Function of PL Power (b).

Figure 5-5(b) illustrates the impact of the SPM by showing the spectral distribution of the mid-IR beam generated at 3.6 µm as a function of the PL power. At low power (10 mW), we observe a near-Gaussian spectral profile for the generated mid-IR beam. As the PL power was increased, spectral broadening was observed and then the double-peak structure became more pronounced. It is important to note that similar spectral broadening was evidently observed for the PL pulse at the output fiber (before the PPLN), but no spectral broadening was observed for both the PL and MOPA before the output fiber (i.e. after the WDM) at their maximum power. These observations clearly point to the 2-m long output fiber as the origin of the SPM. The use of a shorter fiber, or simply bypassing such fiber will definitely minimize the SPM.

Figure 5-6 shows the linear relationship between the mid-IR output power and the MOPA power injected into the PPLN crystal. The FWHM for the laser beam focused inside the PPLN was around 35 µm, which corresponds to a peak power density of 9 MW/cm^2 at the maximum injected power. Interestingly, by preserving the same power density in the PPLN, we could scale up the pump to 5 watts by focusing it to a diameter of 440 µm in the PPLN. Finally, by preserving a similar quantum efficiency of 44%, we could expect the generation of more than 100 mW of mid-IR output around 3.6 µm wavelength.

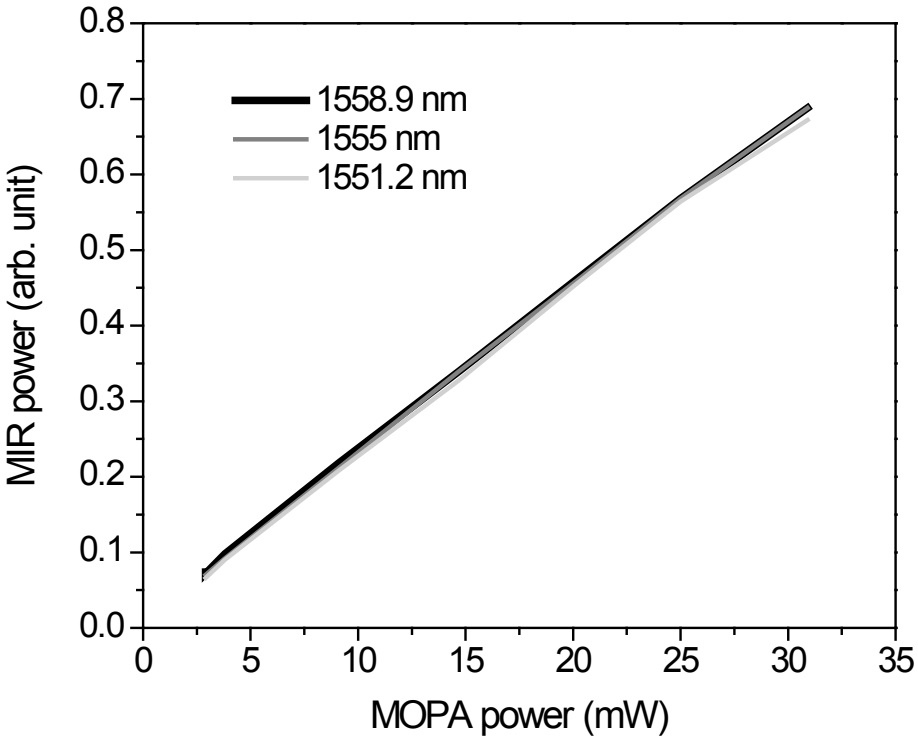

Figure 5-6: Mid-IR Power as a Function of MOPA Power. The PL power was maintained at its maximum for these measures.

The tunability of the mid-IR laser source as presented here was limited by the temperature control for the phase matching, but use of a chirped PPLN crystal would allow much wider tunability and very fast wavelength scanning at a fixed crystal temperature. Such a chirped PPLN crystal could be very long, given that the current 25-mm long PPLN crystal had a QPM bandwidth 10 times larger than the spectral bandwidth of the picosecond laser used in the experiment. By choosing the appropriate wavelengths for the PL and the MOPA, the DFG can be tuned over a wide range of operating wavelengths. For example, by using a tunable PL between 1020 nm and 1110 nm and a tunable MOPA between 1525 nm and 1605 nm the DFG idler can be tuned between 2.8 µm and 4.1 µm. It is also possible to increase by few orders of magnitude the laser powers injected into the chirped PPLN crystal, and consequently, to increase proportionally the mid-IR

output power by using a larger mode area fiber, longer pulsewidth for the SPL, and a shorter transport fiber before the PPLN crystal.

5.2.2 $ZnGeP_2$-Based Systems

ZGP is currently the most mature mid-IR non-linear crystal, offering efficient non-linear conversion in the mid- and long-wave-IR for countermeasures and other applications. ZGP OPOs pumped by Q-switched solid-state Ho:YAG lasers operating in the 2 µm spectral region have demonstrated very impressive results. Progress in fiber and fiber laser development has led to an increase in output power achievable from pulsed fiber systems. The high peak power and near diffraction-limited beam quality of these fibers make them an ideal source for driving non-linear frequency conversion in ZGP.

Daniel Creeden and co-workers reported the first mid-IR ZGP OPO pumped by a pulsed Tm-doped fiber laser [14],[15]. The fiber pump laser is a Master-Oscillator/Fiber-Amplifier (MOFA) configuration (Figure 5-7). The seed signal is generated by gain-switching a Tm-doped fiber, which produces 30 ns pulses at 1.995 µm at 100 kHz repetition rate. These pulses are amplified in a dual-stage Tm-Doped Fiber Amplifier (TDFA) chain. At the output of the TDFAs, the seed has been amplified more than 24 dB to 21 W of average output power (30 ns pulses, 100 kHz PRF) in a near-diffraction-limited beam with an M^2 of 1.1 ± 0.05 (Figure 5-8(a)). An optical isolator is placed in-line after the amplifiers to prevent feedback and to polarize the beam. Only 60% of the power is transmitted by the isolator, leaving 12.7 W of linearly polarized 1.995 µm light to pump the OPO, enough to produce 2 W of output power in the mid-IR in the 3.4 – 3.9 µm and 4.1 – 4.7 µm spectral regions simultaneously (Figure 5-8(b)).

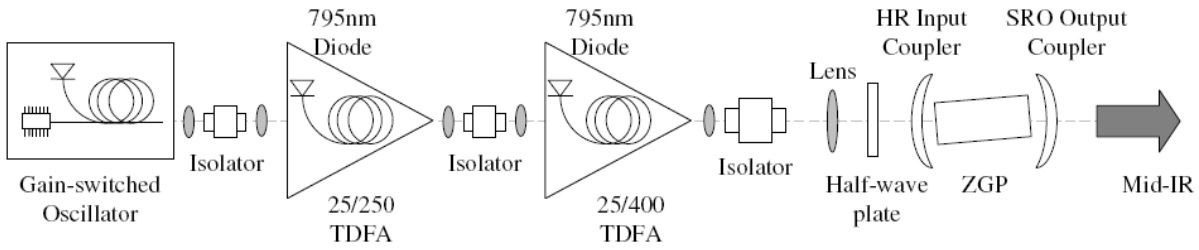

Figure 5-7: Schematic of the Tm-Fiber Amplifier Chain and ZGP Mid-IR OPO.

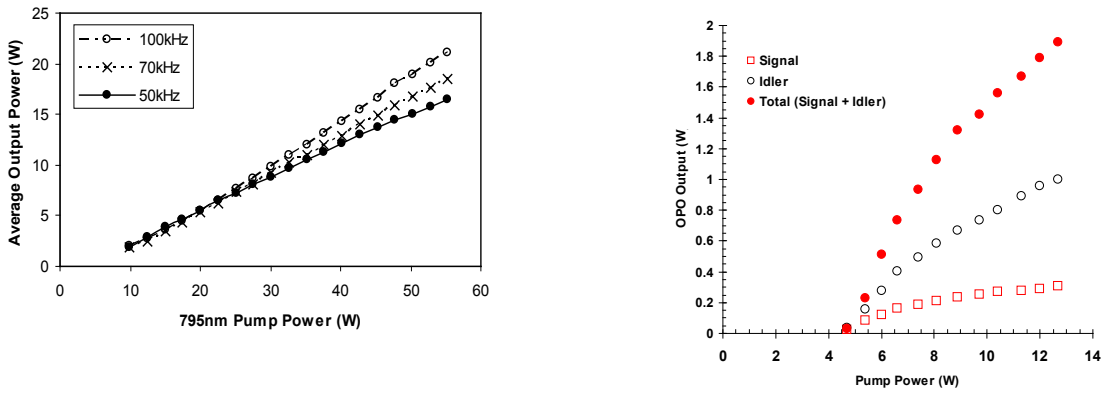

(a) **(b)**

Figure 5-8: Tm-Doped Fiber Amplifier (TDFA) Average Output Power vs. Pump Power (a) and ZGP OPO Output vs. 2 µm Pump Power (b).

The authors claimed that the set-up was not optimized, and suggested that future work focus on reducing the OPO threshold and improving conversion efficiency by power scaling the pump and reducing the oscillator pulse width such that a larger pump spot may be used to produce a high optical intensity in the ZGP. These changes could reduce walk-off, increase the interaction length in the crystal, and reduce the thermal lensing, thus decreasing the OPO threshold and improving conversion. They also mentioned that they have planned to examine various cavity configurations and the use of engineered materials, such as orientation-patterned GaAs, as ways to improve conversion efficiency.

A workshop on Mid-Infrared Fiber Lasers (NATO SET-171) was organized at the French-German Research Institute of Saint-Louis (ISL) on 28-29 September 2010 [16]. At the workshop, Daniel Creeden presented an overview of considerations for rare-earth-doped fibers used in pumping non-linear frequency conversion devices. He suggested that efforts should concentrate on promising Tm and Tm:Ho fiber development, because of their high efficiency and wavelength advantages. He also emphasized the need to develop fibers and components especially to eliminate free-space coupling in future fiber systems, allowing systems that are completely optically confined.

Since 2010 efforts in industry have concentrated on the development of fibers based on Tm and Ho, and on fiber components for the 2 µm wavelength range, and research groups have published mid-IR ZGP OPO results obtained using a pulsed Tm-doped fiber laser.

Australia's Defence Science and Technology Organisation reported highly efficient 2 µm fiber lasers based on Tm- and Ho-doped fibers, and reported the use of a 2 µm fiber source for parametric generation of mid-IR output in ZGP [17]. In this experiment, a pulsed master oscillator generated low energy pulses at a high repetition rate: 60 µJ pulses, 50-ns long at 150 kHz prf. (Figure 5-9, Figure 5-10 and Figure 5-11). These were then amplified in a Large-Mode-Area (LMA) Tm-Doped Fiber (TDF) with a 25-µm diameter core, producing 300 µJ pulses at a wavelength of 2050 nm. The output of the amplifier was then focused into an OPO cavity containing a 16-mm ZGP crystal. The cavity consisted of mirrors with a 200 mm radius of curvature, separated by 20 mm, with 10% outcoupling at 3.5 – 5 µm. The publication claimed that optical parametric oscillation was achieved but without giving performance data. In this fiber pump set-up (master oscillator and fiber amplifier), most of the components were still bulk components with free space coupling.

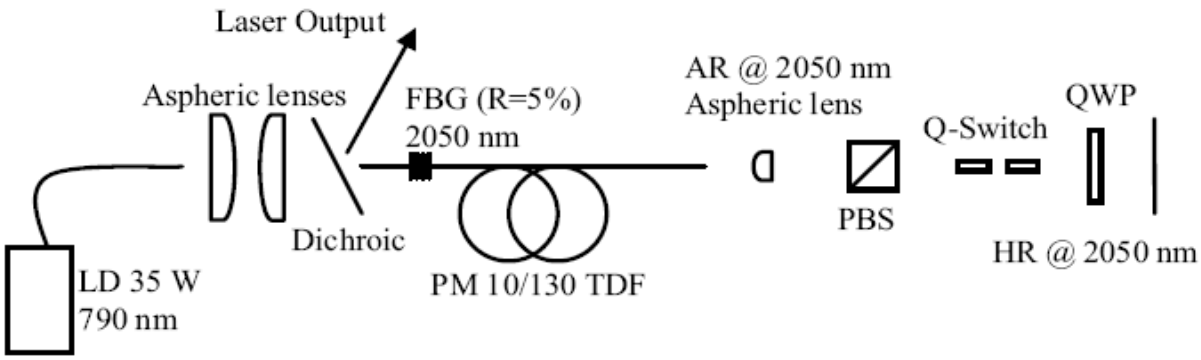

Figure 5-9: Schematic of Electro-Optically Q-Switched Master Laser.

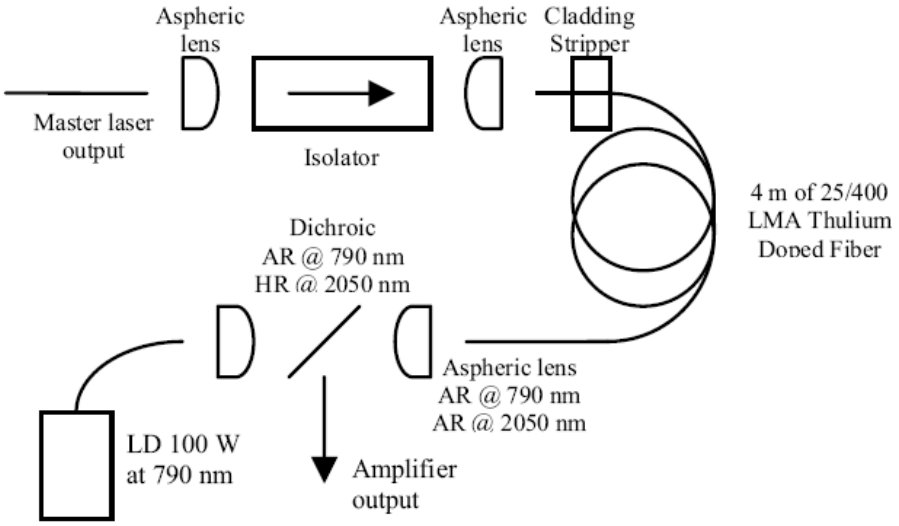

Figure 5-10: The Output of the Master Laser is Propagated Through an Isolator and Coupled into the Core of the Amplifier. The amplifier is pumped from the output end.

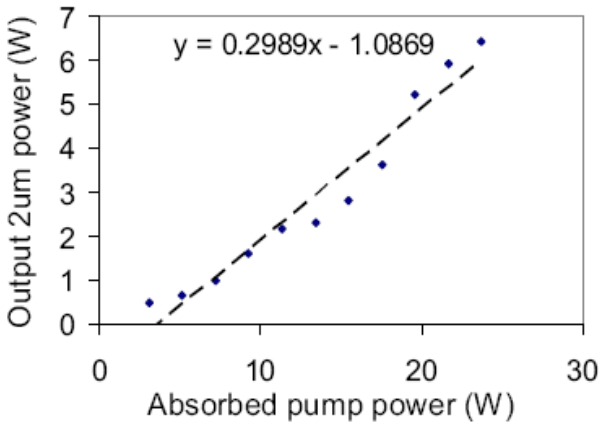

Figure 5-11: Output Performance of the Amplifier as a Function of Pump Power.

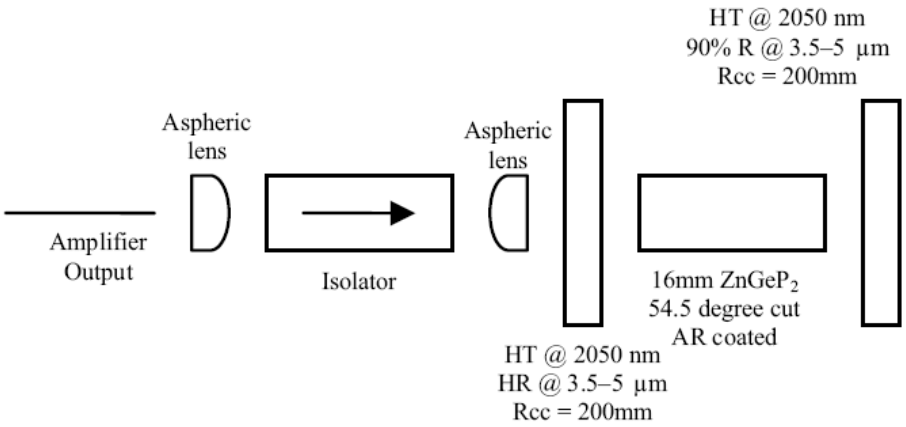

Figure 5-12: Zinc Germanium Phosphide Parametric Oscillator Pumped by Output of the Fiber Amplifier.

In 2012, the Australian group presented a power-scalable, all-fiber, monolithic-pulsed source based on a thulium-doped fiber MOPA design (Figure 5-13) [18]. This source produced 200 µJ pulses 20 – 40 ns in duration at a repetition rate of up to 75 kHz, resulting in up to 12 W of linearly polarized output at 2.044 µm. This was used to pump a walk-off-compensated ZGP OPO which generated 3 W in the mid-IR, with a conversion efficiency of 25% (Figure 5-14).

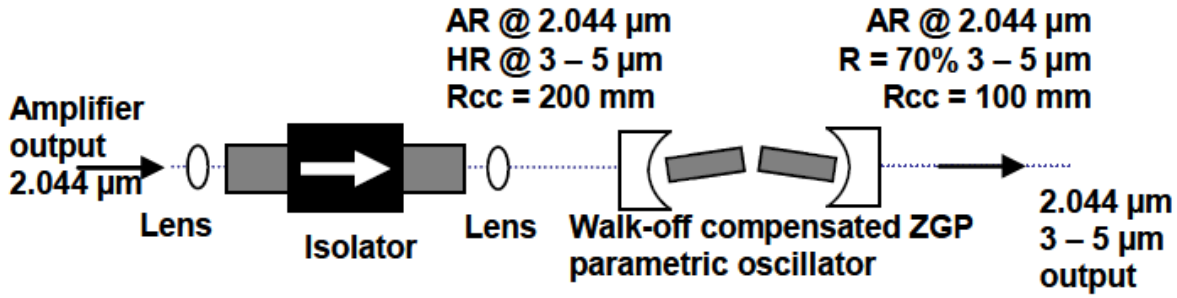

Figure 5-13: Schematic of Tm-Doped MOPA Pumping Dual-Crystal ZGP OPO.

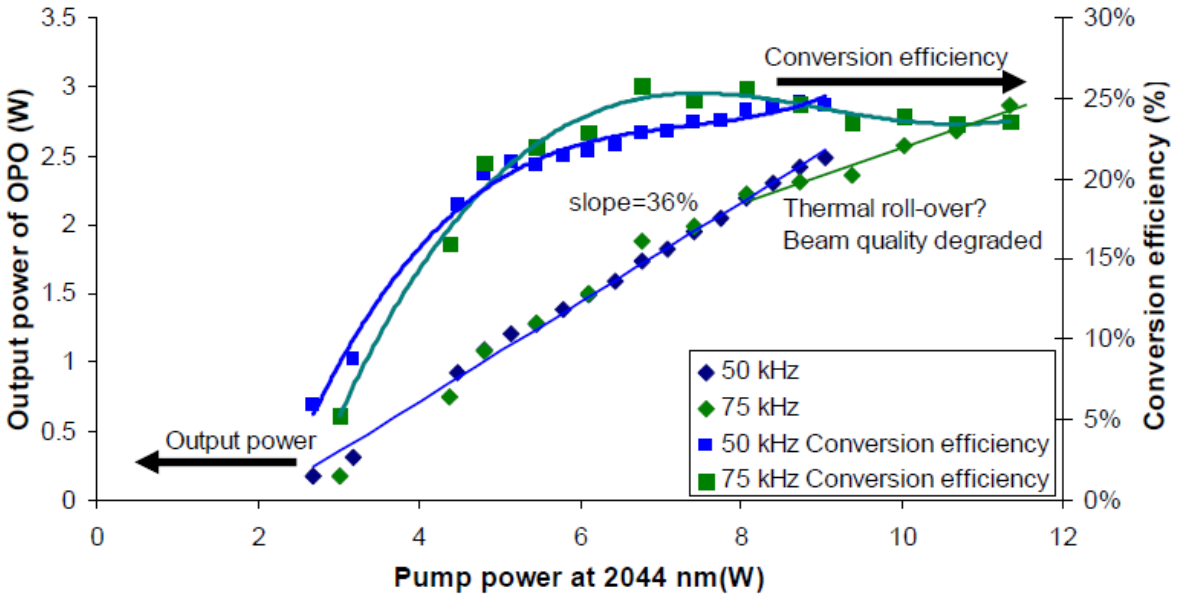

Figure 5-14: Output Power vs. Input Power and Conversion Efficiency of the OPO when Operating at 50 kHz and 75 kHz.

Pankaj Kadwani and co-workers from CREOL, University of Central Florida (USA) and Friedrich-Schiller-Universität (DEU) reported a Tm-fiber MOPA system using a power amplifier based on a Photonic Crystal Fiber (PCF), generating over 40 kW peak power in ~ 6.5 ns pulses as a tunable, narrow linewidth pump for mid-IR ZGP OPOs [19]. The initial experimental OPO set-up can be seen in Figure 5-15. The Q-switched oscillator is based on a Tm fiber pumped by a 35 W laser diode operating at 790 nm. Pulse energies of > 200 µJ were achieved at 20 kHz, and > 400 µJ at 1 kHz, with ~ 6.5 ns pulse duration. The spectral linewidth was < 1 nm FWHM. The output passed through an optical isolator and an extra-cavity EO pulse picker, before being focused by a 400 mm focusing lens to a ~ 225 µm diameter waist in a ZGP crystal with dimensions of 4 mm x 5 mm x 12 mm cut at $\theta = 57.5°$. The ZGP crystal was placed between two flat mirrors forming a doubly resonant OPO cavity. The input coupler was > 99% reflective and output

coupler ~ 50 % reflective over the 3 – 5 µm wavelength range, while both mirrors were highly transmissive at the pump wavelength. A longpass filter removed residual pump light. The use of PM fiber increased the overall efficiency compared with the first demonstration by Creeden et al. using an unpolarized pump beam.

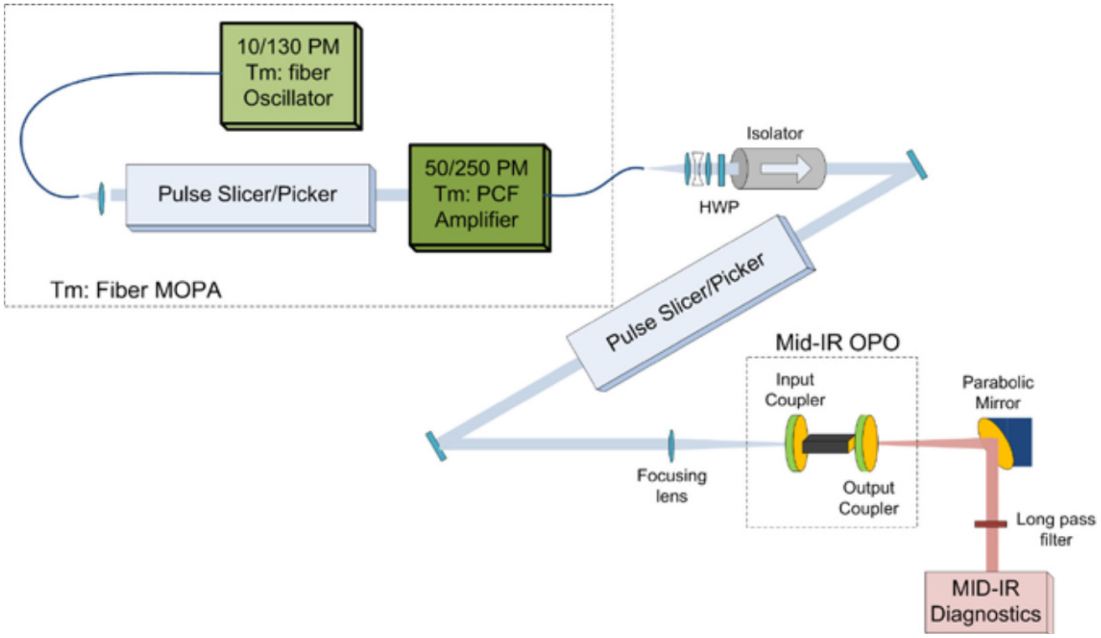

Figure 5-15: MOPA System Where a 10/130 SMF Fiber Oscillator Seeds a Flexible Tm:PCF Amplifier Through a Pulse Slicer. The output is passed through a pulse picker and focused into a ZGP OPO by a 400-mm lens. The output is then collimated by a parabolic mirror and sent through a mid-IR filter to beam diagnostics.

Figure 5-16 shows the output characteristics of this ZGP OPO for three different repetition rates. The maximum total mid-IR energy is ~ 24 µJ which corresponds to about ~ 2 kW peak power for the signal (~ 3.55 µm). At the Mid-Infrared Coherent Sources (MICS) conference held in Paris in October 2013, the CREOL group reported the generation of 28 kW peak power in a mid-IR ZGP OPO, pumped by a Tm:fiber MOPA system delivering ~ 8 ns pulses with ~ 120 kW of usable pump peak power at 1980 nm [20].

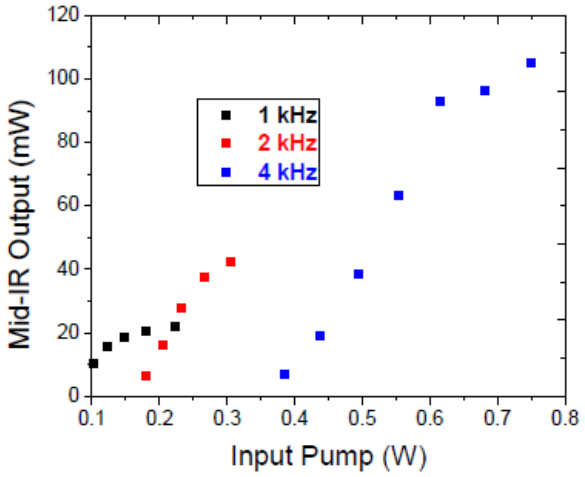

Figure 5-16: OPO Output for Several Repetition Rates, at ~ 6.8 ns Pulse Duration.

5.2.3 OPGaAs

OPGaAs is a Quasi-Phase-Matched (QPM) non-linear crystal allowing for tight focusing, long interaction length and alignment insensitivity required for efficient conversion in a fiber-coupled device. It was the first material to demonstrate the potential of all epitaxial-grown QPM semiconductors and it is already achieving record output powers and efficiencies in the mid-IR. Its IR transparency is broader than that of PPLN and even ZGP. It also offers a higher non-linear coefficient, higher thermal conductivity, low losses when grown from the vapor phase, and is relatively insensitive to pump polarization, compared with other non-linear materials.

5.2.3.1 OPGaAs OPO Directly Pumped by a 2.09 µm Q-Switched Tm,Ho:silica Fiber Laser

The ISL group demonstrated an OPGaAs OPO directly pumped by a 2.09 µm Q-switched Tm,Ho:silica fiber laser [21],[22]. The experimental set-up is shown in Figure 5-17. The pulsed fiber laser is based on a Tm,Ho-doped double clad fiber (OFTC Sydney, Australia), Q-switched by a high diffraction efficiency (> 85%) TeO_2 Acousto-Optic Modulator (AOM) in an external cavity set-up [23]. A Volume Bragg Grating (VBG) was used to narrow the spectral line width emitted. Optical isolation was used between the fiber laser and the OPO cavity. The pump beam is split in two polarized beams by a Brewster plate, allowing separated optical isolation in two arms. The slightly multi-mode nature of the fiber used and the superposition of the two separated isolated beams led to a non-optimized beam in the non-linear crystal. The recombined pump beam was focused by a f = 200 mm lens to a ~ 200 µm spot inside the OPGaAs sample. Figure 5-18 plots the averaged powers curves for a plane-plane OPO cavity and plane-rcc 50-mm OPO cavity. The fiber laser was operated at a stable point of operation for repetition rates from 40 to 75 kHz. With a 2.09 µm Q-switched Tm,Ho:silica fiber laser pump source, up to 2.2 W of average output power was achieved at 40 kHz repetition rate, 1.9 W at 60 kHz and 1.1 W at 75 kHz with the plane-plane OPO-cavity. With the plano – 50 mm – radius-of-curvature OPO cavity, 1.88 W was achieved at 40 and 60 kHz, and 1.2 W at 50 and 75 kHz. Experiments were pump-power limited.

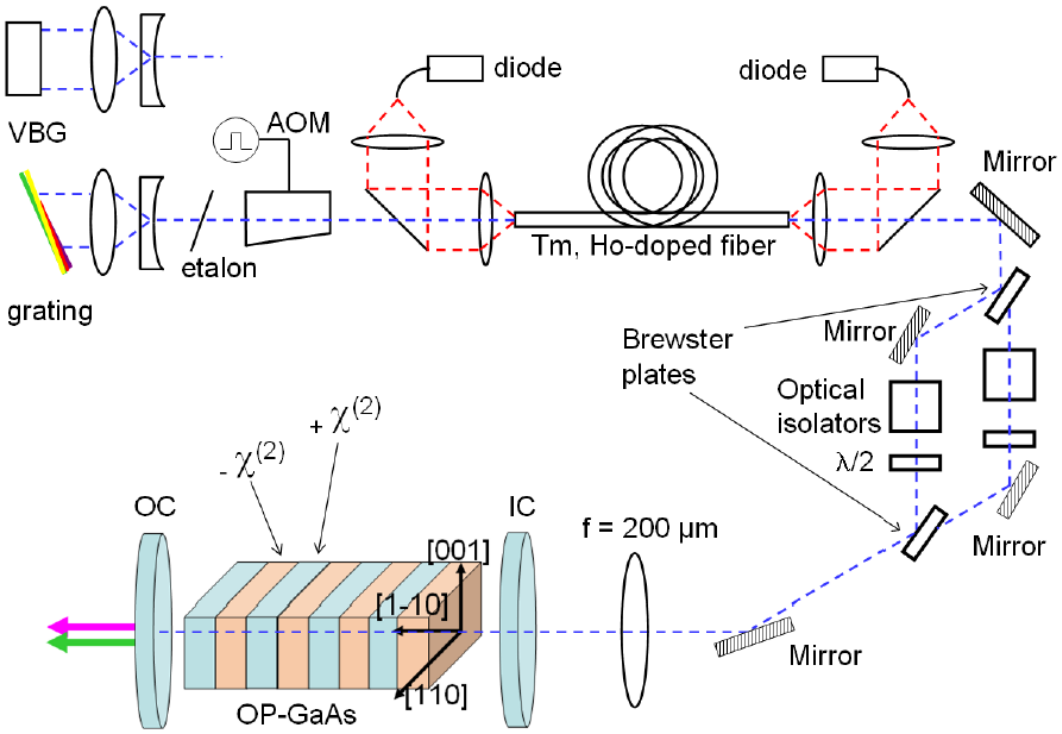

Figure 5-17: Experimental Set-Up for the OPGaAs OPO Pumped by a Tm,Ho-Doped Fiber.

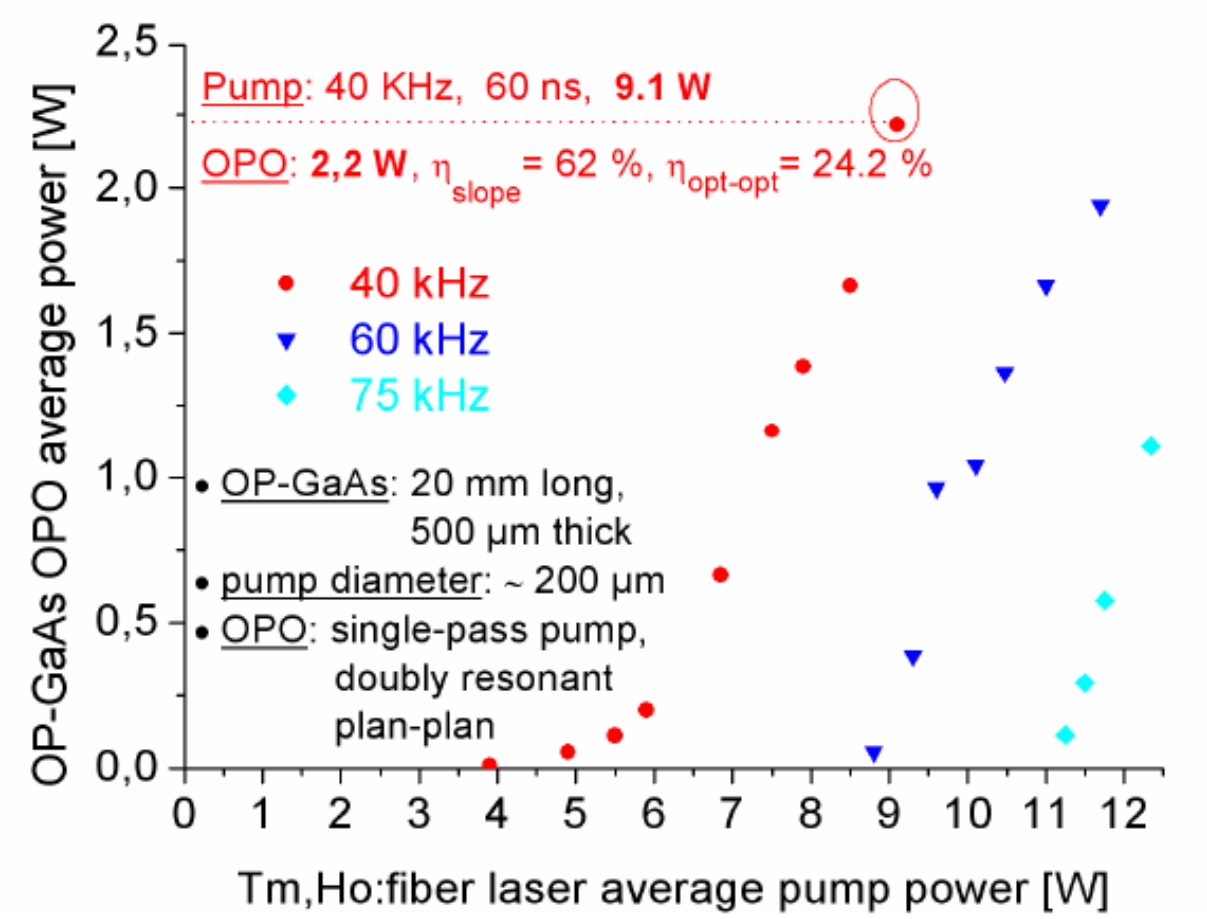

Figure 5-18: Output Average Power Performance of the Fiber Laser Pumped Plane-Plane OPGaAs OPO at 40, 62 and 75 kHz Repetition Rates.

The ISL group is currently working on a new pump set-up allowing for higher pump power and based on a monomode, polarization maintaining Tm,Ho-doped fiber to increase the overall conversion efficiency.

5.2.3.2 Mid-IR Conversion Efficiency from an OPGaAs Pumped by a 1.5 µm Erbium:Fiber Laser

5.2.3.2.1 Simulation

Contributors to this section: Pierre Mathieu[9], Denis Vincent[9], Francis Théberge[9]

Development of a multi-wavelength pump source emitting around 1550 nm is part of the concept put forward by DRDC-Valcartier to achieve the emission of radiation around 4 µm. One of the key concepts is to use the laser at 1535 – 1565 nm as an optical pump for OPO conversion by using the appropriate non-linear medium, here an Orientation-Patterned Gallium Arsenide (OPGaAs) crystal. For this section, we describe briefly the dual-wavelength Erbium fiber laser developed by Institut National d'Optique (INO), Canada, for a research project of the Defence R&D Canada. Experimental results for the difference frequency mixing in OPGaAs pumped by this laser cannot be presented because the OPGaAs crystal was not yet available when this report was written. However, simulation of the OPGaAs pumped by a multi-watt Er:fiber laser is presented using laser pump parameters very similar to the one acquired by DRDC-Valcartier.

[9] DRDC Valcartier, 2459 route de la Bravoure, Québec (Québec) G3J 1X5, Canada.

The Er:fiber laser acquired by DRDC-Valcartier emits an average output power of 18 W at 1535 nm and 1563 nm with modulation at the rate between pulsed and continuous wave regimes. This laser uses the MOPAW technology (Master Oscillator with Programmable Amplitude Wavefront) developed at INO and it is used to control the shape and repetition rate of the pulses. The repetition rate can be varied from 200 kHz to 1 MHz with a pulse width of 20 ns. The laser can also operate in a quasi-continuous regime at 100 MHz. The choice of wavelength (1535 nm or 1565 nm), repetition rate and pulse modulation can be varied at a rate greater than 3 kHz via TTL signals.

The simulations of the difference frequency generation using an OPGaAs crystal into an Optical Parametric Oscillator (OPO) pumped by such Er:fiber laser pulse have been done by using both SNLO and SiSyFos (software from G. Arisholm at Norwegian Defence Research Establishment). Because of the limitation of SNLO, for the first series of simulation presented in this section, we compare the calculations from SNLO and SiSyFos for the pump laser parameters with a Gaussian temporal profile and we neglect the two-photon absorption. In the second set of simulation, we use only the SiSyFos software with a high-order super-Gaussian temporal profile pump pulse (similar to the acquired dual-wavelength Er:fiber laser). For these simulations, we considered a single longitudinal mode for the pump which can underestimate the peak intensity and consequently the Two-Photon Absorption (TPA).Therefore, we considered three different values for the two-photon absorption, including one value being two-times larger than the TPA measured in [25]-[26].

First, for the comparison of the SNLO and SiSyFos simulations, we used a 1563 nm pump pulse with 20 ns Gaussian pulsewidth at FWHM and waist diameter of 165 µm centered into the OPGaAs crystal. The parameters of the OPGaAs for the simulation were a crystal length of 15 mm, a grating period around 28 µm maintained at 80 deg. C, a linear absorption of 0.03 cm^{-1} for the three wavelength involved (pump, signal and idler), and a non-linear coefficient d_{14} = 94 pm/V. The parameters of the OPO cavity used for the simulations were a singly resonant double concave cavity using two mirrors having a radius of curvature of 250 mm. The gap between the ends of the OPGaAs crystal and the mirror surfaces were 7.5 mm. As shown in Figure 5-19, the reflectivity of the first mirror was 0%, 99% and 99% for the pump, signal and idler, respectively. The reflectivity of the second mirror (output coupler) was 99% and 0% for the pump and idler, respectively. For the output coupler, the reflectivity for the signal was adjusted to optimize the idler output power.

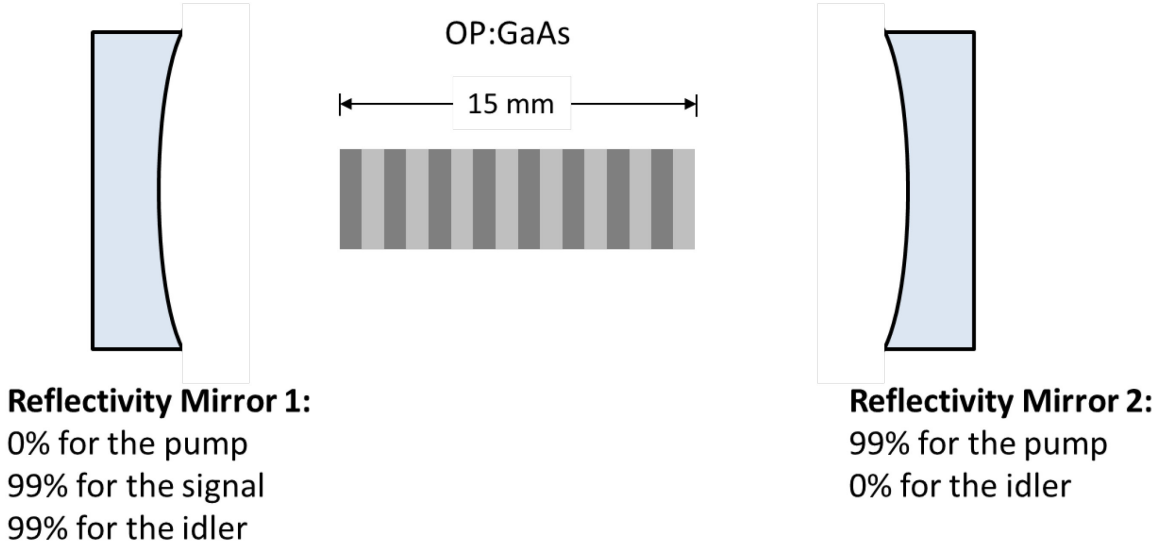

Figure 5-19: Schematic Diagram of the OPGaAs Optical Parametric Oscillator Used for the Simulations.

Table 5-1 presents the simulated output energies of the generated Idler (I) and Signal (S) for different 1563 nm pump pulse energies (P) and for the optimum signal reflectivity of the output coupler (RS,OC), for both the SNLO and the SiSyFos software. When comparing the SNLO and SiSyFos simulation results for pump energy far from the threshold energy for oscillation, we observe a fair agreement between the results of these two simulations for both the optimal signal reflectivity of the output coupler and the parametric conversion efficiency.

Table 5-1: Simulated Optimum Reflectivity of the Output Coupler and Corresponding Conversion Efficiency for Different Pump Pulse Energy.

Pump Energy	$R_{S,OC}$		Ratio I/P		Ratio (I+S)/P	
µJ	%		%		%	
	SNLO	SiSyFos	SNLO	SiSyFos	SNLO	SiSyFos
12	85	95	23	5	46	8
24	60	80	26	19	62	41
48	60	60	28	24	67	56

For the second step of these simulations, we simulate the optical parametric generation with an OPGaAs OPO similar to the one presented in Figure 5-19, but this time the crystal length was fixed at 10 mm. Also we use only the SiSyFos software with a 12-order super-Gaussian pump laser pulse of 20 ns pulsewidth (FWHM), which is very similar to the top-hat pulsewidth from the acquired Er:fiber pump laser. For these simulations, we will compare also different values of the two-photon parameter of the GaAs at 1563 nm (β_{1563nm}). From values available in open literature, the GaAs two-photon parameter corresponds to β_{1563nm} = 10 cm/GW [23],[24]. In Figure 5-20, we compare the parametric conversion efficiency for different pump energy and different value of β_{1563nm} corresponding respectively to 0 cm/GW, 10 cm/GW and 20 cm/GW. From the results presented in Figure 5-20, we observe that a variation of β_{1563nm} and/or the peak intensity of pump pulse do not affect too severely the pump absorption and the parametric conversion efficiency.

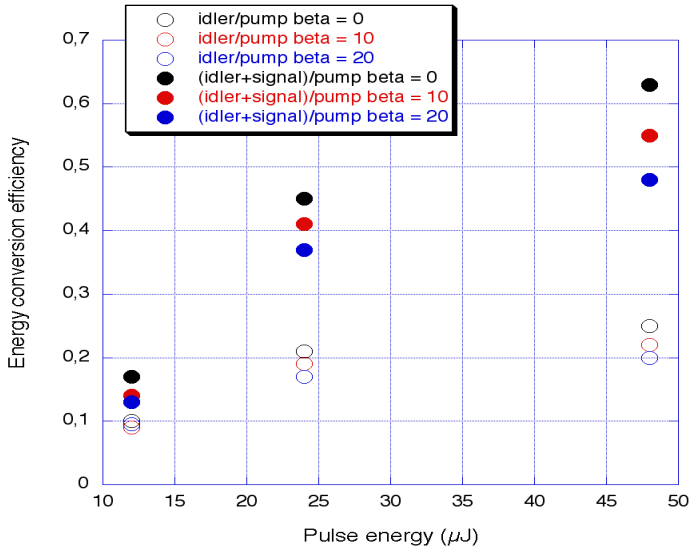

Figure 5-20: Ratio of the Parametric Energy Over the Pump Energy as a Function of the Pump Energy for Different Values of the GaAs Two-Photon Absorption (Beta).

Figure 5-21 presents the temporal evolution of the pump, signal and idler pulses in the OPGaAs OPO for a neglected two-photon absorption (β_{1563nm} = 0 in Figure 5-21(a) and a two-photon parameter of β_{1563nm} = 10 cm/GW (Figure 5-21(b)). For these two cases, the optimum reflectivity of the signal for the output coupler was also calculated and corresponds to 40% and 35% for Figure 5-21(a) and Figure 5-21(b), respectively. By comparing these two results, we observe again that two-photon absorption does not have too severe an impact on the parametric conversion, at least for the range of pump power/energy used for these simulations.

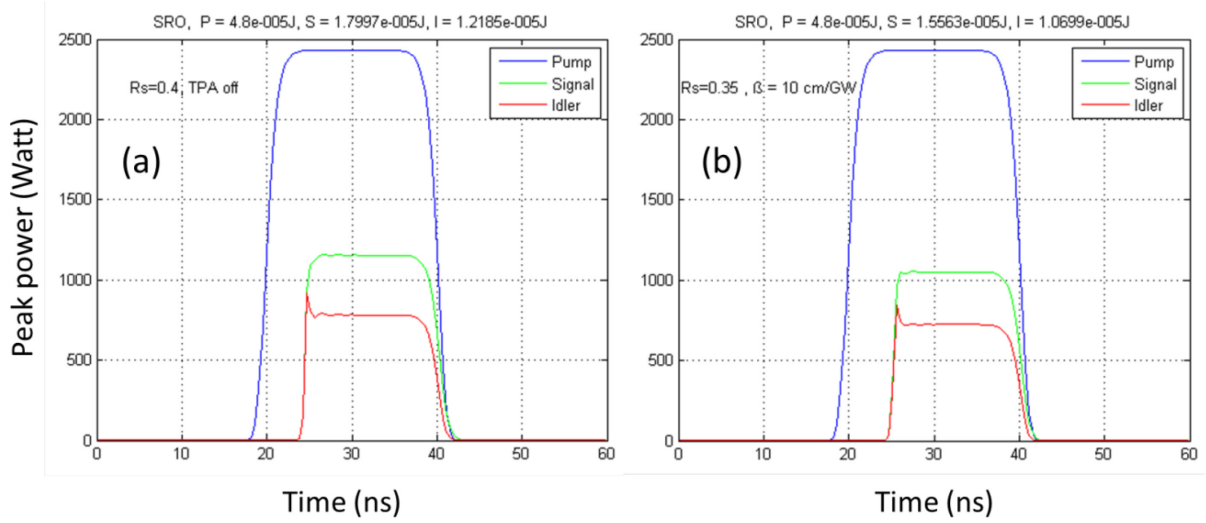

Figure 5-21: Temporal Evolution of the Pump, Signal and Idler Laser Pulses for a Two-Photon Absorption Parameter of (a) β_{1563nm} = 0 cm/GW, and (b) β_{1563nm} = 10 cm/GW.

5.2.3.2.2 Growth of OPGaAs for 1.5 µm Pumping

Contributor to this section: Rita D. Peterson[10]

Producing mid-infrared (3 – 5 µm) output using a 1.5 µm pump in OPGaAs requires a period around 27 – 28 µm. Air Force Research Laboratory (AFRL) had on-hand two template segments with periods in the 27 – 29 µm range, suitable for this interaction. A growth run was made on one of these in April 2011, in the HVPE reactor then located at Hanscom Air Force Base, using a process documented in the literature [25]. This was one of the last growth experiments performed before the laboratory was relocated to Ohio, USA.

The growth run was unfortunately unsuccessful. The domain structure was completely overgrown within the first 100 µm of growth. This was not unexpected, since most material grown in this process to date has had periods larger than 50 µm, and previous thick growth attempts of domains < 20 µm have produced poor results. After the laboratory is back in service in its new location, the remaining template piece will be used to test modifications to the growth conditions. If interest remains in 1.5 µm pumping of OPGaAs, a new template will be fabricated with the required periods, for use in future growth experiments. Understanding how to adjust growth conditions to produce smaller periods is of general interest as the repertoire of OPGaAs-based devices continues to expand.

As part of a consolidation of AFRL facilities, the HVPE growth laboratory was relocated from Hanscom Air Force Base in Massachusetts to Wright-Patterson Air Force Base in Ohio in the summer of 2011. The last growth experiments at Hanscom AFB were completed in May 2011. The growth laboratory includes three

[10] Air Force Research Laboratory, AFRL/RYJW Bldg 620, 2241 Avionics Circle, Wright-Patterson AFB, OH 45433, United States.

HVPE reactors, for growth of GaAs, GaP, and nitrides respectively; all of which received new components and upgrades when reassembled in the new location. The OPGaAs reactor was the first to return to service, beginning with short calibration runs to validate growth conditions. Long growth runs to produce thick samples for device experiments resumed in June 2013. The material quality of these samples is comparable to that of samples grown prior to the lab relocation. A representative cross-section showing the domain structure is shown in Figure 5-22 where the period is 116 µm.

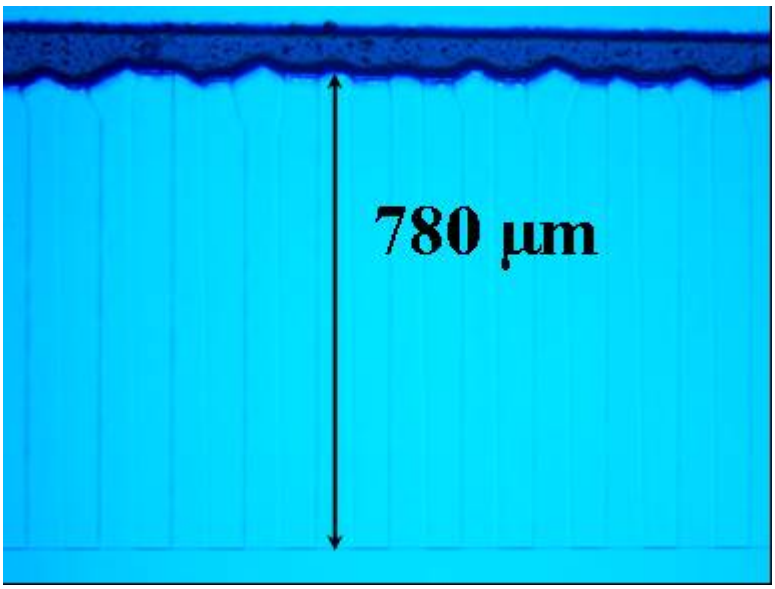

Figure 5-22: Cross-Section of Recent Thick GaAs Growth.

5.3 CONCLUSION AND OUTLOOK

Efficient pumping of OPGaAs and ZGP depends upon pump sources emitting at wavelengths higher than 1.73 nm and 2 µm respectively, to avoid absorption losses while minimizing quantum defect. Analysis of the state-of-the-art indicates that more progress is needed on pump fibers and optical components in this wavelength region, to support the eventual goal of eliminating free-space coupling in future mid-IR fiber sources, allowing systems that are completely optically confined.

The experimental demonstration of mid-infrared (3 – 5 µm) output using a 1.5 µm pump in OPGaAs has to be performed to confirm the DRDC simulation results that predict reasonably efficient output, despite the reported severe two-photon absorption at wavelengths shorter than 1.7 µm.

Continued progress in QPM semiconductors for mid-IR frequency conversion has been reported [26],[27]. This includes the introduction of Orientation-Patterned Gallium Phosphide (OPGaP) as an alternative to OPGaAs having negligible two-photon absorption in the convenient pumping range from 1 µm to 1.7 µm where efficient fiber lasers are readily available. OPGaP material up to 350 µm thick has been grown, but device experiments have yet to be reported.

5.4 REFERENCES

[1] Suter, J.D., Bernacki, B.E. and Phillips, M.C. Angle-resolved scattering spectroscopy of explosives using an external cavity quantum cascade laser, Proc. SPIE 8268, 82681O (2012).

[2] Neese, C.F. Infrared/terahertz double resonance for chemical remote sensing: signatures and performance predictions, Proc. SPIE 7671, 76710F (2010).

[3] Fuchs, F., Hinkov, B., Hugger, S., Kaster, J.M., Aidam, R., Bronner, W., Köhler, K., Yang, Q., Rademacher, S., Degreif, K., Schnürer, F. and Schweikert, W. Imaging stand-off detection of explosives using tunable mid-IR quantum cascade lasers, Proc. SPIE 7608, 760809 (2010).

[4] Seddon, A.B., Tang, Z., Furniss, D., Sujecki, S. and Benson, T.M. Progress in rare-earth-doped mid-infrared fiber lasers, Opt. Expr. 18(25), 26704-26719 (2010).

[5] http://www.wsof2013.org/isla-integrated-disruptive-components-2-%CE%BCm-fibre-lasers.

[6] www.inradoptics.com White Paper (2013).

[7] Bonetti, Y. and Faist, J. Quantum cascade lasers: Entering the mid-infrared, Nature Photonics 3, 32-34 (2009).

[8] Matsuoka, N., Yamaguchi, S., Nanri, K., Fujioka, T., Richter, D. and Tittel, F. Ybfiber laser pumped mid-IR source based on difference frequency generation and its application to ammonia detection, Jpn. J. Appl. Phys., 40, 625-628 (2001).

[9] Jiang, J., Chang, J.-H., Feng, S.-J., Mao, Q.-H. and Liu, W.-Q. Mid-IR dual-wavelength difference frequency generation using fiber lasers as pump and signal light sources, Chin. Phys. Lett.26(12), 124214 (2009).

[10] Winters, D.G., Schlup, P. and Bartels, R.A. Subpicosecond fiber-based soliton-tuned mid-infrared source in the 9.7-14.9 μm wavelength region, Opt. Lett.35(13), 2179-2181 (2010).

[11] Chang, J., Mao, Q., Feng, S., Gao, X. and Xu, C. Widely tunable mid-IR difference-frequency generation based on fiber lasers, Opt. Lett.35(20), 3486-3488 (2010).

[12] Neely, T.W., Johnson, T.A. and Diddams, S.A. High-power broadband laser source tunable from 3.0μm to 4.4μm based on a femtosecond Yb:fiber oscillator, Opt. Lett. 36(20), 4020-4022 (2011).

[13] Salhany, J. and Burgoyne, B. FIBER LASERS: Programmability comes to fiber lasers, Laser Focus World 48(3) (2010).

[14] Creeden, D., Ketteridge, P.A., Budni, P., Zawilski, K., Schunemann, P.G., Pollak, T.M. and Chicklis, E.P. Multi-Watt Mid-IR Fiber-Pumped OPO, Conference on Lasers and Electro-Optics CLEO 2008, paper CTuII2 (2008).

[15] Creeden, D., Ketteridge, P.A. Budni, P.A., Setzler, S.D., Young, Y.E., McCarthy, J.C., Zawilski, K. and Schunemann, P.G. Mid-infrared ZnGeP2 parametric oscillator directly pumped by a pulsed 2 μm Tm-doped fiber laser, Opt. Lett. 33(4), 315-318 (2008).

[16] http://ftp.rta.nato.int/public//PubFullText/RTO/MP/RTO-MP-SET-171///%24MP-SET-171-T.pdf.

[17] Simakov, N., Hemming, A., Davidson, A., Carmody, N., Bennetts, S., Davies, P. and Haub, J. Power Scalable 2 μm Source for Parametric Generation of Mid-infrared Radiation in $ZnGeP_2$, 35th Australian Conference on Optical Fibre Technology (ACOFT) (2010).

[18] Simakov, N., Davidson, A., Hemming, A., Bennetts, S., Hughes, M., Carmody, N., Davies, P. and Haub, J. Mid-Infrared Generation in ZnGeP2 Pumped by a Monolithic, Power Scalable 2 μm Source, Proc. of SPIE Vol. 8237, 82373K-1 (2012).

[19] Kadwani, P., Gebhardt, M., Gaida, C., Shah, L. and Richardson, M. A High Peak Power, Nanosecond Tm:fiber MOPA System for Mid-IR OPO Pumping, Conference on Lasers and Electro-Optics CLEO 2013, Paper JW2A.29 (2013).

[20] Gebhardt, M., Gaida, C., Kadwani, P., Sincore, A., Geh-lich, N., Shah, L. and Richardson, M. Nanosecond Tm:fiber MOPA System for High Peak Power Mid-IR Generation in a ZGP OPO, Mid-Infrared Coherent Sources (MICS) – Paris, Paper MW3B.2 (2013).

[21] Kieleck, C., Hildenbrand, A., Eichhorn, M., Faye, D., Lallier, E., Gérard, B. and Jackson, S.D. OP-GaAs OPO Pumped by 2µm Q-switched Lasers: Tm;Ho:Silica Fiber Laser and Ho:YAG Laser, Proc. SPIE 7836, 783607 (2010).

[22] Eichhorn, M. and Jackson, S.D. High-pulse-energy, actively Q-switched Tm^{3+},Ho^{3+}-codoped silica 2µm fiber laser, Optics Letter, 33 (10), 1044-1046 (2008).

[23] Tani, M., Lee, K.-S. and Zhang, X.-C. Detection of terahertz radiation with low-temperature-grown GaAs-based photoconductive antenna using 1.55 µm probe, Appl. Phys. Lett. 77, p. 1396 (2000).

[24] Hurlbut, W.C., Lee, Y.-S., Vodopyanov, K.L., Kuo, P.S. and Fejer, M.M. Multiphoton absorption and nonlinear refraction of GaAs in the mid-infrared, Opt. Lett. 32(6), 668-670 (2007).

[25] Bliss, D.F., Lynch, C., Weyburne, D., O'Hearn, K. and Bailey, J.S. Epitaxial growth of thick GaAs on orientation-patterned wafers for nonlinear optical applications, Journal of Crystal Growth, Vol. 287 673-678 (2006).

[26] Schunemann, P.G. and Setzler, S.D. Future directions in quasi-phasematched semiconductors for midinfrared lasers, Proc. of SPIE Vol. 7917, 791750 (2011).

[27] Tassev, V., Snure, M., Peterson, R., Schepler, K.L., Bedford, R., Mann, M., Vangala, S., Goodhue, W., Lin, A., Harris, J., Fejer, M. and Schuneman, P. Progress in orientation-patterned GaP for next-generation nonlinear optical devices, Proc. of SPIE Vol. 8604, 8604-31 (2013).

Chapter 6 – SUMMARY AND RECOMMENDATIONS FOR FUTURE WORK

Mid-infrared laser technology is critical to the development of active sources for defeating a growing spectrum of heat-seeking missiles, as well as for remote sensing of targets and threats. These coherent sources must be resistant to environmental changes, and sufficiently compact and conformable to fit in a variety of platforms including large transports, combat aircraft, helicopters, and even UAVs. Fiber lasers have distinct advantages over conventional bulk solid-state lasers for these applications. Their optical confinement reduces the need for free space optics which are sensitive to misalignment, and to such environmental conditions as dust, vibration, and moisture. The small dimensions of the modes propagating in the core of the fiber provide low-threshold and high-gain characteristics with near-maximum efficiency. Their inherent geometry simplifies thermal management and supports distributed system architectures.

Fiber lasers and fiber technology devoted to telecom applications are very well developed and sources delivering kW output powers have been demonstrated. Recent advances in the 2 µm wavelength range have also been demonstrated, but there is still a lack of fiber components. Passive transport fiber and fiber-based optical devices for the mid-IR are still rare, lossy and relatively fragile. Theoretical modelling and designs of fiber lasers emitting beyond 3 µm have been done, but demonstrations have been limited primarily to supercontinuum devices. Extending into the mid-IR the considerable advantages of fiber technology would provide laser sources that are efficient, robust, compact, potentially high in power, and spectrally suited to critical military applications like infrared countermeasures.

For this reason, the SET-170 Task Group focused its efforts on fiber sources operating at wavelengths longer than 3 µm, and fibers based on glasses other than silica. By sharing our diverse expertise, facilities, and materials, we were able to make progress in each of the three areas outlined in our programme of work.

In investigating direct lasing in fibers, we chose to focus on two rare earth dopants: dysprosium (Dy^{3+}) and holmium (Ho^{3+}), with lasing transitions at 4.3 µm and 3.9 µm respectively which have been demonstrated in other host materials. We selected fluoroindate fiber as the host material, because of its broader mid-IR transparency and lower phonon energies relative to the more-developed ZBLAN. Initial spectroscopic evaluation was done on glass samples doped with each rare-earth ion, due to the much greater cost of pulled fiber. This led to the abandonment of Dy^{3+}:fluoroindate as a candidate, due to the inability to observe any fluorescence on the desired transition.

Work with Ho:fluoroindate glass material proved much more successful. Spectroscopic analysis was conducted, specifically measurement of absorption, emission, and fluorescence lifetime, including measurements at low temperature using a cryostat system. The Ho^{3+} transition at 3.9 µm suffers from an unfavorable lifetime ratio, with the upper laser level lifetime typically two orders of magnitude shorter than that of the lower level, resulting in significant bottlenecking. Spectroscopic results were therefore critical as inputs to a model to evaluate the possibility of developing a viable Ho:fiber laser, and to identify a suitable fiber specification. Modelling results indicate that, despite the short lifetime, efficient lasing is possible in a double-clad fiber given the correct choice of concentration, taking advantage of up-conversion processes to help recirculate the active ions. Cascade lasing of the 2.9 µm transition improves performance significantly by alleviating the bottlenecking at the lower laser level, caused by its much longer lifetime relative to that of the upper laser level. Co-doping is also proposed as a means of relieving the bottlenecking, but appears not to help in this case.

The most significant achievement on the direct lasing task is demonstration of lasing in a sample of Ho:fluoroindate glass. A flashlamp-pumped Cr^{3+}:LiSAF laser operating at 890 nm pumped the Brewster-cut sample, in a cavity originally assembled using a crystal of the better-known Ho:BYF material. Results were modest: just over 5 mJ of output, and a slope efficiency of 1.3%. This is the first demonstration of lasing in

this material, however, and given the nature of the sample and the far from optimal resonator conditions, bodes well for the performance of a Ho:fluoroindate fiber. A journal paper on these results is in preparation.

Work on frequency conversion in fibers focused on obtaining broadband mid-IR output via supercontinuum generation, specifically with pump pulses on the picosecond or nanosecond scale for greater average power than most sources reported to date. The end-goal is development of ruggedized, ready-to-use, multi-watt supercontinuum sources. Highlights of the results obtained by the SET-170 Task Group include:

- Demonstration of the highest average power (0.565 W) and the broadest spectrum (1.9 – 4.8 μm) directly emitted from a step-index chalcogenide (As_2S_3) fiber supercontinuum source;
- The first demonstration of watt-level (2.09 W in the 1 – 3.05 μm spectral band) and broadband (2.7 – 4.7 μm) mid-IR supercontinuum generation in a step-index fluoroindate fiber;
- The first demonstration of watt-level (1.08 W) supercontinuum generation (1.9 – 3.6 μm) in ZBLAN fiber pumped by an actively Q-switched and mode-locked Tm-doped fiber laser;
- The first demonstration of watt-level (1.25 W in the 1.8 – 4.15 μm spectral band) supercontinuum generation in a step-index ZBLAN fiber pumped by a fast gain-switched Tm-doped fiber laser and amplifier system; and
- Demonstration of the most efficient supercontinuum power distribution towards the mid-IR, with over half the output at wavelengths longer than 3 μm.

Practical realization of high average power mid-IR supercontinuum sources that meet military requirements remains a challenge, in terms of both the pump laser system and the non-linear fiber itself. The most significant factors limiting the long-wavelength edge of the supercontinuum spectrum are fiber non-linearities, bend-induced loss and bulk absorption. The most promising non-linear fibers are telluride, chalcogenide and fluoride-based fibers. Tellurides and chalcogenides have broad absorption and high non-linearity, but are susceptible to thermally induced damage at high powers. Fluoride fibers demonstrate better power handling, especially with careful thermal management, with the fluoroindate fiber featured in many |of our results offering broader mid-IR transparency than the more familiar ZBLAN, covering the entire 3 – 5 μm region. An average output average power of > 20 W can be expected from a single-mode fluoride fiber covering the mid-IR band within the next 2 – 5 years.

The third task, fiber pump sources for bulk frequency conversion, considered pumping strategies for ZGP, PPLN, and OPGaAs, representing the current spectrum of non-linear materials from birefringent crystals to quasi-phase-matched materials based on poling of ferroelectric crystals, and orientation-patterned growth of semiconductors. While successful and even impressive device demonstrations have been reported with each of these materials, most still rely on bulk crystal lasers as pump sources. Progress is still needed on fiber-based pump sources as well as optical fiber components in this wavelength region, to support the eventual goal of all optically confined systems.

A particularly intriguing result of this task was OPGaAs OPO modelling which suggests that it may be possible, even practical, to pump OPGaAs at wavelengths as short as 1550 nm despite the material's well-known two-photon absorption in this region. A key limitation of OPGaAs has been the need to pump it at wavelengths longer than about 1.7 μm, which rules out the many mature and commercially available lasers operating around 1 μm and 1.5 μm, based on Nd, Yb, and Er active ions. Unfortunately OPGaAs material with the right pattern was not available during the Task Group's tenure, so we were unable to investigate this experimentally and it is left as future work. New materials that do not have 2-photon absorption in this region such as OPGaP are being developed, but the relative maturity of OPGaAs makes the prospect of being able to pump it at these shorter wavelengths tantalizing.

The programme of work laid out at the start of SET-170 was decidedly ambitious, and not all activities under every task could be completed successfully, due partly to the inevitable technical challenges that arise, as well as to the familiar financial, staffing, and schedule constraints. Decisions on how to proceed were made with an eye to maximizing the Task Group's contribution to the field given resources available. To that end, we were successful in that each task produced results that were noteworthy, and more importantly, useful in the further study of mid-IR fiber lasers. The Task Group activities resulted directly in 10 journal publications, plus two planned; as well as several conference presentations and proceedings – these are listed in Annex B.

Recommendations for future work are best grouped by task, following the programme of work.

Direct Lasing in Fibers

- Lasing of the Ho:fluoroindate glass sample was quite encouraging, but lasing still remains to be demonstrated in an actual fiber pulled from similar material, whose design is based on results obtained on this task. While any demonstration of lasing will be scientifically interesting, a practical device based on this gain material will require a more convenient pump source than Cr:LiSAF, specifically a diode laser. While diode lasers at the needed wavelength of ~ 890 nm are available, the unfavorable lifetime ratio on the desired transition limits energy storage in such a way that diode pumping at useful repetition rates and duty cycles may be quite a challenge.

- The Dy^{3+} ion was abandoned early on due to an inability to see any fluorescence at the 4.3-μm transition of interest in the two samples available. These were doped with ~ 1 – 2 % Dy, and it may be enough simply to use more highly doped material. It is worth revisiting this material, and at least modelling gain on this transition using published results for similar materials as a starting point. The slightly longer wavelength may be even more useful than the 3.9 μm Ho^{3+} transition.

- In terms of host materials, the present work focused on fluoride glass, specifically fluoroindate glass with its lower phonon energies and longer wavelength transmission relative to the more established ZBLAN. Chalcogenide fibers have long been attractive due to their transparency at even longer wavelengths, but the lack of stable sites for the dopant has frustrated attempts to pull usable fibers from the glass, leaving tantalizing spectroscopic results, but no lasers. Addressing the relevant glass chemistry issues to create stable sites for the ions would be a significant advance, and would open a whole new host fiber system for development. Of course there are yet other fibers worth considering, such as tellurites and other fluoride compositions.

- More broadly, there is the question of whether rare-earth-doped lasers of any kind are inherently limited vis-à-vis most military applications simply due to their narrow emission bands and minimal tunability. Countermeasure systems require wavelength agility to keep up with the variety of threat sensors in operation, and most remote sensing applications require much more broadband output. An obvious alternative is lasers based on transition metal ions like Cr^{2+} and Fe^{2+}, but successful incorporation of these ions into fibers has proved elusive. Development of a viable transition-metal-doped fiber would be a significant advance in mid-IR fiber technology.

Frequency Conversion in Fibers

In addition to overall output power, a principal concern for mid-IR supercontinuum sources is the fraction of output power at longer wavelengths ($\lambda > 3$ μm). This directly affects their practical use in such areas as direct infrared countermeasure or infrared spectral fingerprinting. This concerns both the non-linear fibers themselves, as well as the pump lasers. The most significant factors that limit the long-wavelength edge of the supercontinuum spectrum are fiber non-linearities, fiber material absorption, and bend-induced loss. Addressing these factors is a particularly pressing direction for future research.

Tellurite and chalcogenide fibers are characterized by very high non-linearity facilitating efficient spectrum extension over short fiber lengths, but are susceptible to thermally induced damage at high powers, thus limiting the output average power < 2 W. Improved thermal management and heat dissipation techniques may help, but improvement in the material quality of the fibers themselves may be necessary to achieve useful power levels.

- Fluoride fibers have shown better power-handling ability while using only modest thermal management strategies, but so far are limited to around 5.5 μm in transparency.

- The entire category of microstructured fibers was not addressed in this work because the achieved output power has generally been low, i.e. less than 100 mW in the mid-IR spectral range. This may bear reconsidering as fiber fabrication methods and the resulting devices continue to develop.

- Work on this task was limited to supercontinuum generation based on the interests and expertise of Task Group participants. An obvious extension is to consider fiber Raman lasers, or fiber-based OPO and OPA. These technologies have received increasing interest in recent years. While they will not provide the broad spectral output of a supercontinuum device, they offer the possibility of a more narrowband but tunable source when paired with a tunable pump laser. Successful four-wave-mixing processes in particular, however, have relied on microstructured optical fiber which is even more costly than the custom fluoroindate fiber necessary for demonstrating a Ho:fluoroindate fiber laser.

Fiber Pump Sources for Bulk Frequency Conversion Devices

- The most pressing recommendation on this task is to verify experimentally whether OPGaAs can be pumped at 1.5 – 1.6 μm, and if so, to establish the potential and limitations of this method as an alternative to the usual 2 μm pumping.

- The peak power or pulse energy available from a fiber laser continues to be an issue in pumping frequency conversion devices, since the non-linear process is intensity-driven. Damage to fiber facets or splices is neither uncommon nor trivial to repair, especially in a packaged device. Simply increasing the core size is generally not an option, as a good Gaussian beam profile is also required. Clever approaches like tapered end caps provide some relief, but this remains an area requiring further development.

- Finally, while an optimized fiber pump source is all well and good, reaching the end goal of an all-optically-confined system will also require the development of fiber-based components like isolators, modulators, switches, and beam combiners. These components are often not exciting or eye-catching enough to attract the funding necessary for their proper development, yet they can easily end up as the weak (or missing) link in an otherwise high-performing system, limiting the success of the system as a whole.

The SET-170 Task Group recommended, and the Fall 2013 SET Panel Business Meeting approved, creation of a new Exploratory Team to continue the collaborative investigation of mid-IR fiber-based sources. This ET, which we hope will lead also to a new Task Group, will consider these recommendations along with ongoing developments in the field of fiber lasers, to identify the best way forward and outline a new programme of work. As before, we expect that we will be able to accomplish more on behalf of NATO and our individual Nations through sharing our resources and expertise than any of us could accomplish alone.

Annex A – PARAMETERS USED IN Ho^{3+} LASING MODELS

A.1 HO:ZBLAN MODEL PARAMETERS USED IN VALIDATION CASE 1

VARIABLE	SYMBOL	VALUE	UNIT	COMMENT
Signal core radius	A	5	µm	
Core numerical aperture	NA	0.2		Cut-off wavelength: 2.6 µm
Pump core radius	R_{cl}	62.5	µm	
Ionic density	N	$5.4 \cdot 10^{20}$	cm^{-3}	3 mol %
$^5I_5$-level:				
Lifetime	T_4	40	µs	
Zero-line energy	E_{04}	11270	cm^{-1}	
$^5I_6$-level:				
Lifetime	T_3	3.5	ms	
Zero-line energy	E_{03}	8675	cm^{-1}	
$^5I_7$-level:				
Lifetime	T_2	150	µs	Pr^{3+} co-doping
Zero-line energy	E_{02}	5166	cm^{-1}	
Laser transitions:				
$^5I_6$ to $^5I_7$:				
Wavelength	Λ_3	2.94	µm	
Emission cross-section	σ_{e32}	$1.4 \cdot 10^{-21}$	cm^2	
Absorption cross-section	σ_{a23}	$8.3 \cdot 10^{-22}$	cm^2	
Fiber attenuation	α_4	0.21	dB/m	0.1 dB/m ZBLAN + 0.11 dB/m Pr^{3+}
Output mirror reflectance	R_3	0.04		
$^5I_8$ to $^5I_6$(pump):				
Wavelength	λ_p	1.15	µm	
Absorption cross-section	σ_{ap}	$1.8 \cdot 10^{-21}$	cm^2	
Fiber attenuation	α_3	0.1	dB/m	
Up-conversion:				
	k_{2241}	$3.2 \cdot 10^{-18}$	cm^3/s	
	k_{4122}	$3.2 \cdot 10^{-18}$	cm^3/s	
	k_{3215}	$1.0 \cdot 10^{-16}$	cm^3/s	

A.2 HO:ZBLAN MODEL PARAMETERS USED IN VALIDATION CASE 2

VARIABLE	SYMBOL	VALUE	UNIT	COMMENT
Signal core radius	A	5	µm	
Core numerical aperture	NA	0.16		Cut-off wavelength: 2.1 µm
Pump core radius	R_{cl}	25	µm	
Ionic density	N	$2.16 \cdot 10^{20}$	cm^{-3}	1.2 mol %
$^5I_6$-level:				
Lifetime	τ_3	3.5	ms	
Zero-line energy	ε_{03}	8675	cm^{-1}	
$^5I_7$-level:				
Lifetime	τ_2	12	ms	
Zero-line energy	ε_{02}	5166	cm^{-1}	
Laser transitions:				
$^5I_6$ to $^5I_7$:				
Wavelength	λ_3	3.0	µm	
Emission cross-section	σ_{e32}	$3.3 \cdot 10^{-22}$	cm^2	
Absorption cross-section	σ_{a23}	$1.4 \cdot 10^{-22}$	cm^2	
Fiber attenuation	α_3	0.05	dB/m	
HR mirror reflectance	R_{HR30}	0.99 or 0.04		
Output mirror reflectance	R_3	0.04		
$^5I_7$ to $^5I_8$:				
Wavelength	λ_2	2.07	µm	
Emission cross-section	σ_{e21}	$0.5 \cdot 10^{-20}$	cm^2	
Absorption cross-section	σ_{a12}	$9.3 \cdot 10^{-22}$	cm^2	
Fiber attenuation	α_2	0.1	dB/m	
HR mirror reflectance	R_{HR2}	0.6 or 0.04		
Output mirror reflectance	R_2	0.04		
$^5I_8$ to $^5I_5$ (pump):				
Wavelength	λ_p	1.15	µm	
Absorption cross-section	σ_{ap}	$1.8 \cdot 10^{-21}$	cm^2	
Fiber attenuation	α_p	0.1	dB/m	
Up-conversion:				
	k_{2241}	$2.5 \cdot 10^{-18}$	cm^3/s	
	k_{4122}	$2.5 \cdot 10^{-18}$	cm^3/s	
	k_{3215}	$1.7 \cdot 10^{-17}$	cm^3/s	

A.3 ESTIMATED HO:FLUOROINDATE MODEL PARAMETER VALUES

VARIABLE	SYMBOL	VALUE	UNIT	COMMENT
Signal core radius	A	5	µm	
Core numerical aperture	NA	0.16		Cut-off wavelength: 2.1 µm
Pump core radius	R_{cl}	25	µm	
Ionic density	N	$1.8 \cdot 10^{21}$	cm^{-3}	10 mol %
$^5I_5$-level:				
Lifetime	τ_4	30	µs	
Zero-line energy	ε_{04}	11240	cm^{-1}	
$^5I_6$-level:				
Lifetime	τ_3	1.1	ms	
Zero-line energy	ε_{03}	8621	cm^{-1}	
$^5I_7$-level:				
Lifetime	τ_2	10.2	ms	
Zero-line energy	ε_{02}	5025	cm^{-1}	
Laser transitions:				
$^5I_5$ to $^5I_6$:				
Wavelength	λ_4	3.905	µm	
Emission cross-section	σ_{e43}	$4.3 \cdot 10^{-21}$	cm^2	
Absorption cross-section	σ_{a34}	$2.8 \cdot 10^{-21}$	cm^2	
Fiber attenuation	α_4	0.1	dB/m	
Output mirror reflectance	R_4	0.5		
$^5I_6$ to $^5I_7$:				
Wavelength	λ_3	2.95	µm	
Emission cross-section	σ_{e32}	$1.1 \cdot 10^{-21}$	cm^2	
Absorption cross-section	σ_{a23}	$3.3 \cdot 10^{-22}$	cm^2	
Fiber attenuation	α_3	0.1	dB/m	
Output mirror reflectance	R_3	0.8		
$^5I_8$ to $^5I_5$ (pump):				
Wavelength	λ_p	0.895	µm	
Absorption cross-section	σ_{ap}	$5 \cdot 10^{-22}$	cm^2	
Fiber attenuation	α_p	0.1	dB/m	
Up-conversion:				
	k_{2241}	$1.0 \cdot 10^{-19}$	cm^3/s	
	k_{4122}	$6.0 \cdot 10^{-18}$	cm^3/s	
	k_{3215}	$6.0 \cdot 10^{-16}$	cm^3/s	

ANNEX A – PARAMETERS USED IN HO^{3+} LASING MODELS

Annex B – LIST OF PUBLICATIONS RESULTING FROM TASK GROUP ACTIVITY

B.1 JOURNAL PAPERS

Gattass, R.R., Shaw, L.B., Nguyen, V.Q., Pureza, P.C., Aggarwal, I.D. and Sanghera, J.S., "All-fiber chalcogenide-based mid-infrared supercontinuum source", Optical Fiber Technology **18**, 345-348 (2012).

Hudson, D.D., Judge, A., Jackson, S., Dekker, S., Magi, E., Li, E., Sanghera, J.S., Shaw, L.B., Aggarwal, I.D. and Eggleton, B., "Octave spanning supercontinuum in an As_2S_3 taper using ultralow pump pulse energy", Optics Letters, Vol. 36, No. 7, pp. 1122-1124 (2011).

Shaw, L.B., Gattass, R.R., Sanghera, J.S. and Aggarwal, I.D., "All-Fiber Mid-IR Supercontinuum Source from 1.5 to 5 μm", SPIE, Vol. 7914 (2011).

Swiderski, J., Maciejewska, M., Kwiatkowski, J. and Mamajek, M., "An all-fiber, resonantly pumped, gain-switched, 2 μm Tm-doped silica fiber laser", Laser Phys. Lett. 10, 015107 (2013).

Swiderski, J. and Michalska, M., "Mid-infrared supercontinuum generation in a single-mode thulium-doped fiber amplifier", Laser Phys. Lett. 10, 035105 (2013).

Swiderski, J., Michalska, M. and Mazé, G., "Mid-IR supercontinuum generation in a ZBLAN fiber pumped by a gain-switched mode-locked Tm-doped fiber laser and amplifier system", Opt. Express 21, 7851-7857 (2013).

Swiderski, J. and Michalska, M., "Generation of self-mode-locked resembling pulses in a fast gain-switched thulium-doped fiber laser", Opt. Lett. 38 (10), 1624-1626 (2013).

Swiderski, J. and Michalska, M., "Over three-octave spanning supercontinuum generated in a fluoride fiber pumped by Er & Er:Yb-doped and Tm-doped fiber amplifiers", Opt. & Laser Technol. 52, 75-80 (2013).

Swiderski, J., Théberge, F., Michalska, M., Mathieu, P. and Vincent, D., "High average power supercontinuum generation in a fluoroindate fiber", Laser Physics Letters 11, 015106 (2014).

Swiderski, J., Michalska, M., Kieleck, C., Eichhorn, M. and Mazé, G., "High power supercontinuum generation in fluoride fibers pumped by 2 μm pulses", IEEE Photonics Technology Letters 26 (2), 150-153 (2014).

Théberge, F., Daigle, J.-F., Vincent, D., Mathieu, P., Fortin, J., Schmidt, B.E., Thiré, N. and Légaré, F., "Mid-infrared supercontinuum generation in fluoroindate fiber", accepted Optics Letters (2013).

Théberge, F., Daigle, J.-F., Villeneuve, A., Salhany, J., Burgoyne, B., Soudagar, Y., Châteauneuf, M. and Dubois, J., "Tunable mid-infrared generation using synchronized programmable fiber lasers", Laser Technology for Defense and Security VIII: 2012 SPIE Proceedings Volume 83810E, May 2012.

B.2 PRESENTATIONS AND PROCEEDINGS

Hudson, D.D., Judge, A., Jackson, S., Dekker, S., Magi, E., Li, E., Sanghera, J.S., Shaw, L.B., Aggarwa, I.D. and Eggleton, B., "Octave Spanning Supercontinuum in an As_2S_3 Taper using Ultra-low Pump Pulse Energy", Proc. CLEO, Baltimore, MD, USA, May 2-6, 2011.

Shaw, L.B., Gattass, R.R., Frantz, J., Nguyen, V.Q., Pureza, P., Busse, L., Sanghera, J.S., Aggarwal, I.D, Stegeman, R. and Park, E., "Wavelength Conversion in IR Fiber", Proc. MSS IRCM, Monterey, CA, USA, April 26-28, 2011.

Shaw, L.B., Gattass, R.R., Sanghera, J.S. and Aggarwal, I.D., "Infrared Supercontinuum Fiber Source", Proc. OSA Specialty Optical Fiber, Toronto, Ontario, Canada, June 12-15, 2011.

Shaw, L.B., Gattass, R.R., Sanghera, J.S. and Aggarwal, I.D., "Broadband Mid-IR Fiber Supercontinuum Source for Hyperspectral Image Projection", Proc. IEEE Summer Topical 2011, Mid-Infrared Solid State Light Sources Challenges and Application, Montreal, Québec, Canada, July 18-20, 2011.

Shaw, L.B., Gattass, R.R., Frantz, J., Nguyen, V.Q., Pureza, P., Busse, L., Sanghera, J.S. and Aggarwal, I.D., "Fiber Nonlinear Sources", Proc. MSS Active E-O Systems, San Diego, CA, USA, September 13-15, 2011.

Théberge, F., Mathieu, P., Châteauneuf, M., Dubois, J., Daigle, J.-F., Villeneuve, A., Salhany, J. and Burgoyne, B., "Tunable Mid-Infrared Generation Using a Synchronized Programmable Fiber Lasers", IEEE Photonics Society Summer Topical Meetings, Montreal, Québec, Canada, July 18, 2011.

REPORT DOCUMENTATION PAGE

1. Recipient's Reference	2. Originator's References	3. Further Reference	4. Security Classification of Document
	STO-TR-SET-170 AC/323(SET-170)TP/600		NATO UNCLASSIFIED RELEASABLE TO PFP

5. Originator

Science and Technology Organization
North Atlantic Treaty Organization
BP 25, F-92201 Neuilly-sur-Seine Cedex, France

6. Title

Mid-Infrared Fiber Lasers

7. Presented at/Sponsored by

Final Report of Task Group 095.

8. Author(s)/Editor(s)	9. Date
Multiple	April 2015
10. Author's/Editor's Address	**11. Pages**
Multiple	138

12. Distribution Statement

This document is distributed in accordance with NATO Security Regulations and STO policies.

13. Keywords/Descriptors

Fiber lasers	Infrared spectroscopy	Non-linear frequency conversion
Fiber materials	Laser materials	Non-linear optics
Fiber optics	Laser modelling	Optical parametric processes
Fluoride fiber	Laser spectroscopy	Optical resonators
Fluoride glass	Lasers	Rare earth lasers
Guided wave sources	Mid-infrared	Supercontinuum generation

14. Abstract

The objective of SET-170 was to advance the state-of-the-art in mid-IR fiber lasers, to support development of active sources primarily for countermeasures and remote sensing applications. The Task Group made significant advances in each of the three areas of its program of work. (1) In direct-lasing fibers, we identified trivalent holmium operating ~ 3.9 µm as the active ion most likely to result in a successful laser; and fluoroindate fiber as the most promising host material. Spectroscopic analysis and modelling were used to evaluate feasibility and to calculate fiber specifications, and led to demonstration of lasing in a sample of Ho-doped glass. (2) Supercontinuum work focused on increasing output power and especially extending the output spectrum and improving efficiency at longer wavelengths. Results include power scaling demonstrations in fluoride and chalcogenide fibers; demonstration of efficient power distribution at wavelengths longer than 3 µm; and a comparison of different fiber-based pumping techniques. (3) As an intermediate step to all-fiber mid-IR sources, SET-170 considered how best to use fiber lasers to pump bulk non-linear ($\chi^{(2)}$) devices. Pumping strategies were investigated and demonstrated for ZGP, PPLN, and OPGaAs, representing the current spectrum of birefringent, poled ferroelectric, and orientation-patterned non-linear materials.

NORTH ATLANTIC TREATY ORGANIZATION

BP 25
F-92201 NEUILLY-SUR-SEINE CEDEX • FRANCE
Télécopie 0(1)55.61.22.99 • E-mail mailbox@cso.nato.int

SCIENCE AND TECHNOLOGY ORGANIZATION

DIFFUSION DES PUBLICATIONS

STO NON CLASSIFIEES

Les publications de l'AGARD, de la RTO et de la STO peuvent parfois être obtenues auprès des centres nationaux de distribution indiqués ci-dessous. Si vous souhaitez recevoir toutes les publications de la STO, ou simplement celles qui concernent certains Panels, vous pouvez demander d'être inclus soit à titre personnel, soit au nom de votre organisation, sur la liste d'envoi.

Les publications de la STO, de la RTO et de l'AGARD sont également en vente auprès des agences de vente indiquées ci-dessous.

Les demandes de documents STO, RTO ou AGARD doivent comporter la dénomination « STO », « RTO » ou « AGARD » selon le cas, suivi du numéro de série. Des informations analogues, telles que le titre est la date de publication sont souhaitables.

Si vous souhaitez recevoir une notification électronique de la disponibilité des rapports de la STO au fur et à mesure de leur publication, vous pouvez consulter notre site Web (http://www.sto.nato.int/) et vous abonner à ce service.

CENTRES DE DIFFUSION NATIONAUX

ALLEMAGNE
Streitkräfteamt / Abteilung III
Fachinformationszentrum der Bundeswehr (FIZBw)
Gorch-Fock-Straße 7, D-53229 Bonn

BELGIQUE
Royal High Institute for Defence – KHID/IRSD/RHID
Management of Scientific & Technological Research for Defence, National STO Coordinator
Royal Military Academy – Campus Renaissance
Renaissancelaan 30, 1000 Bruxelles

BULGARIE
Ministry of Defence
Defence Institute "Prof. Zvetan Lazarov"
Blvd "Totleben" 34
1606 Sofia

CANADA
DGSIST
Recherche et développement pour la défense Canada
101 Colonel By Drive, 6 CBS
Ottawa, Ontario K1A 0K2

DANEMARK
Danish Acquisition and Logistics Organization (DALO)
Lautrupbjerg 1-5
2750 Ballerup

ESPAGNE
SDGTECIN (DGAM)
C/ Arturo Soria 289
Madrid 28033

ESTONIE
Estonian National Defence College
Centre for Applied Research
Riia str 12
Tartu 51013

ETATS-UNIS
Defense Technical Information Center
8725 John J. Kingman Road
Fort Belvoir, VA 22060-6218

FRANCE
O.N.E.R.A. (ISP)
29, Avenue de la Division Leclerc
BP 72
92322 Châtillon Cedex

GRECE (Correspondant)
Defence Industry & Research General Directorate, Research Directorate
Fakinos Base Camp, S.T.G. 1020
Holargos, Athens

HONGRIE
Hungarian Ministry of Defence
Development and Logistics Agency
P.O.B. 25
H-1885 Budapest

ITALIE
Centro Gestione Conoscenza
Secretariat General of Defence
National Armaments Directorate
Via XX Settembre 123/A
00187 Roma

LUXEMBOURG
Voir Belgique

NORVEGE
Norwegian Defence Research Establishment
Attn: Biblioteket
P.O. Box 25
NO-2007 Kjeller

PAYS-BAS
Royal Netherlands Military Academy Library
P.O. Box 90.002
4800 PA Breda

POLOGNE
Centralna Biblioteka Wojskowa
ul. Ostrobramska 109
04-041 Warszawa

PORTUGAL
Estado Maior da Força Aérea
SDFA – Centro de Documentação
Alfragide
P-2720 Amadora

REPUBLIQUE TCHEQUE
Vojenský technický ústav s.p.
CZ Distribution Information Centre
Mladoboleslavská 944
PO Box 18
197 06 Praha 9

ROUMANIE
Romanian National Distribution Centre
Armaments Department
9-11, Drumul Taberei Street
Sector 6
061353 Bucharest

ROYAUME-UNI
Dstl Knowledge and Information Services
Building 247
Porton Down, Salisbury SP4 0JQ

SLOVAQUIE
Akadémia ozbrojených síl gen. M.R. Štefánika, Distribučné a informačné stredisko STO
Demänová 393
031 06 Liptovský Mikuláš 6

SLOVENIE
Ministry of Defence
Central Registry for EU & NATO
Vojkova 55
1000 Ljubljana

TURQUIE
Milli Savunma Bakanlığı (MSB)
ARGE ve Teknoloji Dairesi Başkanlığı
06650 Bakanliklar – Ankara

AGENCES DE VENTE

The British Library Document Supply Centre
Boston Spa, Wetherby
West Yorkshire LS23 7BQ
ROYAUME-UNI

Canada Institute for Scientific and Technical Information (CISTI)
National Research Council Acquisitions
Montreal Road, Building M-55
Ottawa, Ontario K1A 0S2, CANADA

Les demandes de documents STO, RTO ou AGARD doivent comporter la dénomination « STO », « RTO » ou « AGARD » selon le cas, suivie du numéro de série (par exemple AGARD-AG-315). Des informations analogues, telles que le titre et la date de publication sont souhaitables. Des références bibliographiques complètes ainsi que des résumés des publications STO, RTO et AGARD figurent dans le « NTIS Publications Database » (http://www.ntis.gov).

NORTH ATLANTIC TREATY ORGANIZATION

BP 25
F-92201 NEUILLY-SUR-SEINE CEDEX • FRANCE
Télécopie 0(1)55.61.22.99 • E-mail mailbox@cso.nato.int

SCIENCE AND TECHNOLOGY ORGANIZATION

DISTRIBUTION OF UNCLASSIFIED STO PUBLICATIONS

AGARD, RTO & STO publications are sometimes available from the National Distribution Centres listed below. If you wish to receive all STO reports, or just those relating to one or more specific STO Panels, they may be willing to include you (or your Organisation) in their distribution.

STO, RTO and AGARD reports may also be purchased from the Sales Agencies listed below.

Requests for STO, RTO or AGARD documents should include the word 'STO', 'RTO' or 'AGARD', as appropriate, followed by the serial number. Collateral information such as title and publication date is desirable.

If you wish to receive electronic notification of STO reports as they are published, please visit our website (http://www.sto.nato.int/) from where you can register for this service.

NATIONAL DISTRIBUTION CENTRES

BELGIUM
Royal High Institute for Defence – KHID/IRSD/RHID
Management of Scientific & Technological Research for Defence, National STO Coordinator
Royal Military Academy – Campus Renaissance
Renaissancelaan 30
1000 Brussels

BULGARIA
Ministry of Defence
Defence Institute "Prof. Zvetan Lazarov"
Blvd "Totleben" 34
1606 Sofia

CANADA
DSTKIM
Defence Research and Development Canada
101 Colonel By Drive, 6 CBS
Ottawa, Ontario K1A 0K2

CZECH REPUBLIC
Vojenský technický ústav s.p.
CZ Distribution Information Centre
Mladoboleslavská 944
PO Box 18
197 06 Praha 9

DENMARK
Danish Acquisition and Logistics Organization (DALO)
Lautrupbjerg 1-5
2750 Ballerup

ESTONIA
Estonian National Defence College
Centre for Applied Research
Riia str 12
Tartu 51013

FRANCE
O.N.E.R.A. (ISP)
29, Avenue de la Division Leclerc – BP 72
92322 Châtillon Cedex

GERMANY
Streitkräfteamt / Abteilung III
Fachinformationszentrum der Bundeswehr (FIZBw)
Gorch-Fock-Straße 7
D-53229 Bonn

GREECE (Point of Contact)
Defence Industry & Research General Directorate, Research Directorate
Fakinos Base Camp, S.T.G. 1020
Holargos, Athens

HUNGARY
Hungarian Ministry of Defence
Development and Logistics Agency
P.O.B. 25
H-1885 Budapest

ITALY
Centro Gestione Conoscenza
Secretariat General of Defence
National Armaments Directorate
Via XX Settembre 123/A
00187 Roma

LUXEMBOURG
See Belgium

NETHERLANDS
Royal Netherlands Military Academy Library
P.O. Box 90.002
4800 PA Breda

NORWAY
Norwegian Defence Research Establishment, Attn: Biblioteket
P.O. Box 25
NO-2007 Kjeller

POLAND
Centralna Biblioteka Wojskowa
ul. Ostrobramska 109
04-041 Warszawa

PORTUGAL
Estado Maior da Força Aérea
SDFA – Centro de Documentação
Alfragide
P-2720 Amadora

ROMANIA
Romanian National Distribution Centre
Armaments Department
9-11, Drumul Taberei Street
Sector 6
061353 Bucharest

SLOVAKIA
Akadémia ozbrojených síl gen M.R. Štefánika, Distribučné a informačné stredisko STO
Demänová 393
031 06 Liptovský Mikuláš 6

SLOVENIA
Ministry of Defence
Central Registry for EU & NATO
Vojkova 55
1000 Ljubljana

SPAIN
SDGTECIN (DGAM)
C/ Arturo Soria 289
Madrid 28033

TURKEY
Milli Savunma Bakanlığı (MSB)
ARGE ve Teknoloji Dairesi Başkanlığı
06650 Bakanliklar – Ankara

UNITED KINGDOM
Dstl Knowledge and Information Services
Building 247
Porton Down, Salisbury SP4 0JQ

UNITED STATES
Defense Technical Information Center
8725 John J. Kingman Road
Fort Belvoir, VA 22060-6218

SALES AGENCIES

The British Library Document Supply Centre
Boston Spa, Wetherby
West Yorkshire LS23 7BQ
UNITED KINGDOM

Canada Institute for Scientific and Technical Information (CISTI)
National Research Council Acquisitions
Montreal Road, Building M-55
Ottawa, Ontario K1A 0S2, CANADA

Requests for STO, RTO or AGARD documents should include the word 'STO', 'RTO' or 'AGARD', as appropriate, followed by the serial number (for example AGARD-AG-315). Collateral information such as title and publication date is desirable. Full bibliographical references and abstracts of STO, RTO and AGARD publications are given in "NTIS Publications Database" (http://www.ntis.gov).